Universidade de Aveiro
2020

Departamento de Electrónica, Telecomunicações e Informática

DEBARATI MUKHERJEE

DEPOSIÇÃO DE FILMES DO DIAMANTE PARA DISPOSITIVOS ELECTRÓNICOS

DEPOSITION OF DIAMOND FILMS FOR ELECTRONIC DEVICES

Universidade de Aveiro
2020

Departamento de Electrónica, Telecomunicações e Informática

DEBARATI MUKHERJEE

DEPOSIÇÃO DE FILMES DO DIAMANTE PARA DISPOSITIVOS ELECTRÓNICOS

Tese apresentada à Universidade de Aveiro para cumprimento dos requisitos necessários à obtenção do grau de Doutor em Engenharia Eletrotécnica, realizada sob a orientação científica do Doutor Luis Nero Alves, Professor (Professor auxiliar) do Departamento de Electrónica, Telecomunicações e Informática da Universidade de Aveiro e sob a co-orientação do Dr. Joana Mendes (Investigadora auxiliar) do Instituto de Telecomunicações, Aveiro

DEPOSITION OF DIAMOND FILMS FOR ELECTRONIC DEVICES

Thesis presented to the University of Aveiro to fulfill the necessary requirements to obtain the degree of Doctor of Philosophy in Electrical Engineering, conducted under the scientific guidance of Doctor Luis Nero Alves, Professor (Assistant Professor) of the Department of Electronics, Telecommunications and Informatics of the University of Aveiro and under the co-guidance of Dr. Joana Mendes (Senior researcher) at the Instituto de Telecomunicações, Aveiro

Apoio financeiro dos projectos Estrategico 2019- UID/EEA/50008/2019
HeatIT-CENTRO-01-0247-FEDER-017942
Estrategico 2015- UID/EEA/50008/2013
PTDC/EEA-TEL/104004/2008

This thesis is dedicated to parents: Madhumita and Prabir, Lurdes and Tony

o júri/ the jury

presidente/ president

Professor Dr. Armando Jorge Domingues Silvestre
Professor Catedrático, Universidade de Aveiro

Dr. Julian Anaya Calvo
Engenheiro Doutorado, Vestas Design Centre, Porto

Professora Dr. Maria do Rosário Alves Calado
Professora Auxiliar C/ Agregação, Universidade da Beira Interior

Dr. Jordi Llobet Sixto
Investigador Doutorado, International Iberian Nanotechnology Laboratory, Braga

Professor Dr. João Nuno Pimentel da Silva Matos
Professor Associado, Universidade de Aveiro

Dr. Joana Catarina Martins Mendes
Investigadora Doutorada, Instituto de Telecomunicações, Aveiro

Acknowledgements

This work has reached completion due to the support of the many people that have been in my life during its course. I would like to thank the late Dr. José Graçio for the opportunity to move to Aveiro and Dr. Dinis Santos for the support I received during my initial years here. I thank Dr. Joana Mendes for her unfaltering support from day one of my life here in Portugal, her encouragement and belief in my abilities, without which this thesis would not have taken the shape that it has today. I would also like to thank Dr. Luis Nero for the several constructive discussions that we shared and lab activities that he initiated. Both of my supervisors had an undeniable role in boosting my confidence in bringing together the various strings of this work into a consistent piece of scientific writing. In the same vein, I would like to thank my colleagues in the Laboratory of Basic Sciences and Integrated Circuits, at Instituto de Telecomunicações, Aveiro for their criticisms and commendations that have made me a better public speaker today.

I would also like to take this opportunity to thank Instituto de Telecomunicações for providing the facilities that made it possible to carry out the PhD work. Thanks also to Dr. Miguel Neto (for his help with the HFCVD systems), Dr. Rui Silva (for letting me use the tools at the Department of Material Sciences, University of Aveiro), Dr. Filipe Oliveira and Dr. Marta Ferro (for helping me capture some beautiful SEM images) and Ana Queiros (for help with the contact deposition at INESTEC, Porto). I would also like to thank Dr. Shlomo Rotter and Dr. Luiz Perreira for their invaluable scientific and personal insights. Thanks also to my co-authors in the scientific publications that we published in this period for their scientific input.

I would like to thank the administrative staff at Instituto de Telecomunicações as well as DETI for their willingness to help and unfailing co-operation.

I would like to thank the friends I have made during my time in Portugal, who were always around with a kind word or available to join in a fun activity- both necessary for a healthy PhD brain.

Thanks to my family- my sister Prakriti for the wisdom and the silliness that she brings into my life. My mother Madhumita and my father Prabir, without whom, none of this would be.

Thanks also to the reader, for taking their time to peruse the contents of this thesis which represent the scientific acheivements of the past 6 years of my life.

And most importantly, thank you Vitor, for being my rock and much more- I could not have done this without you.

palavras-chave

HFCVD, diamante policrystalino, NNP, Si, SAW, HEMTs, high power electronic devices

resumo

Este trabalho discute a utilização de diamante em aplicações electrónicas. É apresentada uma revisão detalhada das propriedades de diamante e dos respectivos mecanismos de crescimento utilizando deposição química a partir da fase vapor com filament quente (hot filament chemical vapour deposition - HFCVD). Os detalhes experimentais relativos à otimização desta técnica tendo em vista o crescimento de diamante em vários substratos com relevância em eletrónica são apresentados e discutidos com detalhe. A discussão inclui a análise dos parâmetros tipicamente envolvidos em HFCVD, em particular do pré-tratamento que o substrato recebe e que é conhecido na literatura como "novel nucleation procedure" (NNP), assim como das temperaturas de crescimento e da química do plasma, bem como a influência de todos estes parâmetros nas características finais dos filmes. A caracterização morfológica dos filmes envolveu técnicas de microscopia e espetroscopia.

keywords **HFCVD, polycrystalline diamond, NNP, Si, SAW, HEMTs, high power electronic devices**

abstract

This PhD thesis presents details about the usage of diamond in electronics. It presents a review of the properties of diamond and the mechanisms of its growth using hot filament chemical vapour deposition (HFCVD). Presented in the thesis are the experimental details and discussions that follow from it about the optimization of the deposition technique and the growth of diamond on various electronically relevant substrates. The discussions present an analysis of the parameters typically involved in the HFCVD, particularly the pre-treatment that the substrates receive- namely, the novel nucleation procedure (NNP), as well as growth temperatures and plasma chemistry and how they affect the characteristics of the thus-grown films. Extensive morphological and spectroscopic analysis has been made in order to characterise these films.

The greatest challenge to any thinker is stating the problem in a way that will allow a solution.

Bertrand Russell

TABLE OF CONTENTS

1. INTRODUCTION 15

1.1 Motivation for the current work 17

1.2 Objectives of the work 18

1.3 Layout of the thesis 18

1.4 Prime novelty 19

1.5 Scientific output 19

2. NATURAL AND SYNTHETIC DIAMOND 23

2.1 Introduction 25

2.2 Natural diamond 25
2.2.1 Structure 25
2.2.2 Formation 26

2.3 History of synthetic diamond 27

2.4 Optical, mechanical and thermal properties of diamond 31

2.5 Electronic properties of diamond 33
2.5.1 Band structure 33
2.5.2 Carrier characteristics of intrinsic diamond 34
2.5.3 Carrier characteristics of doped diamond 34
2.5.4 Recombination/generation mechanisms 36
2.5.5 Diamond vs other WBGs 37

2.6 Applications of diamond 40
2.6.1 Mechanical applications 40
2.6.2 Optical applications 41
2.6.3 Thermal management 41
2.6.4 SAW devices 42
2.6.5 Field emission devices 43
2.6.6 RF MEMS and NEMS 44
2.6.7 Particle detectors 44
2.6.8 Electrodes 45
2.6.9 Power diodes 45
2.6.10 Transistors 46
2.6.11 CMOS and beyond 47

2.7 Challenges 49

2.8 Conclusions 51

3. DIAMOND GROWTH BY CVD 53

3.1 Introduction **55**

3.2 Undoped diamond **55**
3.2.1 Gas phase chemistry *58*
3.2.2 Surface kinetics and growth *60*
3.2.3 Nucleation processes *64*

3.3 Doped diamond **67**

3.4 Characterisation of CVD diamond **69**
3.4.1 Optical microscopy *69*
3.4.2 Optical profilometry *70*
3.4.3 SEM and EDS *71*
3.4.4 Raman spectroscopy *73*

3.5 Optimization of HFCVD for diamond- conformal coating for electronics **77**
3.5.1 Experimental details- Cleaning of samples *77*
3.5.2 Experimental details- NNP *78*
3.5.3 Results and discussion *80*

3.6 Conclusions **91**

4. DIAMOND FILMS FOR ELECTRONIC DEVICES 93

4.1 Introduction **95**

4.2 Diamond for SAW devices **96**
4.2.1 Experimental details- Diamond films on $LiNbO_3$ *97*
4.2.2 Results and discussion- Diamond films on $LiNbO_3$ *98*
4.2.3 Experimental details- Diamond for SAW using reverse fabrication *99*
4.2.4 Results and discussion- Diamond for SAW using reverse fabrication *101*

4.3 Patterned diamond holders for electronic devices **106**
4.3.1 Experimental details *107*
4.3.2 Results and discussion *107*

4.4 Low temperature growth of diamond on SiC and GaN **110**
4.4.1 Passivation of SiC and GaN devices *111*
4.4.2 Experimental details- Diamond on SiC *112*
4.4.3 Results and discussion- Diamond on SiC *113*
4.4.4 Experimental details- Diamond on GaN *122*
4.4.5 Results and discussion- Diamond on GaN *123*

4.5 Doped diamond films on SiC **132**
4.5.1 Experimental details- BDD deposition *132*
4.5.2 Results and discussion- BDD deposition *133*
4.5.3 Ohmic contacts to BDD *140*
4.5.4 Experimental details- Ohmic contacts to BDD *142*
4.5.5 Results and discussion- Optimization of ohmic contacts to BDD *143*
4.5.6 SiC-BDD heterojunctions *148*
4.5.7 Experimental details- SiC-BDD heterojunctions *148*
4.5.8 Results and discussion- SiC-BDD heterojunctions *149*

4.6 Conclusions **150**

5. CONCLUSIONS AND FUTURE WORK 151

5.1 Conclusions 153

5.1.1 Influence of the PT film 153

5.1.2 Influence of seeding suspensions 153

5.1.3 Other insights 154

5.2 Optimization matrices 154

5.3 Future work 156

6. BIBLIOGRAPHY 157

7. APPENDIX 181

LIST OF FIGURES

Figure 2-1 The structure of diamond, with a bond length of 0.15 nm (After [6]) 26
Figure 2-2 Phase diagram of C detailing the synthetic techniques for inter-conversion between phases 28
Figure 2-3 (Top) Commercially available CVD, PCD wafers of diameters 5 mm, 8 mm and 25 mm (Diamond Materials ®) (Bottom) Commercially available single crystal, electronic grade diamond (Applied Diamond, Inc.) 31
Figure 2-4 Radar graph of material properties of diamond, accompanied by the implications that they have on the devices characteristics designed out of them 37
Figure 2-5 Diagrammatic representation of thickness of semiconductor material required to block 10kV 39
Figure 2-6 A comparison of the charrier characteristics, i.e., the variation of the drift velocity vs. electric field of diamond with other WBG materials 39
Figure 2-7 Device concepts for (a) Graphene FET (GFET) (b) Carbon nano-tube FET (CNTFET) where the substrate is diamond 49
Figure 3-1 Schematic of the most important chemical reactions involved in thin film synthesis. It is important to note that not all the reactions represented here need occur for every CVD process, and are often, in fact, not even desirable (After [376]) 55
Figure 3-2 The fundamental factors involved in the CVD process, in a schematic representation of the process with the atoms and radicals involved in the diamond deposition process 56
Figure 3-3 One of the possible procedures of diamond growth: Schematic representation of reactions (3-11) through (3-17) (Adapted from [419]) 62
Figure 3-4 (a) An optical microscope image at 40x magnification of edge of a diamond film (b) Using an optical microscope to measure feature dimensions of a SAW device 70
Figure 3-5 Optical profilometry of film surfaces provide information about thickness of films as well as (a) sizes of features and (b) surface roughness 71
Figure 3-6 SEM images of the surface of the three types of diamond film: (a) MCD, showing randomly-oriented grain sizes around 1 µm, (b) PCD, with a mixture of grain sizes (c) NCD with grain sizes between 50-100 nm (d) UNCD showing typical cauliflower growth with grain size below 50 nm 72
Figure 3-7 Raman spectra of CVD diamond film collected using (a) Ar (b) HeNe lasers. Note that both spectra show the SCD peak at 1332 cm^{-1} 75
Figure 3-8 SEM image of surface of the PT film 80
Figure 3-9 Micro-Raman spectra collected from (a) no-PT and (b) PT samples after seeding different colors correspond to different positions on the same sample 81
Figure 3-10 SEM images of samples of series B_1, seeded with (a) ND_7 and (b) ND_8 82
Figure 3-11 SEM images of samples after 30 min diamond growth at 873 K. Samples were seeded with suspension (a) ND_1, (b) ND_2, (c) ND_3, (d) ND_4, (e) ND_7 and (f) ND_8 84
Figure 3-12 SEM images of samples seeded with ND_7 after 15 min diamond growth at 873 K, (a) with PT (b) without PT 85
Figure 3-13 SEM images of Si samples after 10 min diamond growth seeded with ND_7 (a, b) and ND_8 (c, d), (a, c) received PT (b,d) did not receive PT 86
Figure 3-14 SEM images of samples after 5 minutes diamond growth at 873 K (a,b) samples seeded with ND_7 (c,d) samples seeded with ND_8. (a, c) received PT (b,d) did not receive PT; insets: same samples after 30 min diamond growth at 873 K 87
Figure 3-15 SEM images of samples after 30 min diamond growth, seeded with (a,b) grit_1 (c,d) grit_2 (e,f) grit_4 and (g,h) girt_5. Images on the left (a, c, e, g) are of samples that received PT, images on the right (b,d, f, h) are samples that did not 88

Figure 3-16 SEM images of samples after 30 min diamond growth, seeded with grit_3 (a) with PT and (b) without PT 89
Figure 3-17 SEM images of samples after 10 min diamond growth, seeded with (a,b) grit_1 (c,d) grit_2 (e,f) grit_3 (g,h) girt_4 and (i,j) grit_5. Images on the left (a, c, e, g and i) are of samples that received PT, images on the right (b,d, f, h and j) are samples that did not 90
Figure 4-1 Schematic representation of (a) P1 and (b) P2 95
Figure 4-2 EDS spectra of Si sample without trace of contamination 96
Figure 4-3 SEM images of samples LNB_grit_1 and LNB_grit_2 98
Figure 4-4 Raman spectra of samples (a) LNB_grit_1 (b) LNB_ND_1 99
Figure 4-5 (a) As-purchased die; (b) Optical microscope image of detail of the IDTs 100
Figure 4-6 SEM images of films deposited during growth cycles D (a,b), E (c,d) and G (e,f) Seeding was performed with (a, c, e) DND and (b, d, f) 6-10 µm grit suspensions. 102
Figure 4-7 (a, b) SEM images of diamond film deposited during run F, seeding performed with grit (c, d) SEM images of the middle section of the IDT fingers showing delamination of diamond from the $LiNbO_3$ surface (series G) 103
Figure 4-8 Raman spectra of samples deposited during runs (a) D and F; (b) E and G 104
Figure 4-9 S_{21} of (a) as-purchased die; dies coated with diamond during run F, seeded with (b) DND and (c) grit suspensions, ... 105
Figure 4-10 SEM images of cross-section of films (a) Si_10h, after 10 hours (b) Si_20h, after 20 hours of growth 108
Figure 4-11 (a) 10kx SEM image of bare Si “negative”, (b) 2.5kx SEM image of growth surface of fully coalesced diamond film (Si_neg_1) (inset with high magnification image) 108
Figure 4-12 Raman spectrum of the nucleation surface of Si_neg_1 109
Figure 4-13 SEM images of nucleation surface of the film Si_neg_50h (a,b) 500kx showing details of features (c,d) showing details of edge of feature and nucleation surface (e) profilometry capture of film cross-section 110
Figure 4-14 Profilometry measure of heights of v-grooves on nucleation surface of free-standing diamond 110
Figure 4-15 Low magnification SEM images of samples (a) POL_PT1_S1_G11 and (b) POL_PT1_S1_G14. High magnification SEM images of samples (c) POL_PT1_S1_G11, (d) POL_PT1_S1_G12, (e) POL_PT1_S1_G13 and (f) POL_PT1_S1_G14 115
Figure 4-16. Raman spectra of samples from series (a) A and (b) B 116
Figure 4-17. SEM images of samples (a) POL_PT2_S2_G21, (b) POL_PT2_S2_G22, (c) POL_PT2_S2_G23 and (d) POL_PT2_S2_G24. Insets: details of isolated grains 117
Figure 4-18 SEM images of samples (a), (b) POL_PT2_S3; (a) inset: visible polishing lines (c), (d) EPI_PT3_S4 118
Figure 4-19 SEM images of samples (a) POL_PT2_S3_G3 and (b) EPI_PT3_S4_G3 (60 minutes’ growth); (c) POL_PT2_S3_G4 and (d) EPI_PT3_S4_G4 (180 minutes’ growth). (a) inset: magnified view of a hole in film on sample POL_PT2_S3_G3 119
Figure 4-20 Raman spectra of samples (a) POL_PT2_S3_G3, EPI_PT3_S4_G3 and EPI_PT4_S5_G5 (60 minutes’ growth); 120
Figure 4-21 (a, b) SEM images of sample EPI_PT4_S5_G5 121
Figure 4-22 SEM images of samples GaN_A2_1 (a,b) and GaN_A1_1a (c,d) 124
Figure 4-23 Raman spectra of samples (a) A1_1a (b) A1_3a and (c) A1_5a. Also detected was the 734 cm^{-1} of GaN (not shown) 125
Figure 4-24 SEM images of samples GaN_B1_1a (a,b) and GaN_C1_1a (c,d), showing delamination of film with increasing temperature 126

Figure 4-25 SEM images at low (left) and high (right) magnification of exposed GaN surface of sample GaN_C1_1a, inset at 40k magnification shows detail of pit 127
Figure 4-26 SEM images of (a) GaN_A1_3 (b) GaN_A1_5 at the same magnification 127
Figure 4-27 SEM images of etch pit at same magnification for (a) GaN_A1_5 and (b) GaN_B1_5 and at low magnification for (c) GaN_C1_5 128
Figure 4-28 Raman spectrum of sample GaN_C1_5 129
Figure 4-29 Raman spectrum of sample GaN_B1_3 129
Figure 4-30 SEM images of GaN_B1_3 at (a) 50kx and (b) 120kx magnification and GaN_C1_3 at (c) 2kx and (d) 100kx magnification 130
Figure 4-31 SEM images of (a) diamond grown on GaN (b) as-supplied HEMT die (c) diamond coated HEMT 131
Figure 4-32 I-V characteristics of the as-supplied and diamond-coated dice 132
Figure 4-33 SEM images of samples (a) A1' (b) A5' (c) A4 (d) A4' 134
Figure 4-34 Raman spectrum of sample A4' (red) and A4 (black), with the sharp peak at 764 cm^{-1} of 4H-SiC, fitting shown at the bottom of the plot 135
Figure 4-35 Raman spectra of samples A3' (red) and A3 (black)- fitting shown at the bottom of the plot 136
Figure 4-36 SEM images of sample (a) A5 (b) A2 137
Figure 4-37 SEM images of samples (a) A3 (b) B2 138
Figure 4-38 SEM image of sample B2' 138
Figure 4-39 SEM images of samples (a) B1 and (b) B2 139
Figure 4-40 SEM images of samples (a) A6 (b) A1 140
Figure 4-41 Profilometry image of sample with contacts deposited 142
Figure 4-42 (a) 2 wire sense set-up for DUT using a Keithley 2400 (b) Corresponding circuit diagram 144
Figure 4-43 (a) Pulse measure timing, with delay, and an overhead of 80µs (b) Linear pulse sweep (c) Cyclical pulse sweep 144
Figure 4-44 IV curves of samples (a) A3_Au and (b) A3_AuPd 145
Figure 4-45 (a) Contacts used for four point probe measurements (b) Measurement set-up for the four point probe technique 146
Figure 4-46 Equivalent circuit diagram of 4 point probe set-up where R_s is the sample resistances, R_c is the contact resistance, and R_L the lead resistance 146
Figure 4-47 Plot of average resistance and its variation with % of CH_4 for samples of series BDD (a) with PT (b) without PT 148
Figure 4-48 IV curves of samples SiC_Ni (top) and SiC_Ni_ann (bottom) 150

LIST OF TABLES

Table 2-1 A summary of the optical, mechanical and thermal properties of the different varieties of diamond and other common semiconductors.......... 32
Table 2-2 Available grades of CVD diamond, with a brief description of its identifying property and its application 33
Table 2-3 The electronic properties of diamond and other WBG materials 40
Table 3-1 A comparison of the advantages and disadvantages of the various CVD techniques.......... 57
Table 3-2 Primary peaks in the Raman spectrum of diamond.......... 76
Table 3-3 Standard cleaning for wafers prior to CVD treatment.......... 78
Table 3-4 Summary of PT and diamond deposition conditions.......... 79
Table 3-5 Summary of ND suspensions used for seeding.......... 80
Table 3-6 Summary of grit suspensions used for seeding 80
Table 3-7 List of Raman bands in spectra of *Figure 3-9* b, as obtained by fitting, the average $I_{diamond}$ / $I_{non-diamond}$ ratio is 1.5 81
Table 3-8 Nucleation densities obtained for grit samples 91
Table 4-1 Deposition conditions used for diamond growth on $LiNbO_3$ samples.......... 98
Table 4-2 Deposition conditions used for diamond growth on SAW dies 100
Table 4-3 Thickness and average grain size of diamond films.......... 101
Table 4-4 Deposition conditions used for diamond growth on Si samples 107
Table 4-5 Deposition conditions used for diamond growth on SiC samples 113
Table 4-6 Deposition conditions used for diamond growth on GaN samples 123
Table 4-7 Deposition conditions used for BDD growth on SiC samples- Samples not given PT are marked with ' 133
Table 4-8 Summary of ohmic contacts to SCD, PCD and natural diamond, of p-type conductivity, using various fabrication techniques 142
Table 4-9 Deposition conditions used for second round of BDD growth on SiC samples- samples not given PT are marked with ' 143
Table 4-10 Summary of samples fabricated for ohmic contact characterization.......... 145
Table 4-11 Average resistance values of samples of series BDD 147
Table 4-12 Summary of samples fabricated for ohmic contact optimization for SiC 149
Table 5-1 Optimization matrix for Si substrates.......... 155
Table 5-2 Optimization matrix for $LiNbO_3$ substrates.......... 155
Table 5-3 Optimization matrix for SiC substrates.......... 155
Table 5-4 Optimization matrix for GaN substrates.......... 155
Table 5-5 Optimization matrix for BDD on SiC substrates.......... 156

LIST OF ABBREVIATIONS

a-C	Amorphous carbon
BDD	Boron doped diamond
BJT	Bipolar junction transistor
CVD	Chemical vapour deposition
DFT	Density functional theory
DLC	Diamond like carbon
DND	Detonation diamond
EBIC	Electron beam induced current
EDS	Energy dispersive X-ray spectroscopy
EPM	Empirical pseudopotential method
FBG	Fibre Bragg grating
FET	Field effect transistor
FOM	Figure of merit
FWHM	Full width half maximum
GC	Growth conditions
HEMT	High-electron-mobility transistor
HF	Hot filament
HFCVD	Hot filament chemical vapour deposition
HFET	Heterojunction field effect transistor
HRTEM	High resolution transmission electron microscopy
IC	Integrated circuit
IR	Infra-red
IDT	Inter-digitated transducer
IGBT	Insulated gate bipolar transistor
LDA	Local density approximation
LHC	Large hadron collider
MCD	Microcrystalline diamond
MCM	Multi-chip module
MEMS	Micro-electro-mechanical systems
MESFET	Metal-semiconductor field effect transistor
MFC	Mass flow controller
MiPD	Metal-intrinsic p-type diode
MIT	Metal-insulator transition
MOSFET	Metal-oxide-semiconductor field effect transistor
NCD	Nanocrystalline diamond
ND	Nano-diamond
NEA	Negative electron affinity
NEMS	Nano-electro-mechanical systems
PCB	Polymer circuit board
PCD	Polycrystalline diamond
PEM	Piezo-electric material
PiND	P-type-intrinsic-n-type diodes
PT	Pre-treatment

RF	Radio frequency
RTA	Rapid thermal annealing
SAW	Surface acoustic wave
SBD	Schottky barrier diode
SBH	Schottky barrier height
SEM	Scanning electron microscope
SRH	Shockley-Reed-Hall
TCT	Transient current technique
TEC	Thermal expansion coefficient
ToF	Time-of-flight
UNCD	Ultra-nanocrystalline diamond
US	Ultrasound
XPS	X-ray photoelectron spectroscopy

LIST OF CHEMICAL SYMBOLS

Ag	Silver
Al	Aluminium
Al_2O_3	Aluminium oxide
AlN	Aluminium nitride
Au	Gold
B	Boron
$B(OCH_3)_3$	Trimethyl borate
B_2H_6	Diborane
B_2O_3	Boron trioxide
BC	Boron carbide
BN	Boron nitride
$C_2CoN_2S_2$	Cobalt (II) thiocyanate
C_2H_2	Acetylene
$[C_2H_2]_n$	Poly-acetylene
C_2H_5OH	Ethanol
C_3H_9B	Trimethyl borane
$C_6H_{15}B$	Triethyl borane
CH_3	Methyl
CH_3COCH_3	Acetone
CH_3OH	Methanol
CH_4	Methane
CO	Carbon monoxide
CO_2	Carbon dioxide
Cu	Copper
DMSO	Dimethyl sulfoxide
Fe	Iron
GaAs	Gallium arsenide
GaN	Gallium nitride
Ge	Germanium
H_2	Hydrogen
H_2O_2	Hydrogen peroxide
HF	Hydrogen fluoride
Hg	Mercury
$K_2Cr_2O_7$	Potassium dichromate
$KNbO_3$	Potassium niobate
Li	Lithium
$LiNbO_3$	Lithium niobate
$LiTaO_3$	Lithium tantalate
Mo	Molybdenum
N_2	Nitrogen
Nb	Niobium
NH_4OH	Ammonium hydroxide
Ni	Nickel
NO_x	Nitrous oxide
P	Phosphorus
PH_3	Phosphine

Pt	Platinum
PZT	Lead zirconate titanate
S	Sulphur
Si	Silicon
SiC	Silicon carbide
Ta	Tantalum
Ti	Titanium
W	Tungsten
Y_2O_3	Yttrium (III) oxide
ZnO	Zinc oxide
ZnSe	Zinc selenide

1. Introduction

If "a snowflake is a letter to us from the sky" (Nakaga) then "a diamond is a letter to us from the depths, and a letter more worth reading since we can visit the sky"- Sir Charles Frank

For a material that is made up of one of the most abundant elements on the planet- carbon, diamond has long fascinated us because of its unique properties. Diamond has a unique combination of physical and electronic properties; the key word here being "combination". If each individual physical property is selected for comparison, even if there may eventually be materials which have superior values for such property, no other material is comparable to diamond when compared in terms of the combination of mechanical, thermal, electrical, optical, and chemical properties that it possesses. These properties make diamond an exceptional candidate for applications in varied fields- from mechanics and optics to electronics.

The story of synthetic diamond is almost as fascinating as diamond itself. Since its first successful synthesis in the laboratory, this field of research has come a long way and reached levels of reproducibility due to its industrial applications that have been occurring in parallel. Diamond crystals and films can be produced using any of the various means of synthetic fabrication. Of these means of producing diamond, one of the most versatile and commonly used techniques is chemical vapour deposition (CVD), of which hot filament chemical vapour deposition (HFCVD) is the undoubtedly the most economical. This technique is most commonly used to fabricate diamond films on both diamond and non-diamond substrates with varying properties; by optimizing the deposition parameters, diamond films can be tailored according to their application requirements. These deposition parameters affect the characteristics of the film such as the grain sizes, grain orientation, ratio of the grains to their grain boundaries, film uniformity and thickness, average surface roughness; the desired characteristics are specific to the application it is intended for. The work undertaken in this thesis can be succinctly expressed as the optimization of the HFCVD process in order to obtain polycrystalline films of diamond that lend themselves to usage in electronics. These films were grown on several *electronically* relevant substrates such that diamond can be included in the schematic of devices fabricated out of them.

1.1 Motivation for the current work

Out of the conventionally accepted four fundamental forces of nature, electromagnetism provides the best compromise between the magnitude of force, relative size of the associated materials, and the ease with which information and power is utilized. Keeping this in mind, it is a matter of little surprise that the field of electronics has been the key contributor in the technological advancements of humankind in the last two hundred years. Progress in the field of electronics has meant the rise in both the production and consumption of electrical energy. On the one hand where the progress of electronics has benefitted modern society, it has brought about demands on power supply that have never before been faced. There is also a new ecology in the field of electronics: one may not simply produce more power, power systems must be made as efficient as possible, sustainable and compatible with environmental restrictions and regulations. Global drivers such as energy efficiency, reduction of greenhouse gases are increasingly becoming more and more important in every layer of the value chain, contributing to this new ecology. These demands are to be met by electronic systems and devices operating at higher frequencies, higher power densities, and high temperatures. Si based switching devices have almost approached the theoretical limitations with respect to temperature, frequency operations and voltage blocking capabilities. Bearing in mind also the failures associated with high temperature operation, one of the places to start the evolution is at the device level- be it with effective passivation and/or thermal management schemes. Diamond is a particularly attractive material in this regard- being a very efficient thermal conductor but uniquely and simultaneously, an electrical insulator. The thorough investigation of its usage in several avenues of electronic devices because of these properties is the primary motivation

for the current work.

1.2 Objectives of the work

This thesis presents the process optimization of the HFCVD technique to deposit diamond on substrates used to commonly fabricate electronic devices and provides definitive inferences about fabricating the films with a certain degree of reproducibility. In order to do this, certain objectives were identified and met during the course of this work; these are listed as follow:

- Literature review of properties and applications of diamond- A review of the properties of both natural and synthetic diamond was carried out. The purpose of this review was to highlight the unique properties of diamond as well as justify its usage in electronics. Following this, a state of the art review was carried out on existing applications of diamond which served to highlight the versatility of this material.

- Literature review of the HFCVD process- A further review of the growth process involved in HFCVD diamond growth was performed to highlight the importance of the process parameters involved in a typical growth cycle. This was considered particularly relevant as the bulk of the experimental work in this thesis involved the variation of deposition parameters and analyzing its effects on the film properties.

- Experimental work- The first part of the experimental work involved the growth of diamond films on Si substrates by optimizing the novel nucleation procedure (NNP). Si is a commonly used substrate for the CVD of diamond; with suitable pre-treatments, it is relatively easy to obtain diamond films on it. In this part of the work, it was used to ascertain the optimum pre-growth treatments that a substrate might receive to obtain good quality films of diamond, useful for electronics applications. This was followed by the deposition of diamond on various substrates- $LiNbO_3$ (a piezoelectric material, or PEM, used commonly to fabricate wireless devices) as well as direct growth on surface acoustic wave (SAW) dies, and wide band-gap (WBG) materials, SiC and GaN that are finding increasing research and industry applications. Besides these depositions, a unique way of fabricating all-diamond holders using the nucleation surface of a CVD diamond film was also investigated. Finally, doped diamond films were deposited on SiC and ohmic contacts to this device were optimized to fabricate heterostructures. The main tools used to characterize the films throughout the work were morphological (scanning electron microscopy- SEM) and spectroscopic (Raman spectroscopy).

1.3 Layout of the thesis

This thesis is laid out in the same order as the objectives presented in the previous section.

- The first chapter is the introduction. The introduction serves to inform the reader about the objectives and contents of the thesis and has been kept concise.

- The second chapter presents the review of the properties of diamond, a summary of the story of synthetic diamond and the state of the art on diamonds' varied applications in the modern world.

- The third chapter summaries the process of HFCVD for the growth of diamond as well as the material characterization techniques used in this work. The significance of the NNP is described, followed by experimental results of diamond growth on Si substrates using the same. An in-depth study of the properties of the thus-produced films are then presented followed by inferences.

- The fourth chapter presents experimental details and subsequent discussions about the growth of diamond on the several different non-diamond substrates- $LiNbO_3$, SiC, GaN as well as Si. In each sub-section, the relevance and benefits of adding diamond to these substrates are first discussed followed by details of the process optimization in order to obtain the same.

- The fifth and final chapter summarizes the main conclusions of the thesis and discusses the future tasks that were identified during the course of this work.

Chapters 2, 3 and 4 each begin with a short introduction of their contents and end with a paragraph summarizing its main conclusions.

1.4 Prime novelty

Although the usage of diamond in electronics is not itself a novel concept, this thesis serves a niche purpose. It brings together knowledge about the usage of the HFCVD technique to deposit diamond on various electronically relevant substrates. It addresses the challenges that have hitherto been faced when the same has been attempted previously using either different deposition techniques and/or deposition parameters. By making extensive morphological and spectroscopic analysis of the films, these parameters have been fine-tuned to successfully obtain diamond on several substrates. The scientific novelties of this work are as follow

- Insight into the nature of the C film grown during the NNP, and the effectiveness of using different seeding suspensions

- Direct growth of diamond on SAW dies using a reverse fabrication procedure

- Optimization of the growth of HFCVD diamond on SiC and GaN, of which growth on GaN is known to be particularly challenging

- Fabrication of PCD- SiC heterostructures

1.5 Scientific output

The results of this work have been disseminated in several international conferences and published in various peer-reviewed journals during its course. Since the publication of scientific work is one of the indicators of its relevance in the field, it is important to enlist the same-

International conferences-

- CVD diamond films for thermal management applications, D. Mukherjee et. al., Proceedings of the 7th International Conference on Microwaves, Communications, Antennas and Electronic systems (COMCAS), Israel (2019)

- Fabrication of patterned diamond holders for electronic devices, D. Mukherjee et. al., Proceedings of the 43rd Workshop on Compound Semiconductor Devices and Integrated Circuits (WOCSDICE), France (2019)

- Deposition of diamond films on GaN substrates without interlayer, D. Mukherjee et. al., Diamond D-Day- Workshop hosted by the Centre for Device Thermography and Reliability of the University of Bristol and the GaNDaME Programme, United Kingdom (2019)

- Deposition of diamond on SiC for power electronics, D. Mukherjee, Second place in 3 Minute Thesis contest, 25th European Signal Processing Conference (EUSIPCO), Greece (2017)

- Diamond-SiC heterojunctions – the influence of CH_4 ratio on the electrical behavior of CVD diamond, D. Mukherjee et. al., Proceedings of 41st WOCSDICE, Gran Canaria (2017)

- Diamond/SiC heterojunctions, D. Mukherjee et. al., Proceedings of PRIME- 12 th Conference of PhD research in Microelectronics and Electronics, Portugal (2016)

- Polycrystalline Diamond (PCD)/SiC heterojunctions, D. Mukherjee et. al., Proceedings of 40th WOCSDICE, Portugal (2016)

- Deposition of polycrystalline diamond films on GaN, SiC and $LiNbO_3$, D. Mukherjee et. al., Proceedings of Hasselt Diamond workshop, Belgium (2016)

- Deposition of diamond films for effective passivation of SiC devices, D. Mukherjee et. al., Proceedings of WOCSDICE - 39th Workshop on Compound Semiconductor Devices and Integrated Circuits, Slovakia (2015)

- Diamond-SAW devices: A Reverse Fabrication Method, D. Mukherjee et. al., Proceedings of Hasselt Diamond workshop, Belgium (2015)

- Selective Nano-Diamond Deposition using Soft-Lithography, D. Mukherjee et. al., Proceedings of International Conference on Advanced Nanomaterials, Portugal (2014)

- Combined effect of seeding suspensions and novel nucleation process (NNP) on HFCVD diamond initial growth, D. Mukherjee et. al., Proceedings of International Conference on Diamond and Carbon Materials, Italy (2013)

International journals-

- The HFCVD growth of diamond on non-diamond substrates- A review, **D. Mukherjee**, M. Neto, F. Oliveira, R. Silva, J. C. Mendes, Crystals, 2019 (under review)

- Deposition of diamond films on single crystalline silicon carbide substrates, **D. Mukherjee**, F. J. Oliveira, S. C. Trippe, S. Z. Rotter, M. Neto, R. F. Silva, A.K. Malik, K. Haenen, C. Zetterling, J. C. Mendes, Diamond and Related Materials, 2019 (DOI: 10.1016/j.diamond.2019.107625)

- Thermal management of photonic integrated circuits: impact of holder material and epoxies, S. Kyatam, **D. Mukherjee**, H. Neto, J.C. Mendes, Applied Optics, 2019 (DOI: 10.1364/AO.58.006126)

- Small signal analysis of MPCVD diamond Schottky diodes, J.C. Mendes, H.L. Gomes, S.C. Trippe, **D. Mukherjee**, L. Pereira, Diamond and Related Materials, 2019, (DOI: 10.1016/j.diamond.2019.02.008)

- Why Moore might love diamond, **D. Mukherjee**, L.N. Alves, J.C. Mendes, IEEE Potentials, 2018 (in line for publication)

- HFCVD nanostructured diamond films deposited by a combination of seeding suspensions and novel nucleation process (NNP), **D. Mukherjee**, R. Polini, V. Valentini, S. Z. Rotter, J. C. Mendes, International Journal of Surface Science and Engineering, 2017 (DOI: 10.1504/IJSURFSE.2017.085622)

- Diamond-SAW devices: a reverse fabrication method, **D. Mukherjee**, F. J. Oliveira, R. F. Silva, J. F. Carreira, L. Rino, M. R. Correia, S. Z. Rotter, L. N. Alves, J. C. Mendes, Physica Status Solidi C, (2016) (DOI: 10.1002/pssc.201510313)

- A manuscript based on the growth of diamond on GaN is being prepared using the results presented in the fourth chapter

- A manuscript based on the growth of doped diamond on SiC is being prepared using the results presented in the fourth chapter

Book chapter-

- Recent advances in SiC / diamond composite devices, **D. Mukherjee**, M. Neto, F. J. Oliveira, R.F. Silva, L. Pereira, Shlomo Rotter, J. C. Mendes, in IOP ebook on Widebandgap Semiconductors, (2020), S. Pearton & F. Ren (eds.)

2. Natural and synthetic diamond

2.1 Introduction

This chapter serves as a bibliographic review of synthetic diamond. It introduces the reader to the history of synthetic diamond; its unique properties are compared with those of natural diamond. The electronic properties of diamond are discussed in detail and this is followed by a review of the current applications of diamond in the industry. A review of the challenges that currently face the field are presented at the end of the chapter.

2.2 Natural diamond

The first documented mining of diamond happened in India in the fourth century BCE [1]. Initially a stone solely regarded for its brilliance, its "industrial" uses as the hardest material on the planet, were quickly realized by the Chinese as early as the second century; scientists have found traces of diamond in Chinese tools dated back to 2500 BCE. Diamond edged knives and engraving tools have been used by stone cutters for millennia [2]. This is with good reason- it is a remarkable material; often called an extreme material because of its extreme properties: be it structural, electrical, optical or mechanical, property values associated with diamond are almost always at list extremities when compared with materials known to have similar characteristics.

2.2.1 Structure

C is the most versatile element known to us, forming the building blocks of virtually all of organic chemistry, which given that it makes up 79% of all the molecules known to us (round-about 20 million, in totality [3]), is a very significant number. It is accorded versatility also because of its ability to exist in the form of various thermodynamically stable allotropes, of which diamond is one among many- graphite, fullerenes, amorphous C, lonsdalite etc. being several of the others. It has been known since the 18th century that diamonds are composed of C atoms but their complete structure only ascertained much later in 1913 with the help of x-rays [4]. C exists in nature in two stable isotopes C^{12} and C^{13} with average abundances of 98.9% and 1.1%, a ratio reflected in natural diamonds which are known to demonstrate slight variations of the C isotope composition.

The ground state electronic configuration of C is $1s^2$ $2s^2$ $2p^2$, where the 2s and 2p orbitals exist in a form of hybridization of the s and p orbitals. Depending on the hybridization, there may be sp^3, sp^2 or sp hybrid orbitals for example, thus being able to form single, double or triple covalent bonds, respectively, with other atoms and most importantly, very stable covalent bonds with other atoms of C itself, giving rise to organic chemistry in the former case and a wide variety of allotropes, in the latter. Because of the size of the C atom, these bonds between C-C are very strong; as a comparison, the bond strength of a C-C single bond has a value of 356 $kjmol^{-1}$ compared to a value of 226 $kjmol^{-1}$ for the equivalent Si-Si bond, making it able to form extended chains with variety of structures. Diamond is the allotrope of C in which the atoms are sp^3 hybridized and each C-atom is σ-bonded (head-on overlapping of atomic orbitals, making it the strongest type of covalent bond) to four neighbouring C atoms. The resultant structure is a 3D network of a combination of two interpenetrating *fcc* (face-centered cube) sub-lattices displaced along the body diagonal of the cubic cell by 1/4th length of that diagonal – this structure is called the diamond cubic structure (*Figure 2-1*). Thus, diamond has tetra-hedral bonding in which all bonds are essentially purely covalent and equivalent, all 0.15 nm in length. Consequently, the number of chemical bonds per unit volume 3.5×10^{23} cm^{-3}, is the highest among all known crystallographic structures [5]. The only weakness lies in the octahedral planes, where diamond crystals can be cleaved with relative ease.

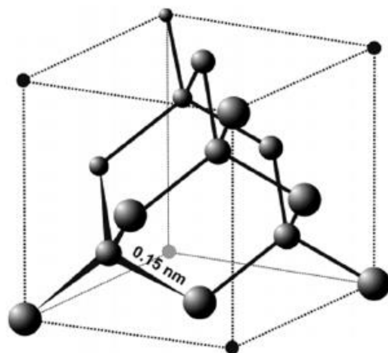

Figure 2-1 The structure of diamond, with a bond length of 0.15 nm (After [6])

This is different from the structure of graphite, for example, which is another allotrope of C, in which C atoms are sp^2 hybridized. As a result, each C atom has 3 bonds with neighbouring C atoms due to its 3 sp^2 orbitals in a trigonal plane; due to the fourth electron in its p orbital, the structure of graphite consists of many "sheets" lying one on top of the other (*Table 2-1*). The fourth electron of each C atom (pertaining to the un-hybridized p-orbital) is in fact de-localized within this structure making it electrically conducting. Thus graphite exists in sheets with strong hexagonally bonded C—C atoms (with short bond lengths of 0.142 nm) and weak C-C bonds between the sheets (with long bond lengths of 0.335 nm). These sheets are sometimes referred to as being held by the weak van der Waal's force, with the long bonds being so weak that they result in the lubricating properties of graphite. Many other forms of C, such as charcoal, consist of disordered fragments of the graphite structure.
The binding energy between atoms of C is very large (for example, the cohesive energy of diamond is 717 kJ mol^{-1}). Once C atoms are locked into a given phase configuration, a large amount of activation energy is required to produce a different stable phase. In order to transform graphite to diamond, the energy barrier is consequently exceptionally high. Since the extreme pressure and temperature conditions required to supply this energy occur in only some specific zones on earth, diamonds are rarer to find in nature compared to graphite- making graphite the standard state of C, and giving diamond a non-zero value for the standard enthalpy of formation (1.863 kJ mol^{-1}, measured at 298 K and 101.325 kPa or 1 atm [8]).

Hybridization	Valence orbitals	Geometry	
sp	SP, SP, P,P	Linear	
sp^2	SP^2, SP^2, SP^2, P	Trigonal planar	
sp^3	SP^3, SP^3, SP^3, SP^3	Tetra-hedral	

Table 2-1 Summary of the VSEPR theory to predict the geometry of atoms with hybridized orbitals (After [7])

2.2.2 Formation

Diamond being the densest allotrope of C, is most stable at high temperatures and pressures; at atmospheric pressure and ambient conditions, it is metastable (i.e., kinetically stable but thermodynamically unstable) compared to graphite. From its higher density (3.52 g/cm^3), compared to

graphite's (2.26 g/cm^3), it also becomes apparent that high pressure conditions can lead to the formation of diamond from other forms of C [9].
Diamond formation, in nature, occurs under very specific conditions, and contrary to popular belief is not just a result of the metamorphosis of coal. A convincing evidence of this is obtained from the C dating of diamond- the earliest diamond deposits have been dated to the earliest period in Earth's history- the Precambrian Eon [10], that ended about 541 million years ago; whereas life, in the form of terrestrial plants, the debris of which is the main source of coal on our planet, did not appear till about 475 million years ago, as observed from direct evidence [11]. Natural diamond on Earth has been produced either in the mantle, about 150 km below the Earth's surface, or in subduction zones between tectonic plates, that can be anywhere between 80 to 650 km below the Earth's surface and natural phenomena such as volcanoes and earthquakes bring these glittering natural marvels to the earth surface. Diamond can naturally form also at asteroid impact sites, that have resulted in extreme temperature and pressure conditions. What is common for these three sources of diamond is the existence of critical pressure and temperature conditions- in the Earth's mantle, temperatures exceed 1323 K whereas in the subduction zones, temperatures might be as low as 473 K but pressure conditions are extreme. In the case of asteroid impacts, both extreme temperature and pressure conditions are produced. The source of C in all of these cases is rarely coal, instead limestone, marble and dolomite are the primary sources of C for the production of diamond [12].

2.3 History of synthetic diamond

Humans have long tried to add to the three ways that diamonds are formed on Earth, with numerous efforts to synthesize it under artificial conditions, in the laboratory, having realized that diamond was just C in a very rare and attractive form. The very first trials for creating diamond in a lab date back to the 19th century which involved transforming carbonaceous materials into diamond by recreating the conditions that lead to naturally occurring diamond. The story of the "diamond makers" is a fascinating tale and a number of popular accounts can be found on the subject [2, 13, 14].
J.B. Hannay was among the first reporting success in 1880 [15], at making diamond by sealing organic material with Li into Fe tubes and heating until red hot. The majority of his tubes exploded, but some did not and were claimed to contain diamonds. Just before the turn of the century, H. Moissan used the known solubility of C in solid Fe to attempt diamond synthesis by quenching such a white hot solution, using an electric arc furnace [16]. The pressure generated by the contraction of the outer parts of the Fe was claimed to have produced diamonds. Over a thirty year period C. Parson attempted to duplicate these and other synthesis experiments, but finally came to conclude that neither he nor anyone else had succeeded [17]. These experiments were not reproducible and had not sufficiently studied the actual products. There have in fact been several early claims of having produced diamond in the laboratory, but with our current knowledge about the conditions required for artificial diamond synthesis (see phase diagram of C, *Figure 2-2*), it is easy to see that none of these claimed experiments attained these conditions [9].
Following the second World War, there was an increasing effort world-wide to achieve successful artificial diamond synthesis, primarily in Allmänna Svenska Eliktriska Aktiebolaget (ASEA) in Sweden and the General Electric (GE) Corporation in the United States, with the motivation to remove the dependence on "unfriendly" states for this precious mineral. In 1955, GE reported successful synthesis of diamond by replicating the extreme conditions of diamond formation in a high pressure high temperature (HPHT) reactor [18]. Curiously enough, using the high pressure process, almost any form of C can be used to make diamond. One study reported over 20 C source substances used with success [19]. Some of these sources, like naphthalene, first form graphite, which then converts to diamond. Others, such as paraffin, the combination of a cubic wax or sugar, convert directly to diamond. In five minutes at 2273 K and 13.8 Gpa

of pressure, even peanuts yielded 60% diamond [9]! The mention of high pressure processes warrants the mention of P.W. Bridgman [20], without whose work on high-pressure systems, these processes would not have come about when they did. Modification on his high pressure anvil by the original GE High Pressure diamond group [18], enabled them to achieve pressures up to 1×10^7 kPa at high temperatures.
It was only 15 years later when the catalytic HPHT technique was performed using a seed crystal of diamond [21, 22] in which a small natural diamond was "bathed" in molten graphite together with Ni, helping to bring down the process temperature to 1772 K and pressure to 5 GPa, that large size synthetic diamond crystals could be produced. The C precipitated on the diamond seed and slowly crystallised into a stone only a few mm^3 in volume. The role of Ni in the process is due to the fact that molten Ni can dissolve graphite, for which it has a high solubility, while at the same time crystallizing out diamond, for which its solubility is much less. At one time it was thought that the metals used, such as Ni, acted as a catalyst, but it is now certain that the metals serve purely as solvents [9, 23]. To this day, billions of carats of synthetic diamonds are manufactured annually for commercial and industrial applications using this process.

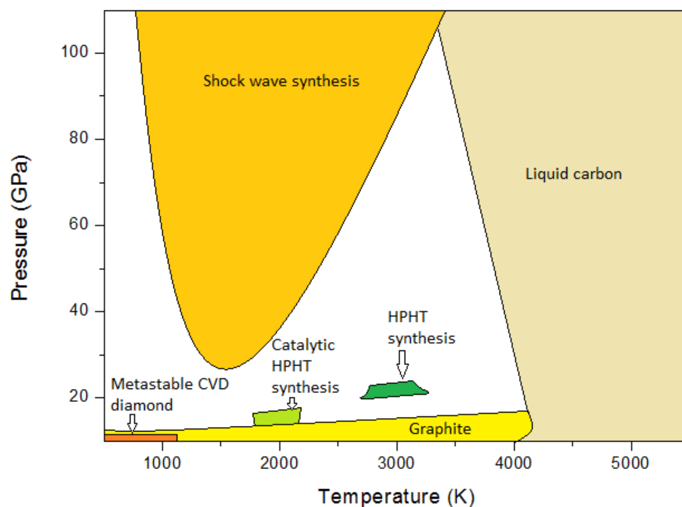

Figure 2-2 Phase diagram of C detailing the synthetic techniques for inter-conversion between phases

Another popular technique, a slightly modified version of which is still used today to produce detonation diamond (DND) (diamonds stones a few µm in size, commonly used for seeding process prior to low pressure synthesis of diamond), came about in 1961 and was reported by DeCarli and Jamieson [24]; it is called the shockwave synthesis technique. Using an explosive charge, 30 GPa was applied as a shock wave to graphite for a very short duration (10^{-6}s); the result of which was a small amount of tiny particles of diamond.
At the same time the HPHT method was being developed, scientists were trying to deposit diamond at low pressures from the gas phase – using a process known as CVD. The low pressure (i.e., pressures below atmospheric pressure) growth of diamond was intriguing because it offered the possibility of growing diamond in simpler laboratory conditions, without the need for expensive high pressure equipment or access to explosives. CVD differs fundamentally from the HPHT growth process, since it involves the production of diamond from a gaseous precursor, typically a hydrocarbon such as CH_4. As the hydrocarbon molecules are energized by a high energy source, they form radicals whose C atoms bond with atoms at the substrate to form diamond; the process also creates non-diamond bonds, like graphite, and much of

the efforts of CVD research has gone into reducing the non-diamond content and optimising the ratio of diamond/non-diamond components.

The first documented growth of diamond at low pressures was reported by Eversole in 1954, whereby he deposited diamond on diamond powder from low molecular weight hydrocarbons and CO, with a growth rate of the order of only 2-3% per hour [25]. The method was initially met with scepticism since at these pressures diamond is thermodynamically unstable with respect to graphite. The scepticism was due in part also to the extremely low rates of deposition. The growth was also restricted to only diamond (or graphite) substrates. In 1962, a patent by Eversole of the Union Carbide Corporation [26] outlined a CVD method that produced diamond without the great amounts of graphite that had been associated with CVD deposition of diamond up until then. The discovery that H_2 in the CVD plasma, at high temperatures and low pressures, is able to etch away the non-sp^3 components of the deposited film faster than the sp^3 content [27] led to further optimization in this competitive process and improvement in the growth rates. These were some of the first reports in literature (by Angus *et al.* of Case Western Reserve University, Cleveland [28, 29] and by Deryagin *et al.*, at the Physical Chemistry Institute, Moscow [30] in the 1960s) which reported optimization of the growth rates. The details of how the two groups in turns co-operated and exchanged their knowledge is succinctly summarised in a review by Angus *et al.* [28]. With a growing understanding of the diamond growth environment and the multi-faceted role played by H_2, the growth of diamond on non-diamond substrates was achieved as well [31].

The modern era in the growth of synthetic diamond can be said to have started in the early 1980s, when the NIRIM group from Japan reported successful growth of diamond on various substrates from a mixture of CH_4 diluted in H_2 [32]. In a series of remarkable papers, the NIRIM group reported the low pressure synthesis of diamond using a hot filament (HF), followed by microwave (MW) [33] and radiofrequency (RF) discharge plasmas [34]. These reports were accompanied with papers detailing the extensive characterisation of the samples obtained [35]. Furthermore, the NIRIM laboratories were open to visitors; as a result of which a large number of Japanese companies, universities and research institutes entered the field, as well as a few American universities which led to the dissemination of these results in the United States as well as Europe. This in turn caused an explosion of CVD research with reports published about diamond deposition using excitation by electrons [36], DC plasmas [37] and the popular oxyacetylene torch method [38].

Since then, there has been considerable progress towards understanding the chemical process and kinetics involved in the growth of CVD diamond, including the effects of process parameters and the role of H_2 in the growth, in detail, like never before. Some important milestones along the way were the introduction of the instructive C-H-O triangular elemental diagram, pin-pointing the favourable conditions for faster diamond growth with O_2 addition in the plasma [39], gas phase and surface mechanism studies and their relationship with concentrations of atomic H and hydrocarbon radicals [40-42], modelling studies of diamond CVD [43, 44], and spectroscopic studies of the diamond-growing environment [45-52]. Using CVD, homo-epitaxial diamond films can now be deposited on diamond substrates, usually obtained by the HPHT process, to obtain single crystal diamond (SCD) films. Hetero-epitaxial diamond films can also be deposited on non-diamond substrates; although the properties of the substrate affect the properties of the diamond grown, the deposition process of CVD remains essentially the same, requiring just an extra seeding step to enrich the substrate with diamond nanoparticles that start growing during the CVD process until they coalesce and form a closed diamond film. The 90s also saw optimization of such pre-treatment (PT) methods for more uniform, high quality films, even at temperatures as low as 400 K, using enhanced nucleation methods and substrate heating [53-59], as well as growth of PCD films with different grain sizes [60-62].

With the possibility of doping diamond films during the CVD process, one could have semiconducting diamond [63, 64]. The interest in diamond for electronics thus moved in conjunction with the growth of diamond CVD research; with increasing knowledge of growth mechanisms and improving film qualities

[65], diamond films could be better tailored for electronics applications [66, 67]. By the turn of the 21st century, the CVD of diamond was a well-established field not only of research, but in the industry as well, primarily for the development of cutting tools. In fact, because of its superior material properties, diamond lends itself to usage in a versatile number of ways and although the use of natural diamond for industrial applications is limited by their relative scarcity and the prohibitive price of obtaining large enough pieces for some applications, the relative ease of fabricating CVD synthetic diamond has resulted in their usage for various applications, in some cases replacing other materials.

Although natural and HPHT diamond continue to find use in a number of applications, these are limited by size because the cost of SCD increases exponentially with size. CVD deposition on the other hand allows the production of continuous diamond films on surfaces other than just diamond. The technology is significantly more cost effective and flexible because diamond can also be deposited on a number of different shaped and contoured surfaces from the gas phase. There are several companies in the industry now that produce diamonds of electronic wafer quality. Because of its availability in optical, thermal and electrical grade wafers (*Figure 2-3*), synthetic diamond has been since used in innovative ways to demonstrate a variety of electronic device applications, such as diodes and power transistors, electrochemical sensors, micro and nano-scale devices, and because of the biocompatible nature of diamond [68], even biomedical devices. These applications are discussed in further detail in the latter part of this chapter. 4 inch PCD wafers can be purchased from vendors around the world and they come as a cheaper alternative without necessarily compromising on performance [69-72]. Furthermore, post growth techniques can be used to enhance the certain properties of the film. For example, high temperature post growth treatments have been successfully carried out at low pressure and a consequent improvement in optical properties has been produced by these annealing techniques. Significant changes in UV– visible and IR absorption spectra are correlated with changes in extended defects and diamond vacancy centers [73].

Hence, one can see how in the last 60 years, the deposition of diamond under conditions where it is meta-stable, that is low pressure CVD synthesis, went from a technology that was met with scorn, and in some circumstances publicly discredited [28], to one that now has a significant industrial applications and still throws up considerable research and applications. CVD diamond research has peculiarly opened more doors rather than following an established development path.

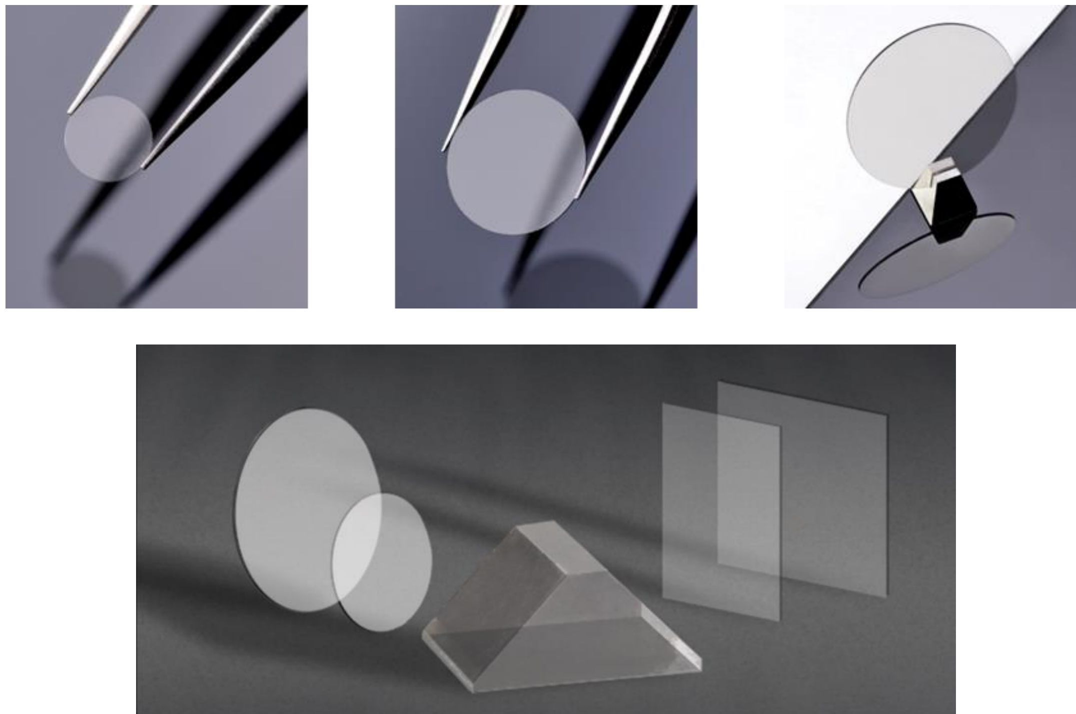

Figure 2-3 (Top) Commercially available CVD, PCD wafers of diameters 5 mm, 8 mm and 25 mm (Diamond Materials ®) (Bottom) Commercially available single crystal, electronic grade diamond (Applied Diamond, Inc.)

2.4 Optical, mechanical and thermal properties of diamond

Diamonds were first classified, based primarily on their optical properties, into several categories, characteristics due in part to the particular impurity present in the diamond lattice. Impurities give rise to a colour when compared to the optically transparent natural diamond- type (I)- that contain 0.025 to 0.25 % N, and type (II) diamonds that contain less than 0.001 % N. Furthermore, the sub- type, type (l)a is classified as containing N impurities in the form of different aggregations (platelets), and type (l)b in which the N occurs in a dispersed para-magnetic. The type (II), "N-less" category is also sub-divided into type (ll)a, which are colorless and essentially free of impurities [9]; and type (ll)b which are blue and semiconducting, and contain B [74]. Type (II)b diamonds occur naturally in nature and their spectral energy distribution was first noted, in 1952, to show three maxima at 4665, 5310 and 5720 Å, peaks that were not present in most other spectra of natural diamond [75]. These diamonds also show conductivity, as opposed to the insulating crystals of other types of diamond. There are also diamonds in which one part of the diamond possesses the properties of a type (I) diamond, and the other part has the properties of a type (II) diamond [4].

All of the exceptional material properties of diamond are due to the structure of its lattice [76, 77]- the combination of light C-atoms held by high strength covalent bonds. These strong covalent bonds imply that a large amount of energy is required to remove a C atom from the diamond lattice, making diamond a robust and abrasion resistant material, and the hardest known material on any scale [78]. It also means that a diamond can only be scratched by another diamond. The rigidity of the lattice also implies that though it is a hard material, it is also brittle, when struck at the right crystallographic planes. Cleavage occurs mainly on the [1 1 1] planes, but other planes have been reported, for example the [1 1 0] and [2 2 1] [79]. Its properties of elastic modulus, robustness, low coefficient of thermal expansion and resistance to both radiation damage as well as chemical corrosion are also due to these strong covalent bonds. On the other hand, the strongly bonded covalent lattice gives a negligible probability of thermal excitation of electrons from the valence band to the conduction band at room temperature; unlike graphite in which

the dislocated electron makes it electrically conducting. However, as a consequence of the high rigidity of the bonds of the C-atoms in its lattice and the fact that C-atoms are "light", they can vibrate at extremely high frequencies (40×10^{12} Hz for diamond compared to 16×10^{12} Hz for Si). This makes diamond an excellent conductor of thermal energy (through crystal vibrations, "phonons"): its room temperature thermal conductivity (1000-3500 W/m/K [79]) is 4 times that of Cu and is the best thermal conductor known to us. It also gives diamond the highest acoustic wave velocity for both longitudinal and transverse waves [80] making it an extremely attractive candidate for SAW devices.

The properties of HPHT diamond and SCD both compare quite favourably with natural diamond. In fact, natural diamonds show a higher density of defects than HPHT single crystals of diamond [69, 70, 76]. However, the area of most available HPHT substrates is limited to a few mm^2, an obvious limitation for electronics applications. Yet, niche applications continue to be served very well by this kind of diamond [81]. 1 inch HPHT diamond substrates recently became available but they are still prohibitively expensive [71, 82].

As both HPHT and SCD still face the problem of size limitation, hetero-epitaxial diamond films can be deposited on non-diamond substrates using CVD, thus overcoming the problem of small area HPHT substrates. Depending on the size of the diamond grains, the hetero-epitaxial diamond films are classified as ultra-nano-crystalline (UNCD) with grain sizes below 10 nm, nano-crystalline (NCD) with grain sizes between 10-100 nm, or micro-crystalline (MCD) with grain size between 1-5 µm and PCD if a mixture of grain sizes is present. In the case of PCD, although some properties such as the Young's modulus and hardness maybe compromised, others such as acoustic velocity and coefficient of thermal expansion remain uncompromised. A summary of the optical, mechanical and thermal properties of the different varieties of diamond and the corresponding values for other well-known semiconductors for comparison, is presented in *Table 2-*.

Different grades of both SCD and PCD, with specific properties, appropriate for use in the particular applications are also available for sale and these are summarized in *Table 2-1*.

Property	Natural diamond	Single crystal HPHT diamond	Single crystal CVD diamond	Polycrystalline CVD diamond	Si	Ge	SiC	GaN
Optical properties								
Refractive index (at 591 nm)	2.417 [79]	2.383-2.417 [83]	2.385-2.417 [83]	2.417-1.9 (depending on H content) [84]	3.5 [85]	4 [85]	2.56 [86]	2.29 [87]
Mechanical properties								
Young's modulus (GPa)	1141 [79]	1140 [88]	1050 [82]	900-1100 [70]	185 [89]	103 [89]	748 [90]	181 [91]
Hardness (GPa)	64-67 [92]	125 [76]	90 [82]	75 [92]	13 [93]	10 [93]	24 [90]	16.67 [91]
Density (g/cm^3)	3.515 [79]	3.515 [88]	3.515 [82]	3.515 [70]	2.329 [94]	5.323 [95]	3.211 [96]	6.15 [97]
Acoustic velocity (V_L) (km/s)	17.52 [80]	18.04 [98]	18.22 [99]	18.18 [100]	9.36 [94]	4.87 [95]	12.5 [90]	6.9 [91]
Thermal properties								
Thermal conductivity (W/m/K)	1000-2500 [79]	2500 [101]	2000-3500 [72, 79, 82]	1800-1900 [70, 72]	130 [102]	58 [102]	370 [97]	130 [103]
Coefficient of expansion ($\times 10^{-6} K^{-1}$)	0.8 [79]	1 [104]	0.8 [105]	1 [70]	2.6 [102]	5.9 [102]	4.06 [106]	3.17 [107]

Table 2-2 A summary of the optical, mechanical and thermal properties of the different varieties of diamond and other common semiconductors

Single crystal CVD diamond	Polycrystalline CVD diamond
Single crystal-Engineered replacement for type (II)a diamond	Optical grade-Far infra-red laser applications
Optical grade-low absorption, birefringence diamond	Electronic grade-ultrahigh purity for power electronics applications
Detector grade-ultrahigh purity for quantum optics & electronics, radiation detectors applications	Thermal grade- heat spreading applications
	Mechanical grade- high strength for mechanical applications like precision machining
	Electro-chemical grade- boron doped, for electrodes

Table 2-1 Available grades of CVD diamond, with a brief description of its identifying property and its application

2.5 Electronic properties of diamond

In comparison with more mature semiconductor materials such as Si or GaAs, the understanding of several of the electronic properties of diamond is comparatively poor, although there has been considerable experimental and theoretical work- this gap in the knowledge can be attributed to the difficulty in growing high-quality single crystals, the wide energy gap and difficulties in achieving effective n or p doping [108]. Of particular difficulty are ascertaining conduction band masses experimentally because of the low activation of n-type dopants in diamond. This section summarizes the current state of the art in the knowledge of the electrical properties of undoped and doped diamond.

2.5.1 Band structure

The earliest band structure calculations of diamond were performed in 1935; a good review of the calculation methods from then until 1979 can be found in [109]. The state-of-the-art approach for calculating the electronic band structure is by incorporating the local density approximation (LDA) of the density functional theory (DFT) into the augmented plane wave method (APW) and the empirical pseudopotential method (EPM), details of which are beyond the scope of this thesis and maybe be found elsewhere [110]. Numerous results obtained from theoretical calculations can and have been verified experimentally [111].

Diamond has four valence bands- analysis of the nature of the wave functions to identify the atomic-like character of these states shows that the lower valence states are primarily s-like, and the upper valence states are p-like, with hybridization in the middle range reflecting the sp^3 bonding, with a total width (absolute energy difference between top and bottom of the valence band) of diamond obtained experimentally being 21.00 $\pm$1 eV [112]. It has been noted that the conduction band minimum is located at different ***k*** points from where the maximum of valence band is situated, in the Brillouin zone. Therefore, the band gap of diamond is indirect- this has been established in theory and experiment using optical constant measurements [112, 113]. The indirect energy gap at 295 K and its rate of change with temperature between 135 and 295 K, obtained from absorption data, are 5.470 ± 0.005 eV and -5.4 ± 0.5 x 10^{-5} eV /K [112, 114], making diamond a WBG material. In nominally undoped diamond thin films, the Fermi level lies about 0.75-0.85 eV above the valence band [115]. The WBG of diamond is a direct consequence of the strong covalent bonds between the C atoms (which itself is due to the strong electronic interaction of the electrons close to the atomic nucleus due to the small size of the C atom). This large band gap in addition to diamond's low relative permittivity (5.68) ensures a high voltage withstand thanks to a high breakdown electric field of 10 MV/cm (breakdown voltage measurements have been performed for both lateral and vertical Schottky barrier diodes (SBDs)) [116, 117] .

2.5.2 Carrier characteristics of intrinsic diamond

No truly intrinsic diamond with conductivity activation energies in the range of 2.5 eV expected for the large band gap of 5.470 ± 0.005 eV of diamond is available. At room temperature such activation energy causes a carrier density much less than one electron per 10^{15} cm^3 diamond [118]. In real diamond defects, extrinsic contaminants, grain boundary or surface effects govern the electronic properties and generate activation energies smaller than 2.5 eV. The mobilities of these charge carriers cannot be measured using the Hall effect; as a consequence, the time-of-flight (ToF) method, also often referred to as the transient current technique (TCT), is thus utilized. In this technique, electron-hole pairs are created by α- and β-particles, pulsed electron beams, pulsed x-rays, or a pulsed UV laser; the motion of the created free charge carriers in an applied electric field induces a current which is then measured. By this technique, the mobilities and drift velocities of carriers in SCD have been measured. The electronic properties such as high electron (4500 $cm^2V^{-1}s^{-1}$) and hole mobilities (3800 $cm^2V^{-1}s^{-1}$) and high carrier saturation drift velocity (1.5 x 10^7 cms^{-1}), all values at room temperature for SCD are now well established [119]. The measured drift velocities show very little spread across the different SCD diamond samples studied, indicating that the quality of the SCD diamond layers has come to stage where it is possible to talk not only about the properties of the specific sample, but also about the material's electronic properties [120]. They are also comparable to theoretical values [121, 122]. The saturation velocity for fields greater than 30 kV/cm is 1.5 x 10^7 cm/s for electrons, and 1.05 x 10^7 cm/s for holes [121]. The mobility for both electrons and holes follows the typical $T^{3/2}$ dependence for temperatures below 280 K, which is an indication that acoustic phonon scattering is the limiting mechanism in this temperature range [120]. Because diamond is a non-polar semiconductor, piezoelectric scattering and polar optical phonon scattering are negligible; other scattering sources that may contribute are neutral impurities and dislocations, both of which commonly exist in diamond [111, 123]. In the temperature range of 70 to 500 K, for low electric fields, the measured mobilities of holes and electrons show good agreement with theoretical values [122].
Dislocations are common defects in both natural and PCD, and they contribute strongly in determining carrier mobilities and lifetimes [111]. Carrier mobilities in nominally undoped PCD diamond have been characterized by transient photoconductivity experiments-in these experiments, both electrons and holes contribute to the transient photocurrent, so that the result is a combined mobility. With increasing film quality the transport properties of CVD diamond approaches those of SCD and natural diamond; at low carrier density, the combined mobility is about 4000 $cm^2V^{-1}s^{-1}$, comparable to SCD [116]. Furthermore, with increasing grain size there is improvement in electrical behaviour correlating also to higher growth temperatures, and improved purity of the diamond films [124, 125].

2.5.3 Carrier characteristics of doped diamond

The ideal doping is supposed to result in a substitutional solid solution in which dopant atoms are randomly distributed in the diamond structure and no other defects are electrically active; such type of doping will not influence the energetic characteristics of the host lattice. Given the crystal structure of diamond and the bond length of 1.54 Å, to fill the empty spaces existing in the diamond lattice, eight extra spheres with diameter of 1.54 Å are required, indicating that the diamond structure makes several possible positions available for the impurity atoms. Due to the small tetra-hedral radius of C (0.77 Å) almost all impurity atoms (with the notable exception of B) are considerably larger and will deform the lattice [5]. Collins *et al.* made the first clear demonstration of p-type behaviour in some rare electricity-conducting diamond crystals in 1971 [126]; it has since been shown that B is in fact the only p -type dopant that can be incorporated into the diamond structure with high reproducibility, and techniques of doping with B using CVD have been developed [127, 128].
Despite the fact that N atoms are present in natural diamond, an efficient n-type doping is difficult to bring about using synthetic techniques. Evaluation of the formation energy of an n-type impurity (like P,

Li and Na) on the basis of bulk cohesive energy of diamond and the impurity shows that solubility is low for these dopants, indicating the difficulty of the n-type doping of diamond [5]. N for example, does not form a shallow donor level in diamond as might be expected from the analogy with Si [5]. The N energy level is 1.7 eV below the bottom of the conduction band; it is electrically inactive but acts as a recombination centre in radiative transitions [129]. An important breakthrough was the success of P-doped n-type diamond by Koizumi *et al.* who experimentally demonstrated the growth of P-doped n-type diamond on (111)-oriented diamond substrates by PECVD using a mixture of PH_3 /CH_4 as a dopant source; by carefully controlling the growth conditions to improve crystallinity and avoid undesirable impurities [130-132]. There have been, since then, improvements on n-type doping for diamond films [133-135], however, the problem remains that the resistance of P-doped films is usually too high and mobilities of carriers too low for electronic applications [5].

Doping diamond with B creates states in the fundamental band gap; substitutional B in diamond forms an acceptor ground level with energy 0.37 eV above the valence band [126, 136, 137]. A considerable density of states exist, starting at or close to the valence band edge and extending 1-2 eV into the band gap, consistent with the relatively high, and process-dependent, extrinsic p-type electrical conductivity [115, 138]. This, however, is difficult to reconcile with the demonstrated sensitivity of the electrical conductivity of diamond thin films to doping with B, which produces an acceptor level at 0.37 eV, at levels as low as tens of ppm, suggesting that it is possible that as one approaches the valence band edge, the density of states distribution goes through a maximum followed by a minimum in the vicinity of the acceptor energy [115]. It is also known that as the impurity concentration increases, the probability of B atoms occupying additional positions also greatly increases i.e., their nearest environment will consist not only of C atoms, but form complexes such as B-B, B-C-B, B-C-C-B, B-N-B, B-N-C-B, and so on; such non-trivial states form shallow acceptor levels with an energy lower than 0.37 eV. This gives rise to one of the most interesting properties of B-doped diamond (BDD)- the gradual evolution from a semiconductor to a metal when the B doping level is increased above 5×10^{20} cm^{-3}[139-141]. The ionization energy of B which is around 0.37 eV at low doping levels tends toward zero as the B content increases (approaching 4×10^{21} cm^{3} [142]), causing a metal-insulator transition (MIT). The fraction of the B atoms that occupy these non-trivial states depends on both statistical laws and conditions of sample growth [143, 144]. One can conclude that inclusion of B atoms can support splitting of diamond energy band as well as creation of impurity states near/at Fermi level and hence enhance electron/ion conductivities of BDD thin films; B atoms either substitute C atoms and/or assemble at grain boundaries (interstitial sites) inducing impurity levels close to the top of the valence band.

The total conductivity of the BDD consists of the valence-band conductivity and the hopping conductivity. At low temperatures, conductivity is due to both the thermal activation from these shallow levels and the hopping mechanism. As the energy of the levels of the additional states is close to that of the level of an excited B state in the conventional position, hopping conductivity occurs along the additional B states assisted by the excited B states in the conventional position, leading to the high hopping conductivity [144, 145]. At high temperatures, the activation energy of carriers has been found to decrease with increasing doping concentration; increasing doping concentration increases the acceptor band width which ultimately reduces the activation energy of acceptors resulting in a transition in the conduction mechanism from localized hopping to band conduction at higher temperature, as the amount of doping is increased [145, 146]. The temperature at which this transition occurs may vary from 252 K to 408 K, varying inversely with the concentration of B in the BDD. The difference in activation energy of the carriers is reflected in conductivity (σ) vs 1000/T plot, indicating two different conduction mechanisms responsible for the semiconducting behaviour of the film.

The B level in PCD films, identified by thermo-luminescence, is manifested by an intense glow peak at 226 K has an activation energy of about 0.37 eV. At 77 K, another emission band has been observed, with an activation energy of 2.22 eV. These observations seem to be in agreement with the fact that the

recombination mechanisms involve two different recombination centres and, therefore, phosphorescence at 77 K and the main peak at 226 K are of different natures, i.e. the TL peak at 226 K is due to B while the phosphorescence is probably due to a shallow donor level [147, 148].
There seems to be an upper limit to the hole mobility (μ_{h}) in BDD [118]- at hole densities larger than 10^{15} cm^{-3}, ionized impurity scattering at B acceptors becomes dominant, causing a decrease in mobility that follows a $\mu_{\mathrm{h}} = \frac{1}{p}$ law, where *p* is the density of holes that is proportional to the density of ionized acceptors (N_a). In B-doped PCD, on the other hand, the mobilities are 10-50 times smaller, varying between 3 and 40 $cm^2V^{-1}s^{-1}$at 300 K. [118]. These significantly lower mobilities are generated by grain boundaries, common to both doped and undoped PCD films- where the effective mobility can be calculated as demonstrated by Orton and Powell (1980)[149]

$$\mu_{\mathrm{eff}} = \mu_{\mathrm{B}} \exp\left[-\frac{E_{\mathrm{GB}}}{\mathrm{k_B}T}\right] \tag{2-1}$$

where μ_{B} is the mobility in the grains, and E_{GB} the energy barrier at grain boundaries.
Taking into account typical bulk mobilities of SCD in the grains (μ_{B} = 200-1800 $cm^2V^{-1}s^{-1}$) and the effective mobility in PCD (μ_{eff}= 40-165 $cm^2V^{-1}s^{-1}$), this results in grain boundary energy barriers E_{GB} of 5-100 meV. On analyzing the mechanism of electrical conduction in PCD films, the role of the grain boundaries is still unclear. The grain boundaries are a source of disordered graphitic material, along which variable range hopping occurs. When PCD films are annealed at 943 K, however, the conductivity decreases dramatically suggesting that grain boundaries are paths for current conduction that upon annealing are reduced [150, 151]. A gradient in the electrical properties of CVD diamond films has also been observed that exists through the thickness of the film [152], this gradient has also been reported in the thermal properties [153] and in luminescence [154]. It is known that the average grain size increases with film thickness, thereby, correlating the grain size with the electrical properties; this correlation does not, however, identify the role of the grain boundaries.
In addition to bulk conductivity, a high p-type surface conductivity has been observed on as grown H-terminated CVD diamond surfaces [155-158]. Hall effect measurements on H-terminated B-doped CVD diamond films, show that the number of carriers (holes) per unit area is four to five orders of magnitude larger than that of a comparable oxidized B-doped film at room temperature and is nearly constant in the temperature range between 120 and 400 K, while that of the oxidized B-doped film shows a strong temperature dependence with an activation energy 0.37 eV [159]; this suggests the existence of shallow acceptors originating from H incorporated in the subsurface region of as-deposited hydrogenated diamond films, introducing levels that are expected to be responsible for the high conductivity and resulting in conductivity in the top 10-20 nm of the surface [158, 159], sometimes referred to as a 2D hole gas [160]. CL spectra and secondary ion mass spectroscopy analysis, in fact, suggest the existence of shallow acceptors originating from H incorporated in the sub-surface region of as-deposited hydrogenated diamond films, expected to be responsible for the high conductivity [159]. A work function of 4.9 eV of H-terminated diamond is obtained, and a Fermi level 0.7 eV below the valence band minimum at the H-terminated surface and indicating p-type conductivity [156, 157, 159]. Illumination of the sample results in a shift of the surface Fermi level by as much as 0.2 eV, a phenomenon ascribed to photo-voltage [156]. When diamond is O_2 terminated, or given an acid treatment post CVD growth, this is not observed and the surface has insulating characteristics [157]. This surface conductive layer is ideal for the channel of FETs because it has a high sheet carrier concentration of $>10^{12}$ cm^{-2}, a shallow depth of <10 nm, and a low activation energy [161, 162].

2.5.4 Recombination/generation mechanisms

Since diamond is an indirect band gap material, band to band recombination is highly unlikely, until free carrier excitation density reaches 10^{19} cm^{-3} [111]. The mechanism for recombination prevalent in most semiconductors, especially ones with large concentrations of deep traps (trap levels > $3k_BT$) is of the

Shockley-Reed-Hall (SRH) type, in which the deep donor level is involved in recombination [111]. This type of recombination has been shown, at least for natural type IIa diamond, to be the dominant mechanism with which diamond relaxes to thermal equilibrium at excitation densities of Δn (or Δp) < 10^{18} cm^{-3}.
For B-doped SCD, two distinct free carrier decay mechanisms, a fast and a slow mechanism were observed [163, 164]- the fast component is believed to be associated with the coupling of valence and acceptor states whereas the slow component is due to the coupling of donor and acceptor state. The hole capture cross section for an ionized B acceptor has been estimated to be approximately $4x10^{-13}$ cm^{-2} , with carrier decay times between 120-300 ps, at room temperature [165].
Using the TCT, the carrier decay times have also been measured for PCD films; CVD diamond shows a low excitation free carrier lifetime (limited by point defects, and approaching 800 ns). Also of significance amongst results from TCT is the observation that the decay of transient currents is not single-component but multi-component- this implies that the decay time of a transient current does not result in a unique carrier lifetime. In addition, as the operating temperature is increased to well above room temperature, the decay time of the photoconductive current is greatly reduced. This can be understood from the point of view that the trapped carriers can be thermally emitted to either the valence or the conduction band thereby increasing the probability for recombination at some later time [111, 147].

2.5.5 Diamond vs other WBGs

The full potential of diamond as an electronic material can be understood by comparing the properties of different WBG materials. Semiconductors with wide energy band gaps are known for some time to be superior semiconducting materials for high-temperature and high-speed electronics [166]; in addition to the WBG, they exhibit high values of properties such as breakdown field, saturation velocities and mobilities of carriers, as well as thermal conductivity, as a result of which devices that function at higher temperatures, voltages, powers and frequency can be fabricated with them. *Figure 2-4* presents as a radar graph a comparison of these properties between diamond and other common WBG materials- SiC and GaN.

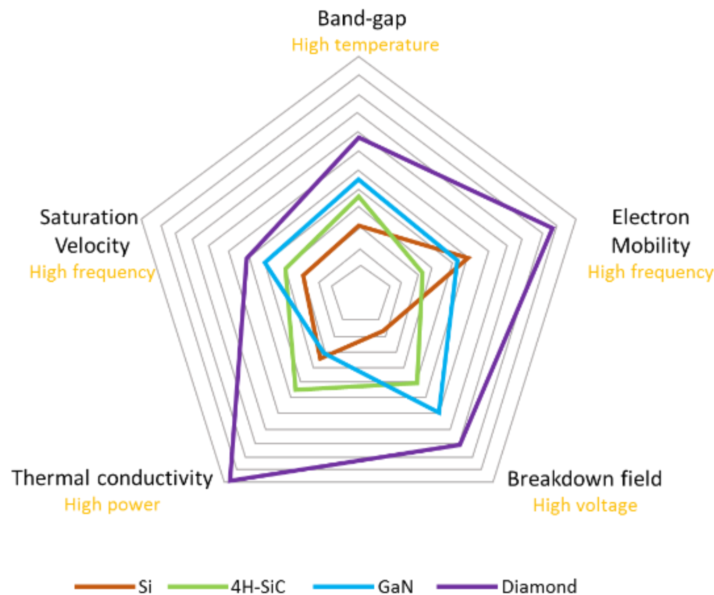

Figure 2-4 Radar graph of material properties of diamond, accompanied by the implications that they have on the devices characteristics designed out of them

In order to evaluate and compare the merits of semiconductor materials, certain figures of merit (FOM) are useful- these FOMs are derived from analyses of the impact of material parameters on the performance of semiconductor devices. The Johnson's FOM (JFOM) defines the power-frequency product for a low-voltage transistor, in terms of the critical electric field of breakdown, E_c and the saturated drift velocity, v_s [167], it illustrates that for a given device cut-off frequency, there is a trade-off in the maximum allowable voltage in a charge controlled device such as a transistor.
The Keyes' FOM (KFOM) provides a thermal limitation to the switching behaviour of transistors used in ICs and is dependent on the dielectric constant, ϵ and the thermal conductivity, σ_c [168]. In general, the delay through a semiconductor device is related to the thickness of the device and an *RC* time constant, which leads to the general conclusion that the smaller the device, the faster it can operate. However, one must take into account that there is a lower limit on the size set by the relatively size-independent amount of power that is generated and must be conducted away from the device as heat. As the device size decreases, this thermal resistance increases causing undesirable device temperature increase. The KFOM relates the thermal conductivity value of a material with the properties that govern the minimum thickness required to obtain a certain speed of operation.
Finally the Baliga FOM (BFOM) defines material parameters to minimize the conduction losses in power FET's in terms of the band gap, E_G and mobility, μ [169], and is based on the assumption that ohmic losses are the dominant source of power dissipation, which holds for low frequency applications.
The FOMs are usually normalized to the value for Si for ease of comparison and these values are presented in *Table 2-2*- a perusal of JFOMs and KFOMs coupled with the present desire for devices for GHz logic, microwave communications, high temperature microprocessors and radiation hard applications, makes obvious the reason for the present interest in the growth and characterization of and device development in diamond, SiC and GaN. Furthermore, comparing the values for diamond with other WBG materials, it is clear that diamond possesses a unique combination of desirable properties which make it attractive for a variety of electronic applications. The JFOM value for diamond demarcates, in fact, one of the main fields of application for diamond devices, power electronics at high frequencies tolerating high temperatures, heat extraction being one of the key elements for reliable power operation. The primary advantages of diamond over other materials are in fact, more prominent at higher operating temperatures, possibly higher than 473 K [170-172]. In addition, CVD diamond has been shown to have higher values of maximum electric field, meaning the diamond diodes can be made significantly thinner (*Figure 2-5*) than their respective state of the art counterparts [167, 173, 174]. A diagrammatic representation of the thickness of semiconductor material required to block 10 kV helps to compare the advantage diamond provides in terms of material content and device sizes possible [174]. Diamond diodes are also meant to operate at much higher frequencies because of the high-saturation velocity of the carriers (*Table 2-2* and *Figure 2-6*) and, at least in theory, exhibit much lower leakage currents during blocking mode because of the very low intrinsic carrier concentration at both room and high temperatures [170, 175-177]. However, defects arising from the poor material quality and the absence of large area diamond substrates have lowered the actual performance of diamond diodes by causing low forward current capability, relatively high leakage current and poor reverse blocking voltage [178-180]. The experimentally obtained on-resistance for diamond is lower than the unipolar limit for Si and is, at the moment, comparable to that of SiC with promising usage in power devices; the values however are still much higher than the expected characteristics for diamond. This is thought to be due to the as-yet un-optimized doping and thickness of drift layers and defect densities and consequent high leakage currents through defects [181, 182].

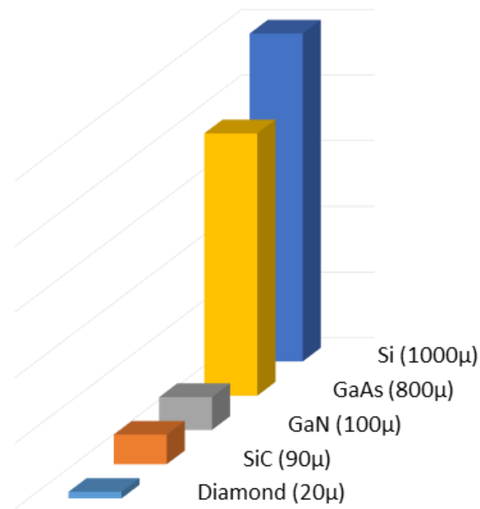

Figure 2-5 Diagrammatic representation of thickness of semiconductor material required to block 10kV

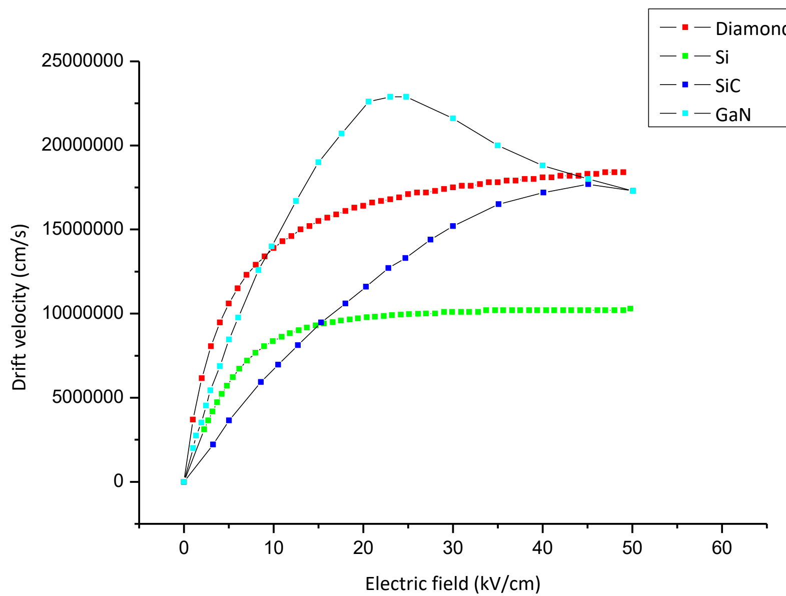

Figure 2-6 A comparison of the charrier characteristics, i.e., the variation of the drift velocity vs. electric field of diamond with other WBG materials

Table 2-2 presents a summary of the electronic properties of diamond discussed in the preceeding sections and other WBG materials for comparison.

Electrical property (at 300 K)	Natural diamond	Single crystal HPHT diamond	Single crystal CVD diamond	Polycrystalline CVD diamond	Si	Ge	SiC (4H-)	GaN
Dielectric constant	5.70±0.05 [79]	5.7 [101]	5.7 [82]	5.6 [70]	11.7 [85]	16.2 [183]	9.66 [184]	8.9 [185]
Band gap (eV)	5.47-5.5 [79, 186]	5.48 [101]	5.48 [82]	5.48 [70]	1.12 [85]	0.66 [187]	3.2 [188]	3.3 [185]
Hole mobility ($cm^2V^{-1}s^{-1}$)	1800 [70]	2000 [189]	3800 [119]	1000-1600 [70, 72]	450 [190]	1900 [191]	115 [188]	170 [192]
Electron mobility ($cm^2V^{-1}s^{-1}$)	2200 [70]	1814 [193]	4500 [119]	480-1800 [70, 72]	1400 [194]	3900 [195]	800 [70]	1000 [192]
Hole saturation velocity ($\times 10^7 cm\ s^{-1}$)	1.1 [122]		1.05 [121]		1 (near saturation) [196]			
Electron saturation velocity ($\times 10^7 cm\ s^{-1}$)	1.5 [121]	2.3 [197]	1.5 [121]		2.4 [196]	0.6 [188]	0.8 [198]	1.5 [199]
Breakdown field ($\times 10^6\ Vcm^{-1}$)	10 [200]	10 [201]	10 [202]	0.7-5 [203-205]	0.3 [206]	0.1 [207]	3 [208]	
BFOM (normalized to Si) $= \epsilon.\mu.E_G^3$	6751 [169]	200-18000 [180]	51 [209]		1.0		1500 [210]	1300 [211]
JFOM (normalized to Si) $= \left(\frac{E_c v_s}{2\pi}\right)^2$	2601 [166]		8200 [78]		1.0	0.1 [166]	410 [78]	281.6 [212]
KFOM (normalized to Si) $= \sigma_c(\frac{c.v_s}{4\pi\epsilon})^{1/2}$	32 [166]				1.0	0.27 [166]	5.8 [212]	1.76 [212]

Table 2-2 The electronic properties of diamond and other WBG materials

2.6 Applications of diamond

The applications of diamond in the industry are versatile- it can and has been used for its mechanical and optical properties for respective applications. CVD diamond is also finding increasing applications in nano- and micro- electromechanical (NEMs and MEMs) devices as well as SAW devices. In electronics, it can and has been used either for thermal management, electron emission or as a WBG semiconductor. The various categories of the existing applications of diamond are discussed in detail in the following sub-sections.

2.6.1 Mechanical applications

The mechanical applications of diamond stem from its extraordinary hardness, making it the obvious choice from time immemorial, in fact, in cutting tools [2]. The use of HPHT diamond to coat cutting tools has been around for a number of years. However, although SCD is extremely hard and wear-resistant, it is also prone to cleave easily [76]. In these cases, PCD CVD diamond has been used to overcome problems associated with adhesion of diamond coating onto tools [213] and PCD coated cutting tools have become an industry product for some time now [214, 215]. Diamond coated tool bits are used to machine stone, timber, reinforced plastics, Al and other non-ferrous metals; they cannot however be used to machine metals and alloys that are Fe, Ni or Ti based because C is soluble in these materials at the high contact pressures and temperatures associated with the machining [216]. CVD diamond is also used to coat length gauge tips and other wear resistant components e.g. for textile machines, inserts for dresser tools [217]. Besides cutting tools, there are companies that fabricate medical scalpels coated with diamond, that are used in ophthalmic operations requiring extremely sharp high-precision instruments [218].

When terminated with H, as is the case in typical CVD deposition of diamond, the surface of diamond has an extremely low coefficient of friction combined with its stiffness and hardness properties, it is ideal for coating oil-less bearings [70]. Among other applications of CVD diamond in the mechanical industry- CVD diamond has been used to coat moulds typically employed in the injection moulding systems with some success [219].

The high stiffness of diamond has led to its usage as tweeter domes for loudspeakers. The ideal tweeter dome for a loudspeaker should perform as a perfect piston, without deformation, at all frequencies. In practice, the frequency up to which a tweeter shows ideal (or near ideal) behaviour is called the break-up frequency, a common technique of increasing this break-up frequency is obtained by using modified geometries, such as reducing the diameter. Such modifications usually also imply a compromise in the sound pressure level, an undesirable effect in high end audio systems. Because of the high value of Young's modulus of diamond, practical diamond tweeters have been used to obtain with a break-up frequency of over 70 kHz compared to 30 kHz for a similar high quality Al tweeter [78]. In commercial units, diamond tweeters are already finding usage, with the most superior frequency range available on the market [220].

2.6.2 Optical applications

Diamond has broadband optical transparency, and with technological improvements in CVD technology allowing for fabrication of large diameter optical-grade diamond, it has found industrial usage as optical windows; its extreme thermal properties and hardness only adding to its utility in usage as high power laser or detector window applications. Especially in the infra-red (IR) region, diamond's resistance to thermal shock and its transparency has encouraged CVD diamond production for use as a window material in high power IR lasers. The high thermal conductivity prevents local heating of the window, which is a common factor in material failure. Another proposed use of diamond windows is as an IR airborne sensor detector window for use on missiles, where working conditions might typically involve harsh environments such as hail and sandstorms, replacing materials such as such as ZeS [221]. Diamond is also transparent to X-rays, finding applications as X-ray windows in detectors and tubes. Diamond may also be used in future lithography techniques for similar reasons [222].

Optical fibre sensors with an inscribed fibre Bragg grating (FBG) are able to decode small variations of strain; temperature; pressure; loading; bending; or even refractive index, by means of a shift in the reflected wavelength. CVD coating of such fibres with diamond exploits it properties of high thermal conductivity, hardness and resistance to hazard environments; furthermore, its well-known biocompatibility makes it suitable as a coating material for biological sensors [223, 224].

Diamond finds usage as a photodetector as well; with a large band gap, it is effectively transparent to visible light but can be used to detect deep ultraviolet (UV) light. This is an advantage compared to conventional photodetectors that are generally sensitive to both visible and UV light because of the band gap of their detector material. Being an extremely robust material, diamond is an excellent candidate for use in hostile environments, such as in environmental monitoring or military applications.

2.6.3 Thermal management

As high-power electronic and optoelectronic devices continue to become smaller, the efficient removal of large quantities of generated heat is of prime importance, contributing toward efficient device performance and slower degradation. With the availability of high quality SCD CVD substrates, this application potential looks promising. By utilizing diamonds' unequalled thermal conductivity, freestanding thick CVD films can also be used as a medium to 'spread' the heat from the device to the cooling system, particularly for multichip modules (MCMs), laser diode arrays, power modules, etc. Its low heat capacity relative to metals such Al or Cu makes it preferable for heat spreading applications rather than for dissipating the heat flux itself (as a heat sink). CVD diamond heat spreaders are

commercially available from several vendors around the world [71, 82]. The field of thermal management of electronic devices has seen several patents using diamond [225-228]. It has seen innovative usage such as printable, flexible, and stretchable forms of UNCD with applications in thermal management of plastic electronic systems [229, 230] and diamond nano-wires for nano-devices [231], as well as innovative designs such as Cu "micro-pillars" on CVD diamond to obtain a thermal power dissipation of more than 600 W/cm^2 [232]. Diamond being an electrical insulator provides an important advantage over other high thermal conductivity materials in high-density electronic packaging by satisfying the requirement for an electrically insulating layer between any metallization and active cooling channels. The optimization of the PCD deposition process has resulted in high quality films with a very good grain (where diamond properties prevail, such as heat conduction and electrical insulation) to grain boundary ratio (where non-diamond properties such as current leakage and reduced thermal conductivity prevail) and large areas, in an optimum configuration for thermal heat spreaders. In addition to heat spreaders, packaging and heat sink, diamond has also been evaluated as an efficient. material for substrate for high power electronic devices, such as the insulated gate bipolar transistor (IGBTs) [233], and more recently demonstrated in integration with AlGaN/GaN high electron mobility transistors (HEMTs) [234-237] using NCD and UNCD.
With respect to optoelectronic devices that are also going through a similar trend of downsizing, the increasing integration densities has caused subsequent higher heat production- with components such as lasers and high power light emitting diodes (LEDs) [238] that have more stringent working temperature requirements than CMOS (complementary metal-oxide-semiconductor) technologies; diamond has been successfully evaluated for its thermal management abilities in these cases as well [239-241].

2.6.4 SAW devices

SAW devices are widely used as high quality filters in cell phones, for example, and are one of the main drivers behind the miniaturization of cell phones. SAW resonators replace larger and bulkier RF filters composed of discrete resistors, capacitors and inductors. The operating frequencies of a SAW filters based on standard PEMs remain under 1 GHz due the limitation of optical photolithography resolution. This is because of the dependence of the operating frequency (*f*) of the device proportionally on the acoustic wave velocity (*v*) and inversely proportional to wavelength (λ), which in turn, is equal to the period of interdigitated transducers (IDTs), according to the following equation

$$f = \frac{v}{\lambda} \qquad (2\text{-}2)$$

To increase the operation frequencies on SAW filters one may either decrease the wavelength, i.e. the period of IDTs or use substrates with higher propagation velocity or to use different propagation modes with high propagation velocities, e.g. leaky waves [242].
Although due to its isotropic, crystalline structure, diamond is not piezoelectric, it has the highest acoustic wave velocity for both longitudinal and transverse waves [80]; due to the high Young's modulus of diamond films deposited by CVD, the SAW wave velocity can reach values as high as 17.1 km/s [243]. This makes it an extremely attractive candidate for SAW substrates, when combined with PEMs. For the same IDT geometry, the operating frequency of these multilayer devices is expected to increase. For example, a 5 GHz SAW filter can be fabricated with the electrodes of width 0.5 µm using a diamond substrate, compared to widths less than 0.2 µm that are necessary when using conventional SAW materials [244]. Since it is not piezoelectric, diamond has been combined with piezoelectric films in order to obtain SAW operation; materials such as $KNbO_3$ [245], ZnO [244, 246-248], PZT [80], $LiNbO_3$ [249] and AlN [250] have been investigated theoretically and experimentally. While research on diamond-based SAWs still remains an open topic, some diamond SAWs devices are already a commercial product exploiting diamond based SAW filters in commercial mobile phone equipment [105]. The high thermal conductivity of diamond in addition to its growth by CVD onto large surfaces has encouraged both investigation and production of diamond based SAW filters operating in the GHz range [247, 251]. Moreover, due to the versatility of the

CVD process, by adjusting the parameters, films with appropriate characteristics, such as low grain size, which has been known to reduce wave reflection, can be easily obtained [252]. Because of its remote sensing ability, SAW devices have found applications in harsh or biological environments; diamond being extremely chemically stable and bio-inert has found usage in such sensors. The surface of diamond is particularly stable when functionalized with biomolecules and is in fact considered a nearly ideal substrate [253]. This makes diamond of particular interest for bio-sensing applications [254, 255].

A challenge in using CVD diamond as a substrate for SAW devices is the roughness of the growth surface of diamond. For acoustic applications, surfaces must be flat if wave scattering and propagation losses are to be prevented. The roughness must also be compatible with the photolithographic pattern resolution and deposition of piezoelectric thin films [80]. To address this challenge, several approaches have been successfully used; diamond polishing, despite its difficulty, has been used to obtain smooth and large PCD wafers. In some cases, reducing the grain size, i.e., using NCD, the surface roughness has been reduced- some have used NCD films with RMS roughness of 50 nm to address the problem [256, 257]. Yet others have used the nucleation side of CVD diamond, which is smooth, to fabricate SAW devices [258-260]; in some cases the flat nucleation side of thick freestanding diamond layer grown on Si substrates. However, when growing layers of a PEM on a diamond substrate, the differences in the nature of atomic bonding and crystalline structure of the two result in a high interfacial energy. In particular, stoichiometric films of $LiNbO_3$ are difficult to achieve because at the temperatures required for good crystal growth (>700°C) using vapour phase deposition, the vapour pressure of Li is high, which in turn gives rise to the Li deficient phase, $LiNb_3O_8$ [261]. In addition, the mismatch between the thermal expansion coefficients [262] of $LiNbO_3$ and diamond is high leading to high thermal stress in the deposited films [263]. Films of $LiNbO_3$ obtained by RF sputtering and metalorganic deposition on the other hand are found to be porous and with very small grain size [264, 265]. Films deposited at lower temperatures (500 °C) are also reported to have lower acoustic wave velocity [266]. These reasons prevent taking full advantage of the layered structure for the wide bandwidth applications. Despite these drawbacks, PEMs have been deposited directly on the surface of the diamond film. Different authors have successfully deposited $LiNbO_3$ thin films on diamond substrates and have shown that these structures are potential candidates for the fabrication of SAW devices [265, 267, 268].

2.6.5 Field emission devices

Electron field emission is the emission of electrons from a solid surface induced by an electrostatic field; one of its applications is to be used as an electron gun, a typical usage of which is in electronic information displays. RF electron guns work by establishing an RF electromagnetic field inside a cavity having conducting walls. Electrons from a cathode are generated in the injector and immediately become accelerated by the RF electric field, and exit the gun as a series of electron bunches. Finding simple solutions for electron injection is a long standing problem [269]. Experimental evidence explaining the extremely low-threshold electron emission from diamond, a phenomenon first reported in 1996, was first obtained in 2009 [270]. The attractive negative electron affinity (or NEA-is desired to obtain efficient cathodes that can supply electrons to the vacuum with little energy loss) property of diamond (both H-terminated, B-doped and N-doped) surfaces has attracted a lot of interest in recent years owing to its potential application as a low-voltage field emission device [271-273]. The applications of low-voltage field emission are varied- they can be used as field emitter cathodes for planetary mass spectrometry, specifically, gas-phase ionization of target molecules, in which a low power means of generating an electron beam of the appropriate performance could benefit resource-constrained missions to remote planetary targets throughout the solar system. UNCD field emitters also show promise for use as field emission displays- films prepared by laser ablation process showing good field emission properties have been used to fabricate a 1 inch flat panel display [274]; and for massive parallel electron field emission

lithography, to fabricate ferroelectric nanostructures for the fabrication of the next generation high-density (Gb to Tb) non-volatile ferroelectric memories [275]. Argonne Laboratories is one of the premier institutes investigating the utilization of UNCD films for field emission-based science and devices in addition to other research groups investigating NCD [276].

2.6.6 RF MEMS and NEMS

It has been recognized that NCD and UNCD films have strong potential in MEMS, and important advances have been achieved in improving mechanical properties and reducing film stress [277]. Piezo-resistance- which is a change in the electrical resistance of a semiconductor or metal when mechanical strain is applied, and which in contrast to the piezoelectric effect, causes a change only in electrical resistance, not in electric potential, is a particularly useful effect for realizing a diamond physical sensor; BDD films exhibit this effect and have been shown to possess a longitudinal piezo-resistive effect greater than the transverse effect [278]. Moreover, the WBG of diamond indicates that the piezo-resistive effect is ‘‘hard’’ which means that it is preserved or even accentuated at higher temperatures and in radiation environments that would severely limit other currently used materials [279]. It has been found that the piezo-resistive gauge factor of even the crudest PCD strain sensor is sufficient for practical devices and the gauge factor- for homo-epitaxial diamond films is at least 550, compared to that of crystalline Si (120-170) [280, 281]. Diamond piezo-resistive pressure [282, 283], acceleration [284], and vibration sensors [285], uniquely suited to chemically harsh, high radiation, and high-temperature environments have been fabricated. Other important demonstrations include CVD diamond high-Q resonators, integration of UNCD films with RF-MEMS and CMOS technologies, as a dielectric [286], as well as with PEMs such as PZT [287] and AlN [288], enabling fabrication of high-performance piezoelectric-driven MEMS/NEMS. Capacitive RF MEMS switches using UNCD have been demonstrated with isolation around 19-20 dB and a loss around 0.3-0.4 dB at 10 GHz [289]. Diamond based NEMS switches with ultra-low power consumption, high switching speeds, and operation at high temperatures, have also been demonstrated [290, 291]; similar performance on wafer-scale level PCD however is yet to be reported. Fundamental understanding of mechanical dissipation in diamond cantilevers as well as electrical properties at very low temperature have led to designing ultrasensitive SQUID (Super-conducting quantum interference device) with the possibility of detecting a very weak magnetic field, promising for developing specialized sensors/detectors [286].

2.6.7 Particle detectors

Diamond particle detectors have been a subject of investigation for quite some time now and with the advent of CVD diamond, they are now finding usage in practice; from particle level detection to intensity levels [292]. Diamond devices have become ubiquitous in the large hadron collider (LHC) experiments, finding applications in beam background monitoring and luminosity measuring systems [293]. CVD diamond has been used extensively in beam condition monitors as the innermost detectors in the highest radiation areas of Babar, Belle, CDF and all LHC experiments [294]. These are niche applications where volume sensitivity, radiation hardness and/or temperature insensitivity are paramount. When compared to other solid state radiation detectors, which use reverse biased diodes, high purity intrinsic diamond can act as a solid state ionization chamber at room temperature. In a solid state ionization chamber, a charge must be able to travel freely through the lattice and the key to this is purity and high crystalline quality [78]. Solid state ionization chambers when compared to the gaseous ionization chambers, offer a much higher atomic density (which when diamond is used is about 1000 times higher than the latter) and thus offers significant potential for miniaturization. Diamond’s radiation hardness has of course, been widely studied and reported [295-297], a detailed explanation of the underlying high energy physics is of course, beyond the scope of this thesis. However, it may be enough to say that the first beam test results

of prototype diamond devices with improved 3D detector geometry shows further enhancement of the radiation tolerance of this material. In addition to retaining significantly more signal than other Si sensors currently deployed in collider experiments, these diamond sensors have very low leakage currents – even after large doses of radiation. Since leakage currents dictate the ultimate lifetime of solid-state particle detectors, diamond sensors survive longer [298]. In terms of detection itself, diamond is able to detect a large variety of particles, even generating a response signal to neutrons [292, 299].

2.6.8 Electrodes

BDD electrodes have attracted increasing interest from researchers due to their potential for application for electro-analysis, spectro-electrochemistry, neurochemistry, chemical/ biological-sensing, and water disinfection/purification [300]. Electrodes based on BDD can be readily obtained and are most useful for fundamental studies of interfacial structure as well as grain boundary and crystallographic effects on rates of electrochemical reactions. Polycrystalline thin-film electrodes, whereby diamond is deposited on properly pre-treated substrates (e.g., Si, W, Mo, Nb, and Pt), are however the most commonly used form of diamond due to the ease of uniform diamond deposition on these thin metallic needles [300]. Diamond electrodes also can be patterned into microelectrode array structures (e.g., discs and bands). Because of the diversity in fabrication (and the other properties of diamond such as biocompatibility and ability to withstand harsh chemical environments), these electrode arrays find application as a platform for nerve cell growth, neural stimulation, and action potential monitoring for reading short duration changes in the membrane potential of an excitable cell [301, 302]. *In vitro* measurements using diamond microelectrodes have been used to detect human biological markers such as histamine [303], dopamine [304], and GSH (an indicator of oxidative stress in cells and existing in high concentration in cancerous tissues) [305].

2.6.9 Power diodes

The progress in information technology and mobility has resulted in a network of innumerable devices, that are indispensable to us now, and although each single instrument on this network does not consume massive amounts of energy, their aggregations are expending a great amount of energy, putting demands on power generation and transmission like never before. This also includes demands on conversion of power from its various sources to the type of power consumed at the load. The branch of electronics that deals with electrical power generation, conversion and in general, control, is termed as power electronics. Power electronic devices have seen a doubling of efficiency every three years for the last 18 years [306], with the target being making them smaller, lighter, more reliable, and with consequent reductions in overall system cost. Si technology currently has been used, albeit within its constraints, to satisfy these demands but the intrinsic properties of diamond may provide some advantages over the material limits of existing Si-technology; there has in fact been increasing research interest in diamond based power devices [170]. The ideal power semiconductor device combines zero conduction losses with zero switching losses, with near-ideal switching characteristics in the absence of stored charge, thus maximizing the efficiency of power electronics systems. As of 2019, with the improvements in diamond growth techniques and doping control methods for p, p+, n-type and intrinsic diamond, the electrical properties of these materials have been characterized and used experimentally to develop several power devices structures. Diamond diodes are thought to bring particular impact in the area of high blocking voltages of several 10 kV, avoiding cascading of diodes and for operation under very high temperature, possibly above 1000 °C [307]. Diamond diodes have been fabricated with synthetic and natural SCD as well as PCD grown on Si or other non-diamond substrates.

The material properties of diamond, particularly its high breakdown field, which is about 10MV/cm for SCD and in the range of 0.7-5MV/cm for CVD diamond [205], have favoured the development of several power diodes- p-type diamond unipolar SBDs [171, 172, 180, 308-312], metal-intrinsic-p-type diodes

(MiPDs) [313, 314], as well as bipolar p-type-intrinsic-n-type diodes (PiNDs) [315], Schottky- pn diodes (SPNDs, that merge the Schottky and p-n diode architectures) [316]. The highest V_{max}, (>11.5 kV) has been obtained for a PiND without a mesa-structure [315]. A current density of more than 60 kA cm^{-2}, which corresponds to an on-resistance of 0.03 mΩ-cm^2, was reported by Makino *et al.* for a SPND [316], which is impressive when compared to the state of the art SiC power devices that lie in the order of a few hundred A cm^{-2}. In all cases, p-type conductivity was obtained by B doping and where applicable (for example, in p-n structures), n-type conductivity was obtained by N doping. HPHT SCD SBDs operating in the range of 298 K to 584 K have been experimentally confirmed for their fast recovery, the long-term high temperature stability [317] and depending on the rectifying junction, up to 1273 K [318, 319]. PCD diodes SBDs have also been fabricated and exhibited rectification $>10^6$, leakage currents <1 nA, no indication of reverse bias breakdown at 100 V and an ideality factor of 1.1 [320].

2.6.10 Transistors

The research aimed at utilization of diamond for switching devices began as early as the 1980s using natural diamond crystal, with the fabrication of a bipolar junction transistor (BJT) using a natural p-type diamond crystal as a base electrode with an n-type emitter and collector regions formed by C ion implantation [321]. This primitive device had a low-current amplification factor of 0.11 (attributed to fabrication issues) and the absence of a reliable shallow donor still remains the bottleneck for diamond bipolar devices. Hence work on diamond BJTs has been sparse, utilizing N in some cases [322] and P in some, to obtain n-type conductivity [323]. Some have approached the solution to this bottleneck by fabricating heterojunction BJTs with SiC [324].

However, as was seen from the discussion of the material properties of diamond, the FOMs and extraordinary theoretical performance of diamond merits the attraction towards it for high frequency RF electronics and especially RF power circuits, where the important parameters are high speed, high power density, efficient thermal management and low signal loss in high power/frequencies. Much of the research has been focused towards diamond field effect transistors (FETs), in particular utilizing the p-type conductivity of H-terminated surface [H-terminated FETs (HFETs)- also referred to as surface channel FETs] and BDD (B-doped FETs).

The working principle of HFETs is based on the surface transfer doping which can be achieved by exposing H-diamond to different surface acceptors with high work functions [162]. HFETs aim to achieve high frequency performance that is made possible with diamond because of its high reported values of carrier mobility and saturation velocity [325] and they have shown promising results- a variety of transistor structures (such as low on-resistance FETs, triple-gate FETS, vertical type with trench gate FETs) using primarily the conductive H-terminated diamond surface and oxides such as Al_2O_3, Y_2O_3 and high-k ZrO_2 have been fabricated with sub-micron gate lengths [326, 327]. The H-terminated surface of diamond has proved useful in fabricating metal-semiconductor FETs (MESFET) [158] and metal-oxide-semiconductor FETs (MOSFETs) [328] with high current capabilities. The high sheet carrier concentration, the low depth and low activation energy makes this surface ideal for the channel of FETs. The Schottky barrier height (SBH) can be controlled based on the electronegativity of the metal; therefore, low-resistance ohmic contacts can be produced by deposition of Au or Pt on the surface, and Schottky contacts are obtained with Al or Cu. Utilizing the intrinsic p-type H-terminated surface, diamond metal-insulator-semiconductor FETs (MISFETs) have been realized with a cut-off frequency of 23 GHz and maximum frequency of oscillation of 18 GHz [329]; the same has been noted to be 45 and 120 GHz respectively, for a PCD HFET [325]. More recently such high frequency performance was demonstrated in diamond FETs at temperatures up to 473 K [279]. Homo-epitaxial SCD substrates have been used to demonstrate the RF performance of a 50-nm gate length H-terminated diamond FET with a cut-off frequency of 53 GHz, believed by the authors to be the highest value reported for a diamond-based transistor [330]. H-diamond

NOT and NOR logic circuits composed of depletion and enhancement mode MOSFETS have also been demonstrated [331].

B-doped diamond transistors, however, in particular the B- δ doped FETs are often regarded as the best solution for RF power transistors because although HFETs have shown remarkable properties, the H-related surface acceptor concept is not yet fully verified and the surface is thermally and chemically unstable [332]. The δ -doped technique allows one to localize the impurity atoms within a few atomic monolayers, thereby generating a V-shaped potential well with a 2D hole gas. In the case of BDD, this is relatively easy to obtain because of the low diffusivity of impurities in diamond, thanks to the rigidity of its structure [333]. In addition, increasing the impurity concentration has been shown to lower the activation energy of carriers in BDD (this effect peaks at a concentration of 10^{20} cm^{-3}), allowing one to obtain full activation at room temperature [334]. Over the years, several δ doped FETs have been fabricated that have shown operation in a temperature range of 20 K to 474 K [335, 336], MESFETs with cut-off frequency and maximum oscillating frequency of 1 and 3 GHz respectively [337], high temperature MISFETs based on PCD [338], with gate leakage currents below 10 nA at 25 V [339]. A sub-category of B-doped diamond transistors are junction FETs that exploit the p-n junction (utilizing n-type N-doped diamond with BDD) as the control diode [334] because compared to Schottky contacts, they show lower leakage current and high breakdown as well as the higher built-in voltages, leading to a shift in the pinch-off voltage towards enhancement-mode operation (normally off at zero gate-source voltage) [340]. These JFETs have shown operation up to 473 K [336].

2.6.11 CMOS and beyond

Transistors have fueled the growth of the information technology sector. Having more transistors on a chip means more speed and possibly, more functions and the industry has faithfully maintained this tendency since the early 1970s because this scaling brings a good performance-to-cost ratio of products, with the current SOA being transistors shrinking to dimensions < 10 nm [341] and about 10^{10} transistors placed into a single chip [342]. The continuous miniaturization has enabled consumer electronics to keep evolving, launching smaller and lighter personal computers, smartphones and tablets every year, at increasingly competitive prices. By reducing the critical dimensions of the transistor, while keeping the electrical field constant [343], higher speed and reduced power consumption can be simultaneously obtained for a MOS device. However, as scaling down continues and transistor features as well as interconnects approach < 10 nm range, the shortage of horizontal space and the problems that come with such tiny features are becoming evident; for example, increasing leakage and tunnelling currents, in addition some fundamental power-thermal limits. Consequently, performance frequencies have plateaued in the few GHz range since the middle of last decade and at the forefront now, is the minimization of power consumption. With respect to lowering power consumption, the CMOS technology remains unmatched in the industry [344]. CMOS technology makes use of 2 MOSFETs to implement logic gates and other digital circuits and their defining characteristics are high switching speeds, enabling high density of integration, and very low static power dissipation. Current reduction in CMOS is accomplished by complementing every n-MOSFET with a p-MOSFET and connecting the gates and drains together. A high voltage at the gate will "open" the n-MOSFET (and "close" the p-MOSFET) whereas a low voltage at the gate causes the reverse. This complimentary arrangement allows for power to be consumed only during state transitions making it very efficient and a vital component in battery-powered devices, where they are currently included in a variety of components: microprocessors, microcontrollers, static RAM and other logic circuits and memory/storage components. The International Technology Roadmap for Semiconductors (ITRS) predicts that challenges with respect to chip power and power density, and associated thermal management, particularly those that have arisen in the last 5 years, may be addressed in two ways: improvement in materials to enable and maintain CMOS scaling by substrate engineering,

for example, or with “beyond CMOS” technologies [345]. Diamond lends itself to a number of these schemes.

The primary advantage that diamond can bring is due to its exceptionally high thermal conductivity and low thermal expansion coefficient, to be used as an addendum to the substrate material for CMOS technologies, improving thermal management [346] and enhancing the performance of Si based transistors by reducing their thermal load. SOI (Si-on-insulator) substrates are used to reduce parasitic device capacitance in CMOS chips, providing better dielectric isolation in both vertical and horizontal directions, improving performance and enabling harsh environment operation. The integration of diamond and Si in order to have SOD (Si -on-diamond) wafers that serve the same purposes as SOI but are functionally more efficient, is a subject of eager investigation [347-349]. For SOI applications, the substrate is not defect sensitive, it only needs to be sufficiently insulating. Because of its extremely high room temperature resistivity (of the order of 10^{13} Ω cm), diamond is especially attractive as it transfers heat efficiently while being an electric insulator. The relief of thermal load brings a lot of individual advantages. For example, the properties of high-*k* materials used as gate-insulators degrade as temperature rises. Features such as these benefit directly from better thermal management. Another advantage of SOD is related with the lattice properties of diamond and Si. Si and diamond share the same diamond lattice structure, however, their lattice constants are different. This induces strain in the Si layer fabricated on top of the diamond. The strained-Si layer is useful: it has been known to improve carrier mobilities and in fact, is already a widely used technique in CMOS scaling. Ionizing radiation causes degradation in CMOS circuits by creating electron-hole pairs in the gate; the difference in the carrier mobilities leads to undesirable charge accumulation. Since diamond is immune to the effects of radiation, diamond substrates would also, not suffer from this problem [350, 351].

The smallest Si transistor yet reported is a FinFET with a gate length of 7 nm [352], and simulations show that the use of multi-gate architectures will allow Moore’s law to continue to at least the 2 nm node [353]. However, at sizes below this limit, where the gate oxide becomes only a few atoms thick, quantum confinement effects start to play a role. Quantum effects such as tunnelling might actually be used in the future to make even more innovative chips with TFETs (tunnelling FETs) for example. According to the ITRS, with innovations as these, we may soon be moving into the regime of beyond CMOS. Beyond CMOS can be interpreted in a number of different ways, for example, More-than-Moore applications, new kinds of logic/memory devices, new architectures, devices using spintronics and quantum tunnelling, and extreme materials like graphene and carbon nanotubes (CNTs). These materials offer even greater opportunities for miniaturization- the intrinsic switching speed of a 50 nm-long CNT transistor has been estimated to be about 950 GHz![354, 355] This happens because C-based materials such as CNTs and graphene, have carrier mobilities in excess of 200,000 $cm^2V^{-1}s^{-1}$ [356]. For these properties to be fully exploited, however, the choice of the substrate is very important. Defects created in the substrate under radiation, for example, will result in an electrical response dominated by the substrate. Diamond is a radiation hard material uniquely positioned to serve as substrate material for these C-based transistors [357, 358].

The similarities in the diamond lattice and honeycomb structure of graphene and CNTs provide a much more natural, less strained interface. With the right substrate, graphene FET mobilities can increase to several thousand $cm^2V^{-1}s^{-1}$ enabling device performance to match and exceed CMOS, potentially up to 1 THz [359]. *Figure 2-7* shows a device concept for one such transistor. Although this line of research is still in its infancy, preliminary results look very promising- current induced breakdown in graphene is thermally activated [360], and experimental results show that the current carrying capacity of graphene can be improved not only on with SCD substrates but also the relatively inexpensive, UNCD [357] as well as NCD [361]. Several significant results have already been obtained from MOSFETs fabricated using graphene-diamond hetero-structure [362, 363]. A device concept (also *Figure 2-7*) for CNT FET enables

higher drive current density because of the higher carrier mobilities of CNTs, however when compared to graphene-diamond heterostructures, diamond-CNT work has been rarer [364].

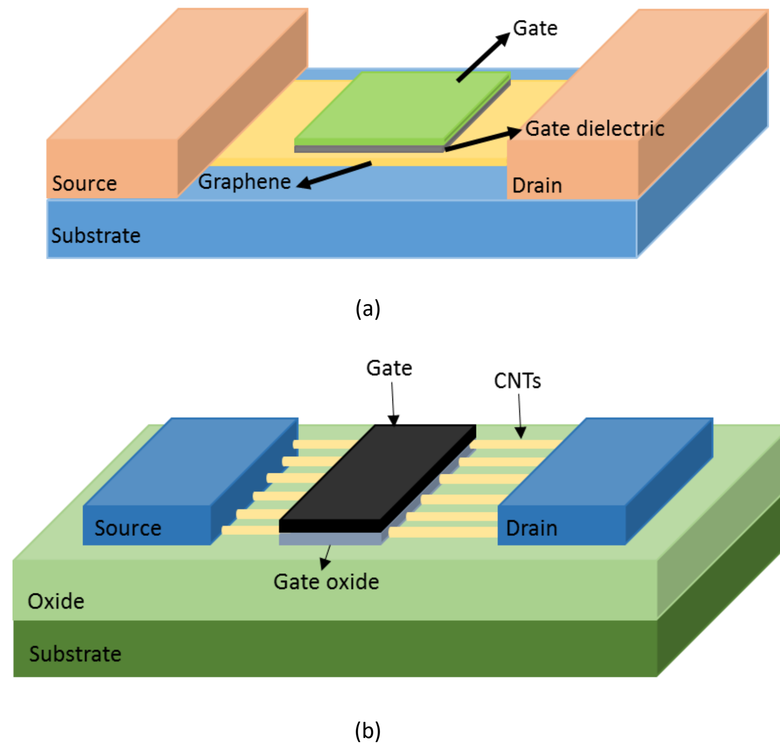

Figure 2-7 Device concepts for (a) Graphene FET (GFET) (b) Carbon nano-tube FET (CNTFET) where the substrate is diamond

For critical device dimensions < 10 nm, thermal transport is no longer governed by the diffusion equation. It becomes a much more complicated process involving optical and acoustic phonons governed by the Boltzmann transport equation. This allows the emergence of novel nano-devices that utilize the wave nature of the phonon instead of "conventional" electronic charges. By utilizing corresponding phonon depletions regions, phonon stop bands, phonon waveguides and phonon lenses, diodes, transistors and solid-state quantum memories can be designed. Even though the first two have so far only been theorized, the diamond lattice was used to demonstrate, for the first time, this very memory, at room temperature. Albeit for a very short period of time, a write and consequent read unit obtained information stored in the memory for about 7 picoseconds [365, 366]. There are significant technical obstacles to be overcome to extend this storage time, but if diamond can be isotopically enhanced, this remains an extremely exciting application avenue.

2.7 Challenges

Although numerous diamond based devices are already in the marketplace, as discussed above and some have irreplaceable place in research-for example, the detectors at the LHC, commercialization of this material is still in its infancy. Large-area single-crystal substrates are now available in the market, however, defect densities and resistances can still be improved and these remain a challenge for the years to come. The most promising candidate for SCD wafer fabrication is the lift-off process based on ion implantation [308]; to achieve this goal, a single large (inch size) seed wafer is required, and further research and development of bulk diamond crystal growth techniques in this direction is ongoing [367].

With respect to homo-epitaxial CVD and HPHT films, It has been seen that the initial orientation of the substrate has influence on the synthesis of thick high-quality intrinsic and doped diamond layers [368]. The [1 0 0] orientation is still the most widely used due to its availability and the relative ease of growth of low defect films, but has limitations in terms of doping: active n-type films are still particularly difficult to obtain and p-type doping with B has a limited efficiency. Hence one way of addressing the challenge of good quality doped diamond is by considering other crystalline orientations. Growth on the [1 1 0] orientation for example, allows for improvements in the doping efficiency of B; at the same time however, this orientation reduces the usable surface area and limits their use to a moderate thickness unless improved growth conditions are developed. The [1 1 1] orientation is probably the most attractive for doping allowing active n-type films with P and the highest B concentrations, but this orientation too is subjected to the formation of twins and macroscopic defects that restrain the growth conditions and the maximum reachable thickness while crystalline quality remains average. There are however, many alternative orientations and these continue to be an area of active research interest; with specific growth strategies based on alternative orientations and substrates playing an important role in exploiting the properties of semiconducting diamond [368]. Optimization of the growth process is particularly important because the electrical properties of diamond that make it particularly interesting, such as the high mobilities of carrier are process dependent- as the diamond purity is improved the mobility increases [205].
To realize the properties of high breakdown field and blocking voltages, the homo-epitaxial growth of ultrahigh purity diamond is required, with very low crystalline defects. So far ultrahigh pure films with N concentration (for n-type doping) lower than ~10^{13} cm^{-3} and B concentrations around 10^{15} cm^{-3} have been demonstrated [369]. For hetero-epitaxial diamond wafers, whose main advantage is the absence of size limitation, there are two main challenges that still need to be addressed next: first, crystal growers have to explore the limits for dislocation density reduction, currently, a state of the art of hetero-epitaxial diamond growth on Ir using bias enhanced nucleation (BEN) starts with a dislocation density above 10^{10} cm^{-2}, and this needs to be brought own drastically, closer to 10^{6} cm^{-2}[370]. Second, the development of devices based on diamond needs to put an impetus in demonstrating that diamond elements really can compete with existing technology based on other semiconductor materials (e.g., SiC, GaN). This may be done on the best single crystal material available with the lowest dislocation density (close to zero) and only afterwards identical devices fabricated on state of the art hetero-epitaxial diamond. In case it turns out that device fabrication only makes sense with crystals containing no dislocations or a maximum of several 100-1000 cm^{-2}, hetero-epitaxy would probably be out of the race for diamond electronics [370]. The hetero-epitaxy of diamond on SiC is promising, mainly because of the lower lattice mismatch between the lattice parameters of diamond and SiC than that between diamond and Si, the most commonly used substrate for hetero-epitaxial growth of diamond [371].
Before there can be large scale application of diamond in electronics, one of the major challenges synthetic diamond must overcome is the deficiencies in doping concentrations and high density of impurities and defects [277]- there is still much room for improvement in terms of wafer quality but most importantly in terms of price. On the other hand, the exploitation of these very same defect and impurity structures for their use as quantum devices is a very luring subject of research. The identification of more shallow dopants (with an energy level that is near the band edge of the semiconductor, so that only a little energy is required to ionize the dopant and produce free carriers) [372] and new quantum defects and effects [373, 374] are still open challenges. The deep impurity levels in diamond result in much lower free carrier densities resulting in high resistance. Although many attempts have been made to identify shallower dopant impurities, shallow impurities have yet to be found. Hence, even though taking advantage of the high breakdown field of diamond, the ultimate in high voltage tolerant devices can be obtained, the low carrier density result in very large on-resistance for such high voltage devices with a long drift layer. Consequently, diamond devices have not demonstrated the theoretically predicted FOMs

when compared to other power semiconductors. Some of the directions undertaken by researchers to reduce the on-resistance have been designing diamond power devices for high temperature operation, and unique devices structure using the properties of diamond (such as NEA of H-terminated surfaces), or utilizing highly conductive hopping transport for high doping [205].
The active p-doped layers that have been produced and integrated in numerous electronic devices are thin and growing thick freestanding layers with heavy doping that can be used as p-type substrates in power devices is much more challenging.
In diamond research, one of the issues that remain under-explored are fundamental charge transport characteristics and carrier dynamics, crucial in applications such as bipolar devices, the lack of which is a serious impediment to the application of diamond in CMOS technologies, for example. CVD diamond and the heterostructures it forms with other semiconductors and metals have been studied although only with respect to specific devices, an understanding of the underlying physics is still missing.
With respect to power devices, predicting the electrical and thermal performance is a key step for their next generation development. For the development of diamond power devices in particular, the implementation of the physical models of CVD diamond into a finite element simulator is mandatory. In addition, to be able to penetrate power electronics applications, diamond power devices will have to reach higher total current capabilities, for which the obvious limitation in the current size of monocrystalline diamond substrates must be overcome.
Researchers and the industry are currently concentrating upon developing methods to scale up the CVD processes and reduce production costs to the point at which it becomes economically viable to use diamond as the material of choice; it is important to note that the biggest challenge is in obtaining semiconducting diamond of suitable quality, the state of the art of industrial CVD diamond for the other applications that were discussed in the previous sections are quite satisfactory. Without prohibitively priced large-area single-crystal or high quality semiconducting substrates, the electronics research will not receive the impetus to enable device development that can take advantage of the processes and equipment used in microfabrication facilities. A fundamental matter that needs addressing with respect to reducing the cost is the improvement in the efficiency of the CVD growth process- for a method that is so versatile and widely used, the current state of the art in CVD has an efficiency of conversion of only 0.6% of the C supplied in gaseous form to diamond [375].

2.8 Conclusions

The properties of diamond- natural and synthetic, were presented in this chapter. A history of the synthesis of diamond that led up to the present state of the art was also discussed. The electronic properties of diamond were discussed in some detail. The role that diamond plays in the industry and its various applications were also discussed. In the end, the challenges that currently face diamond technology were presented.

3. Diamond growth by CVD

3.1 Introduction

In this chapter, the reader is introduced to the details of the CVD process, in particular, the HFCVD technique which was used to fabricate all diamond films investigated in the current work. This is followed by a discussion on the chief analytical techniques used to characterize the diamond. Finally, the experimental details of the optimization of the HFCVD process using the NNP are presented. Insight from this work contributed to the experiments presented in the next chapter.

3.2 Undoped diamond

CVD is a process in which one or more volatile precursors are transported via the vapour phase into a reaction chamber, where they decompose and are consequently, deposited as a thin, solid film on to a heated substrate. Precursors are commonly in gaseous form but can sometimes be liquid. The precursors are the source of the constituent atoms of the desired film and the conditions in the reaction chamber leads to their decomposition and deposition through chemical processes. The kinetics of the flow of the dissociated elements and the surface conditions of the substrate affect the quality and the quantity of the film deposited. Thus, CVD is a chemical process that spans many traditional disciplines: the chemical physics of gases and plasmas, surface science, solid-state chemistry of inorganic materials and organometallic or organic chemistry for precursor synthesis. A schematic representation of the most important chemical reactions that occur in thin film synthesis, in general, is shown in *Figure 3-1*. These reactions include the gas phase reactions, surface reactions and desorption of film precursors or volatile surface reaction products. CVD may indeed be regarded as a chemical process that spans many traditional disciplines: chemical physics of gases and plasmas, surface science, solid-state chemistry of inorganic materials and organometallic or organic chemistry for precursor synthesis.

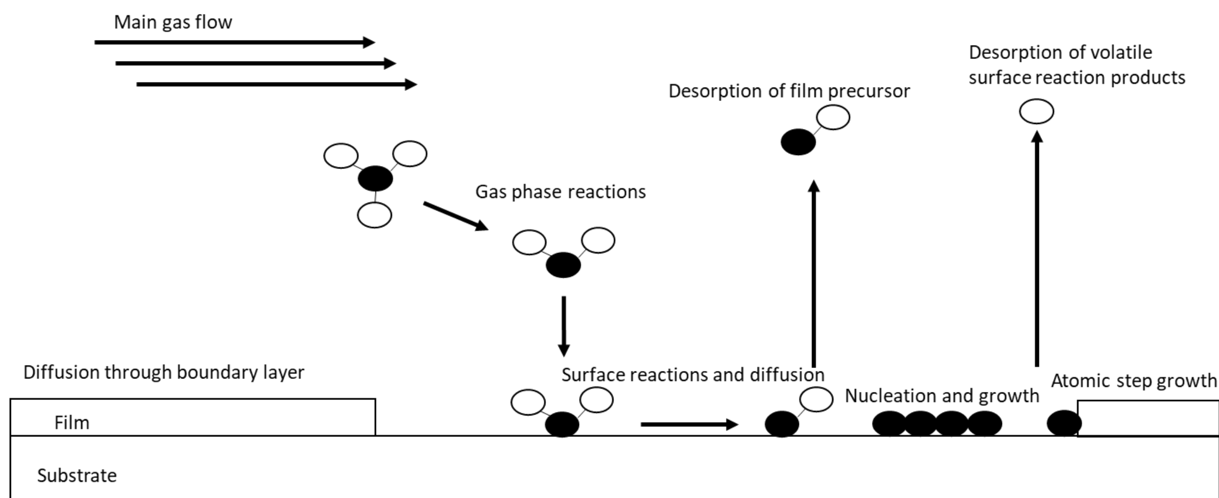

Figure 3-1 Schematic of the most important chemical reactions involved in thin film synthesis. It is important to note that not all the reactions represented here need occur for every CVD process, and are often, in fact, not even desirable (After [376])

In the growth of diamond using CVD, the precursors are therefore C containing gases. It is important to note that in the conditions typically involved in a CVD reactor, diamond is metastable compared to graphite. Hence, in order to obtain a diamond film that has a higher sp^3 content than sp^2, all the factors that can be adjusted to lead to the formation of the former instead of the latter must be finely tuned. In order to arrive at the particular conditions that lead to the preferential growth of metastable diamond instead of graphite or amorphous C, one needs to treat the process of CVD as a result of three separate (but not independent) factors, each of which has a direct influence on the growth of quality diamond. The

first factor is the composition of the precursor gases used for the process. The second involves the type of dissociation processes and reactions that occur between them. The third includes the diffusion of these elements in the gas plasma and the surface conditions and reactions that lead to the actual deposition of diamond on the substrate. These factors are schematically represented in *Figure 3-2*. Another separate, yet, important factor involved in the growth of diamond on non-diamond substrates is the appropriate treatments prior to the deposition itself, in order to enhance the nucleation density of the film.
For the growth of diamond in C-H chemistry, a very dilute hydrocarbon/H_2 gas mixture is used, that is activated utilising one technique out of various options (DC, linear antenna, RF, MW, electron cyclotron resonance (ECR)-MW, HF etc.), to form important radical species and atomic H. The reason why a very dilute hydrocarbon mixture is used is because at higher hydrocarbon concentrations, there is a significant reduction in the amount of atomic H [42, 377], for example, in the case of HFCVD, this is a consequence of a "poisoning" of the heterogeneous production of atomic H [42, 43, 377] through the deposition of C on the filament surface [378, 379]. This is not desirable because atomic H plays a crucial role in the diamond deposition process, and producing high partial pressures of H plays a crucial role in stabilizing the diamond phase and increasing deposition rates up to a few tens of µm/h [368]; this will be discussed in the following sections. The transport of these species to the substrate growth surface is the next consideration; and this may occur by convection or by diffusion (determined by the activation technique used). Gas phase reactions and the gas-surface interactions initiate the necessary chemistry that leads to the deposition of the film.

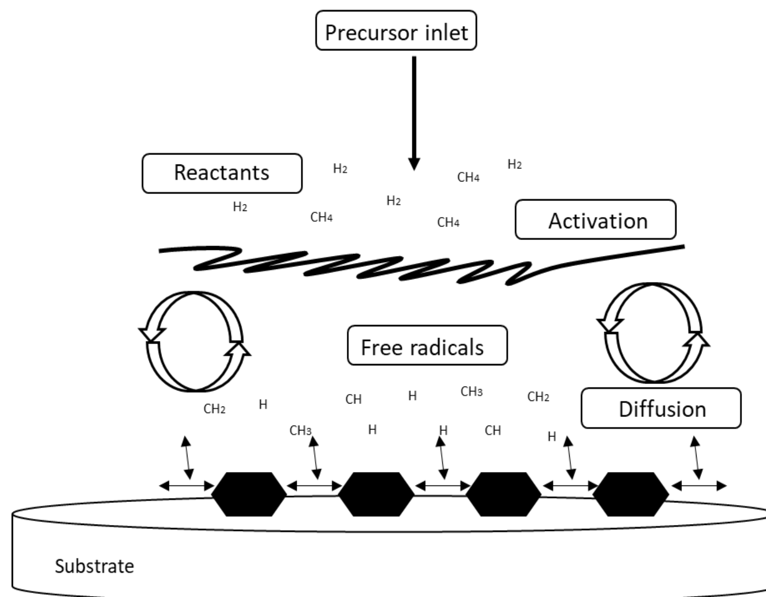

Figure 3-2 The fundamental factors involved in the CVD process, in a schematic representation of the process with the atoms and radicals involved in the diamond deposition process

HFCVD is by far the most commonly used CVD technique to obtain diamond films for laboratory research; it is cheap and highly economical (most industrial production of CVD diamond now involves high power MW systems or, occasionally, use of DC plasma jets). An advantage of HFCVD reactors over MWCVD reactors, for example, is the simplicity of the system and a uniform diamond deposition over large areas [380]. Other advantages of the HFCVD technique are its intuitively easy to understand process parameters. This being the case, HFCVD has also been one of the most widely studied techniques, and there is considerable research on the optimisation of this process. *Table 3-1* presents a comparison of the various CVD techniques, by discussing their respective advantages and disadvantages.

Technique of activation		Advantages	Disadvantages
Hot filament		• Moderate growth rate at low capital cost • Large area deposition with uniformity • Allows for *in situ* diagnostics and mathematical modelling [201]	• Filament contamination • Filament carburization and embrittlement • Other issues that may affect filament over time and affect reproducibility- sagging, deformation • Typically high temperature growth (> 673 K)
Plasma	**DC** **RF** **MW**	• Radical species generated from high energy electrons while gas and substrate remain at relatively low temperature • 2.5 GHz reactors commercially available	• Bombardment of substrate surface with charged particles might cause damage and contamination (DC and capacitatively coupled RF) • Radial non-uniformity and the need for resonant standing wave cavity (for MW) hence problems in scaling up
	ECR-MW	• Large area and high plasma density • Low substrate temperature	• Low growth rate • Small growth area • Poor uniformity and quality
	Plasma torch	• Very high growth rate of good quality films (up to 1mm/hr [381]) • Allows for *in situ* diagnostics	• High gas flow rates and power consumption therefore, expensive • Small growth area
Combustion		• Low capital cost • Reasonably good growth rates	• Worst efficiency of conversion of hydrocarbon to diamond • Non-uniformity and small growth area

Table 3-1 A comparison of the advantages and disadvantages of the various CVD techniques

Devised originally by the NIRIM group in Japan [32], the HF system used industrially today has changed very little. Deposition is usually carried out by passing a gaseous mixture of hydrocarbon gas and H_2 into a deposition chamber, which contains a heated filament mounted near the substrate. The principle function of the HF is to activate the reactants and produce atomic H. Commonly used filaments are Ta, W or Re. Auxiliary components include- a vacuum pump, mass flow controllers (MFCs), power supply for the filament, water cooling for the deposition chamber which itself is made of pressure resistant steel, exhaust pumps, thermocouple for substrate temperature measurement and an IR pyrometer to measure filament temperature. In systems where doping of diamond is desired, an additional supply valve for the dopant is included. Systems for doped diamond growth are usually different from undoped diamond in order to prevent unintentional doping cases, when undesired. Gas flow, current supply and consequent filament-substrate temperatures etc. are controlled either by setting appropriate values manually or through varying degrees of automation, using programmable computer software. Hydrocarbon concentrations are always low; usually between 0.5-5 % up to flow rates of 1.67×10^{-7} m^3/s, at a pressure of 2 to 10 kPa. The filament is maintained between 2173-2773 K, and the substrate at 673-1273 K. The substrate temperature can be controlled either by using a specific substrate heater or using the radiative heat from the filament (if the latter is the case, the temperature is dependent on the filament-substrate distance and this is adjusted accordingly). These aforementioned conditions can be said to be standard HFCVD parameters for deposition of diamond films and each of them have the potential to affect the chemical reactions and properties of the plasma inside the deposition chamber, and hence, the qualities of the film deposited as well.

Although the HFCVD method is versatile, it does have some disadvantages. Since the filament sets an upper limit on the temperature, HFCVD processes produce less atomic H when compared to plasma process. This low gas phase concentration results in lower growth rates when compared to the plasma

methods. Because of the usage of a HF, deposition is usually preceded by a carburization step [379] so that during deposition, stable plasma conditions are obtained. The HF is also sensitive to oxidizing or corrosive gases, limiting the variety of gas mixtures which can be employed. The reports in literature of diamond CVD from C and H_2 containing gas mixtures that have been supplemented by small amounts of oxygen or other oxygen containing compounds to enhance the growth process [382-384] usually utilize a MW reactor, because in an HFCVD reactor even trace amounts of oxygen tends to cause oxidation and rapid destruction of hot metal filaments. Depending on the filament used, a commonly encountered problem is the contamination of the diamond film with filament material. Metallic impurities in diamond films deposited by HFCVD, using various commonly used filament materials have been found and quantified experimentally [385-387], and this is definitively, due to the loss of metal from the HF. In some cases, for example, W and Ta, this is due to evaporation of refractory metal carbide; in other cases, for example, Re, this is due to the high vapour pressure of Re [388] at the typical operating temperatures involved in HFCVD. For some applications of diamond, metallic impurities at the tens of ppm level are not a significant problem, and in some cases, even yield improvements in film quality [387]; however, for electronics applications, the same is unacceptable.
Since the primary technique for diamond growth used in this work was HFCVD, the following sub-sections highlight the diamond growth processes involved in HFCVD, in order to better understand the work done to optimise the HFCVD for the growth of diamond for electronics applications.

3.2.1 Gas phase chemistry

CVD diamond growth occurs in the presence of C containing radicals and molecules that impinge on the substrate and contribute to the growth of diamond, while at the same time, the co-deposited graphite is selectively etched by the atomic H. For a thorough understanding of the CVD of diamond, knowledge about the gas phase environment (which includes the H_2 as well as hydrocarbon chemistry) inside the reaction chamber, and in the vicinity of the film is of utmost importance. Also relevant is knowledge about the diffusion and transport phenomena involved in the species, and the surface chemistry of the substrate where the diamond film grows. Hence there have been several studies (experimental [41, 42, 389] and theoretical [43, 390, 391]) about the phase species present, their sources, interconversion and sinks of the key reactive (radical) species, their spatial distribution and their transport through the gas, the chemistry occurring at the gas/surface interface, and the way in which all of these factors vary with, for example, temperature, pressure and the extent of activation (i.e. filament temperature).
Studies of the gas-phase chemistry during the CVD deposition of diamond [41-43, 392-399] have revealed that atomic H and hydrocarbon concentrations are the most critical determinants of CVD of diamond as well as its quality and growth rate. Thermal dissociation of H_2 is the primary source of H atoms at high temperatures [400]. In HF systems, at pressures about 4 kPa the dissociation of H_2 occurs, according to the following temperature activated reaction [401, 402]

$$\mathrm{H_2} \leftrightarrow 2\mathrm{H} \quad (3\text{-}1)$$

H atoms initiate most of the gas phase chemistry in low power CVD reactors (e.g. HFCVD) [399]. H atoms, thus produced, diffuses rapidly away from nearby the filament, resulting in a concentration profile near the filament [396]. Diffusion is the dominant transport mechanism in low pressure (e.g. HFCVD) reactors [43, 403]. In addition, H concentration profile measurements have shown that the substrate surface, i.e., diamond, is a sink for H at typical substrate temperatures [404]. The level of atomic H at steady state is obtained as the balance between the rate of its production and its destruction. For typical diamond CVD conditions (i.e., pressure far below 20 kPa), destruction, which occurs due to the homogeneous recombination of H, is a slow process, as a result of which, H atoms are able to diffuse to the walls or to the substrate before recombining in the gas [44, 405].
Much of the gas phase chemistry involves reactions between atomic H and the hydrocarbon species. The most commonly used gas in HFVCD is CH_4 but it has been found that gas phase composition in the vicinity

of the filament at temperatures appropriate for optimal diamond CVD is essentially independent of the C source gas [399].

Considering a precursor hydrocarbon like CH_4, the H atoms drive a series of fast "H-shifting" reactions that involve abstractions in the hot regions of the chamber (3-2) and additions in the cold regions (3-3).

$$CH_y + H \leftrightarrow CH_{y-1} + H_2 \quad (3\text{-}2)$$

$$CH_{y-1} + H + M \leftrightarrow CH_y + M \quad (3\text{-}3)$$

Where M is a third body radicle.

The relative densities of the various CH_y species depend on the local H atom density and gas temperature, and thus show a wide spatial variation [400].

For example, in the vicinity of the filament, reactions of the type (3-2), i.e., H atom abstraction from CH_4 are the principal route for forming CH_3 radicals, and this production rate and consequently its mole fraction has a maximum at *d*=0 (*d* being the distance from the filament) [399]. It has also been seen that increasing the filament temperature results in higher CH_3 as well [399].

CH_y species undergo further recombination according to the following reactions to form C_2H_x species.

$$CH_x + CH_y + M \leftrightarrow C_2H_{x+y} + M \quad (3\text{-}4)$$

$$CH_x + CH_y \leftrightarrow C_2H_{x+y-1} + H \quad (3\text{-}5)$$

$$CH_x + CH_y \leftrightarrow C_2H_{x+y-2} + H_2 \quad (3\text{-}6)$$

These C_2H_x species can also cycle through a series of gas phase H-shifting [abstractions and additions analogous to reactions (3-2) and (3-3)]. C_2H_2 is the most thermodynamically favoured out of these C_2H_x species, at high gas temperatures [399]. C_nH_x species may also be created through similar recombination reactions and their numbers increase as the C mole fraction in the input gas mixture is increased.

Transport of these radicals within the chamber, for example, from the activation or the mixing zone closer to the surface of the substrate happens by diffusion, in low pressure techniques. The geometry of this transport is unique for a specific deposition technology (for example, although diffusion occurs in HFCVD systems, in plasma jet or torch systems, the mechanism is convection). What is common though is that the transport time is much longer than characteristic time for hydrocarbon radicals to react with H atoms. As a consequence, these radicals coupled by H transfer reactions quickly equilibrate and their distribution depends directly on the atomic H to molecular H_2 ratio at that location [406].

As one moves away from the filament, the temperature of the gas drops from around 2273 K at the filament to about 773 K at a distance of 20 mm from it [399]. At low gas temperatures, atomic H drives $C_2 \rightarrow C_1$ gas conversion via multi-step sequences, whereas, at much higher gas temperatures (near the HF, for example), unimolecular decay of C_2H_6 [reaction (3-7)] and reactions of the type reaction (3-8) dominate] [399].

$$C_2H_6 + M \leftrightarrow CH_3^{\circ} + CH_3 + M \quad (3\text{-}7)$$

$$H + C_2H_5^{\circ} \leftrightarrow CH_3^{\circ} + CH_3^{\circ} \quad (3\text{-}8)$$

The three-body additive reaction following (3-3) is sufficiently fast at low temperatures, and becomes an efficient source of the CH_4 molecules. These molecules diffuse into the filament region and through an abstraction reaction following (3-2), re-convert to CH_3 radicals. These reactions are presented below.

$$CH_3^{\circ} + H + M \leftrightarrow CH_4 + M \quad (3\text{-}9)$$

$$CH_4 + H \rightarrow CH_3^{\circ} + H_2 \quad (3\text{-}10)$$

This discussion shows that there is much inhomogeneity in the gas phase composition within an HFCVD reactor, due particularly to atomic H concentrations and gas temperatures. It is important to note that detailed studies of the gas phase chemistry prevailing in HFCVD (and precursors containing more than C, H, and O, in the case of MWCVD) that contain B, N, S or P sources, with very few exceptions [407-409], are missing. However, from the above discussion, some important factors related to the optimization of the diamond growth process can be gathered. For example, irrespective of the hydrocarbon source, there is similarity in the relative species concentrations, both in the immediate vicinity of the HF and in the

region of 4-10 mm from it, which is where diamond deposition typically occurs [399]- hence the starting ratio of H_2/hydrocarbon as well as the distance between filament and substrate holder are both important factors. Another important factor is the filament temperature, and rate of gas flows during the CVD growth of diamond.

3.2.2 Surface kinetics and growth

Studies both experimental [45, 397, 404] and modelling [403, 410, 411] have indicated that the most abundant active species at the diamond growth surface are atomic H, CH_3 radicals, and C_2H_2. The role of atomic H is particularly important, not just as seen in the previous section, in the gas phase chemistry and kinetics, but during diamond growth as well. This is because it is simultaneously responsible for passivating the diamond surface and activating surface sites for subsequent growth reactions. The 'standard model' of diamond CVD [400] proposes that the diamond lattice is stabilized and prevented from rearranging into graphitic C by its termination with H atoms (or similar chemical species). The temperature at the film level is too low for any further spontaneous bulk rearrangement to occur (i.e. below the Debye temperature of diamond) [400]. The Debye temperature is the temperature of a crystal's highest normal mode of vibration, and it correlates the elastic properties with the thermodynamic properties such as phonons, thermal expansion, thermal conductivity, specific heat, and lattice enthalpy, derived from the Debye model [412]; in general, a crystal with a large Debye temperature is a "stiffer" crystal, requiring higher energy for reconfiguration of its lattice units. Although simplistic, the standard growth model, that has been around since the 1990s, has been very successful in predicting morphologies observed in typical diamond films [393]. It is also useful to understand the basic processes involved in the thin film growth of diamond before more complicated, stereo-specific cases can be considered. A common assumption made in the standard growth model for thin film HFCVD diamond growth is that there is no significant ionization accompanying filament activation and that C species are added to an electrically neutral, non-stereospecific diamond surface [406, 413]. In the following discussion, surface kinetics according to the generic growth model at the [1 0 0] surface is presented. Incorporation of C atoms into the diamond lattice happens through the deposition of CH_3 and C_2H_2 onto the substrate surface. Spectroscopic studies at the substrate surface have shown that larger hydrocarbons were present only in trace quantities and did not contribute in any considerable way towards the diamond growth [392]. The H atoms abstract H from the surface CH bonds, thereby creating more surface radical sites. Reaction (3-11) represents an activation of a surface site by removal of a surface H atom from a C atom on the diamond surface (C_D). An activated surface site is required for further hydrocarbon addition. This happens when these radical sites occasionally react with gas phase C-containing species, resulting in further adsorbed C. These C-containing species are either a radical ($CH_3°$, for example) or an unsaturated molecule (C_2H_2, for example), and the ensuing reaction is (3-12). It has been found, however, that the concentration at the surface of the C_xH_y species, with the exception of CH_3, is several orders of magnitude lower than previously believed [411]. In general, this implies that reactions that involve direct insertion of C_1H_y (with y=0-2) and/or C_2 into surface C-H or C-C can be neglected and these species do not contribute significantly to diamond growth.

Because the concentration of C-containing species is less than that of atomic H, much more frequently, the radical sites are simply refilled by recombining with gaseous H atoms, reaction (3-13). This constant turnover of the surface-terminating species (H) further drives the surface chemistry to dehydrogenate the adsorbed C species and to incorporate C into the lattice. It is important to note though that the rate of the reaction (3-12), that is, the rate of adding C to the surface, is independent of the atomic H concentration [406, 414].

$$\mathrm{C_DH + H \leftrightarrow C_D^{\circ} + H_2} \quad (3\text{-}11)$$

$$\mathrm{C_D^{\circ} + C_xH_y \leftrightarrow C_D - C_xH_y} \quad (3\text{-}12)$$

$$C_D^{\circ} + H \rightarrow C_D H \quad (3\text{-}13)$$

When a hydrocarbon radical or molecule is added to the growth surface, this new C atom has one bond with the existing lattice. For it to be fully incorporated into the film, at least two more bonds need to be formed, such that the remaining fourth bond is made with the next layer of diamond film. For these two more bonds, a dehydrogenation step is required as the C atoms in the lattice are hydrogenated. For the dehydrogenation to occur, atomic H must be present, and the chemical process follows the reaction (2). As seen previously, this recombination is exothermic, consequently, surface heating via this recombination is a significant contribution to the heat flow in the diamond CVD process [406]. The kinetics of the adsorbed hydrocarbon species and an adjacent H terminated surface site ($CH \cdots HC_D$) are as follows:

$$CH \cdots HC_D + H^{\circ} \leftrightarrow C^{\circ} \cdots HC_D + H_2 \quad (3\text{-}14)$$

$$C^{\circ} \cdots HC_D + H^{\circ} \rightarrow CH \cdots HC_D \quad (3\text{-}15)$$

$$C^{\circ} \cdots HC_D + H^{\circ} \rightarrow C^{\circ} \cdots C_D^{\circ} \quad (3\text{-}16)$$

$$C^{\circ} \cdots C_D^{\circ} \rightarrow C - C_D \quad (3\text{-}17)$$

Reactions (3-16) and (3-17) are essentially the same reaction, and reaction (3-15) is the same as reaction (3-13). The sum of reaction (3-16) and (3-17) represents the incorporation of C into the diamond lattice, and the rate of this incorporation is dependent on atomic H concentration.

$$C^{\circ} \cdots HC_D + H^{\circ} \rightarrow C \cdots C_D + H_2 \quad (3\text{-}18)$$

This reaction (3-18) represents the incorporation of the desired sp^3 atoms in the lattice. At suitable substrate temperatures (typically around 973 K, standard HFCVD growth conditions) adsorbed C species migrate until they meet a step-edge and are added to the diamond lattice. The preferential adsorption of C species at the step edge occurs due to the higher concentration of the surface dangling bonds [415]. The typically elevated substrate temperatures found in HFCVD also allows for the migration of these C species across the surface until they meet such a step edge [416].

This generic growth model of CVD diamond (schematically represented in *Figure 3-3*) shows that under typical conditions:

- The fraction of open sites on the surface is independent of atomic H concentration, but dependent on temperature;
- The incorporation of C into the lattice depends on atomic H concentration;
- The quality of diamond increases with atomic H concentration and decreases with hydrocarbon concentration, i.e., $[C_xH_y]$;
- It has also been seen that the quality has a maximum and falls off at higher temperatures due to competing desorption and decomposition rates [406];
- There is surface termination by H, a plausible mechanism for which is the presence of dangling surface C bonds and C-C unsaturated bonds at typical CVD temperature; molecular H_2 reacts at these sites to produce a H-terminated surface [417, 418]

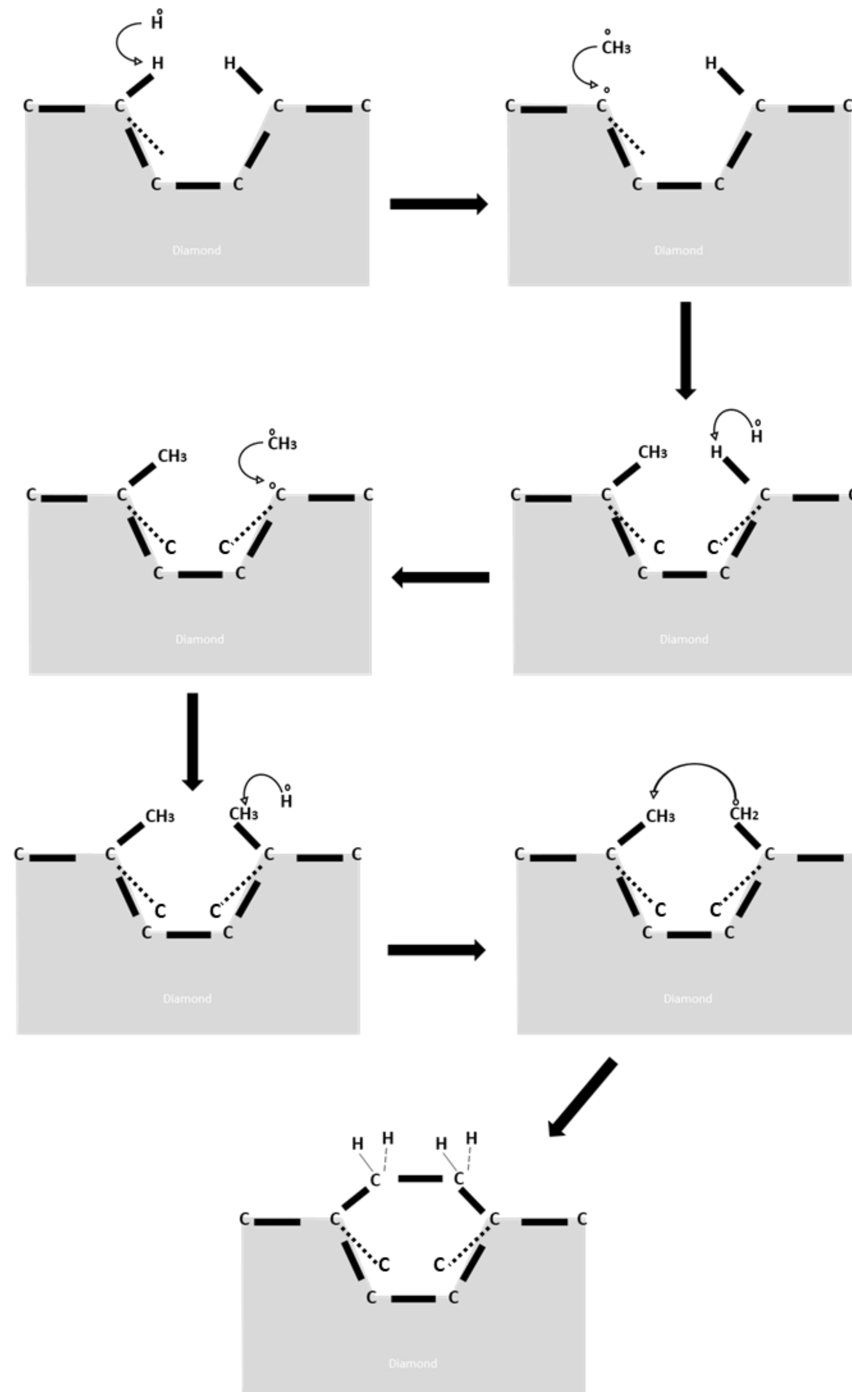

Figure 3-3 One of the possible procedures of diamond growth: Schematic representation of reactions (3-11) through (3-17) (Adapted from [419])

As long as the surface migration of the CH_2 radical (which is induced by H abstractions) is much faster than adsorption of CH_3, the aggregation of CH_2 bridge sites into continuous chains (i.e., void filling) provides normal layer-by-layer [1 0 0] diamond growth [420]. It must be kept in mind that this insertion of C atoms into the lattice cannot be random nor can they be added to sites on a hydrogenated diamond surface as both these cases will lead to an amorphous, lower quality film. It is here that the atomic structure of the surface plays an important role- it must be such that additions of atoms are directed to specific sites.

Because the different principal planes of planes of the diamond-like structure offer different types of vacant sites for C atom addition, the growth mechanisms on these principal planes vary [421]. These effects are particularly significant for diamond because of the high strength covalent bonding between C atoms. On the [1 0 0] planes as considered in the standard growth model, the attachment of single-C atomic species, such as C, CH, or CH_2, is energetically favoured because they can make two bonds with the surface [422].

As the ratio of gaseous CH_x /H increases (but not high enough to cause sp^2 deposition to dominate), the growth of the next layer might be initiated before all the voids in the current layer have been filled. Thus, depending upon the gas mixture and therefore, the relative concentrations of [H]/[CH_3], [C] +[CH]/[CH_3] for example, affects the probability of a re-nucleation event occurring and results in a modification of the average crystal sizes. The morphology of the subsequent film can thus be modified to be micro-, nano- or ultra-nano- crystalline [423]. Precise control of the crystallite size can be obtained by maintaining the deposition conditions in the appropriate atomic H and hydrocarbon ratios. For UNCD for example, this is done by introducing a non-reactive gas, the most common being argon (Ar), into the gas phase. The role of Ar in this case is to provide the third body, *M* [for example, in reaction (3-4)] increasing the dissociation of CH_4 near the filament and making available a high number of C_1 atoms that can then diffuse towards the growth surface [424]. It has been suggested that good quality facetted diamond occurs via adsorbed of C species migrating across the surface and adhering to step-edges, forming islands. The size of these islands varies depending upon growth conditions and can contain tens or hundreds of C species for SCD or MCD, but as little as 5 for NCD [425]. One of the biggest drawbacks of the standard growth model thus far discussed is its inability to predict crystallite size of the resulting film [426]; although, experimentally it has been well established, that tailoring of the gas phase concentrations near the growing diamond results in varying film morphologies- UNCD, NCD, MCD or a combination of these grain sizes, i.e., PCD. A good summary of the gas phase conditions that lead to MCD, NCD or UNCD films can be found in the reference [423].

Solely the addition of C atoms to the growing diamond lattice is not the entire picture of diamond growth in CVD. It is well known that CVD diamond growth is accompanied by deposition of impurities, present primarily as sp^2 species, and that the quality of the film is determined by the ratio of the sp^3 to the sp^2 atoms in the film, a better quality film having a higher ratio of the same. An important part of the diamond growth process is thus the etching of the defects and non-diamond phases in the group, which is what leads to good quality diamond films and not DLC films instead. Uni-molecular decomposition of the $C^{\circ}\cdots HC_D$ entity, by desorption of a hydrocarbon, creates sp^2 lattice bonds that appear as defects in Raman spectrum of the film [427]. As the CH_4 amount in the deposition plasma is increased, it has been observed that the contributions of the sp^2 phases increase and manifest as a gradual broadening of the G and D bands [428] (around 1580 and 1375 cm^{-1}). In addition, the peak of SCD i.e., the sp^3 phase [429] (around 1332 cm^{-1}), also broadens and decreases as the CH_4 amount increases.

$$C^{\circ}\cdots HC_D + C_xH_y \rightarrow C_xH_y - C\cdots HC_D \quad (3\text{-}19)$$

$$C^{\circ}\cdots HC_D \rightarrow C_DH + C_2H_y \quad (3\text{-}20)$$

$$C^{\circ}\cdots HC_D \rightarrow C_{defect}\cdots HC_D \quad (3\text{-}21)$$

H atoms can etch graphitic or sp^2 carbon more efficiently and successfully the sp^3 diamond atoms [29, 411, 422, 425, 430]. This is yet another important role of the H atoms in the low pressure synthesis of diamond. As long as there is a flux of the H atoms on the growth surface, non-diamond C is etched away and sp^3 C left behind. It is known, however, that the rate of etching of sp^3, although negligible depending on the local environment, is not zero . Studies of etch rates of diamond using pure H_2 gas, under otherwise similar conditions to those used for diamond CVD, show that this non-zero rate is a little less than 10 nm/hour [431]. This etch rate is however does not have the same value for the different planes of the

diamond surface- sp^3 atoms are etched away much faster from the [1 0 0] flat diamond terraces than those that are adjacent to a step edge [430]. This preferential etching is also seen to contribute to the step-edge growth discussed earlier.

It is important to note that there exists literature that does not support the theory of preferential etching by H atoms to explain the kinetic competition between diamond and non-diamond phases. Instead, they establish the critical role of aromatics condensation and interconversion of sp^2 and sp^3 C phases mediated by H atoms [410, 432-434]. These studies have not been covered in the presented review of diamond growth processes as they have received much less citations in scientific literature.

3.2.3 Nucleation processes

Hetero-epitaxial growth of diamond can be obtained on any non-diamond substrate that can endure, without disintegration or degradation, the CVD process conditions, and thus, has been used to obtain diamond films on various substrates. Hetero-epitaxial growth thus does not typically face the same limitations in size that are encountered in the homo-epitaxial growth of diamond on SCD. For the hetero-epitaxial growth of a diamond film, there must first be nucleation on the substrate. Once the substrate surface is nucleated, the predicted evolution of crystallites from random oriented seed crystals exhibits a columnar growth [435], as can be expected in the absence of re-nucleation processes following the van der Drift model. Once the film is closed, diamond grows homo-epitaxially on the individual crystal facets of this closed film and the process continues. A detailed understanding and control of the fundamental phenomena associated with diamond nucleation is therefore essential for optimizing the diamond film properties such as thickness, grain size, ratio of grain to grain boundaries, orientation, growth rate, adhesion, and roughness.

Some researchers have studied the spontaneous nucleation (i.e., formation of a stable agglomeration) of diamond in the gas phase itself occurring at pressures typical during CVD processes [410, 436, 437] with the speculation that the nuclei formed in the gas phase may reach the growing surface and increase the surface nucleation. However, it is important to note that these studies were made in RF plasma using various C containing gases as precursors, and not under typical HFCVD conditions. For the HFCVD growth of diamond, surface nucleation processes are of utmost importance. Nucleation processes for the growth of diamond on non-diamond substrates have commonly involved an intermediate layer of DLC or of carbides or graphite, formed at the substrate surface by chemical interactions with the activated gas species and the surface during the incubation period. These intermediate layers provide nucleation sites for diamond crystallite growth [438]. Which of these processes actually occurs during the HFCVD growth of diamond depends primarily on the type of substrate but also on deposition conditions such as the ratio of hydrocarbon to H_2 in the pre-cursor mixture [439]. Nucleation of diamond with an intermediate layer of carbide has been observed for the growth of diamond on Si [440] with further evidence from an atomic force microscopy (AFM) study [441]; these studies have been carried out in both HFCVD and MWCVD [442, 443]. Such spontaneous nucleation phenomena- such as the formation of a graphite deposit or DLC do not provide a nucleation density high enough for efficient growth of good quality PCD films. Hence, numerous nucleation enhancement methods [439, 444-446] have been developed that have allowed researchers to increase the density from 10^5 per cm^2 on untreated substrates up to 10^{11} to 10^{15} per cm^2 on treated substrates; the more commonly used techniques are listed below-

- Spraying/dip-coating with diamond nano-particles

  An obvious approach to enhance diamond nucleation densities is to coat the substrate surface with as many diamond particles as possible, which act as the seeds for epitaxial growth, by spraying them on or dipping of the substrate. Proof of this epitaxial growth is clear from such work as Geis *et al*. [447] who showed that [1 1 1] textured diamond films followed the seed texture; this is probably the earliest example of seeding by dip-coating diamond particles. Diamond

particles can also be sprayed directly on to the substrate to obtain more uniformity [448]. The main advantage of this method is that it does not damage the substrate surface and can be used on three-dimensional surfaces. The disadvantage, however, is the difficulty in ensuring a uniform distribution of the diamond particles [449].

- Mechanical abrasion techniques (scratching)
  An enhancement of the nucleation density by several orders of magnitude has been obtained by scratching the substrate with diamond powder, a technique that has existed for almost 40 years now [450]. This enhancement has also been noticed when non-diamond particles are used but with much less efficiency. The enhancement can be explained by the fact that spontaneous nucleation of diamond crystals is mostly observed on defects on these mechanically damaged wafers, such as in scratches, pits, on grain boundaries etc. [31, 451]. However, the principal mechanism behind the nucleation enhancement is the embedding of small residual diamond particles in the substrate, making the process far more efficient when using diamond particles in the polishing pad or cloth etc. [449]. Alternatively, vibrating and grinding methods have been used to enhance nucleation making use of diamond and non-diamond nanoparticles, that led to improved adhesion of thus grown films to substrates [452]. Smaller diamond particles generally result in higher nucleation densities and better uniformity [453], presumably due to the larger surface to volume fraction of finer scratches and the increase of residual diamond [449]. The main disadvantage of this technique is that it cannot be used for substrates with features as it is highly damaging to the surface. It can also not be used to treat three dimensional surfaces.
- Ultrasonic (US) particle treatment
  Micro-chipping happens to substrates that undergo an US treatment in diamond slurries of a larger grit size and it has been shown to enhance nucleation densities significantly [454]. The mechanism of this technique is very similar to that of mechanical abrasion, with the advantage of better uniformity and reduced damage to surface features. By immersing a substrate into a slurry of micron sized diamond particles, the cavitation of the ultrasound causes similar damage to the substrate as the abrasion processes and also embeds diamond fragments. High resolution transmission electron microscopy (HRTEM) investigations have shown that the predominant nucleation mechanism is homo-epitaxial growth on residual diamond embedded into the substrate [455], i.e. almost identical to the mechanical abrasion techniques. This technique when performed with diamond nano-particles, has resulted in very good nucleation densities, because the substrate surface is enriched by their uniform dispersion over the surface [456].
- BEN
  To perform BEN, the substrate, which must be conductive, is negatively biased by around 100–250 V DC with respect to the (grounded) chamber or a second internal electrode. This process is generally carried out under rather CH_4 rich (4–10% in H_2) conditions as compared to diamond growth otherwise and is most routinely used in MPCVD [457], although it may also be executed in HFCVD [458] and DC plasma CVD [36]. The mechanism behind BEN is generally accepted to be based on the sub-plantation model [458] according to which, incident CH^{x+} ions have an energy distribution of around 80 eV, which is close to the optimum to sub-plant them into an amorphous C layer. The nucleation sites originate from the formation of pure sp^3 C clusters in the layer. High substrate temperature causes annealing of the faults under the presence of H_2 and this results into the growth of these clusters via the transformation of amorphous C into diamond. The main advantage of BEN is that it is *in situ* whereas the main disadvantage is in the limitation it imposes on the substrates, that need to be conducting in order for it to be applicable. In addition, this method may damage the substrate- surface damage; holes as deep as 2–3 mm and as large as 200–300 nm in diameter have been reported on Si substrates [459].

3.2.3.1 Novel nucleation procedure (NNP)

This section details the NNP used throughout the current work that combines the US treatment with a unique PT method for substrates in order to greatly improve not just the nucleation densities but the interface quality and uniformity of the film itself. The indicators that are commonly used to evaluate the efficacy of a seeding method include the seeding or nucleation densities, which are often regarded as parameters that should be maximized for a particular application. While it is widely accepted that an increase in the nucleation density leads to facilitated growth of diamond on non-diamond substrates [460-462], this is not the only parameter to be considered when diamond films are to be used in electronics applications such as passivation or heat dissipation layers. As the seeded substrate is introduced in the CVD system, the nucleation seed centres grow three dimensionally until they coalesce with each other; once this happens they kinetically restrict the supply of gas radicals approaching the substrate, creating a void [53]. The gas radicals trapped in these crevices can then coalesce in to a non-diamond phase (graphitic or amorphous C) [463]. When the purpose of the diamond layer is passivation of electric defects or extraction of heat, these voids (as the ones reported in [463, 464]) have an obvious detrimental effect in the quality of the interface. In addition, the boundaries between individual diamond nuclei are saturated with non-sp^3 bonds; as a consequence, a very large nucleation density usually coincides with a high percentage of non-diamond bonds. This again is a detrimental factor both for electric passivation or heat extraction; on the one hand, if the density of grain boundaries is high enough, the latter may provide channels through which the charge carriers can flow [151, 465] as was discussed before in section 2.5.3; on the other hand, the grain boundaries induce phonon scattering and also compromise the thermal conductivity of the films [466].

Both the existence of voids and the high density of grain boundaries at the nucleation surface can be diminished if, during the initial stages of diamond deposition, the lateral growth of the grains is enhanced. This can be achieved by performing the PT of the substrate surface by exposing it to typical diamond growth conditions for a short period of time, prior to the standard US seeding (with diamond grit or nanoparticles). This procedure, often referred as NNP in the literature, enriches the surface of the substrate with a nm-thick C layer that improves the dispersion of the diamond particles during the seeding procedure and induces a lateral growth mode during the early stages of diamond growth, which in turn accelerates grain coalescence and diminishes the number of voids. This was experimentally verified by Sumant *et al*. [56], who studied thoroughly the nucleation surface of NCD films deposited on previously pre-treated and seeded with diamond nano-powders Si substrates; the roughness of the nucleation surface was as low as 0.3 nm and had only a slightly higher sp^2 content- 1.8%, in comparison with 0.7% on the top side.

The NNP process comprises the following three steps:

(i) Formation of a thin C film by exposing the surface of the substrate to the growth conditions (GC) for a brief period of time (15 to 60 minutes, after which a thickness of 15 nm is reached by the thin C film and no more C is observed as being added [53]). This step is called the PT.

(ii) Seeding in an US bath with a suspension of diamond grit or nanoparticles of diamond (ND) in an organic solvent; in practice, the NNP can be modified to include as step (ii) any of the other nucleation techniques listed in the previous section, except BEN.

(iii) Diamond film deposition under standard CVD GC. The GC are the standard parameters (gas composition, pressure, MW or HF power and substrate temperature) that result in diamond deposition on a seeded surface. It is a common belief that the CVD growth process requires an incubation time in order to saturate the surface with C, before film growth starts to occur [467]. In the regular growth case, C is supplied only from the gas phase and the incubation time is in the order of 15–45 minutes; however, when NNP is used, the C present in the PT film allows the start of crystallite growth with a minimal incubation time. The PT film can be considered as a local C source that ''feeds'' the crystallite growth front- indeed it is, as was experimentally verified in a very interesting study [53]- which used $^{13}CH_4$ gas to

perform the PT, followed by seeding, and an initial growth under atypical GC- in a pure H_2 plasma for 10 minutes. This exposure resulted in small individual diamond crystallites formed on the small seeds left from the US treatment- as there was no other C source in the system to support the small diamond crystal formation, it must have come from the PT film, in fact, the diamond Raman peak (more details about Raman spectroscopy for the characterization of diamond can be found in the latter part of this chapter) for these crystals was positioned at 1280 cm^{-1} where it is expected to be for a ^{13}C isotope-enriched diamond crystal.

The primary advantage of the NNP is that it greatly enhances the nucleation density and uniformity of films- because of step (i), crystallites start to expand laterally, avoiding the formation of the crevices that usually appear on the nucleation surface, unlike the van der Drift model. The diamond/substrate interface of films grown under NNP is thus expected to be much smoother than the interface obtained with the USP alone. The above discussion serves to justify the usage of the NNP in order to optimise the growth of diamond films for electronics applications, in the current work.

3.3 Doped diamond

Doping is achieved by incorporating certain impurity atoms at sites in the diamond lattice where they are electrically active; these impurities should be compatible to diamond in their physical size to not disturb the diamond lattice itself. Impurities incompatible in this regard or unwanted impurities (i.e. those that do not occupy a substitutional site in the lattice) may generate additional defects, which can yield levels deep in the bandgap susceptible to compensate or trap the original useful carriers. The distribution of the impurities must also be uniform through the so there is no accumulation or segregation in certain sites.

The desired properties in a diamond film depend on its application. Consequently, the growth process has to be appropriately tuned- in order to obtain p-type doping in diamond commonly used dopants is B. The primary challenge in the doping of the diamond lattice is the small covalent radius of C (0.077 nm). While the small covalent radius of B (0.088 nm) allows for its substitution in the C, the space is not sufficient for the substitution of another atom of the third column, say, Al (0.118 nm), Ga (0.126 nm) and In (0.144 nm). Because of the higher covalent radius of B (0.088 nm > 0.077 nm), it is expected to expand the diamond lattice. This results in it having striking effects on the structural properties of the films, including ultimately the stability of the diamond phase [468, 469].

The doping of synthetic diamond with B can be done during HPHT synthesis [470], via the gas phase [471], and by ion implantation. Commercially available p-type BDD substrates are prepared by the HPHT method [372]. However, this method has practical limitations in terms of the size of the substrate [472]. The technology of ion implantation is mature for Si, but because diamond is metastable, there might be conversion to graphite during the process or during post-process annealing; it still is a widely investigated and used technique to obtain p-type BDD [473]. The doping of PCD CVD diamond films by B ion-implantation [474, 475] has yielded results comparable to those obtained for single crystal type IIa diamonds, albeit with poorer electrical properties. This indicates that the technology developed for implantation doping of SCD, although leaves much room for improvement, is also applicable to implantation doping of CVD diamond films, a finding that obviously has some important technological implications for the industry.

The CVD growth of diamond allows for it to be doped and this incorporation of B from the gas phase in to the solid phase is highly efficient [469]. Hence, methods to obtain p-type BDD using low pressure techniques have been widely studied. B can be introduced in the gas phase from various precursors. Amongst low-pressure methods, MWCVD has been known to lead to soot formation when preparing p-type layers with a high doping level [472]. This limits growth itself, and possibly becomes an origin of non-epitaxial components. In HFCVD, this problem is avoided even at high doping levels; using the method, resistivity of 1 mΩ cm in BDD has been obtained with a doping level of 10^{21} cm^{-3} [476]. From a model based

on step-flow motion, the lifetime of B-related molecules (τ) on the terrace surface was evaluated; it was found that for HFCVD, τ was ~13 times higher than MWCVD. A consequence of this observation is the longer migration length of B-related molecules in HFCVD than in MWCVD, which limits B incorporation in the latter. In fact the higher flux of atomic H, the very factor that leads to higher growth rates of undoped diamond films in MWCVD has been seen to hinder the growth rate of doped diamond films, by causing surface etching [407].

In order to initiate the growth of BDD on a foreign substrate, similar to undoped film growth, a nucleation step is mandatory. Most work on BDD typically uses the standard seeding procedures [477-481] listed in section 3.2.3. The NNP for BDD has also been investigated but admittedly not for Si substrates nor PCD films. It has been used to enhance the nucleation density prior to NCD BDD growth on Pt electrodes [482]. NNP for BDD has been investigated in the current work and results are presented in the next chapter.

To grow BDD using CVD, B_2H_6, or B_2O_3 oxide dissolved in CH_3COCH_3, C_2H_5OH or CH_3OH, or equivalently $B(OCH_3)_3$, C_3H_9B, $C_6H_{15}B$ have been used to introduce B in the gas phase [469, 483]. Hence, it can be seen that the B source introduces in addition to the B and C species, H_2 or O_2 depending on the source and solvent used. This implies that growth occurs either in B-C-H or B-C-H-O chemistries. The gas phase chemistry and therefore factors such as growth rate and crystal quality of the film thus changes profoundly when growing BDD using HFCVD [484].

When B_2H_6 is added to the gas phase for example, BH radicals are detected. Besides the appearance of this new species, the intensities of the other species are also modified. The [H]/H_2, [CH]/[H] and [CH_2]/H ratios are observed to decrease with the addition of B_2H [485]. In the absence of a definitive model for the growth of BDD in B-C-H chemistry, it has been speculated [485] that the decrease in the concentrations of the aforementioned species diminishes the rates of the reactions (3-2) (H-abstractions) and (3-12) (surface activation). Hence, the addition of B in the gas phase, in general, has a negative effect on the growth rate of diamond. In addition, for B-C-H chemistries, it has been seen that the B concentration in the film increases with the square of the B concentration in the gas phase [486], suggesting that the incorporation of B in the growing film involves a bimolecular process at the surface, i.e., two BH species are needed at the surface to incorporate one B atom in the solid phase.

In the case of B-C-H-O chemistries, it has been speculated [487] that similar to B-C-H chemistries, addition of B here too has a detrimental effect on the growth rate of diamond. The same study also concluded that in addition to diamond growth radicals and B atoms, O_2-rich compounds such as B_2O_2, CO and CO_2, are also present in the gas phase and interact with the substrate and the growing diamond surface. As a result, it was seen that in contrast with undoped CVD diamond growth where there is a surface H-termination, the surface termination for these films included O_2.

It has been seen, however, that low level addition of B (<500 ppm B/C) increases the diamond crystal size as well as growth rate [488]. Furthermore, a linear relation between the concentration of incorporated B and the B/C ratio in the gas phase up to 4000 ppm B/C has been found [489]. However, addition of B at intermediate levels (1000–4000 ppm B/C) results in p-type BDD thin films that have all other crystalline characteristics similar to undoped diamond films i.e., without B addition in the gas phase. Addition of B at high levels (>4000 ppm B/C) results in the loss of crystallinity with increasing graphitic content and reduced B-incorporation [488, 490]. It is important to note that these trends are observed for the HFCVD growth of hetero-epitaxial growth of BDD on non-diamond substrates. For homo-epitaxial growth however the B incorporation in films as well as the growth rate has been seen to increase monotonously with increased (B/C) gas up to almost 13000 ppm B/C without loss in crystal quality or observance of any soot [407, 468, 490].

In general, during the synthesis of BDD films, the filament temperature shows a strong influence on diamond growth rate and morphology, indicating that gas phase reactions activated by the filament, have a favourable effect on the growth rate of diamond deposition [484], whereby, the growth rate and phase purity in the presence of B is also more sensitive to surface temperature than for undoped diamond

growth. Incorporation of the B atoms into both the growing [1 0 0] and [1 1 1] diamond thin film surfaces has been obsevered and the incorporation at the [1 1 1] surface has been found to be almost 10 times greater than that at [1 0 0] surfaces [491-493].

3.4 Characterisation of CVD diamond

Through the characterisation of diamond films obtained with CVD growth, vital information about the efficacy of the deposition process can be obtained. Characterisation techniques help to identify the quality of the film obtained as well as classifying the grain size of the diamond in the film, in order to be able to classify it as UNCD, NCD, MCD or a combination of these grain sizes, PCD. This information is important because the electrical and thermal properties of the diamond films are intricately related to these characteristics-the ratio of the sp^3/sp^2 content, grain size, average film surface roughness and film thickness. One of the most useful aspects of such characterisation is that it divulges the correlation of the characteristics of the film with the CVD parameters used, a very important tool in the optimisation process. This section presents some of the most useful techniques that one may use to obtain and analyse such information from CVD grown diamond films.

3.4.1 Optical microscopy

Optical microscopy is the usually the first step in studying the surface of diamond films and can provide images up to 1000x in magnification. Hence, although it is a good tool to study superficial features about the film surface, it does not provide any other information about the film quality. Because the standard optical microscope uses visible light and because of the wave nature of light, the resolution of the light microscope cannot be smaller than the half of the wavelength of the visible light, i.e., 0.4-0.7 µm. Diffraction restricts the ability of optical instruments to distinguish between two objects separated by a lateral distance less than approximately half the wavelength of light used to image the specimen, i.e., 0.2 µm. That being said, the technique is useful because it involves minimal surface preparation, and provides real time image acquisition. It is also useful to identify points of interest on a film that can later be seen under an electron microscope. By using interference, one can also obtain colour images that provide information about the roughness of the films. With image processing software, one can also utilise the magnification to quantify features of the sample.

In the current work, optical microscopy (Eclipse E200 upright microscope) was a frequently used technique to confirm the presence and uniformity of diamond films immediately after deposition, for example, as shown in *Figure 3-4.* In addition, it was used to measure lengths of features on the substrate surface, where applicable.

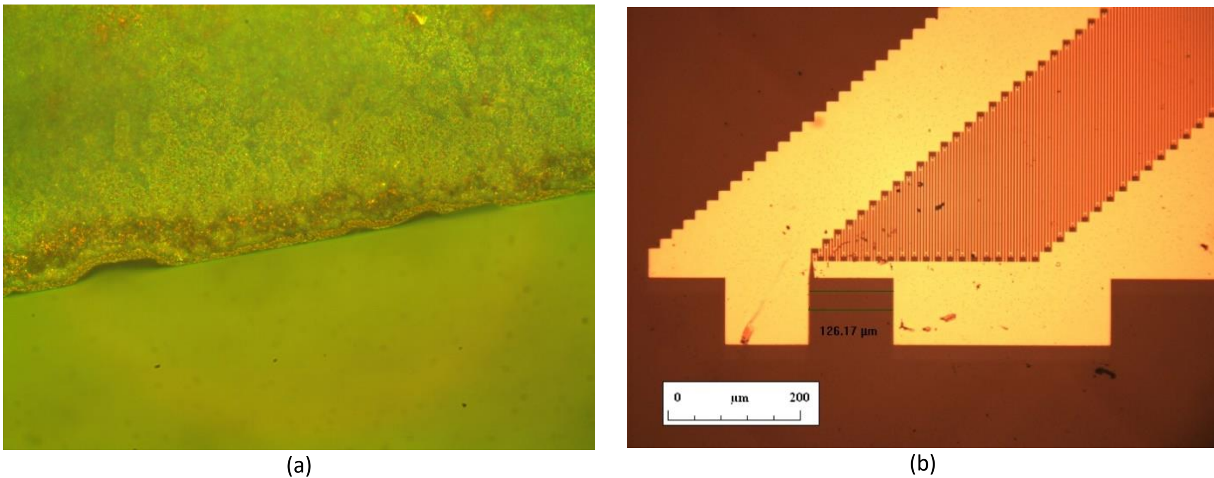

(a) (b)

Figure 3-4 (a) An optical microscope image at 40x magnification of edge of a diamond film (b) Using an optical microscope to measure feature dimensions of a SAW device

3.4.2 Optical profilometry

Non- contact, optical profilometry at its current state of the art can provide profiling with excellent measurement repeatability. It can detect vertical feature heights down to 1 nm and lateral features down to 10 nm. In order to obtain the best precision-accuracy ratio for the measurements a suitable scan speed (where resolution maybe be traded for throughput and processing algorithm must be chosen. The profilometer must be protected from systemic problems that can influence measurements such as temperature drift during a measurement, acoustic noise, or floor vibration.

In the current work, optical profilometry was utilised in two main stages of the work- to validate the growth of patterned diamond on SAW filters and to measure thickness of the electrical contacts for the diamond semiconductor heterojunctions, both of which are presented in the next chapter. To determine the efficiency of patterned diamond growth on SAW devices, for example, measurements were made on various different spots of the film with an average of 5 measurements per spot to confirm the uniformity of films. *Figure 3-5* shows some of the typical images obtained for the films. All profilometry measurements presented in this work were obtained using the Sensofar S Neox instrument.

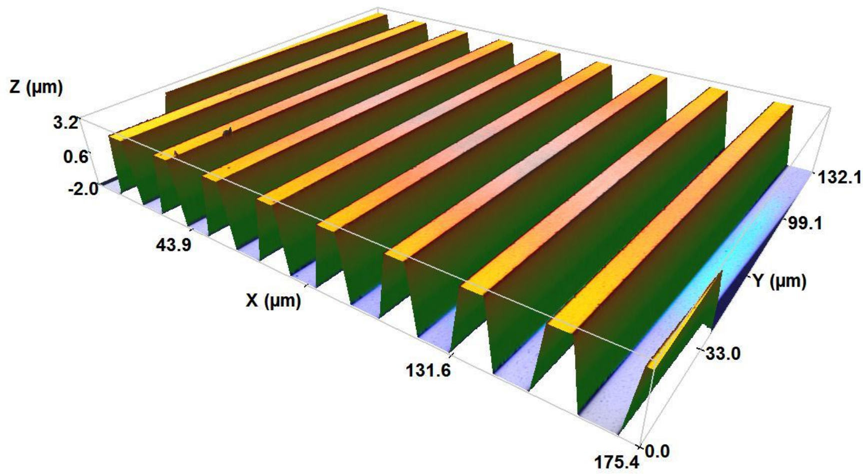

(a)

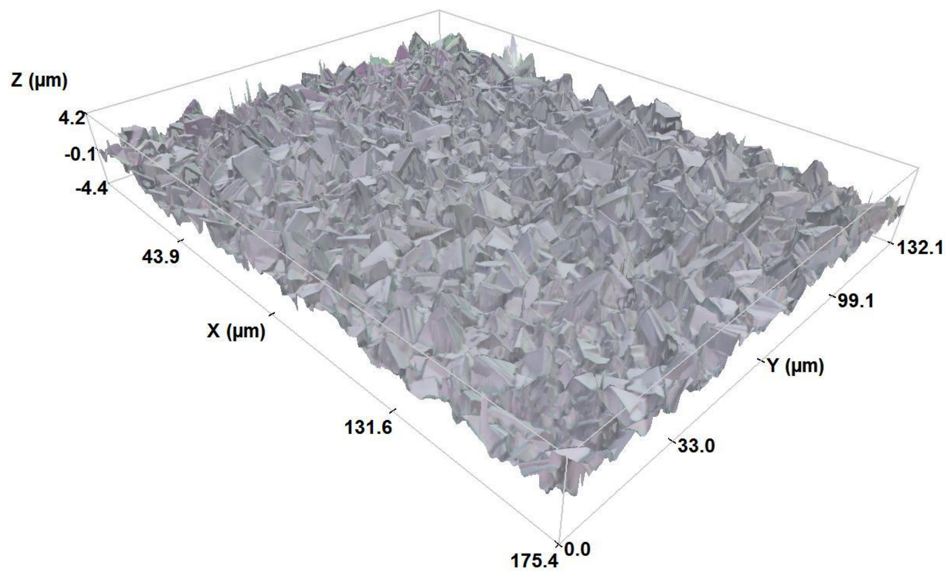

(b)

Figure 3-5 Optical profilometry of film surfaces provide information about thickness of films as well as (a) sizes of features and (b) surface roughness

3.4.3 SEM and EDS

Scanning electron microscopy (SEM) is a very useful technique to study CVD grown diamond films; it can not only provide topographical information about the films, which itself can contain information about the roughness of films, presence of grain boundaries, presence and type of defects, but can also be used to make qualitative analysis of the diamond films. Although unlike spectroscopy, SEM does not allow one to measure the percentage of diamond and non-diamond phases, using the EDS (energy dispersive x-ray spectroscopy) mode one can detect heavier imourities that may have been incorporated into the films during the deposition process.

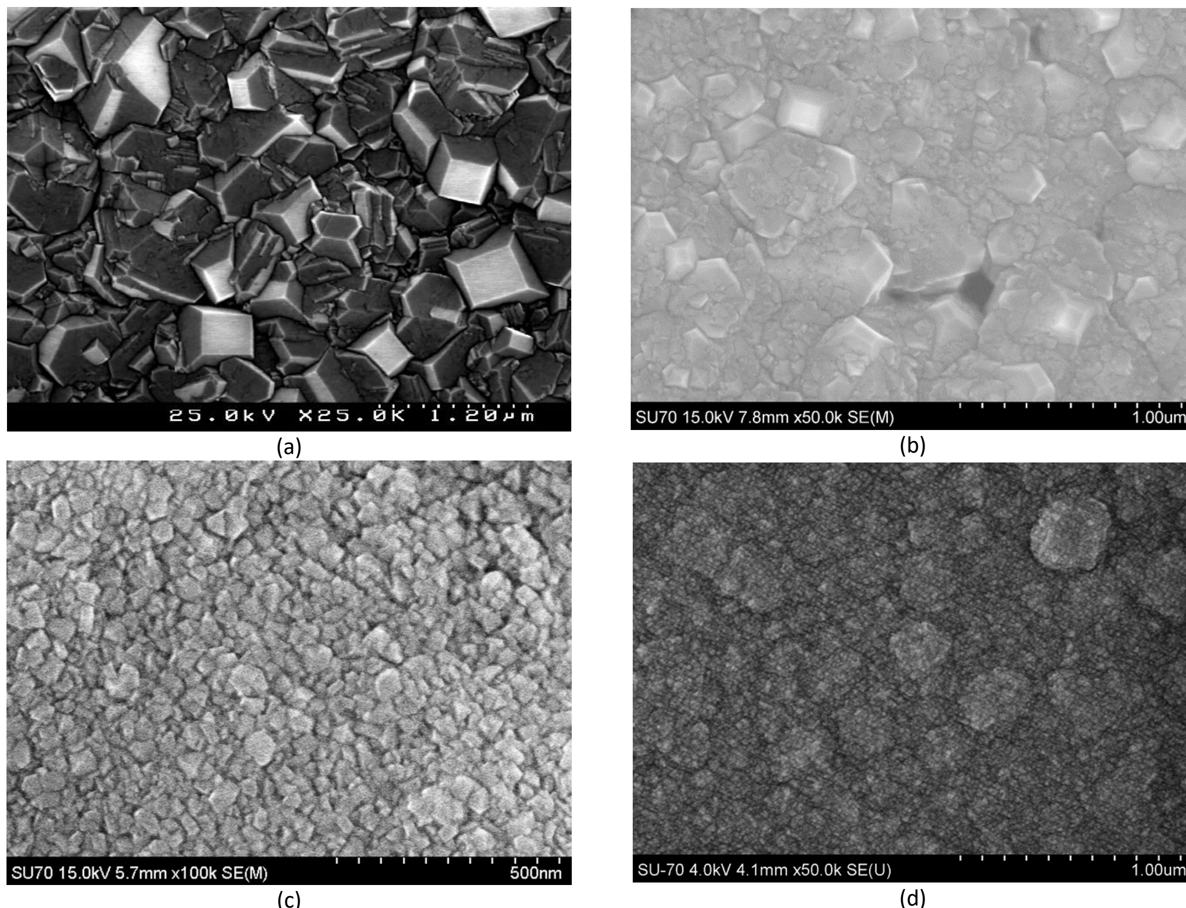

Figure 3-6 SEM images of the surface of the three types of diamond film: (a) MCD, showing randomly-oriented grain sizes around 1 µm, (b) PCD, with a mixture of grain sizes (c) NCD with grain sizes between 50-100 nm (d) UNCD showing typical cauliflower growth with grain size below 50 nm

A state of the art literature survey of CVD diamond growth almost always throws up research where SEM has been used to see the morphology of films obtained [494-500]. It has been used to study the evolution of diamond films during the CVD process- from the state of grain growth from early onset, to formation of diamond crystals and followed to full growth of diamond films [499]. It is known that changes in the parameters of the CVD process result in changes in characteristics of the resulting diamond film. SEM allows one to see how these changes are manifested morphologically. Furthermore, the characteristic of the films (i.e., the grain size) has been correlated to deposition parameters such as total pressure, precursor working gas, flow rates of precursor gases, substrate/deposition temperature, leading to invaluable knowledge about the CVD of diamond process itself. Signature characteristics of the various kinds of diamond films depending on crystallite size- UNCD, NCD, MCD and PCD films have been seen most clearly using the SEM [501] (*Figure 3-6*). Cross-sectional scanning electron images have been used to study the columnar growth of diamond films on [1 0 0] Si [502]. The technique has been used to characterise the morphology of not just diamond films, but more recently, p- and n-type doped CVD grown diamond crystals [498]. The EBIC (electron beam induced current) mode of SEM has been used to study the electrical and thermal properties of diamond [497]. In the current study, all SEM images were obtained exclusively using the Hitachi SU70 instrument or the Leo Supra 35. These SEM images were indispensable for this work- they were utilized at every step of the experimental work of optimizing the deposition process.

3.4.4 Raman spectroscopy

Raman scattering is said to occur when a beam of energy incident on a material is scattered in-elastically, causing a change in the frequency of the incident wave. Although only a small fraction of the incident beam undergoes ineleastic scattering (most of it being scattered elastically, with no change in frequency), the most intense Raman scattering happens in molecules with symmetric vibrations, inducing a large distortion of the electron cloud around the molecule. Raman spectroscopy is thus suitable for the highly symmetric covalent bonds that have little or no natural dipole moment- C-C bonds that make up C and organic materials, for example, allowing for this technique to be used for C-based materials to provide a wealth of structural information [503].

Raman spectroscopy is highly sensitive to the morphology of the material as well. Given that the vibrational frequency of a Raman band is highly sensitive to the orientation of bonds and the size of the bonded atoms, this technique can be used to characterise a whole variety of C nanomaterials. When it comes to characterising C nanomaterials, Raman spectroscopy is used to sort through the allotropes of C such as diamond and graphite as well as more complex structures such as CNTs, and fullerenes simply because this technique is sensitive to the intricate differences in the C-C bonds in these materials. These intricate differences are manifested in changes in the parameters typically obtained from a Raman spectrum-peak position, asymmetry and full width at half maxima (FWHM).

In the Raman spectra of two C allotropes – diamond and graphite –there are easily distinguishable characteristics. These differences arise from the difference in the hybridization of the C atoms in the respective molecules and as a result, the differences in the C-C bonds. Sp^2 hybridized C-atoms in graphite form a planar sheet in which the bond energy between the atoms in the sheets is quite high when compared to the sp^3 tetra-hedrally bonded C-atoms in diamond. In the case of graphite, where the sp^2 bonds have higher energy, the vibrational frequency is also consequently high, pushing the frequency of the band in the Raman spectrum to a higher frequency. A shift of the main band from the 1332 cm^{-1} peak for diamond to around 1582 cm^{-1} in graphite, is thus seen; this band is known as the the G band of graphite [504]. This elucidates the fact that the graphite spectrum has several bands and the presence of these additional bands are indicative of the existence of C bonds with several different bond energies [504]; from this it can be concluded as well that the graphite structure is not as uniform as diamond. The FWHM of the peaks and bands is commonly used to quantify the amount of disordelline material, with a greater FWHM signifying greater disorder [505].

The Raman spectrum of natural diamond was first studied by Ramaswamy in 1930 who noticed that it exhibits a single sharp and intense line with a frequency shift of 1332 cm^{-1} [506]. The Raman spectrum of SCD is dominated by the 1332 cm^{-1} line because this corresponds to the vibrations of the two interpenetrating cubic sub-lattices [507]. This study was followed by Robertson, Fox and Martin's 1934 study which also noted the 1332.2 cm^{-1} frequency shift at 293 K [508]. It is very interesting to note that these early experiments were made using a Hg arc to illuminate the diamond, quartz lenses being used for ultra-violet, and a glass condensing system for the visible region. To weaken the lines of the Hg arc for the limited range of the spectrum, some liquid cell screens containing $K_2Cr_2O_7$ and $C_2CoN_2S_2$ were used. With this instrumentation good photographs were obtained after 30 to 40 hours' exposure!

Robertson *et al.*, also noted that the Raman shift was not affected by lowering of temperature. In 1941, Nayar undertook the study of a number of diamonds and investigated the temperature variation of the frequency shifts and recorded a value of 1332.1 cm^{-1} at room temperature, and found it to diminish slowly at first but more rapidly later to 1316.4 cm^{-1} at 1130 K [509].

Raman spectroscopy has been widely used in the characterisation of diamond films; from the measurement of stress in diamond films [510, 511], to effects of the growth rate on film quality [512-514], texture of films [515], local crystal orientation [516], density of graphite-like defects in films [514], thermal expansion behaviour of natural and CVD diamond [517], to the effect of substrate position during film

growth on the film grown [485]. As can be seen from these references, work using Raman for characterising diamond films has been around for more than 20 years and has been very varied. In more recent years, Raman spectroscopy has been used to analyse the characteristics and quality of BDD [476, 518-520] as well as N-doped diamond [521], in addition to bringing further insight on how various synthesis methods influence quality of diamond films [522].

3.4.4.1 Undoped CVD diamond

In general, the applications of Raman spectroscopy in diamond film science were adequately summarised in a seminal paper by Prawer and Nemanich in 2004 [507] and they are listed as follows:

1) For measuring the phase purity and crystalline quality of CVD diamond
2) To investigate the dependence of films on stress and pressure
3) To investigate the phonon confinement effects for finite crystal domains
4) To make non-contact temperature measurements
5) To investigate probing defects and annealing
6) To investigate the doping of diamond films

The single sharp line of diamond at 1332 cm^{-1} at room temperature differs significantly from amorphous C, glassy C or graphite. It is important to note that CVD diamond films may not demonstrate the sharp line at precisely 1332 cm^{-1}. The diamond peak may appear at 1334 cm^{-1}, the difference suggesting the presence of internal strain and structural imperfections absent in natural diamond [32]. Hence, Raman spectroscopy is useful for the quality assessment of CVD diamond because it can divulge information about the “graphite-like” defects commonly encountered in this material and it is sensitive to the stress state and the size of the diamond crystallites [514]. It can also provide information about disordered crystallites present at the grain boundaries of CVD grown diamond films if a near-IR laser is used for excitation [501].

The peak position and width of the Raman line of PCD films depend on film preparation conditions and have been related to the structural order or crystallinity, temperature, defect density, and the distribution of the internal and/or external stress [523].

Different characteristics of CVD grown diamond films, such as the presence of NCD, amorphous diamond (sp^3 hybridized C, exhibiting non-isotropic hardness and strength, as opposed to diamond, whose mechanical properties are directional), hexagonal diamond (tetra-hedrally bonded sp^3 hybridized C but in a hexagonal unit cell), amorphous C and graphite etc. in addition to sp^3 diamond, each leave their own signature peaks in the Raman spectrum of a sample. By calculating the ratio of the intensities of the signals obtained from the integrated crystalline and amorphous phases, one can draw conclusions about the purity of the obtained diamond films.

One of the challenges in the analysis of the Raman spectra of CVD diamond films is their polycrystalline nature. Non-diamond layers produce many bands that overlap the areas of diamond peaks, hindering the identification of some species and parameters. Graphite-like defects that accumulate in the grain and twin boundaries also complicate matters. In addition, it has been noted that the wavelength of excitation used (the 2 most common being the Ar 488/514.5 nm laser and He-Ne 633 nm laser) resonantly enhance the Raman bands of non-diamond C to different extents [524]. Experimental observations made in this regard are presented in *Figure 3-7*, where the variation in the enhancement of the bands in PCD can be seen when the excitation wavelength is varied. In fact, most authors agree that the intensity of the Raman peaks varies with the excitation wavelength [525]; this phenomenon, interestingly, has provided a useful tool in the analysis of high quality diamond films by providing a basis for comparison [526].

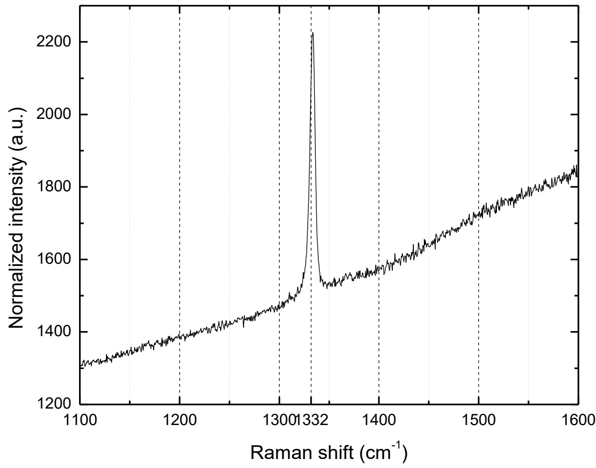

(a)

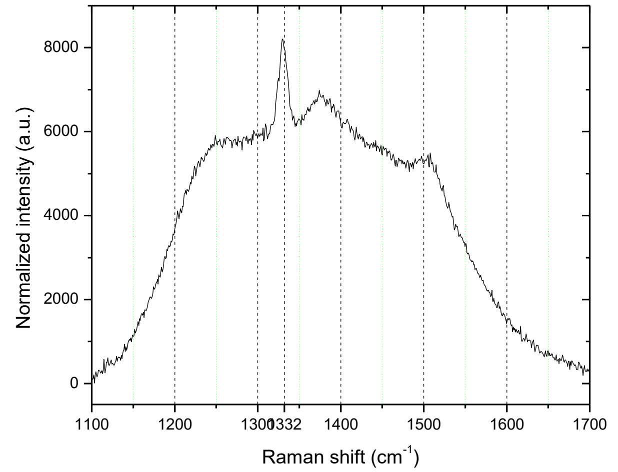

(b)

Figure 3-7 Raman spectra of CVD diamond film collected using (a) Ar (b) HeNe lasers. Note that both spectra show the SCD peak at 1332 cm^{-1}

When the parameters of deposition of the CVD process such as total pressure, flow rates of precursor gases, substrate/deposition temperature, substrate position are varied, the quality of the diamond films varies too. In order to use Raman spectroscopy to monitor these variations, the relative cross-sections for Raman scattering from diamond and non-diamond C need to be determined. Using a Ar^+ (514.5 nm), S. Sails *et al*. [526], obtained the following formula for a quality factor, *Q*, to encapsulate the difference in the diffusion of non-diamond vs diamond phases in diamond films grown using MPCVD:

$$Q = 100 \times \frac{I_{\text{diamond}}}{I_{\text{diamond}} + \frac{I_{\text{non-diamond phases}}}{233}} \qquad (1\text{-}22)$$

Thus, it can be seen that the contribution of non-diamond C to the Raman spectrum of a diamond film is 233-times greater than that from the diamond. Using this, one can determine a quality factor for diamond films that represents that actual percentage of diamond in the film. The FOM of the films need to be modified accordingly. This however is not representative of the absolute purity of the film since the non-diamond phases, in this study, were assumed to be only amorphous C. No differentiation was made between amorphous C (a-C) and graphite, i.e., the difference in the Raman cross-sections of a-C and graphite was not studied.

The spectral lines of most significance often obtained in CVD diamond films are summarised in the following table.

Peak position (cm^{-1})	Possible origin	Reference
520	1st order Si peak	[507]
1137-1170	Nano-crystalline diamond	[527-529]
	Amorphous diamond	[530]
	Presence of H_2	[531]
	1st vibrational mode of trans-$[C_2H_2]_n$	[532]
1240	2nd vibrational mode of trans-$[C_2H_2]_n$	[532]
1315-1326	Hexagonal diamond	[533]
1332	Sp^3 diamond/ good quality MCD	[510, 530]
1350	D band of graphite	[428]
1450	3rd vibrational mode of trans-$[C_2H_2]_n$ (at grain boundaries)	[532]
1480-1560	Amorphous C	[533]
1550-1580	G band of graphite	[427]

Table 3-2 Primary peaks in the Raman spectrum of diamond

As can be seen in *Table 3-2*, several of the peaks belong to microcrystalline graphite. The D band for example is evidence of disordered graphite, and this mode of vibration is absent in perfectly ordered graphite. Graphite-like defects present at grain boundaries strongly affect the intensity of the G-band [514]. Hydrogenated amorphous C has its signature peak at 1520 cm^{-1}. In low quality PCD films, bands associated with amorphous C and hexagonal diamond, that are considered pre-cursors of diamond by some authors, may be present [533]. The band that appears immediately before diamond is associated with hexagonal diamond. A commonly debated peak in the Raman spectrum of polycrystalline peaks is one that appears between 1137 and 1170 cm^{-1}. Some authors attribute it to nano-crystalline [527-529] or amorphous diamond [33]. Some also attribute it to the presence of H_2 in the grain boundaries of the films [531]. Yet others see it as the signature vibrational modes of trans-$[C_2H_2]_n$ chains (a chain of sp^2 hybridized C atoms with a single atom of H connecting them) [532].
The peaks in a typical Raman spectrum are often fitted with a combination of Gaussians and Lorentzians with a sloping background; this background is usually due to photoluminescence (PL) that arise due to several possible causes- as varied as Si or W incorporation into films. In the case of PCD, the PL is due to the recombination of electron-hole pairs within sp^2 bonded clusters and its intensity tends to increase with increasing H concentration [534]. This is usually addressed in the fitting step by subtracting a baseline.

3.4.4.2 Doped CVD diamond

The homogeneous doping of B in the diamond film is complicated because of the tendency of the incorporation of the B into the diamond lattice to be irregular. This is because of the prejudiced and higher incorporation in the octahedral facets of diamond [1 1 1] than in cubic facets [1 0 0] [488]. These differences of B incorporation in various crystal facets result in differences of the Raman spectra and the peak at 1332 cm^{-1} is strongly reduced [488] or shifted [535]. The parts grown via [1 0 0] facets contain at least one order of magnitude less B than parts grown via [1 1 1] and accordingly the latter facets exhibit deterioration of the Raman spectra [491]. Oftentimes, in order to remove added complications due to the presence of non-diamond phases in polycrystalline films, a number of studies that use Raman spectroscopy to evaluate B doping are carried out on epitaxial B-doped diamond layers [518]. Some studies have concentrated on individual crystals grown on Si substrates in order to avoid the local stress fluctuations caused by agglomerations of crystal grains [536]. Even so, there does not appear to be a single simple signature of a local Raman active vibrational mode corresponding to a B-C bond that can be used to assess the level of doping [507]. The signatures of doped films are necessarily much subtler, and involve interactions between vibrational modes of the lattice and the electric continuum of states due to the presence of dopants. Haubner and Rudigier [537] measured the same spot of a doped diamond film

sample with three different laser units (of wavelengths 472.681 nm-blue, 532.1 nm-green, 632.81 nm-red), providing insight into how the details of the Raman instrument itself are of importance when consulting the literature about the Raman spectrum of BDD. In general, the Raman peak due to the Si substrate decreases with increasing B concentration, as the doped material becomes more opaque at the wavelength of light used for the excitation [507]. In addition, for extremely heavily doped films, a wide signal at 500 and 1220 cm^{-1} dominates the spectrum, and although several hypotheses have been proposed, for example, to B-doped disordered diamond [538] or disordered graphite [491], the reasons for this occurrence are not yet obvious [539].
In the current work, Raman spectra of all samples, both doped and undoped were obtained using the Yobin Yvon HR800 spectrometer whereby spectra were excited with a 514.5 nm Ar+ laser focused to a 1 µm-diameter spot and with 5 mW incident beam power. The spectral resolution was 2 cm^{-1} and the spectra were calibrated using the 1332.2 cm^{-1} line of a SCD. Raman spectroscopy was another technique indispensable to the current work, allowing one to quantify to a large extent the diamond films deposited with a more detailed analysis of their constituent phases.

3.5 Optimization of HFCVD for diamond- conformal coating for electronics

The optimization of HFCVD for depositing diamond for electronics is many faceted- as discussed in great detail in the previous sections, the process parameters affect the qualities of the film. In addition, the system and its conditions, must be adapted for the particular substrate in question. For electronics applications, some aspects of the film- the film-substrate interface, the ratio of the grains-grain boundaries, grain size, thickness of the film, all of which in turn depend on the nucleation density, are particularly important. Also important is the quality of the nucleation surface, when the potential application of the diamond film is based on it. The following sub-sections detail the experiments made during the course of this work in order to investigate how the NNP affects the properties of the films and interface. For details on instruments used, the reader is referred to the appendix of this thesis.

3.5.1 Experimental details- Cleaning of samples

Essential to any successful CVD deposition cycle, similar to the rest of the steps involved in electronics fabrication, is the proper cleaning of substrate samples. Cleaning is used to remove potentially harmful contaminants such as adhesive residues, oxides, ionic and heavy metal atomic contaminants and other more general contaminants such as dust and debris present from the substrate wafer manufacturing process. The particulars of the cleaning step are adapted depending on the substrate material. For example, the solvent clean step (introducing substrates in a US bath, in organic solvents such as CH_3COCH_3) removes organic residues and oils. However, solvents sometimes themselves leave residues because of which a 2-step process is generally used, that involves a second step of introducing the substrates in the US bath in a beaker of C_2H_5OH. This cleaning is followed by the standard 3–step RCA cleaning (SC1, oxide clean, SC2). All samples fabricated and discussed in this thesis underwent solvent cleaning steps 1 and 2; all SiC samples underwent SC1, oxide clean and SC2, in addition. After each cleaning step, samples were dried using a filtered air gun. *Table 3-3* details the cleaning steps for the samples.

Cleaning step	Solvent/liquid	Duration (s)	Temperature	Additional notes
Solvent cleaning-1	CH_3COCH_3	300	Ambient	Sample placed in a beaker, in a US bath
Solvent cleaning-2	C_2H_5OH	300	Ambient	Sample placed in a beaker, in a US bath
SC1	i.5 parts DI H_2O ii.1 part NH_4OH (28%) iii. 1 part H_2O_2 (30%)	300	353 K	• Sample placed in beaker, on a magnetic hot plate with a stirrer • Rinsed with DI* H_2O post treatment
Oxide clean	i. 1 part HF (49%) ii. 30 parts DI H_2O	15	Ambient	• Sample placed in Teflon beaker and stirred • Rinsed with DI* H_2O post treatment
SC2	i. 6 parts DI H_2O ii. 1 part HCl (37%) iii. 1 part H_2O_2 (30%)	600	353 K	• Sample placed in beaker, on a magnetic hot plate with a stirrer • Rinsed with DI* H_2O post treatment

*DI stands for deionized water

Table 3-3 Standard cleaning for wafers prior to CVD treatment

3.5.2 Experimental details- NNP

As detailed in 3.2.3.1, one of the ways of obtaining the deposition of thin diamond films on foreign substrates is to use the NNP that involves exposing the sample to diamond GC. This PT leaves a thin C film at the surface of exposed regions. This is followed by the US treatment of the substrate with diamond suspensions- a procedure that leaves seeds on the substrate surface; seeds coalesce and form a closed conformal film during early stages of diamond growth. To get insight on the PT film thus formed and the early growth of these seeds therefore, evaluating the efficiency of the NNP as well as the seeding efficiency of different suspensions, the experiments and results presented in the following sub-sections were designed. These experiments were divided into 3 groups- (i) samples that underwent only the PT and seeding, and analysed to obtain insight into the nature of the film followed by (ii) samples seeded with ND suspensions and (iii) samples seeded with grit suspensions, and called series A, B and C respectively. For series B and C, following the PT and seeding, i.e., the NNP, samples were then introduced again to HFCVD diamond GC, for short durations. The experimental details are presented in *Table 3-4.* The aim of this study was to evaluate the effectiveness of this approach when diamond deposition takes place in a HFCVD system, US seeding is performed with grit and ND suspensions and the role of the suspensions on seeding uniformity and subsequent growth phase. For all three cases, [1 0 0] 460 µm-thick epitaxial Si wafers (Semiconductor Wafer Inc.) were cut into 10 mm ×5 mm samples; this was achieved by pressing the wafer against a hard surface with the epitaxial side facing down and cutting it into smaller pieces with a diamond cutter. All samples received solvent cleaning steps 1 and 2. Experiments were carried out with Re filaments- Re, under typical diamond HFCVD process conditions, does not distort as easily as W or Ta, nor does it break between successive runs. Most importantly, it does not act as a C-sink that other filaments do when used without a carburization step [540]. Hence, using Re provides several advantages, that includes saving time in not performing carburization. The same Re filament was also used in different runs, keeping the experimental set-up without any change in the filament-substrate distance and, consequently, in both the gas phase compositions at the substrate surface and film growth temperature. Re is known to sag with time in a typical HFCVD set-up [387] but by using a special “zig-zag” geometry for shaping the filament, this sagging was completely avoided in this study. The substrate temperature was measured with a standard type K (chromel-alumel) thermocouple; the filament temperature was

measured using an optical pyrometer (Impac Infrared 140) with emissivity set at 0.41 [541]. The desired substrate temperature was obtained by adjusting the filament temperature but keeping it in the range of 2173 to 2473 K. The filament- substrate distance was maintained at 5mm.

<table>
<tr><th rowspan="2">Series</th><th colspan="3">PT</th><th rowspan="2">Pressure (kPa)</th><th rowspan="2">Seeding</th><th colspan="3">GC</th><th rowspan="2">Pressure (kPa)</th><th rowspan="2">PT film thickness (nm)</th></tr>
<tr><th>CH_4/ H_2 (%)</th><th>Substrate temperature (K)</th><th>Duration (min)</th><th>CH_4/ H_2 (%)</th><th>Substrate temperature (K)</th><th>Duration (min)</th></tr>
<tr><td>A</td><td rowspan="11">1</td><td>973</td><td rowspan="11">30</td><td rowspan="11">4</td><td colspan="5">Grit (6-12 µm)</td><td>4.4±0.2</td></tr>
<tr><td rowspan="4">B_1</td><td rowspan="4">973</td><td rowspan="8">ND (refer to Table 3-5 for further details)</td><td rowspan="10">1</td><td rowspan="4">973</td><td>5</td><td rowspan="10">4</td><td rowspan="10">N/A</td></tr>
<tr><td>10</td></tr>
<tr><td>15</td></tr>
<tr><td>30</td></tr>
<tr><td rowspan="4">B_2</td><td rowspan="6">873</td><td rowspan="6">873</td><td>5</td></tr>
<tr><td>10</td></tr>
<tr><td>15</td></tr>
<tr><td>30</td></tr>
<tr><td rowspan="2">C</td><td rowspan="2">Grit (refer to Table 3-6 for further details)</td><td>10</td></tr>
<tr><td>30</td></tr>
</table>

Table 3-4 Summary of PT and diamond deposition conditions

The thickness of the PT films from series A was evaluated by ellipsometry- a technique used to measure thickness of thin films using the interference of light reflected from surface and light travelling through the film. It is typically used for films whose thickness ranges from sub-nm to a few µm; as films become thicker than several tens of µm, interference oscillations become increasingly difficult to resolve, except with longer IR wavelengths. The thin film measurements in this work were made using an AutoSE ellipsometer (HORIBA Scientific) with a total of 218 points in the wavelength interval 450-850 nm, an incidence angle of 70°, a signal quality of 50 and a measurement spot area of 250×250 m^2. In addition, SEM and Raman were used to characterize the films from all 3 series.

Following the PT step, all Si samples were seeded for 90 minutes in an US bath. The series A samples (one with PT and another without) were seeded in the 6-12 µm grit. Series B samples underwent seeding with commercially available seeding suspensions (supplied by ITC, Van Moppes, and Plasma-Chem). The main differences between the ND suspensions investigated here are the dispersive medium (water or DMSO-based suspension) and the nature of ND (ITC and PlasmaChem suspensions contain DND; nanoscale diamond by Van Moppes was jet-milled after HPHT synthesis, oxidised to make the surface hydrophilic, and then graded). These are detailed in *Table 3-5.* Series C samples underwent seeding with diamond grit of varying sizes, in CH_3OH suspensions detailed in *Table 3-6*. After the US seeding step, samples were cleaned in organic solvents and were introduced in the HFCVD system. Short (5, 10, 15 and 30 minutes for series B and 10, 30 minutes for series C) diamond growth cycles were performed, using the same conditions as the PT step *(Table 3-4).*

Suspension #	Supplier	Code	Particle size (nm)	Specifications
ND_1	Plasma Chem	PL-SDND-5p-5g	3.5-5.2	5 w/v% aqueous suspension, single digit ND
ND_2		PL-D-G01-5p-5g	4	5 w/v% enhanced stability aqueous suspension, diamond cluster
ND_3		PL-D-G01P-5p-5g	4	5 w/v% aqueous suspension, positively charged diamond clusters
ND_4	Van Moppes	SYP-GAF-0-0.1	50	Precision graded diamond powder, 100 cts/kg
ND_5		SYP-GAF-0-0.05	25	Precision graded diamond powder, 100 cts/kg
ND_6		SYP-GAF-0-0.03	15	Precision graded diamond powder, 50 cts/kg
ND_7	ITC	Opal seeds	20-30*	0.5 w/v% DND in DMSO suspension
ND_8		Blue seeds	~10*	0.5 w/v% DND in DMSO suspension

* For ITC suspensions, the ND size refers to the average agglomerate size of DND particles, whose primary size is 4-5 nm [542]

Table 3-5 Summary of ND suspensions used for seeding

Suspension #	Particle size (μm)	Specifications
Grit_1	0.25	0.8 g in 80 ml CH_3OH
Grit_2	6-12	
Grit_3	10-20	
Grit_4	30-40	
Grit_5	40-60	

Table 3-6 Summary of grit suspensions used for seeding

3.5.3 Results and discussion

3.5.3.1 Nature of PT film

As mentioned, ellipsometry was used to measure the thickness of the PT film after 30 minutes of treatment, the thickness was measured to be 4.4±0.2 nm. To get information on the nature of the PT film, sample A was prepared by exposing a Si sample for 30 min to 1% CH_4/H_2 ratio, at a substrate temperature of 973 K (*Table 3-4*), i.e., PT followed by seeding in grit suspension. This sample was observed under SEM and the PT film can be clearly seen covering fully the surface of the Si (*Figure 3-8*). Isolated ~80 nm-sized crystals due to spontaneous diamond nucleation can be seen on the surface of the PT film.

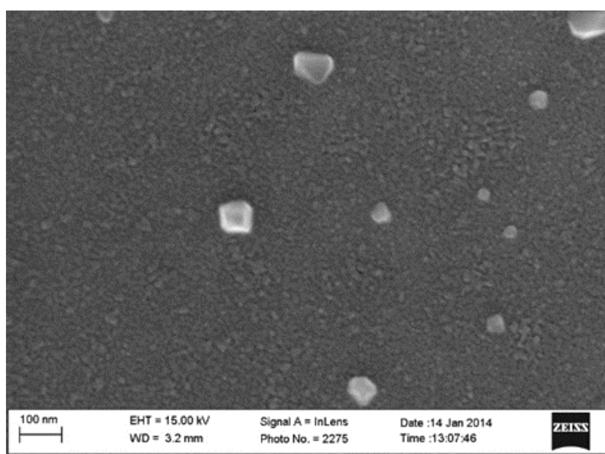

Figure 3-8 SEM image of surface of the PT film

Raman spectra were acquired from different spots of the surface of the PT film as well as the sample that underwent no PT but only seeding. On comparison between spectra in a and b of *Figure 3-9*, one can see clear differences that can provide valuable information, since the difference arises exclusively from the presence of the PT film- Raman spectra collected from several areas of the sample subjected to PT showed several distinct features.

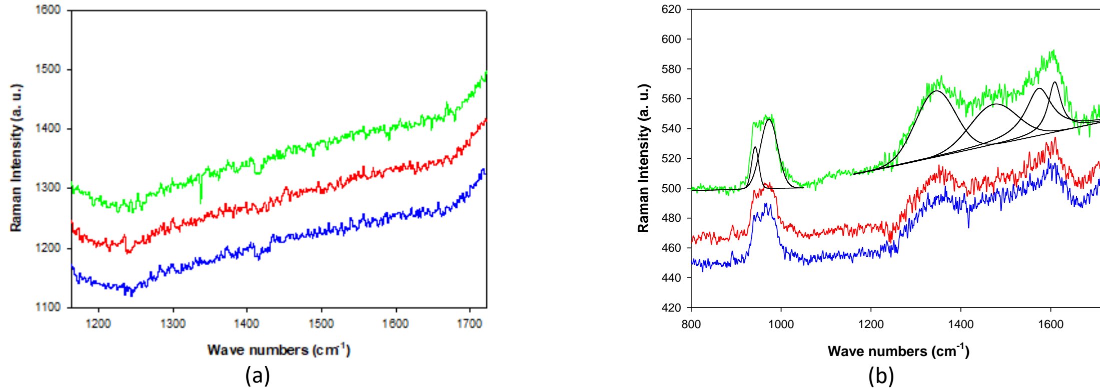

Figure 3-9 Micro-Raman spectra collected from (a) no-PT and (b) PT samples after seeding different colors correspond to different positions on the same sample

All spectra of *Figure 3-9* b show (i) the Si second order band of the substrate at low frequency (964 cm^{-1}) (ii) the D band (~1340 cm^{-1}) due to disorder in graphitic sp^2-C (iii) a band centered at about 1480 cm^{-1} that will be discussed later (iv) the G band (~1580 cm^{-1}) related to the graphitic C and (v) the D' band at higher frequencies (~1610 cm^{-1}). An example of fitting of a Raman spectrum is also shown in the same figure (*Figure 3-9* b). The frequency and the intensity of each band (with the exception of Si second order band) of spectra from the PT sample, along with the ratio of the diamond to non-diamond phases i.e., $I_{diamond}/I_{non\text{-}diamond}$ are summarized in *Table 3-7*.

Spot		1	2	3
D' band	**Position (cm^{-1})**	1612	1610	1605
	Intensity (AU)	10.56	10.33	21.59
G band	**Position (cm^{-1})**	1589	1590	1565
	Intensity (AU)	14.05	18.16	35.81
Amorphous band	**Position (cm^{-1})**	1487	1495	1477
	Intensity (AU)	12.26	10.99	27.70
D band	**Position (cm^{-1})**	1345	1348	1341
	Intensity (AU)	24.15	28.60	42.32
$I_{diamond}$ / $I_{non\text{-}diamond}$		1.7	1.6	1.2

Table 3-7 List of Raman bands in spectra of *Figure 3-9* b, as obtained by fitting, the average $I_{diamond}$ / $I_{non\text{-}diamond}$ ratio is 1.5

The 1480 cm^{-1} band has two possible assignments: amorphous sp^2-C or amorphous sp^3-C. Peaks at 1340 and 1470 cm^{-1} could be assigned to the presence of a high phonon density of states in graphite samples [543, 544], with an estimated crystal planar domain size L_a = 25 Å. According to Robertson *et al.* [545, 546] the graphitic clusters should be terminated by sp^3 sites and the presence of sp^3 C should shift the G peak of graphite to higher frequencies (past 1600 cm^{-1}), an occurrence that was not observed in these samples. In fact, in the PT films the G band was detectable in the 1565-1590 cm^{-1} range (*Table 3-7*). The position of the G peak and the $I_{diamond}/I_{non\text{-}diamond}$ ratio depend on the disordered phases in the film and the sp^3 fraction for as-deposited hydrogenated amorphous C films (a-C:H) [427]. In these samples, the average value of the $I_{diamond}/I_{non\text{-}diamond}$ ratio (1.5) and the position of the G bands suggest that the C layer deposited by

HFCVD during the PT step was mainly composed of nano-crystalline and/or amorphous sp^2 C. This is in apparent contradiction to other reported findings [53, 56] according to which the PT is composed of a sp^3 rich amorphous C layer.
This apparent contradiction may be related to Re contamination from the filament. Higher magnification SEM images of series B_1 samples (seeded with ND_7 and ND_8 followed by GC for 30 minutes) in fact revealed the presence of round particles in-between the diamond crystallites (*Figure 3-10,* red circles); these particles may be Re clusters due to the evaporation of atoms from the filament- to ensure 973 K substrate temperature for samples of series A_1 and B_1, the filament was heated up to 2273 K; implying a higher vapor pressure of Re, and consequent metal contaminations of diamond films when compared to carbide-forming filament materials such as W or Ta [547]. However, the presence of Re in the films could not be confirmed with EDS because the detected Si substrate signal completely masks the Re peaks. In any case, Almeida *et al.* detected W atoms in multilayered diamond films deposited by HFCVD under certain conditions [548]; according to the authors, these impurities had an impact in the nature of the C bonds at the interface. Similarly, the presence of Re atoms on the surface of the Si substrate in these samples, is expected to influence the diamond growth by favouring the formation of sp^2 instead of sp^3 bonding, despite of the low CH_4/H_2 ratios used during growth. As such, the presence of the amorphous sp^2 C in the PT film is considered a consequence of the Re contamination.

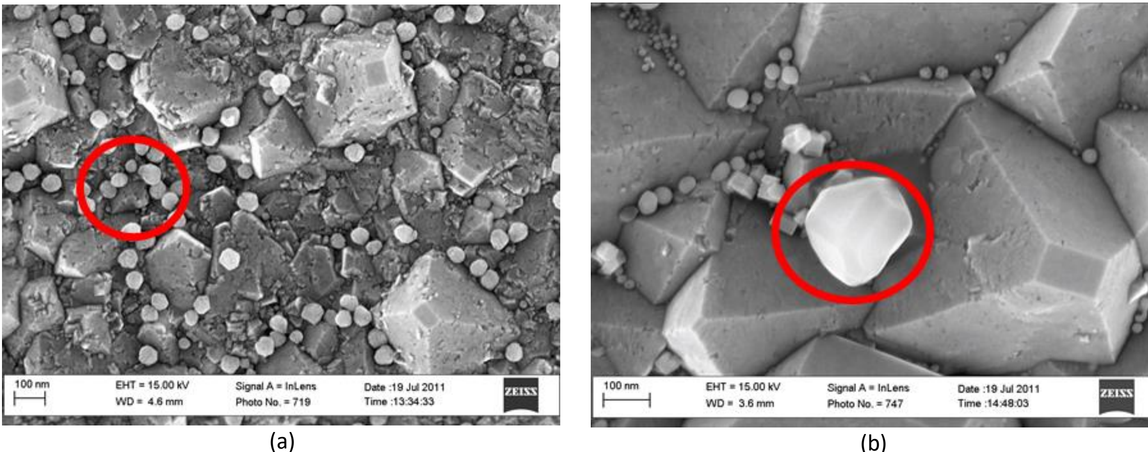

Figure 3-10 SEM images of samples of series B_1, seeded with (a) ND_7 and (b) ND_8

In summary, contradictory to what was observed in the relevant literature for MWCVD, the PT film deposited by HFCVD using a Re filament was mostly composed by sp^2 C rather than nanostructured sp^3 C. This is attributed to the contamination of the substrate with the metal impurities from the Re filament that contributes to disorder in the bonding of the C atoms and thus, its amorphous nature.

3.5.3.2 Seeding effectiveness of ND suspensions

Following the inferences from the previous section, in order to prevent Re contamination, experiments for series B_2 were carried out at 873 K, using a lower filament temperature, while maintaining the same filament-substrate distance. A lower filament temperature (2173 K) is expected to reduce Re contamination significantly as the vapor pressure of Re at 2173 K is 7 times lower than that at 2273 K [547, 549].
From the SEM images of these samples, it was seen that the suspension used during the US procedure influenced the uniformity of the diamond film significantly. *Figure 3-11* shows the SEM images of samples of series B_2 after 30 minute runs. Samples of this series seeded with DMSO-based suspensions were coated with conformal and uniform diamond films, while samples seeded with both Van Moppes and

PlasmaChem water suspensions revealed films that were not coalesced and not uniform, composed instead of isolated crystals and patches of diamond deposits. The tendency was the same for both PT and no-PT samples. Shenderova *et al*. [542] discussed the good seeding behaviour of DMSO-based DND suspensions. DMSO contains a highly polar S=O group, forming strong intermolecular attractions with functional groups existing on the surface of DNDs with positive zeta potential (the potential difference between the dispersion medium and the stationary layer of fluid attached to the dispersed particle). In addition to a highly polar group, DMSO contains two hydrophobic methyl groups. The resulting solvation shell could therefore prevent DND particles from agglomerating via H_2 bond formation. As a result, differently from protic media, DNDs in DMSO have high dispersion. After this preliminary analysis of the samples deposited during 30 minute runs at 873 K, attention was focused on Si samples seeded with DMSO-based suspensions, since seeding with Van Moppes and PlasmaChem water suspensions resulted in non-uniform diamond growth. Results obtained with suspensions ND_5 and ND_6 are similar to results obtained with suspension ND_4, and hence not presented.

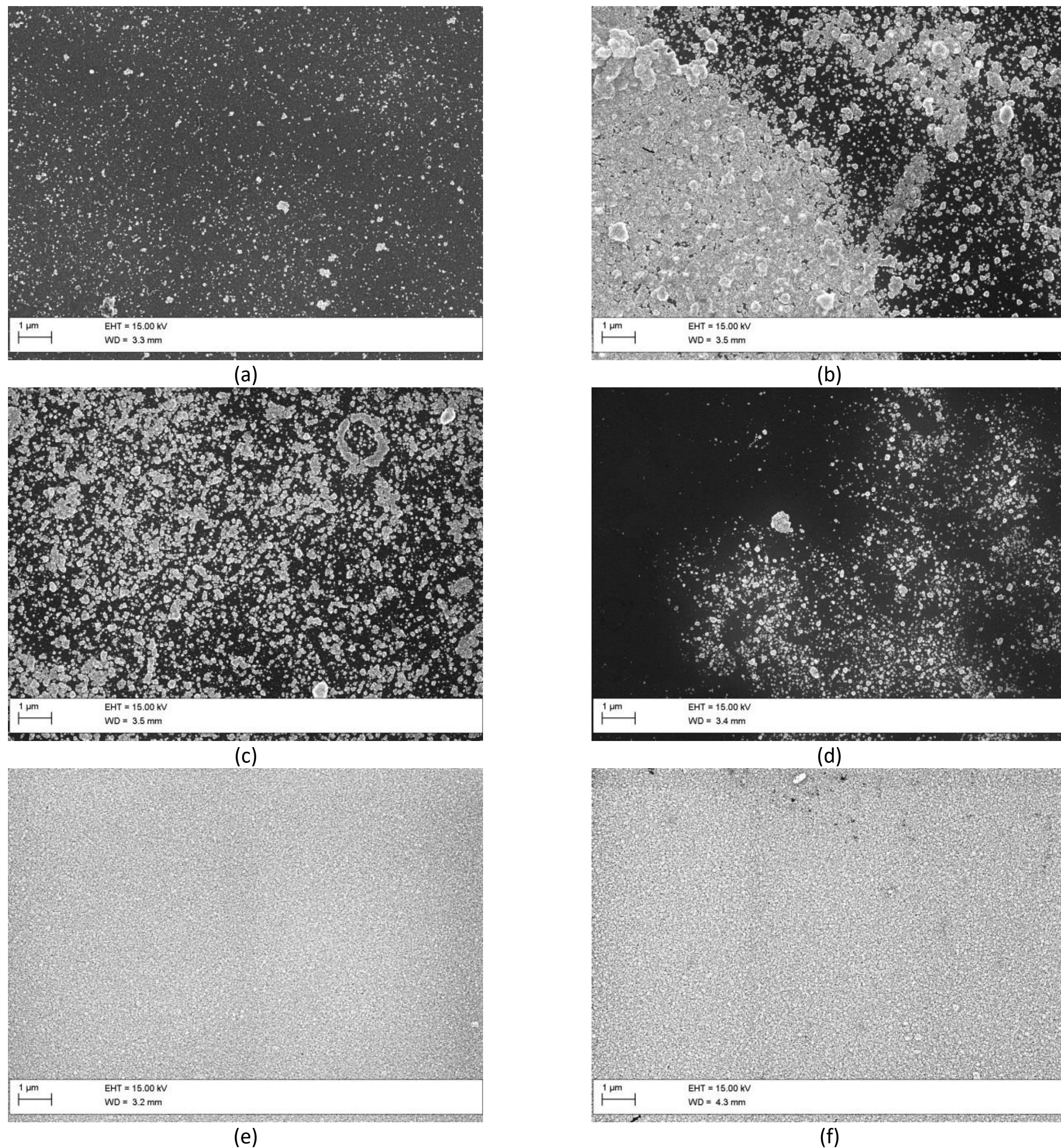

Figure 3-11 SEM images of samples after 30 min diamond growth at 873 K. Samples were seeded with suspension (a) ND_1, (b) ND_2, (c) ND_3, (d) ND_4, (e) ND_7 and (f) ND_8

Figure 3-12 a shows that after 15 minutes deposition, PT samples seeded with suspension ND_7 revealed a coalesced film, in opposition to *Figure 3-12* b no-PT samples, which showed a less coalesced film. Results obtained with suspension ND_8 were similar. EDS spectra (not shown) were collected from PT and no-PT samples. PT samples show a uniform C content all over the sample surface, while no-PT samples show a deficit of C in the spaces between the crystals (green rectangle in *Figure 3-12* b, as well as on comparison of area inside red circles in both a and b).

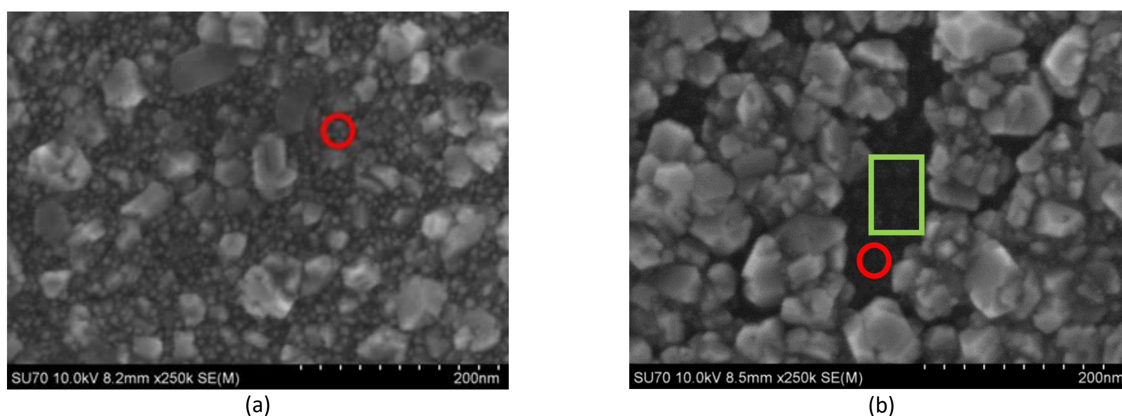

Figure 3-12 SEM images of samples seeded with ND_7 after 15 min diamond growth at 873 K, (a) with PT (b) without PT

Figure 3-13 shows the surface morphology of the Si samples after 10 minutes deposition, having been seeded with DMSO-based suspensions ND_7 (a, b) and ND_8 (c, d). SEM images on the left column (panels a and c) show samples that underwent PT prior to the seeding procedure. One conclusion can immediately be taken: the exposure of the Si surface to diamond growth conditions prior to the US seeding (PT step) increases the number of diamond seeds that remained attached to the Si surface. The seeds of suspension ND_8 (~ 10 nm in size, panels c and d) also show a larger tendency to agglomerate than the seeds of suspension ND_7 (20-30 nm in size, panels a and b). This finding reflects the larger tendency of smaller, DND particles with higher surface area, to agglomerate [550]. However, it is worth noting that the tendency towards agglomeration was much lower on PT samples (panels a and c). It can be concluded that the PT step, prior to US seeding, leads not only to a larger seeding density, but also to a more uniform distribution of less agglomerated diamond nanoparticles at the Si surface. The nature of the PT film might explain the result of SEM observations; from *Figure 3-13* it is clear that there are many DND seeds on the surface of no-PT sample. These seeds are however much more agglomerated and much less homogeneously distributed at the substrate surface suggesting that the effect of the PT films is due to the stronger interaction between the sp^2 film deposited during PT and either the graphitic shell of DND seeds [551] or the hydrophobic methyl groups of adsorbed DMSO molecules. In the case of no-PT samples, the DND seeds tend to interact with each other rather than the PT film on the Si surface, leading to agglomeration and inhomogeneity; this causes an increase of DND "islands" (which act as growth centers in the subsequent CVD step) at the surface. On the contrary, in the case of PT samples the DND seeds interact with the sp^2 film, which causes the islands to be much smaller and more frequent; this, in turn, reduces the deposition time required to get continuous and very thin PCD films. These results imply that thinner conformal films can be grown by HFCVD using both PT and seeding with DND suspension in DMSO.

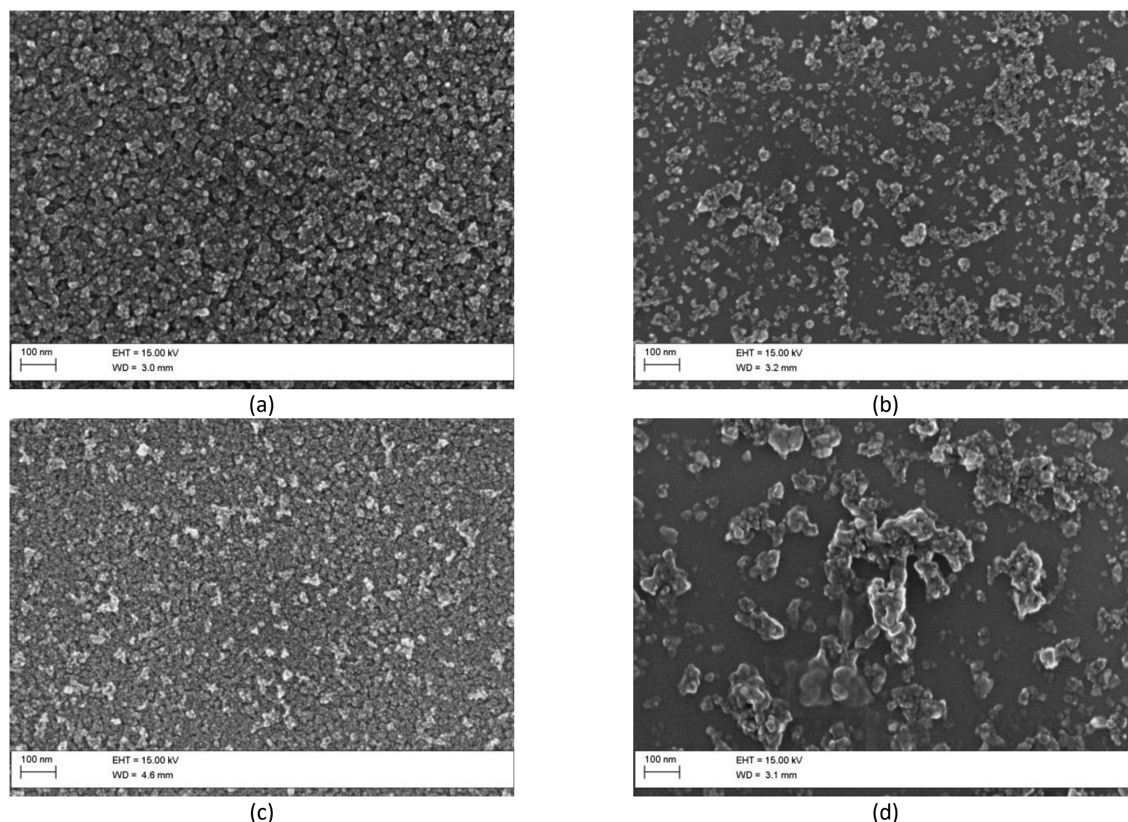

Figure 3-13 SEM images of Si samples after 10 min diamond growth seeded with ND_7 (a, b) and ND_8 (c, d), (a, c) received PT (b,d) did not receive PT

After 5 minutes deposition, the difference between PT and no-PT samples is even more evident –*Figure 3-14.* PT samples (a and c) show a uniform dstribution, with a high density of crystallites, in opposition to the no-PT samples that show isolated crystals, 10-40 nm in size. The nucleation density was estimated to be 2.2×10^{11} cm^{-2} and 2.6×10^{10} cm^{-2} for PT and no-PT samples, respectively; these values were obtained by counting individual nuclei and neglecting particle clusters over five different SEM images and averaging the final result. The insets in *Figure 3-14* show same the samples after 30 minutes deposition: PT samples have coalesced diamond films, with crystals 40-70 µm in size, while the films on no-PT samples are not fully coalesced yet and have a crystal size of 30-50 µm. The influence of the DND particle size used for the US seeding step is not apparent. Although DMSO based suspensions have already been used to obtain superior diamond nucleation densities [552] this finding indicates clearly that the use of PT step prior to seeding with DND suspensions in DMSO is of great help in growing PCD diamond coatings as thin as possible by using a technique as simple and versatile as HFCVD.

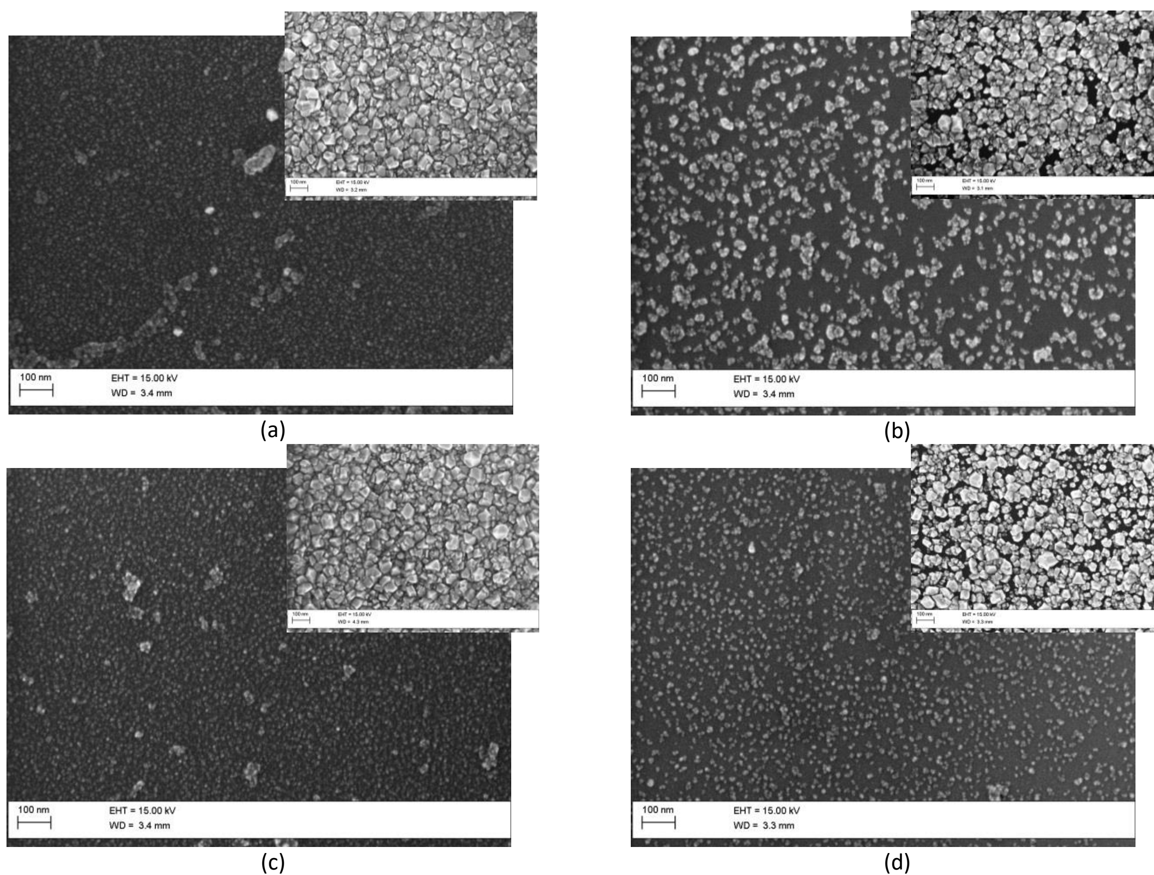

Figure 3-14 SEM images of samples after 5 minutes diamond growth at 873 K (a,b) samples seeded with ND_7 (c,d) samples seeded with ND_8. (a, c) received PT (b,d) did not receive PT; insets: same samples after 30 min diamond growth at 873 K

In summary, comparing with commercially available ND suspensions in deionized water, the seeding with DMSO-based suspensions (supplied by ITC) resulted in uniform diamond films after 30 minutes HFCVD at 873 K. The NNP resulted in a higher nucleation density, in comparison to samples that had not been given the PT. No apparent difference could be detected between seeding with "blue seeds" (~ 10 nm DND agglomerates in DMSO) or "opal seeds" (20-30 nm DND agglomerates in DMSO) suspensions in longer runs. Samples prepared at higher temperature (973 K) revealed the presence of round amorphous-like particles that were tentatively identified as Re clusters resulting from the evaporation of atoms from the filament. The PT has a clear influence: it favors the de-agglomeration of DND particles via interaction between the a-C covered substrate surface and either the graphitic shell of DND or the hydrophobic methyl groups of adsorbed DMSO molecules, allowing a more uniform dispersion of seeds. This, in turn, results in shorter deposition duration to get continuous and conformal HFCVD diamond films.

3.5.3.3 Seeding effectiveness of grit suspensions

As in the previous sections, experiments for testing the seeding effectiveness of grit suspensions were carried out at a lower filament temperature, to prevent Re contamination. From the SEM images of these samples, it was seen that the suspension used during the US procedure influenced the uniformity of the diamond film significantly as did the PT. *Figure 3-15* shows the SEM images of samples of series C after 30 minute runs. Samples of this series were coated with conformal and uniform diamond films for all the substrates that received the PT, while samples that did not receive the PT have a much lower nucleation density as can be seen from the images. Because of the lower nucleation density, the films on these samples did not coalesce and close in the same time as their counterparts that received the PT did, an

effect especially noticeable in samples seeded with smaller grit sizes (grit_1 and grit_2) (*Figure 3-15* b and d). In these samples, higher magnification images of the areas highlighted in red rectangles, an amorphous C structured film can still be seen (insets of *Figure 3-15* b and d).

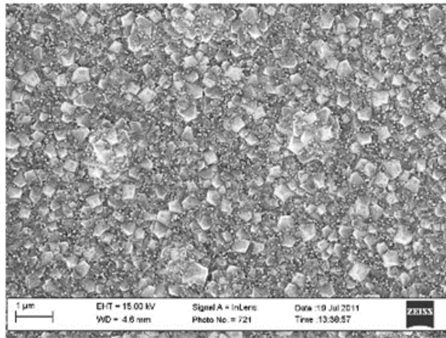

(a)

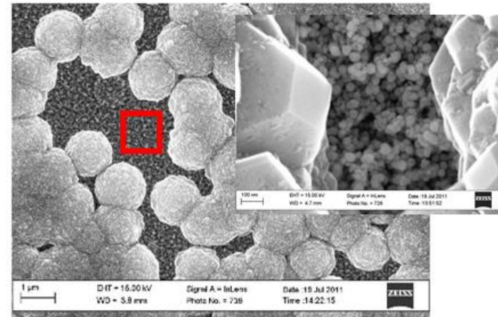

(b)

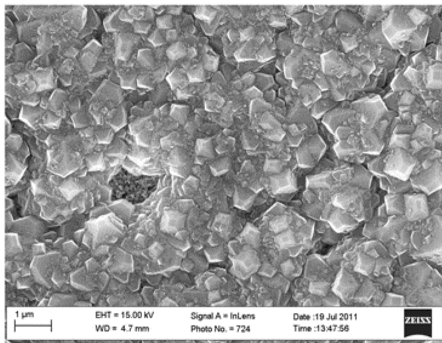

(c)

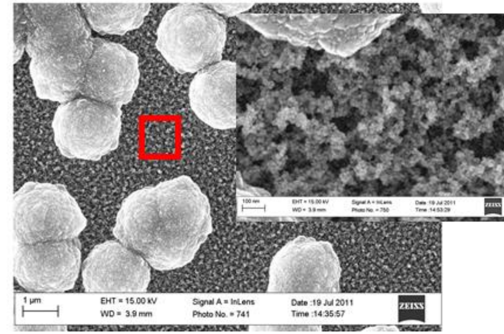

(d)

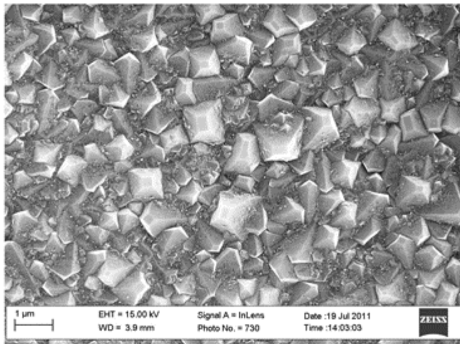

(e)

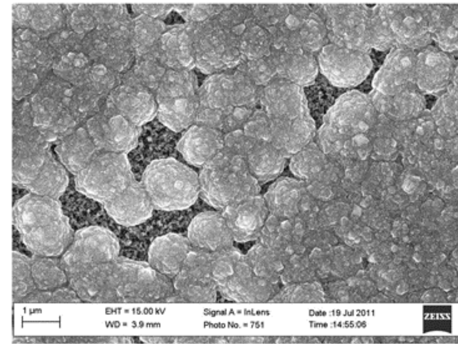

(f)

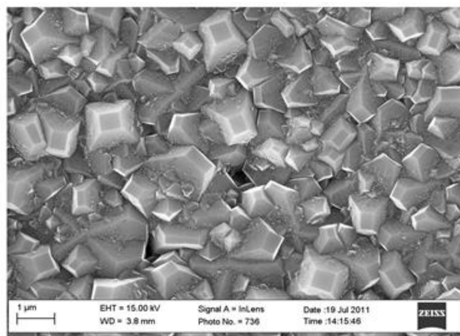

(g)

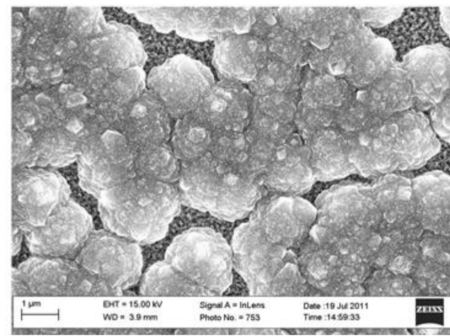

(h)

Figure 3-15 SEM images of samples after 30 min diamond growth, seeded with (a,b) grit_1 (c,d) grit_2 (e,f) grit_4 and (g,h) girt_5. Images on the left (a, c, e, g) are of samples that received PT, images on the right (b,d, f, h) are samples that did not

Samples seeded with larger grit size (grit_4 and grit_5) had films that coalesced to a larger degree although they were not completely coalesced as their counterparts with PT (*Figure 3-15* f and h). In all cases, due to the disparity in the nucleation density, in which the PT clearly had a role, films that underwent NNP show bigger crystals, and better crystalline quality in general (higher grain to grain boundary ratio) when compared to samples that did not receive PT. The PT plays a role in ensuring a more uniform distribution of seeds when samples are seeded with diamond grits, leading to coalesced, conformal films in a short amount of time.
In addition to the influence of the PT that is noticeable in these samples, the grit size also played a role in the characteristics of the films- a decrease in the nucleation density was seen with an increase in grit size causing larger grain sizes in films grown with larger grit sizes *(Figure 3-15* a, c, e and g).
An interesting exception to this trend was seen in samples seeded with grit_3, i.e., the 10-20 µm size diamond particles. As can be seen from the SEM images of both of these samples *Figure 3-16*, i.e., with and without PT, after 30 minutes' growth the films had very similar characteristics implying that the PT did not seem to make any meaningful difference. It is not possible at the moment to identify the cause of this phenomenon.

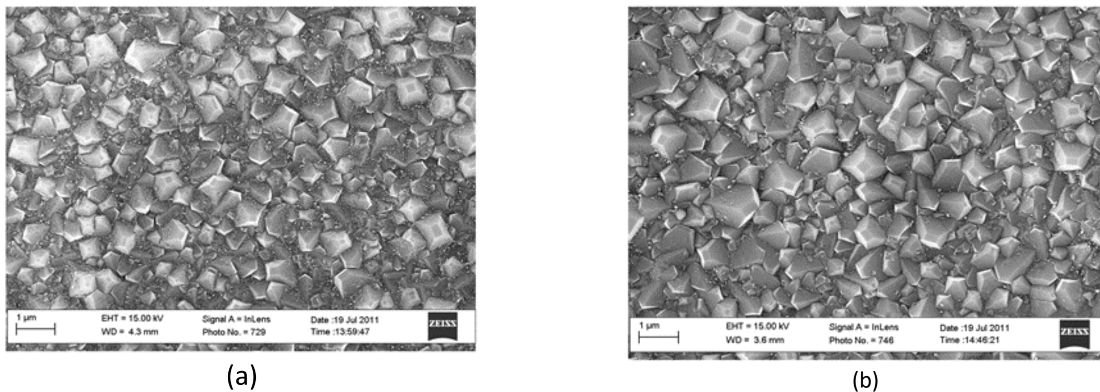

Figure 3-16 SEM images of samples after 30 min diamond growth, seeded with grit_3 (a) with PT and (b) without PT

Figure 3-17 shows the surface morphology of the Si samples after 10 minutes' deposition, having been seeded with grit suspensions 1 through 5. SEM images on the left column show samples that underwent PT prior to the seeding procedure, and on the right samples that did not undergo PT. One conclusion can immediately be taken: the exposure of the Si surface to diamond growth conditions prior to the US seeding (PT step) increases the number of diamond seeds that remained attached to the Si surface, comparing the images in the left column with the ones in the right. It can be concluded that the PT step, prior to US seeding, leads not only to a larger nucleation density, but also to a more uniform distribution of less agglomerated diamond particles at the Si surface. An exception to this was again the sample seeded with grit_3 which showed no meaningful influence of the PT. In these 10 minute samples, the tendency of decreasing nucleation density with increasing grit size that was observed in 30 minute samples *(Figure 3-15)* can again be seen. These calculated values of the nucleation density are presented in *Table 3-8*; these values were obtained by counting individual nuclei and neglecting particle clusters over five different SEM images and averaging the final result. Sample seeded with grit_3 is again a notable exception.

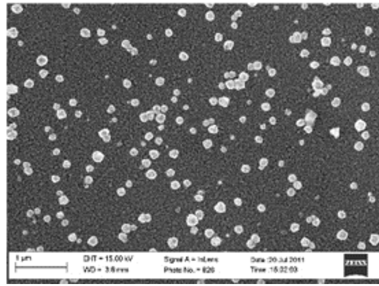

(a)

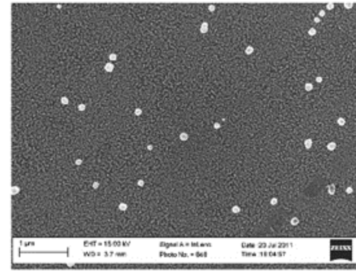

(b)

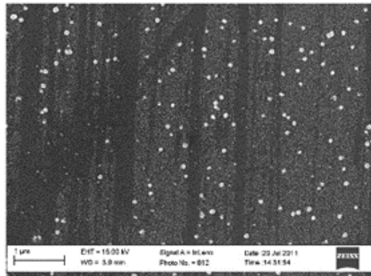

(c)

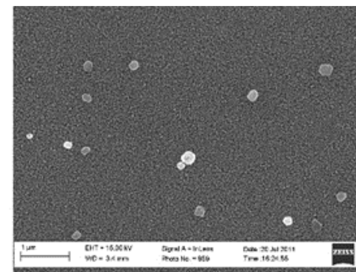

(d)

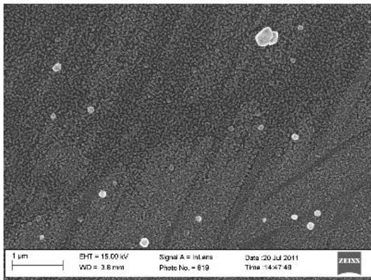

(e)

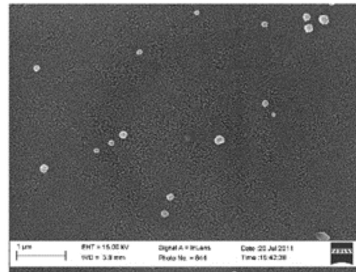

(f)

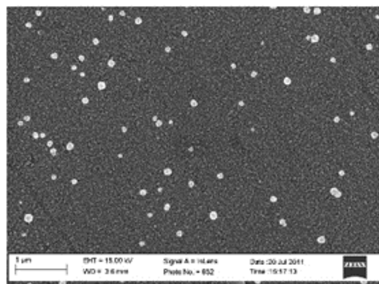

(g)

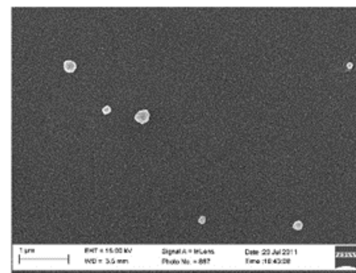

(h)

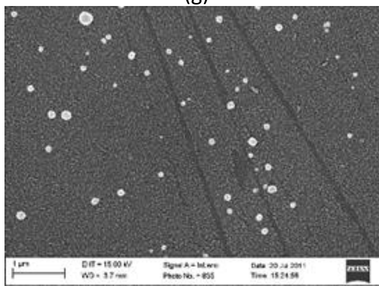

(i)

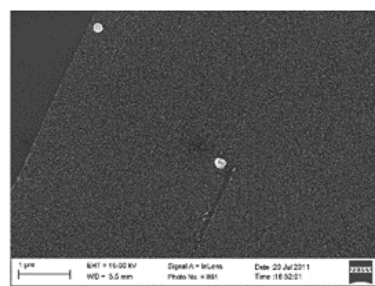

(j)

Figure 3-17 SEM images of samples after 10 min diamond growth, seeded with (a,b) grit_1 (c,d) grit_2 (e,f) grit_3 (g,h) girt_4 and (i,j) grit_5. Images on the left (a, c, e, g and i) are of samples that received PT, images on the right (b,d, f, h and j) are samples that did not

Suspension (Grit_)	Nucleation density for PT sample ($\times 10^8$ cm^{-1})	Nucleation density for no-PT sample ($\times 10^8$ cm^{-1})
1	4.94	0.81
2	4.34	0.18
3	0.8	0.81
4	1.9	0.13
5	1.5	0.12

Table 3-8 Nucleation densities obtained for grit samples

In summary the NNP resulted in a higher nucleation density, in comparison to samples that had not been given the PT. The NNP greatly influenced the grain size, leading to larger grains in samples that received it, when compared with samples that did not receive it but had all other parameters of the GC identical. In addition, grain size was seen to be directly proportional to grit size and the nucleation density, inversely proportional to the grit size. An exception to this trend was the grit size 10-20 µm, in which no discernable influence of the NNP was noted. The NNP was also seen to lead to more coalesced films when compared to their counterparts that did not receive the same NNP treatment, after only 30 minutes of diamond GC.

3.6 Conclusions

A detailed description of the HFCVD process was presented in this chapter, described individually for undoped and doped diamond growth. The typical techniques used to characterise CVD diamond were also presented.

In the final section of the chapter, some experimental aspects and inferences from them were presented- parameters of the CVD process such as the PT and the nature of seeding suspension used were investigated. In conjunction with the right seeding suspension, the NNP resulted in coalesced films in a short amount of time (30 minutes) that samples without the PT were not able to achieve. It is important to note that under the same conditions, using DMSO based suspensions resulted in higher nucleation densities when compared to CH_3OH based grit suspensions. However, an arbitrarily high nucleation density is not always a desirable factor- for good quality diamond films for applications in electronics, what is important is an adequate nucleation density but lateral coalescence of these grains during the initial few minutes of growth. This ensures a good grain to grain boundary ratio. These insights are utilised in the next chapter where the HFCVD has been used to optimize the growth of diamond films for very specific applications in electronics.

4. Diamond films for electronic devices

4.1 Introduction

The preceding chapters presented an in-depth discussion about the growth of synthetic diamond, as well as the experimental optimization of the process of HFCVD itself for the growth of conformal diamond films. This chapter presents experimental results obtained during the work that explores some potential applications of CVD diamond for electronic devices- how diamond films can (1) be combined with SAW devices using a reverse fabrication method, (2) be used to fabricate holders for electronic devices using a novel patterning technique (3) by achieving low temperature growth, be used for passivation of WBG devices (4) doped with B and combined with SiC to form novel heterojunctions. These experiments benefit from the optimization work presented in the last chapter- they were designed keeping in mind the nucleation densities and film qualities observed during the optimization process. The current chapter is divided into 4 main sections that follow the order of applications mentioned above.

The deposition procedure followed in all the sub-sections that can be generalized have been summarised in *Figure 4-1* and will be called, hereafter as protocol 1 (P1) and protocol 2 (P2). As can be seen, P1 is the NNP.

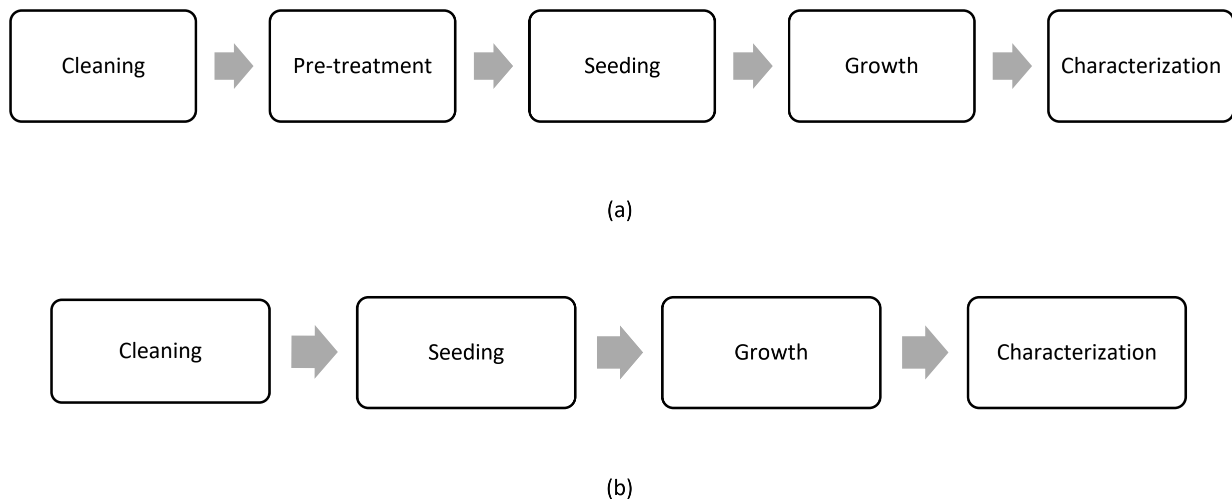

Figure 4-1 Schematic representation of (a) P1 and (b) P2

The experimental details involved in the cleaning step have already been summarised in section 3.5.1 of the previous chapter, and were followed accordingly for the samples mentioned in the current chapter. For the PT and GC, the relevant parameters are the substrate temperature, gas composition, filament substrate distance (maintained at 5 mm unless otherwise mentioned), deposition pressure and duration. As mentioned in section 3.5.2, the desired substrate temperature was obtained by adjusting the filament temperature (within the range of 2173 to 2473 K, unless otherwise specified) and not the filament-substrate distance which was maintained at 5 mm. The substrate temperature was measured with a standard type K (chromel-alumel) thermocouple; the filament temperature was measured using an optical pyrometer (Impac Infrared 140). For all filaments other than Re (in the present work, W and Ta were also used) a carburization step is involved before stable PT or GC conditions can be obtained. For this, the HFCVD system is run with a 5% CH_4/H_2 ratio of gas and filament temperature set to 2673 K for a duration of 30 minutes. During this step, performed prior to PT (where applicable) and GC, the samples are exposed; they are however kept at a much larger distance from the filament (>5 cm). EDS measurements

were taken from test-run Si samples after this step to confirm any traces of filament contamination (W and Ta)- no trace of contamination was found (*Figure 4-2*). Seeding in all cases of US treatment was carried out for 90 minutes. In all cases of deposition, both PT and GC, post growth cooling was carried out in a H_2 atmosphere. Standard characterization techniques used were the FEG SEM and Raman spectroscopy; in some cases, profilometry, experimental details of which have already been specified in the previous chapter. For details about all the instruments used in the work, the reader is referred to the appendix of this thesis.

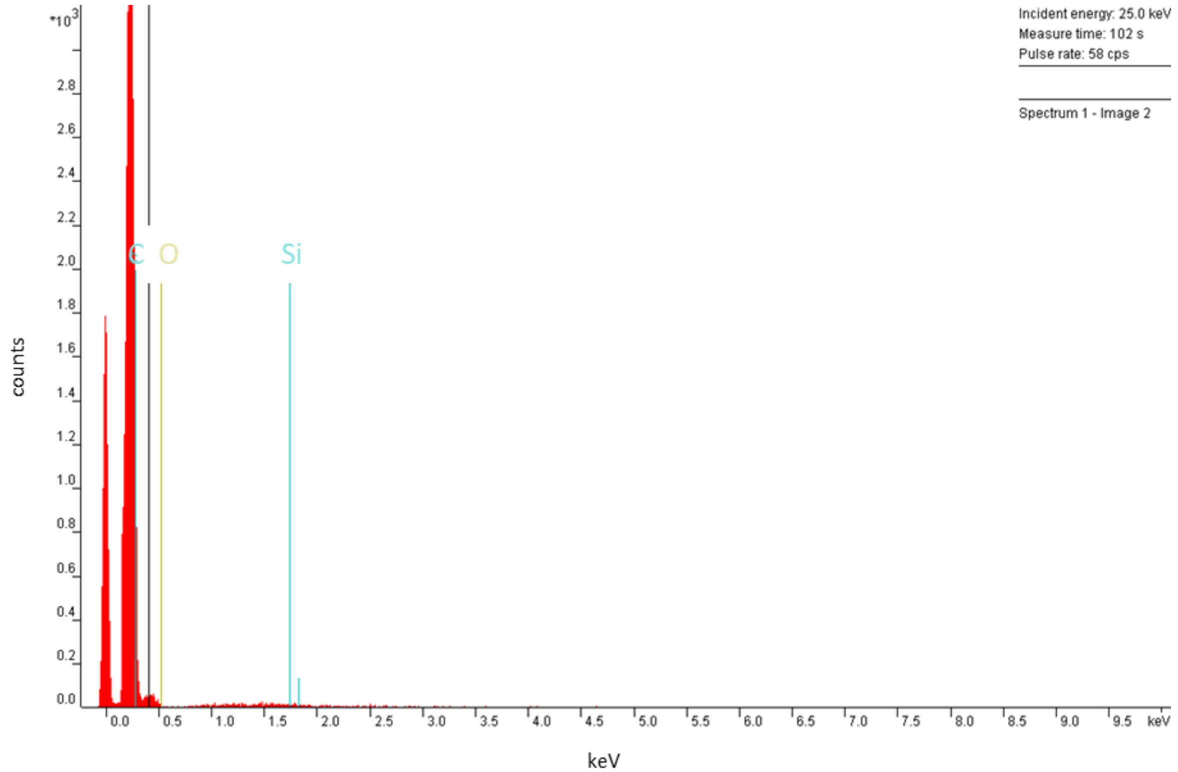

Figure 4-2 EDS spectra of Si sample without trace of contamination

4.2 Diamond for SAW devices

In addition to using diamond as a substrate for SAW devices in conjunction with PEMs, as discussed before in the section 2.6.4, there has been investigation of growing PEM layers on diamond substrate or vice-verse, in order to benefit from the composite structure of diamond-$LiNbO_3$ based SAW devices. The diamond-$LiNbO_3$ composite structure is very useful for SAW devices that can be used in GHz range in frequencies between 2–5 GHz [553] and the fabrication technique usually involves the deposition of PEM films on a good quality diamond wafer. However, the high density of defects in the $LiNbO_3$ films [554, 555] when deposited on diamond substrates has prevented the full exploitation of the theoretical potential of these devices. A lesser used technique is one of growing diamond films directly on the $LiNbO_3$ substrate, that could help overcome the limitations faced by the aforementioned technique of growing PEM-on-diamond. Diamond films of various grain sizes have, in fact, been grown on $LiNbO_3$ substrates [261, 263], enabling the integration of diamond into these SAW devices. By using this reverse approach, Jagannadham *et al.* [261] successfully deposited diamond films by MPCVD on single crystal $LiNbO_3$ and found it to be favorable for formation of SAW devices with low acoustic wave propagation losses.

The conventional fabrication setup for a SAW die, after the choice of a suitable substrate (for example, diamond), typically involves the deposition of the PEM film followed by the deposition of the metal IDTs. In the present work, a reverse fabrication method is proposed, and addresses the primary challenge of performing diamond growth on PEM device dies directly- to deposit diamond at temperatures low enough to not damage the metallization normally present on these un-capsulated devices. The deposition of a diamond film directly on the surface on the SAW die, allows for the simplification of the fabrication procedure to its maximum extent: current SAW fabrication technology (including substrate fabrication and IDT deposition) is simply followed by selective diamond deposition on the final die, prior to encapsulation. Since this diamond film can also function as a protective coating against aggressive or harsh environments, by making patterned diamond growth, one can at the same time utilize diamonds' acoustic and thermal properties and simultaneously obtain devices capable of working in harsh environments, such as in space, or for geo-thermal applications, where either or both radiation and high temperatures are encountered and where due to their wireless operation, SAW devices find much of their usage [556-558]. For the preliminary tests, diamond films were deposited by HFCVD on $LiNbO_3$ substrates. Utilising the results from these studies, a next set of experiments was designed to obtain direct diamond growth on $LiNbO_3$ device dies. These experiments also included the optimization of a patterned diamond growth procedure. The S-parameters of the coated and uncoated dies were then evaluated with a network analyser.

4.2.1 Experimental details- Diamond films on $LiNbO_3$

For this study, a total of 4 $LiNbO_3$ substrates diced into pieces of 6 mm × 4 mm were used. Substrates underwent solvent cleaning 1 and 2, followed by P1 i.e., PT and seeding to prepare them for CVD GC. For this study, Re filaments were used, using the same geometry that prevents sagging (as described in section 3.5.2), hence carburization was not necessary. To prevent Re contamination, the maximum temperature in these experiments were limited to a maximum of 773 K. To obtain optimum nucleation densities, the 6-12µm grit and 20-30 nm DND in DMSO suspensions were chosen. Because of the known disparity in the thermal expansion coefficients of diamond and $LiNbO_3$, a 60-minute-long cooling step was included post growth; this decreases the possibility of delamination of the film during the turning off of the HFCVD system. The parameters used are listed in *Table 4-1*. The films were then characterized using SEM and Raman.

<table>
<tr><th rowspan="2">Sample ID</th><th colspan="3">PT</th><th rowspan="2">Pressure (kPa)</th><th rowspan="2">Seeding</th><th colspan="3">GC</th><th rowspan="2">Pressure (kPa)</th><th rowspan="2">Rate of cooling (°C/min)</th></tr>
<tr><th>CH_4/H_2 (%)</th><th>Substrate temperature (K)</th><th>Duration (min)</th><th>CH_4/H_2 (%)</th><th>Substrate temperature (K)</th><th>Duration (min)</th></tr>
<tr><td>LNB_grit_1</td><td rowspan="4">1</td><td rowspan="2">673</td><td rowspan="4">60</td><td rowspan="4">5</td><td>6-12 µm grit (0.6 g in 60 ml CH_3OH)</td><td rowspan="4">1</td><td rowspan="2">673</td><td rowspan="4">120</td><td rowspan="4">5</td><td rowspan="2">5</td></tr>
<tr><td>LNB_DND_1</td><td>DND (20-30 nm particles in DMSO/CH_3OH 1:3 suspension)</td></tr>
<tr><td>LNB_grit_2</td><td rowspan="2">773</td><td>6-12 µm grit (0.6 g in 60 ml CH_3OH)</td><td rowspan="2">773</td><td rowspan="2">6</td></tr>
<tr><td>LNB_DND_2</td><td>DND (20-30 nm particles in DMSO/CH_3OH 1:3 suspension)</td></tr>
</table>

Table 4-1 Deposition conditions used for diamond growth on $LiNbO_3$ samples

4.2.2 Results and discussion- Diamond films on $LiNbO_3$

Both grit samples (LNB_grit_1 and LNB_grit_2) were covered with good quality diamond films- coalesced and uniform- as can be seen from their SEM images (*Figure 4-3*). The films were MCD with an average crystal size of 1 µm. The good film quality is also attested by the Raman spectra, where the sharp peak of sp^3 diamond is at 1332 cm^{-1} (FWHM 9.4 cm^{-1}), and a smaller band of amorphous C at 1480 cm^{-1} (*Figure 4-4* a).

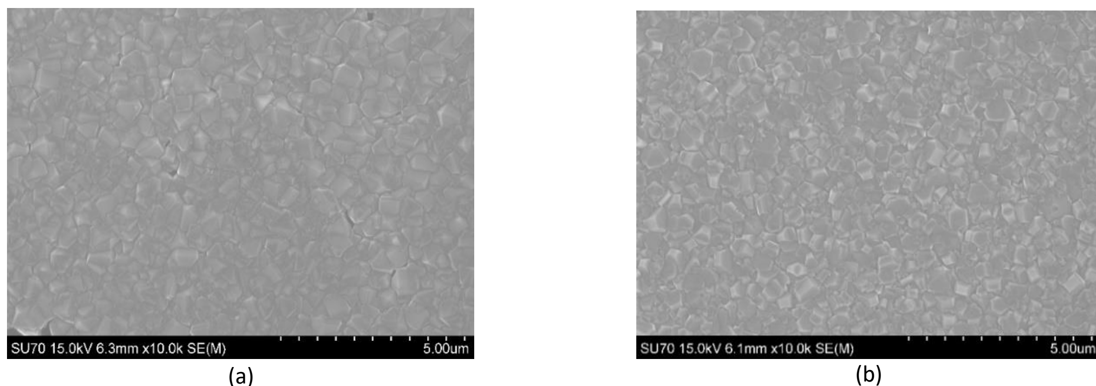

(a) (b)

Figure 4-3 SEM images of samples LNB_grit_1 and LNB_grit_2

However, in the case of both DND seeded samples, although SEM images showed uniform film quality (images not shown), their Raman spectra attest to the large ratio of non-sp^3 content in the film, with a

very large FWHM of sp^3 diamond and significant bands at around 1384 cm^{-1} and 1593 cm^{-1} of the D and G bands of graphite respectively, along with a contribution of amorphous C with a band centered at 1522 cm^{-1} (*Figure 4-4* b). This maybe because of the outer sp^2 shell that DND particles are known to have, by virtue of their fabrication process [551], as was discussed in section 3.5.3.2.

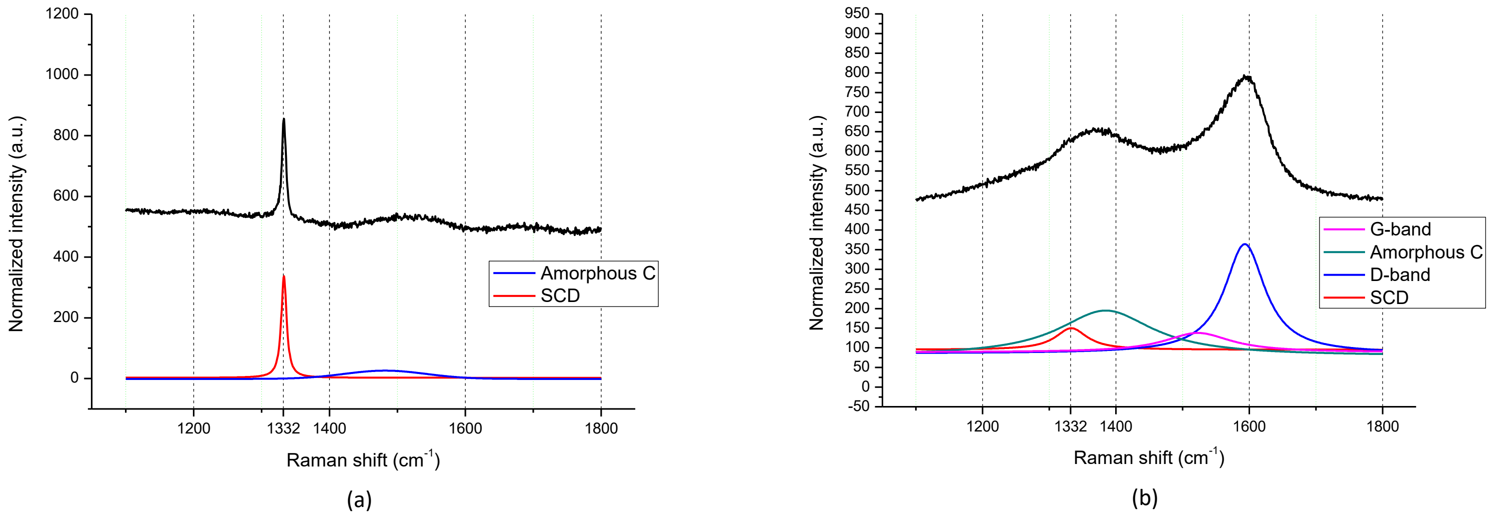

Figure 4-4 Raman spectra of samples (a) LNB_grit_1 (b) LNB_ND_1

Despite the low temperature growth and the 60-minute-long cooling step post growth, however, the films delaminated in all cases. The large grain size of the films lead to a largely increased thermal stress at the interface [263] that these precautions that were taken were not enough to address. Hence, in the next part of the work, which involved the direct growth of patterned diamond on $LiNbO_3$ SAW wafers, it was decided to modify the GCs in order to attain uniform films with smaller grain sizes- NCD and UNCD.

4.2.3 Experimental details- Diamond for SAW using reverse fabrication

For this study, a wafer with dies of commercial 74 MHz delay lines was purchased from SAW Components GmbH, (*Figure 4-5* a). The $LiNbO_3$ substrate is 500 µm thick and the IDTs have a curved structure; no reflectors are present. The IDTs are composed of 100 pairs of double fingers; each finger is ≈ 2 µm wide and the distance between adjacent fingers is ≈ 4 µm (*Figure 4-5* b).

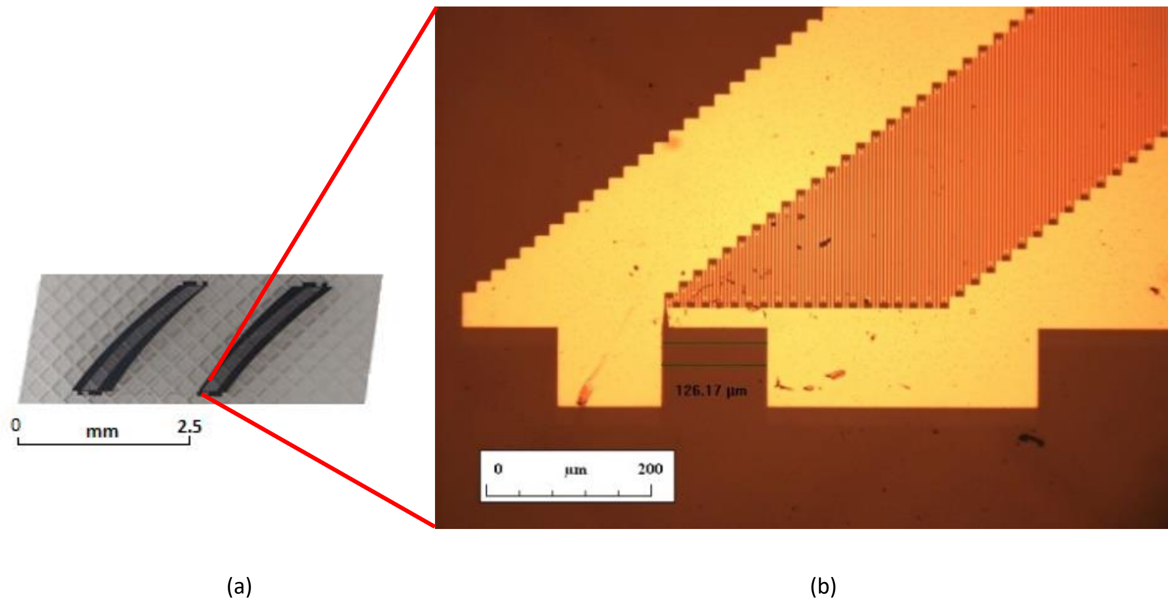

(a) (b)

Figure 4-5 (a) As-purchased die; (b) Optical microscope image of detail of the IDTs

In order to prevent diamond growth on the IDT pads and allow for subsequent electrical probing, they were protected with black wax after which the dies were divided in two groups, named A and B. In order to obtain the black wax masks, the wax was dissolved in limonene and applied on the probe with the help of an optical microscope to magnify the application zone. They were then left in a furnace at 333K for a period of 12 hours. Group A was ultrasonically seeded with DND particles and group B was seeded in a suspension of 6-12 µm diamond grit. After seeding, the wax was removed with limonene, the dies were cleaned in organic solvents and dried using an air-gun. Using the inferences from the previous section, the GCs chosen for this study were to allow for UNCD/NCD growth- i.e., smaller grain sizes to improve film adhesion. Hence, samples underwent P2, i.e., not NNP and dies were placed in an $Ar/H_2/CH_4$ plasma inside an HFCVD system during four different runs (sets D, E, F and G, *Table 4-2*). Again for this study, Re filaments, in the zig-zag geometry, were used so carburization was not necessary, and temperature was limited to 773 K. During each CVD cycle, one die from group A and one from group B were coated together. This guaranteed that any differences between samples coated with the same deposition conditions could be effectively ascribed to the seeding procedure, and not to any other changes. After deposition, coated samples were characterized using SEM and Raman. The thickness of the films was measured by optical profilometry. The S-parameters of as-purchased and coated dies were measured with an Agilent ENA5071B network analyser.

Set	GC			Pressure (kPa)	Seeding
	$Ar/H_2/CH_4$ (%)	Substrate temperature (K)	Duration (min)		
D	81.2/18/0.8	773	120	5	DND (20-30 nm particles in DMSO/CH_3OH 1:3 suspension) [Group A] or 6-12 µm grit (0.6 g in 60 ml CH_3OH) [Group B]
E	98/1/1		120		
F	81.2/18/0.8		60		
G	98/1/1		180		

Table 4-2 Deposition conditions used for diamond growth on SAW dies

4.2.4 Results and discussion- Diamond for SAW using reverse fabrication

Deposition of diamond directly on the surface of a die is a challenging task. The conditions involved during HFCVD growth (for example, the H_2 rich plasma and the high temperatures) may damage the metal electrodes and cause Li to diffuse out; in addition, the difference between the thermal expansion coefficients of diamond and $LiNbO_3$ may induce a high stress at the interface and promote delamination of the diamond film during cooling down. In order to minimize these issues and validate the proposed reverse fabrication method, this study began with the deposition of NCD films in Ar plasma at relatively low temperatures, i.e., 773 K using two different seeding suspensions, as described above.

Figure 4-6 shows films deposited during runs D, E and G. Left and right column samples were seeded with DND and grit suspensions, respectively. Films were deposited for 120 (*Figure 4-6* a, b, c, d) and 180 minutes (*Figure 4-6* e, f) and Ar/ CH_4/H_2/ ratio (%) was 81.2/18/0.8 *(Figure 4-6* a, b) and 98/1/1 (*Figure 4-6* c, d, e, f). The following trend could be seen in all samples: the average grain size of films deposited on samples seeded with grit tends to be larger than the one of samples seeded with DND (*Table 4-3*). In the case of the grit-seeded sample, the surface is covered with a complete layer of diamond nanoparticles that chip off from the larger diamond particles during the US seeding. Once under GC, these particles start growing immediately, without any incubation period. On the other hand, it is known that the DND seeds typically have an outer shell of graphitic or amorphous C [550], even though it is possible to further process these particles and have this shell partially removed [551]- the outer shell delays the effective growth of the diamond seeds, and explains the difference in the size of the grains on the samples. Despite the fact that the film obtained after DND seeding has smaller crystals, it is fully coalesced and no holes can be seen, suggesting that the nucleation density is higher when seeding is performed with DND particles, in comparison with seeding with 6-12 µm grit. The seeding suspension however, does not seem to influence the film thickness (*Table 4-3*). The IDTs were successfully covered with diamond in both cases –*Figure 4-6* (e, d).

Set	Seeding suspension	Film thickness (µm)	Average grain size (nm)
D	DND	0.6	200
	Grit	0.6	500
E	DND	0.2	100
	Grit	0.2	200
F	DND	0.1	60
	Grit	0.1	220
G	DND	0.8	400
	Grit	0.8	800

Table 4-3 Thickness and average grain size of diamond films

In the case of samples deposited with the same GC (D and F, E and G respectively), both thickness and grain size increase with deposition time, as expected. Diamond films deposited for 60 minutes during run F are not fully coalesced; instead, isolated crystals, distributed evenly through the surface of the device, as can be seen in *Figure 4-7* a and b. The area without diamond (*Figure 4-7* a)corresponds to the area that was protected with black wax during the US seeding step. For longer deposition times, the films are almost completely coalesced (*Figure 4-6* e and f). For devices coated during run G, diamond deposited in the middle section of the IDTs delaminated, *Figure 4-7* (c, d). This is related with the difference in the mismatch of the thermal expansion coefficients of diamond/ $LiNbO_3$ and diamond/metal IDTs, resulting in different stresses at both interfaces and causes the diamond film to delaminate from the $LiNbO_3$ between the metal IDTs. The low deposition temperature nor the smaller grain sizes compared to films of

samples of series LNB_grit/DND, could prevent the delamination of the thick films deposited during 180 minutes for this run.

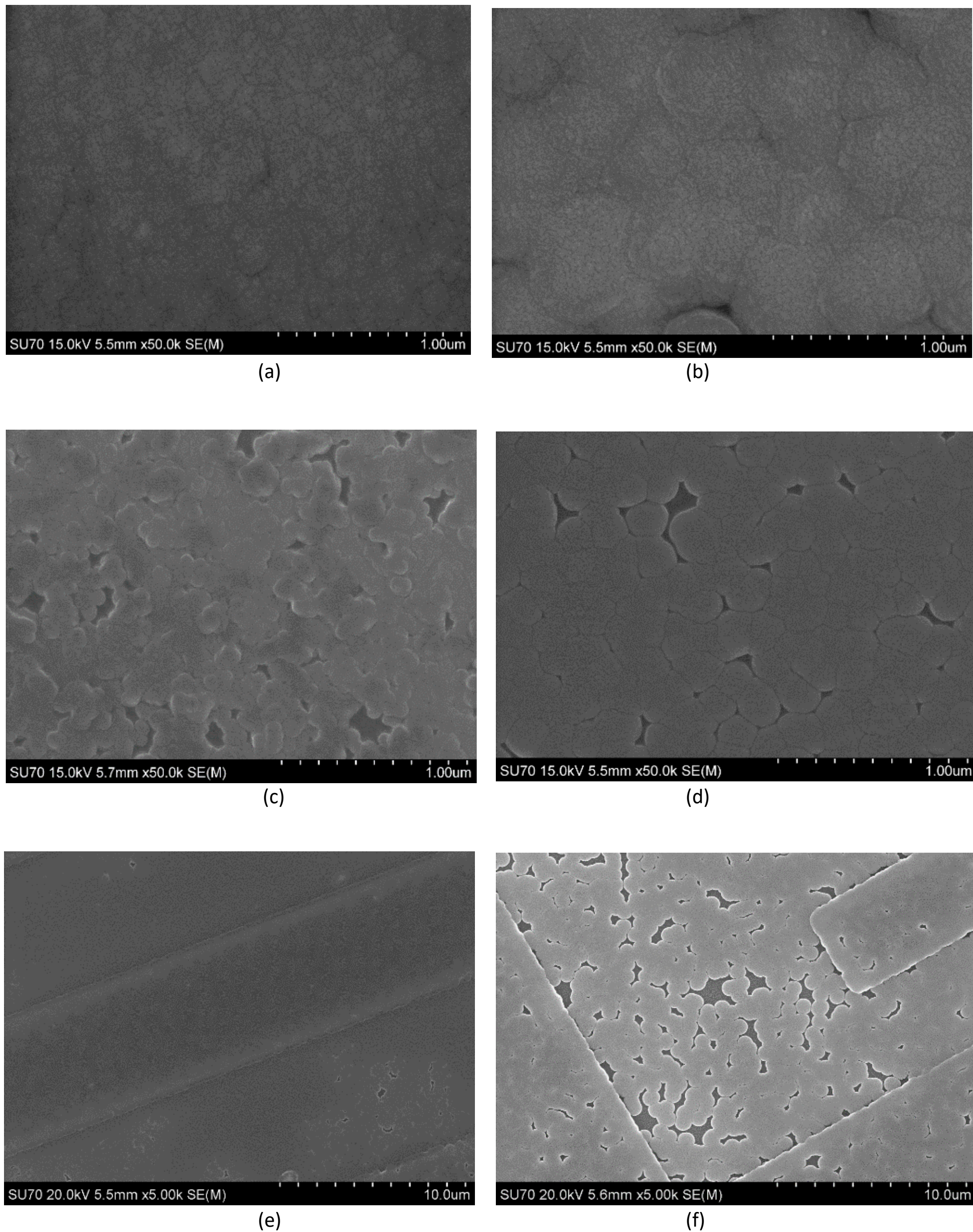

Figure 4-6 SEM images of films deposited during growth cycles D (a,b), E (c,d) and G (e,f) Seeding was performed with (a, c, e) DND and (b, d, f) 6-10 µm grit suspensions.

SEM images of films deposited for 120 minutes (*Figure 4-6* a, b, c and d) present a cauliflower structure. The cluster size of films deposited with larger Ar ratio (series E and G, *Figure 4-6* c, d, e and f) seems to be

smaller than the one of films deposited with higher H_2 ratio, i.e., series D (*Figure 4-6* a, b), reflecting the tendency to deposit UNCD as the H_2 content decreases.

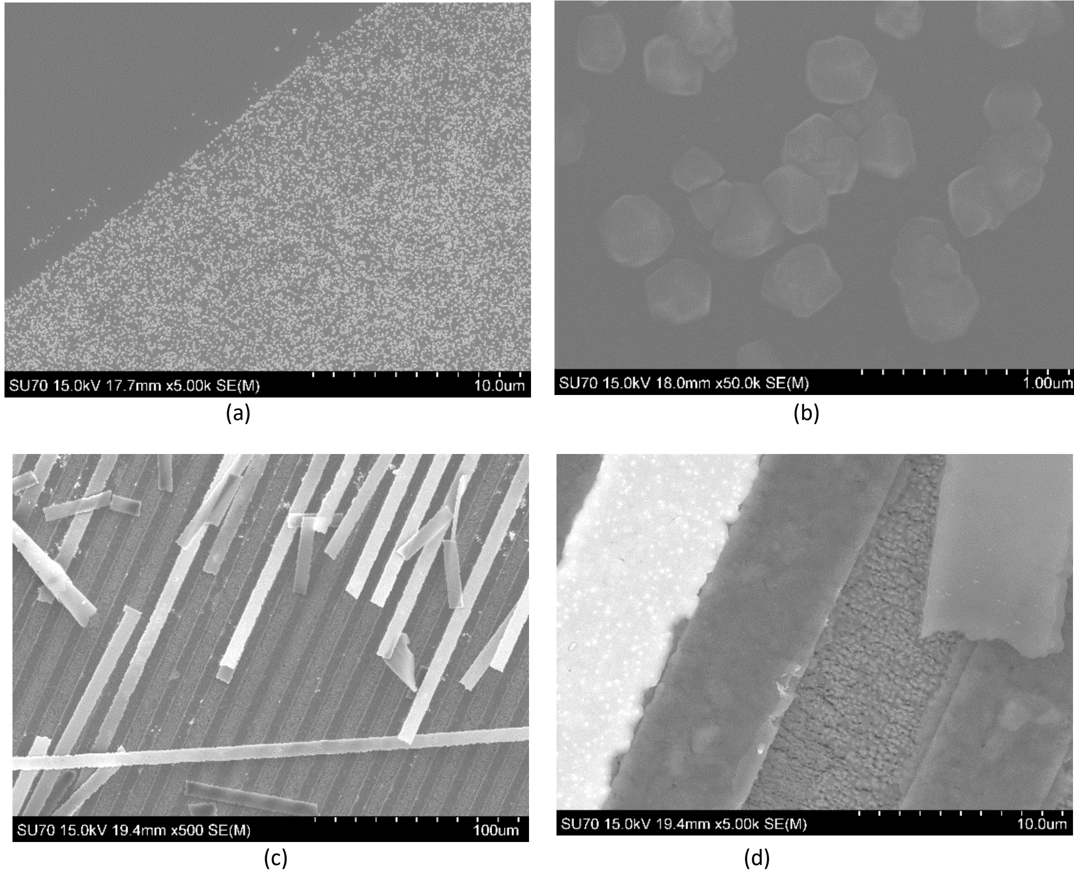

Figure 4-7 (a, b) SEM images of diamond film deposited during run F, seeding performed with grit (c, d) SEM images of the middle section of the IDT fingers showing delamination of diamond from the $LiNbO_3$ surface (series G)

Figure 4-8 shows the Raman spectra taken at the surface of the diamond film deposited on the dies during the different runs. In all the samples, the D and G bands of amorphous C (that are usually centered at 1350 and 1550 cm^{-1}, respectively) can be clearly seen. Fitting (not shown) reveals the presence of smaller peaks around 1150 and 1480 cm^{-1}; associated with NCD. Another peak centered at 1289 cm^{-1} was found at the spectra of sample G seeded with DND suspension; this peak is attributed to the presence of trans-$[C_2H_2]_n$ and explains the apparent broadening of the D band of this sample. The ratio between the D and G peaks is larger for films deposited with larger Ar percentage (series E and G). The sp^3 peak, although detected in all samples, had a large FWHM; signifying relatively poor diamond quality.

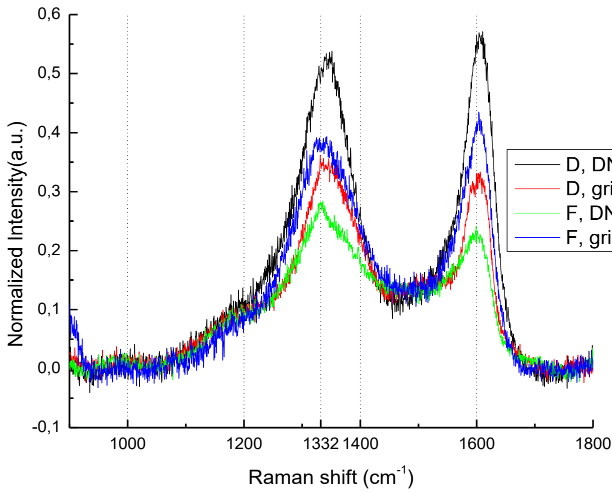

(a)

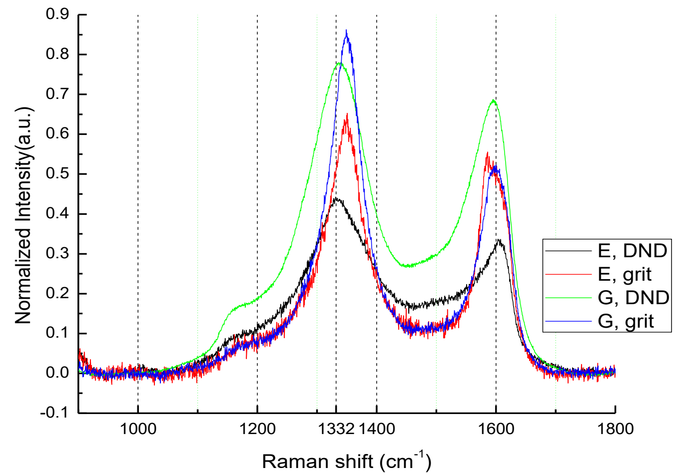

(b)

Figure 4-8 Raman spectra of samples deposited during runs (a) D and F; (b) E and G

The S-parameters of as-purchased dies and of dies coated with diamond during run F were measured with a network analyser. S_{21} graph can be seen in *Figure 4-9.* The transmission frequency window remains centered at 74 MHz and the bandwidth remains the same; this means that the IDTs successfully converted the alternating electric field into a SAW that travelled across the substrate surface, i.e., the piezoelectric properties of the $LiNbO_3$ did not deteriorate due to the deposition of the diamond film. However, these results are accompanied with a drop of more than 20 dB in the signal in both coated dies. This effect may have different origins. One of them may be due to the additional mass loading of the film; however, if this were the case, one would expect to see a shift of the frequency window unless the mass loading caused the formation of bulk waves. Another possible explanation might be the impedance mismatch induced by the presence of the diamond layer on top of the IDTs. In fact, these IDTs are designed to have an impedance that matches the impedance of the network analyser probes (50 Ω) at the operating frequencies. The presence of a diamond layer with a different dielectric constant changes the impedance of the IDTs which might induce an impedance mismatch between the probes and the IDTs and a corresponding signal drop. The stronger attenuation at the central frequency, however, cannot be attributed to this effect; the attenuation is also noted to be more significant in the grit seeded sample. Without further investigation, at this stage it is not possible to provide a definite explanation of this effect. Studies are needed to clearly identify the origin of the central frequency signal attenuation and propose a viable way to overcome it.

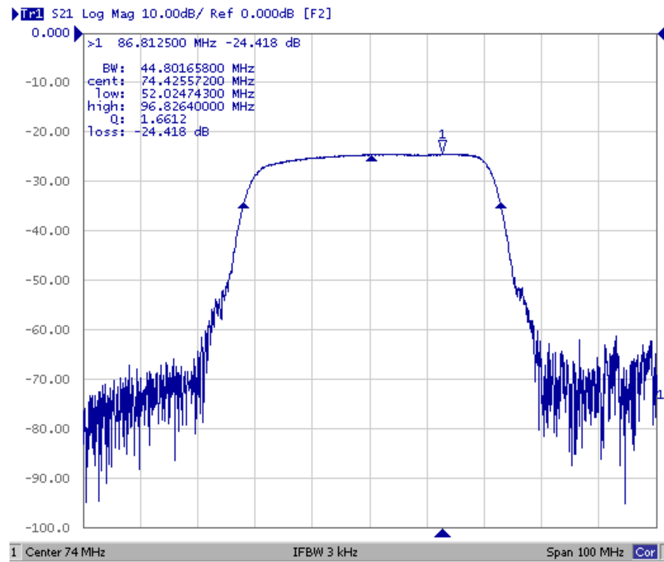

(a)

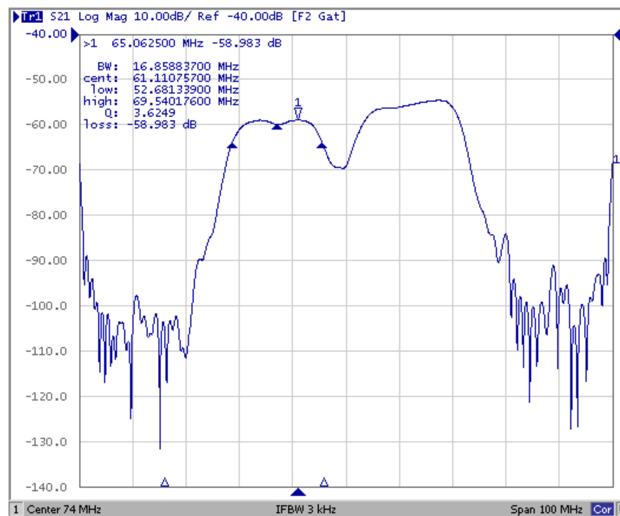

(b)

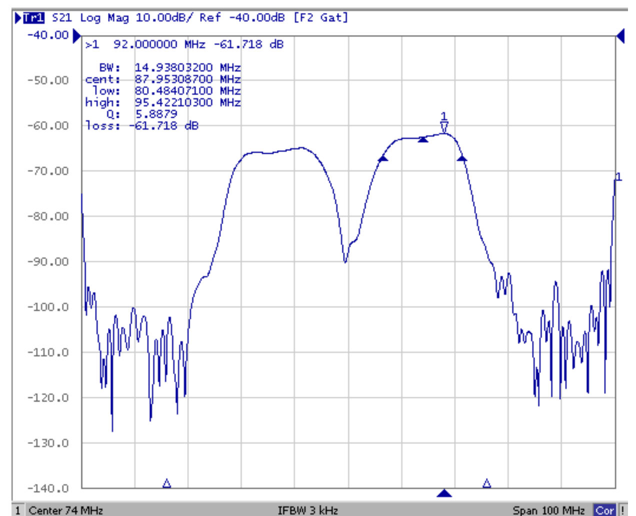

(c)

Figure 4-9 S_{21} of (a) as-purchased die; dies coated with diamond during run F, seeded with (b) DND and (c) grit suspensions, respectively

Despite the NCD film covering the full surface of the $LiNbO_3$, the operating frequency did not increase. To increase the operating frequency, which is one of the prime benefits of the $LiNbO_3$-diamond composite structure, a possible solution would be to protect not only the pads, but the whole IDTs during the seeding step. This would, in addition to keeping the impedance of the IDTs unchanged, also prevent the delamination of the diamond between the fingers due to the accumulated stress at the interface. Another improvement would be to grow thicker films, by decreasing the seeding density and encouraging lateral film growth by using NNP for NCD and UNCD films as well- NNP for UNCD/NCD growth has, thus far, not been investigated. As the growth plasma for the latter involves Ar, detailed investigation is needed into the kinetics and effect of this plasma on the UNCD/NCD PT film. This work was not performed at the moment due to the unavailability of more dies, but is a subject for further studies. These preliminary results, however, opened the door to a simplified fabrication procedure of diamond-based SAW devices.

4.3 Patterned diamond holders for electronic devices

Miniaturization, increasing speeds accompanied by increasing power levels and the related thermal management issues of ICs have made its packaging with conventional materials increasingly difficult [559]. Typical elements involved in a packaged IC are, besides the IC die itself, the substrate, the die-attach (epoxy for example) to mount the die on the substrate, polymer circuit boards (PCB) and metallic interconnects. The packaging of an IC serves several functions such as signal and power distribution, circuit support and protection and also, heat dissipation. As it is widely known that nearly 60% of electronics failures are temperature induced and for every 10°C rise in operating temperature the failure rate nearly doubles [560], packaging designers aim to use materials that afford the maximum thermal conductivity and the minimum thermal expansion [561], not just in terms of materials used, but also the way the die is attached to the package, leading to two kinds of IC packages- the through-hole and the surface mount types. In particular, with the advent of packages with solder balls in the late 1980s, surface mount packages have afforded higher packaging densities on the board compared to through-hole packages. For such packages, it is particularly useful to use a substrate with good thermal properties and the recent advances in diamond technology, as well as the promise of major reductions in the price of synthetic diamond has allowed its consideration for use in electronic thermal management applications, such as MCM substrates [562]. Diamond, with a thermal conductivity about six times greater than AlN or BeO, the two most commonly used substrate materials [563], is most uniquely poised to address thermal management requirements- substrate materials must ideally have high thermal conductivity and electrical resistance and a low thermal expansion coefficient. Diamond fits all of these criteria perfectly. Large area (a few square inches) diamond films can be deposited on foreign substrates by CVD in an economical way, allowing for the usage of PCD films as a substrate. CVD diamond has been investigated as a substrate material using several approaches- as a composite with existing ceramic substrates [230, 564] as well as all diamond packaging panels with built-in interconnects for integrated microsystems [565]. Although PCD retains the superior thermal properties of SCD reasonably well [70, 72, 82], it does face the challenge of surface roughness- the surface roughness of the top growth side of the diamond films increases with increasing film thickness, due to an increase in the average crystal size at the surface and a polishing step is usually required before subsequent metallization and device attachment. Diamond can be polished using diamond powder or more sophisticated chemical techniques, but this step is a prohibitive cost additive to the addition of diamond substrates in the packaging process. An alternative to the growth surface of the PCD wafer is using the nucleation side of the wafer instead- it typically has much lower average roughness and mirrors the roughness (or more appropriately, the smoothness) of the substrate on which it is grown. Currently, EDS signals from the nucleation side show many non-C phases (like Si and O) and non-diamond C peaks, that attest to its poor quality; in addition, this is evidenced by its Raman spectra in the broadening of the peaks in the spectrum which is higher on the nucleation surface when compared to the growth side of otherwise good quality PCD [566]. This poorer quality of the nucleation side leads to compromise in the effective thermal conductivity values and thus hinders its usage.

In this work, a straightforward way of fabricating CVD diamond substrates using the nucleation side of the diamond which addresses directly the surface roughness issue [567] without need for an additional polishing step is proposed. In addition, the technique also allows one to simultaneously fabricate features on the substrate that may be advantageous to the consequent metallization and die attach steps. Such features might be particularly useful for the already commonly used flip-chip bonding technique which removes the need for bonding wires and has been known to improve the thermal contact between the die and the substrate [559, 568, 569]. In addition, such features can be beneficial for the embedded die

packaging systems that are leading to improved packaging densities and thermal contacts as well [570]. Most importantly, however, the work presents novel results that attest to the fine quality of the nucleation side when the NNP is used. NNP is poised to address many of the aforementioned problems that are currently faced when utilizing the nucleation surface of diamond by encouraging the lateral growth of grains.

4.3.1 Experimental details

A total of 4 samples were used in these experiments, 2 5 mm × 5 mm Si pieces (Si_10h and Si_20h), 1 Si sample with negative V-grooves (Si_neg_1) and 1 Si sample with mesa-structures (Si_neg_2). The V-grooves and mesa-structures were obtained in Si, by using typical photolithography processes (an example can be seen in *Figure 4-11* a). All samples underwent the P1. The experimental conditions used are listed in *Table 4-4*. In order to achieve a higher rate of growth, a relatively higher substrate temperature was used [571], and W filaments were chosen for this purpose. Of the commonly used HF materials, W has the highest melting point (3695 K compared to 3458 K for Re and 3290 K for Ta), allowing one to reach higher filament temperatures and subsequently, higher substrate temperatures with very little material evaporation [572]. Filament temperature was monitored using the same pyrometer as described before (section 3.5.2) but with emissivity set to 0.85 [541]. As W is a carbide forming metal, carburization was carried out following the steps detailed in section 4.1. To obtain a good ratio of sp^3 to non-sp^3 content in the films, in line with the thermal conductivity requirements of the proposed holders, the 6-12 µm grit suspension was used. The films were analyzed for diamond quality using SEM and Raman, post growth. After respective analyses, samples underwent a wet chemical etch (a mixture of HF and HNO_3 in 2:3 ratio), following which free-standing diamond holders were obtained with surface features on the nucleation side (that mirror the features of the negative of the Si holder) and the features analyzed again using SEM imaging, Raman spectroscopy and profilometry.

<table>
<tr><th rowspan="2">Sample ID</th><th colspan="3">PT</th><th rowspan="2">Pressure (kPa)</th><th rowspan="2">Seeding</th><th colspan="3">GC</th><th rowspan="2">Pressure (kPa)</th></tr>
<tr><th>CH_4/H_2 (%)</th><th>Substrate temperature (K)</th><th>Duration (min)</th><th>CH_4/H_2 (%)</th><th>Substrate temperature (K)</th><th>Duration (h)</th></tr>
<tr><td>Si_10h</td><td rowspan="4">3</td><td rowspan="4">873</td><td rowspan="4">60</td><td rowspan="4">5</td><td rowspan="4">6-12 µm grit (0.6 g in 60 ml CH_3OH)</td><td rowspan="4">1</td><td rowspan="4">873</td><td>10</td><td rowspan="4">5</td></tr>
<tr><td>Si_20h</td><td>20</td></tr>
<tr><td>Si_neg_1</td><td rowspan="2">50</td></tr>
<tr><td>Si_neg_2</td></tr>
</table>

Table 4-4 Deposition conditions used for diamond growth on Si samples

4.3.2 Results and discussion

The growth rate of the diamond films was first ascertained by using the same conditions as proposed for the final growth on two cleaned Si pieces (Si_10h and Si_20h), and making growth for 10 hours and 20 hours respectively. The cross-section of these samples was observed under the SEM to measure the thickness of the films. After 10 hours of growth, the film had an average thickness of 5µm, and 10 µm after 20 hours. A growth rate of 0.5µm/h was thus ascertained and the SEM images are presented in *Figure 4-10*.

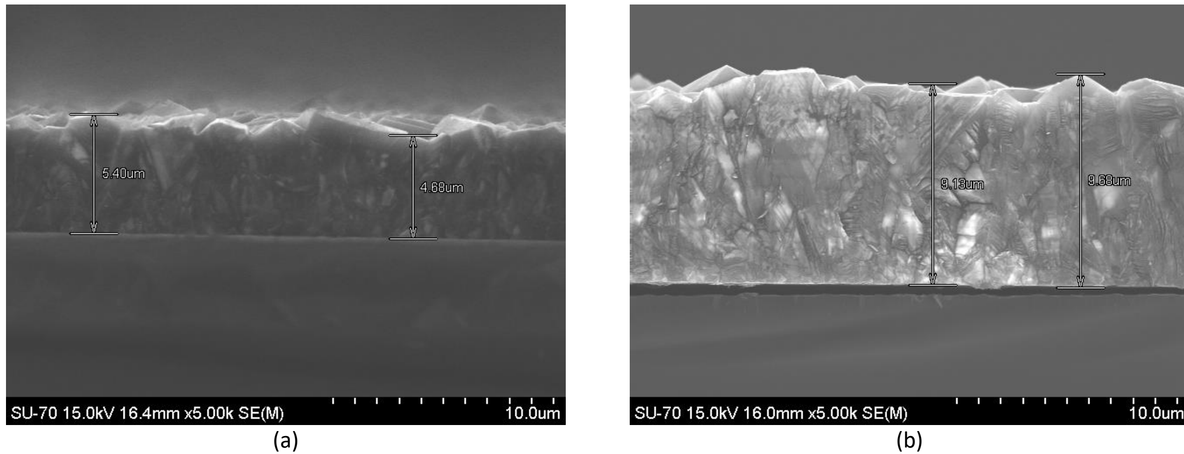

Figure 4-10 SEM images of cross-section of films (a) Si_10h, after 10 hours (b) Si_20h, after 20 hours of growth

The Si holders (Si_neg_1 and Si_neg_2) underwent deposition for 50 hours to obtain 25µm thick films. SEM images of the growth surface are shown in *Figure 4-11* b. A relatively higher initial ratio of CH_4/H_2 (3%) was used for the PT to ensure a high C content in the PT film and good dispersion of subsequent seeding particles. For growth, this ratio was reduced from 3 to 1% to obtain good diamond quality in the film- this was evidenced in the Raman spectrum of the growth surface that showed the characteristic sharp peak of sp^3 diamond at 1332 cm^{-1} (FWHM 15 cm^{-1}) [427] (results not shown). Raman spectrum of the nucleation surface also showed the sp^3 diamond peak at 1332 cm^{-1}; the presence of H_2 at grain boundaries presented itself as a peak at 1450 cm^{-1} (FWHM 98.6 cm^{-1}) and the G- band of graphite at 1540 cm^{-1} (FWHM 69.5 cm^{-1}) (*Figure 4-12*).

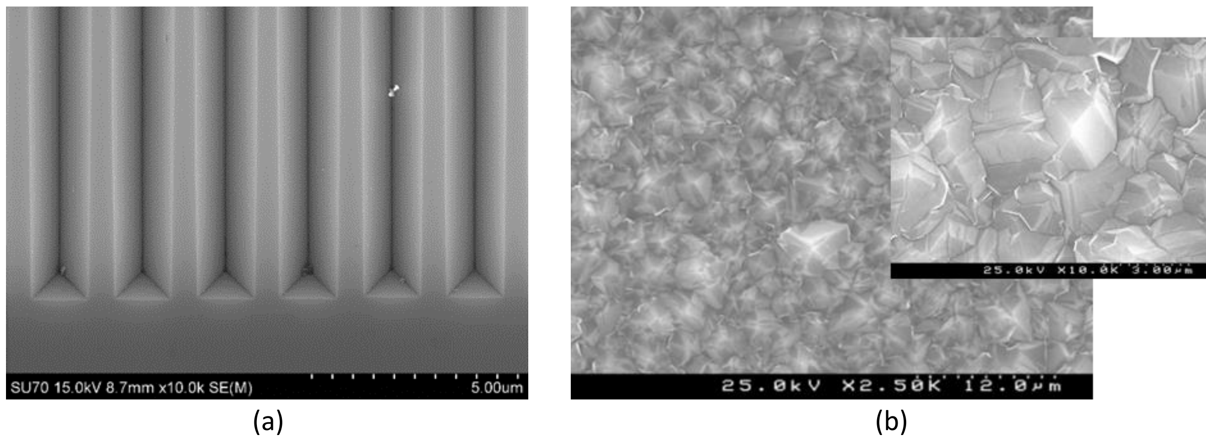

Figure 4-11 (a) 10kx SEM image of bare Si "negative", (b) 2.5kx SEM image of growth surface of fully coalesced diamond film (Si_neg_1) (inset with high magnification image)

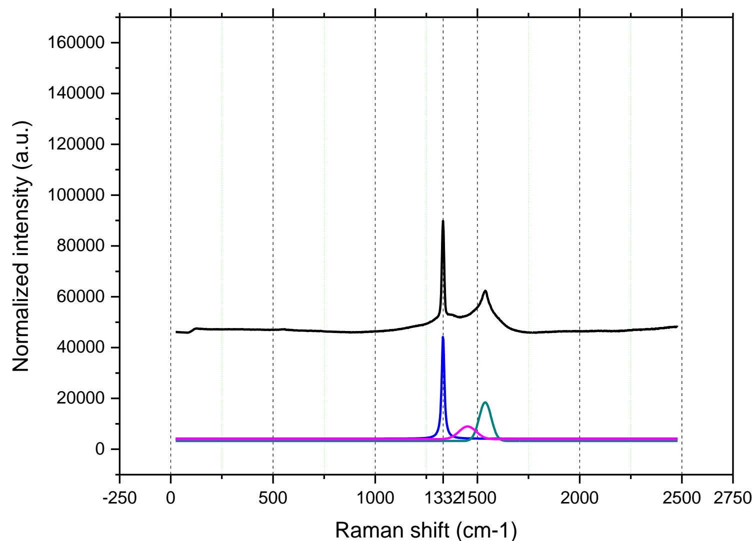

Figure 4-12 Raman spectrum of the nucleation surface of Si_neg_1

As can be seen from the images of the nucleation surface (*Figure 4-13* a, b and *Figure 4-14*), the topography of the Si surface is mirrored. The large grain size (between 550 to 1100 nm) can be noted in the higher magnification images (*Figure 4-13* c and d). What is notable in these pictures is the large crystal size and the extremely good quality of the nucleation surface- the images show the lack of holes in the film and its uniformity.

Profilometry was used to measure the dimensions of the v-grooves and an average value of 3.8303 µm was obtained. Surface roughness was below the detection limit of the optical profilometry (Comparing these to the quality of nucleation surfaces obtained in other work [566], it can also be noted that there are no agglomerations or seed leftovers. This can be directly attributed to the NNP that these samples received that is known to aid in the uniform distribution of the seeds because of the PT film. Roughness of the surface was below the detection limit of the profilometer (<0.3 nm) (*Figure 4-13* e), i.e., these values are considerably lower that the rms roughness of nucleation surfaces obtained by other methods [566, 573].

In summary, using NNP the quality of the nucleation surface can be considerably improved; the described technique can thus be used to fabricate a variety of features by taking advantage of the smooth surface of this high quality nucleation face of diamond. In addition, this technique of growing diamond on negatives Si substrates followed by wet chemical etch also allows one to fabricate the features required for flip-chip and embedded die packaging technologies.

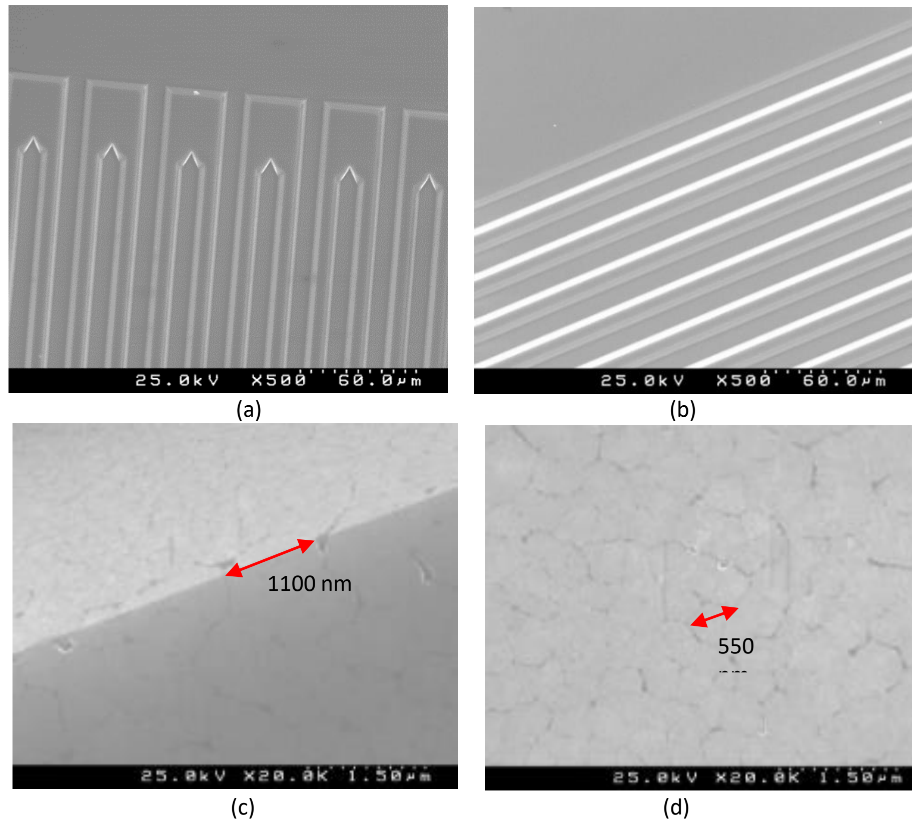

Figure 4-13 SEM images of nucleation surface of the film Si_neg_50h (a,b) 500kx showing details of features (c,d) showing details of edge of feature and nucleation surface (e) profilometry capture of film cross-section

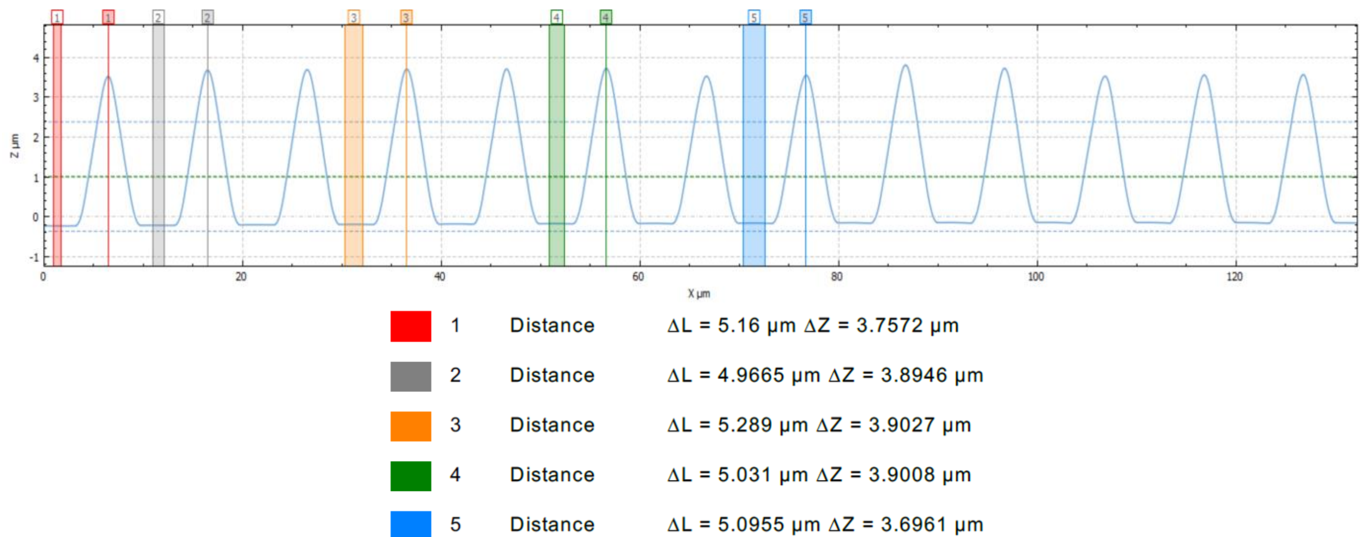

Figure 4-14 Profilometry measure of heights of v-grooves on nucleation surface of free-standing diamond

4.4 Low temperature growth of diamond on SiC and GaN

SiC and GaN are two promising WBG materials, with much potential for use in HPHT electronics. The primary limitation in their full exploitation for the same lies in the lack of effective passivation, making it more difficult to realise their theoretical potentials. The following sections present a contextualization of

utilizing diamond as a passivation layer to overcome several of the limitations faced by devices fabricated with SiC and GaN followed by the experimental details of the growth of conformal diamond films on the two materials.

4.4.1 Passivation of SiC and GaN devices

Despite the promising numbers associated with the performance of SiC and GaN WBG devices [574, 575], there are some disadvantages associated with the use of devices fabricated from SiC and GaN. For example, SiC wafer fabrication technology is mature enough to produce 6 inch wafers with low defect density and p- and n-type epitaxial layers but at a considerable cost compared to that of Si wafers [576]. The cost can be justified if the efficiency and the maximum power values can be significantly improved. This, in turn, depends on the maximum breakdown voltage and leakage currents of a particular device. This makes the challenges of the effective passivation of the SiC surface, as well as the heat removal from the device's hotspots- topics linked to the back-end processes, of crucial importance since they can affect the efficiency of the edge termination. Moreover, as the high operating temperature of SiC power devices will certainly contribute to the market growth and industrial utilization, it will be necessary to develop packages able to withstand high operating temperatures. At the moment, SiC technology has the advantage of being able to utilize the same native oxide, SiO_2 as Si technology for passivation and although this is adequate for the thermal specification and voltage range of todays' commercial SiC unipolar devices, the breakthrough for SiC MOSFETs is severely hampered by the SiO_2/4H-SiC gate properties [577, 578]. Because of the established relationship between the channel mobility behaviour and the passivation of interface states for SiC FETs in particular [579], passivation remains an important challenge to be addressed.

GaN technology on the other hand faces other challenges- GaN boules are difficult to grow. Therefore, pure GaN wafers are not available; instead, GaN wafers are grown on sapphire or SiC [580] making GaN wafers even more expensive than SiC wafers. Annealing studies performed GaN substrates, in particular, thin films with thickness up to 3µm, show promising results- the material itself does not show damage up to 1200°C. However, for higher temperatures, for example at 1300°C, a high density ($\sim 10^8$ cm^{-2}) of small distorted hexagonal pits due to incongruent evaporation from the surface are observed. At 1400°C the substrates shows extensive, non-reversible, disassociation [581]. In addition, analytical studies on GaN HEMTs have shown that increase in temperature is associated with highly undesirable leakage current increases [579]. This behaviour of GaN shows that although it is a suitable candidate for HPHT electronics, given its superior electronic properties, an effective passivation as well as thermal management is crucial. To overcome this limitation and reduce the leakage current in the HEMTs, introducing a thin (10–20 nm) dielectric layer is the most straightforward approach, SiN_x being the most popular choice [579] because of its high permittivity. It is however limited by its relatively poorer thermal conductivity [582].

The above discussion elucidated the importance of passivation in the successful utilization of HPHT devices fabricated with WBG materials. Important physical properties of a passivating layer on a semiconductor are large dielectric constant, large band-gap and sufficient band offsets between the valence and conduction band edges between the passivating dielectric layer and the semiconductor [583]. A high thermal conductivity and a thermal expansion coefficient of similar magnitude as that of the semiconductor are also desirable. Besides the intrinsic properties, the deposition technique itself used to form the passivation layer is critical- it should enhance the overall reliability and electric field durability of the system without damaging the substrate. The interface of the passivating layer and the semiconductor should contain, if at all, only a low and thermally stable concentration of electronic defects such that

properties such as the surface potential, mobility and the recombination of charge carriers are not affected. As the ideal, defect free, interface is technologically difficult to achieve, the deposition technique must aim at minimizing the amount of defects with particular attention to interface quality.

Due to intrinsic material properties, such as a WBG and a high thermal conductivity, diamond films deposited by CVD emerge as a candidate for the passivation of WBG devices, while providing at the same time a highly thermally conductive layer that can spread and dissipate the heat generated during the devices operation. To take advantage of these properties, the interface between the diamond film and the substrate needs to be as intimate as possible, otherwise the electrical passivation may be compromised. As discussed in section 3.2.3.1, the existence of voids and the high density of grain boundaries at the nucleation surface must be diminished in an intimate, good quality interface and it can be done if the lateral growth of the grains is enhanced during the initial stages of diamond deposition- i.e., performing the NNP. The following sections present experimental results that are then discussed in detail to elucidate the influence that NNP may have on this same film quality. In addition, the CVD parameters - substrate temperature, CH_4/H_2 ratio and size of the diamond particles used for the seeding procedure, that most influence the morphology and growth rate of the deposited diamond film are also discussed.

4.4.2 Experimental details- Diamond on SiC

A total of 14 10 mm × 10 mm double side polished 4H-SiC samples were used in this work. Additional films were deposited on 4 n-type epitaxial 6H-SiC wafers. Both polished and epitaxial samples presented a mirror-like surface and the two sets were not distinguishable to the naked eye. Beside standard solvent cleaning 1 and 2, samples also underwent the 2-step RCA clean (SC1, oxide clean and SC2). For this work, Re filaments were used, hence, carburization was not necessary. The protocol followed was P1 and the experimental conditions are listed in *Table 4-5*; samples with same ID prefixes were all coated in the same run. The surface of the SiC substrates from series A was partially covered with flat Si samples; in the remaining experiments (series B, C & D) the whole surface of the SiC was exposed to the plasma. The details of the seeding suspension used, listed in the following table are as follow (i) 40-60 µm- 0.2 g of diamond grit dispersed in 20 ml C_2H_5OH, (ii) 6-12 µm- 0.2 g of diamond grit dispersed in 20 ml C_2H_5OH and (iii) 4-5 nm clusters of DND particles dispersed in DMSO diluted in C_2H_5OH (1:3 ratio). The samples were then characterized using SEM and Raman.

Series	Sample ID	Substrate[1]	PT			Pressure (kPa)	Seeding	GC			Pressure (kPa)	Grain size (nm)	FWHM (cm^{-1})
			CH_4/ H_2 (%)	Substrate temperature (K)	Duration (min)			CH_4/ H_2 (%)	Substrate temperature (K)	Duration (min)			
A[2]	POL_PT1_ S1_G11	Pol	1	873	60	5	40-60 µm grit in CH_3OH	1	773	120	5	500-600	
	POL_PT1_ S1_G12							1	873	60		250-350	
	POL_PT1_ S1_G13							1.5	773	90		400-600	
	POL_PT1_ S1_G14							1.5	873	30		200-300	
B	POL_PT2_ S2_G21	Pol	1	873	60		40-60 µm grit in CH_3OH	1	773	120		600-800	
	POL_PT2_ S2_G22							1	873	60		200-300	
	POL_PT2_ S2_G23							1.5	773	90		400-600	
	POL_PT2_ S2_G24							1.5	873	30		150-250	
C	POL_PT2_ S3	Pol	1	873	60		4-5 nm DND in DMSO	--	--	--		--	--
	POL_PT2_ S3_G3							1	773	60		50-100	63
	POL_PT2_ S3_G4							1	873	180		333-550	19
	EPI_PT3_ S4	Epi	1	873	60		6-12 µm grit in CH_3OH	--	--	--		--	--
	EPI_PT3_ S4_G3							1	773	60		150-350	20
	EPI_PT3_ S4_G4							1	773	180		350-750	16
D	EPI_PT4_ S5_G5	Epi	1	773	60		6-12 µm grit in CH_3OH	1	773	60		125-225	19

1 Epi – epitaxial SiC; Pol – polished SiC.
2 The substrate was partially covered with a Si piece during the PT step

Table 4-5 Deposition conditions used for diamond growth on SiC samples

4.4.3 Results and discussion- Diamond on SiC

Figure 4-15 a and b shows low magnification SEM images of samples POL_PT1_S1_G11 and POL_PT1_S1_G14 (series A), after the growth cycle; the shape of the Si piece used to partially cover the SiC samples is marked in the images with a red line. The films are non-uniform- below the edges of the Si piece the film is coalesced, in contrast to the remaining area under the Si piece. The films deposited on samples POL_PT1_S1_G12 and POL_PT1_S1_G13 follow the same trends (images not shown). Since both seeding and growth cycles were performed with the SiC surface fully exposed, this difference in the film morphology is related with the PT step. Higher magnification images also reveal that the outer boundaries of the closed deposit are sharper than the inner boundaries. This can be explained in the following way- gaseous C radicals that infiltrated below the Si pieces were trapped preferentially along the edges of the Si piece and resulted in a corresponding local artificial increase in the C supply. It is known that for the same temperature and deposition time, the PT film thickness increases with the CH_4/H_2 ratio [53]; this would cause a gradient in the thickness of the PT film, and an additional C supply along the edges would contribute to the formation of a denser film during the growth cycle. This was indeed the case- as was seen when the higher magnification images of these were compared to (1) parts covered further inside

under the Si piece during PT as well as (2) part of the SiC that was left uncovered during the PT step. In the first case, the films were non-uniform and not coalesced and in the second case, uniform but closed (images not shown).
The higher magnification images of the denser zones (marked with an arrow) revealed films with different trends (*Figure 4-15*). The grains of the films deposited at 773 K (*Figure 4-15* c and e) are larger and flatter. This effect seems to be more evident for 1% CH_4/H_2 gas ratio – *Figure 4-15* c. On the contrary, films deposited at 873 K (*Figure 4-15* d and f) reveal sharper crystals. This influence of the substrate temperature on the film morphology has been widely reported in the literature [584].
The deposition times are different for all the samples and it can be seen that for the same temperature (*Figure 4-15* c, d, e and f), longer deposition times resulted in larger crystals *(Table 4-5*). These images suggest that lower deposition temperatures (773 K) and lower CH_4/H_2 (1%) ratios induce the lateral growth mode of the crystals during the initial moments of the deposition; this is not a surprising result, since a lower temperature and/or a lower CH_4/H_2 ratio mean a lower supply of C from the gas phase; on the other hand, the C in the PT film is a steady source of C in the initial moments of deposition. The balance between C supply from the gas phase and from the PT film results is larger two-dimensional grains for lower temperatures and CH_4/H_2 ratios, but also lower growth rates. This in turn may induce lateral growth of the crystals during the first moments of deposition.

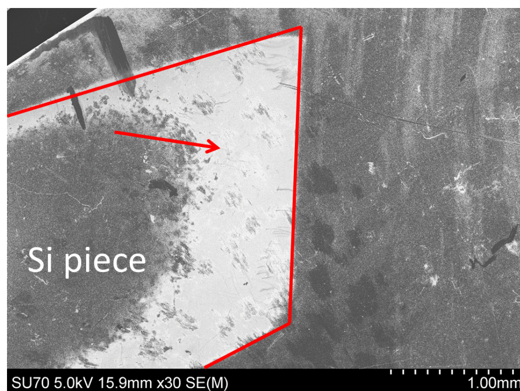

(a)

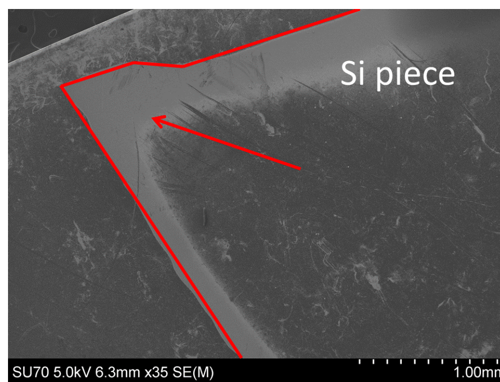

(b)

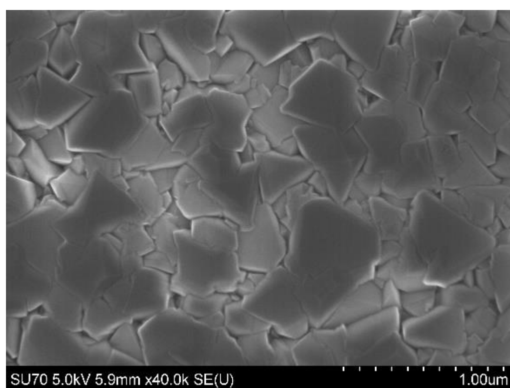

(c)

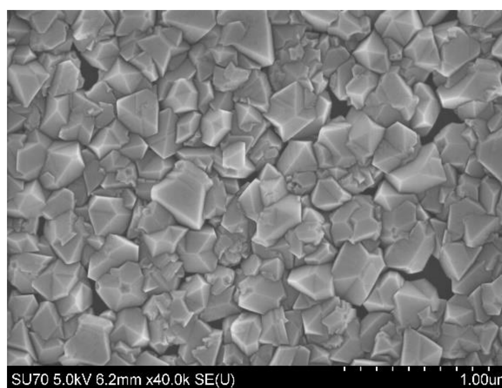

(d)

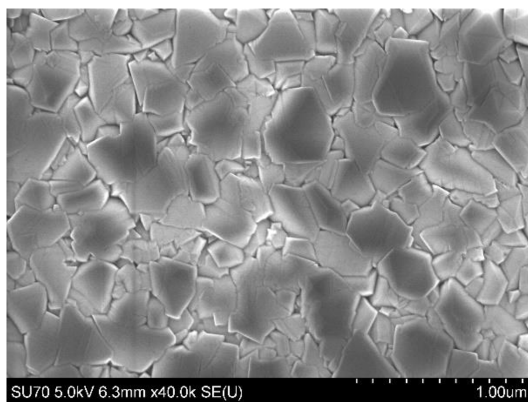

(e)

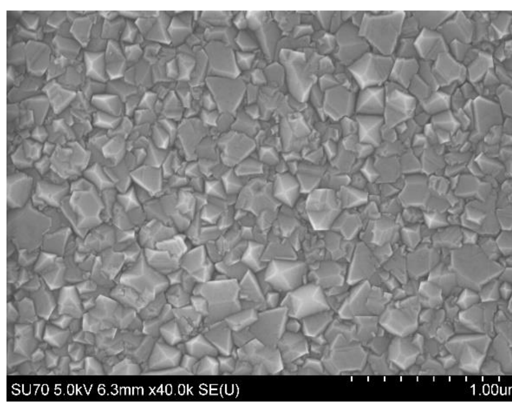

(f)

Figure 4-15 Low magnification SEM images of samples (a) POL_PT1_S1_G11 and (b) POL_PT1_S1_G14. High magnification SEM images of samples (c) POL_PT1_S1_G11, (d) POL_PT1_S1_G12, (e) POL_PT1_S1_G13 and (f) POL_PT1_S1_G14

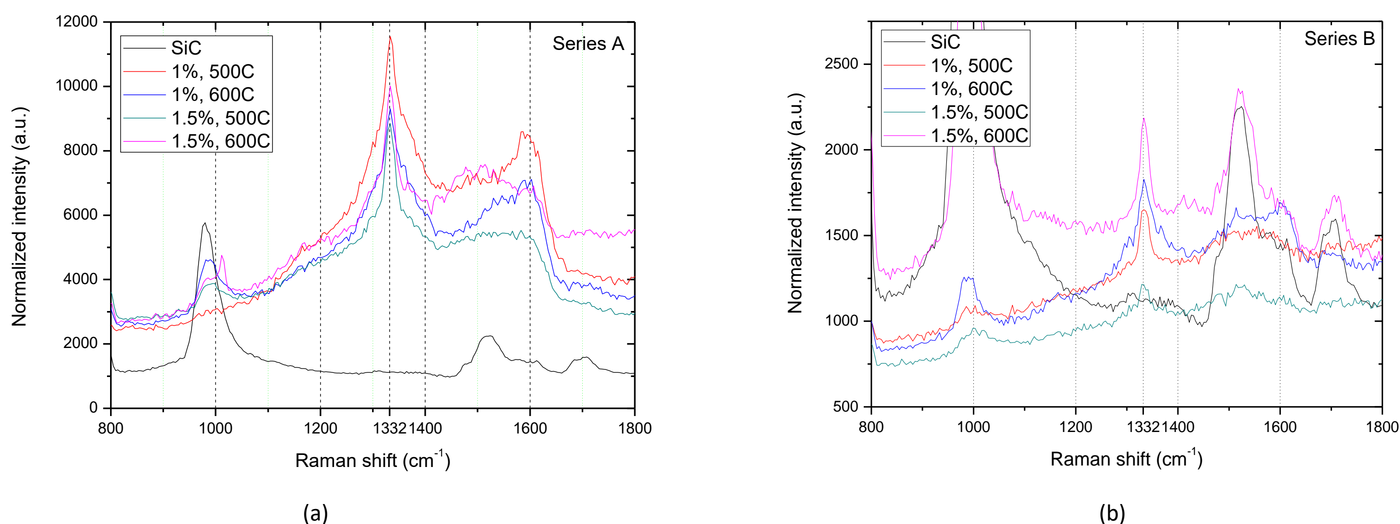

Figure 4-16. Raman spectra of samples from series (a) A and (b) B

Figure 4-16 a shows the Raman spectra obtained from the denser zones; the Raman spectrum obtained from the pristine SiC substrate is included as a reference. The sp^3 diamond peak is centered around 1332 cm^{-1} and is considerably broad for all films, with the exception of the film deposited at 500°C with 1.5% CH_4/H_2; however, as discussed above, if the gas molecules were trapped below the Si surface, the local C content changed, making it impossible to relate the quality of the films with the deposition conditions. A weak band centered around 1150 cm^{-1} is seen in all the films, indicating the presence of NCD or trans-$[C_2H_2]_n$; the films deposited with 1% CH_4/H_2 show the G-band at 1590 cm^{-1}. An additional broad band centered at ~1500 cm^{-1} is seen in some spectra; this is due to the SiC band centered at 1525 cm^{-1} contributed and it is not possible to separate the signals from the substrate and film.

The next set of samples (series B) was prepared under the same conditions as series A (*Table 4-2*), but the PT was performed on the whole surface of the SiC samples thus removing any influence that the Si sample might have had in samples from series A. The deposited films are uniform all over the sample but they are not coalesced (*Figure 4-17*). The degree of coalescence of the films decreases from samples POL_PT2_S2_G21 to POL_PT2_S2_G23 to POL_PT2_S2_G22 to POL_PT2_S2_G24 (*Figure 4-17*). This is expected because of the corresponding deposition times for each sample, decreasing in the same order from 120 minutes to 30 minutes. It was noted that the shape of the individual crystals followed the trend observed in series A, that is, crystals deposited at 773 K (*Figure 4-17* a, c) have a tendency to be larger and flatter. The average size of the crystals in samples from series A and B deposited under the same conditions is also similar *(Table 4-5*). From the analysis of series A and B, it was concluded that the seeding of the SiC substrates with the 40-60 µm diamond suspension was not effective (despite the area with a coalesced film that was observed in samples from series A which however can be ascribed to the accumulation of gas radicals below the Si top pieces).

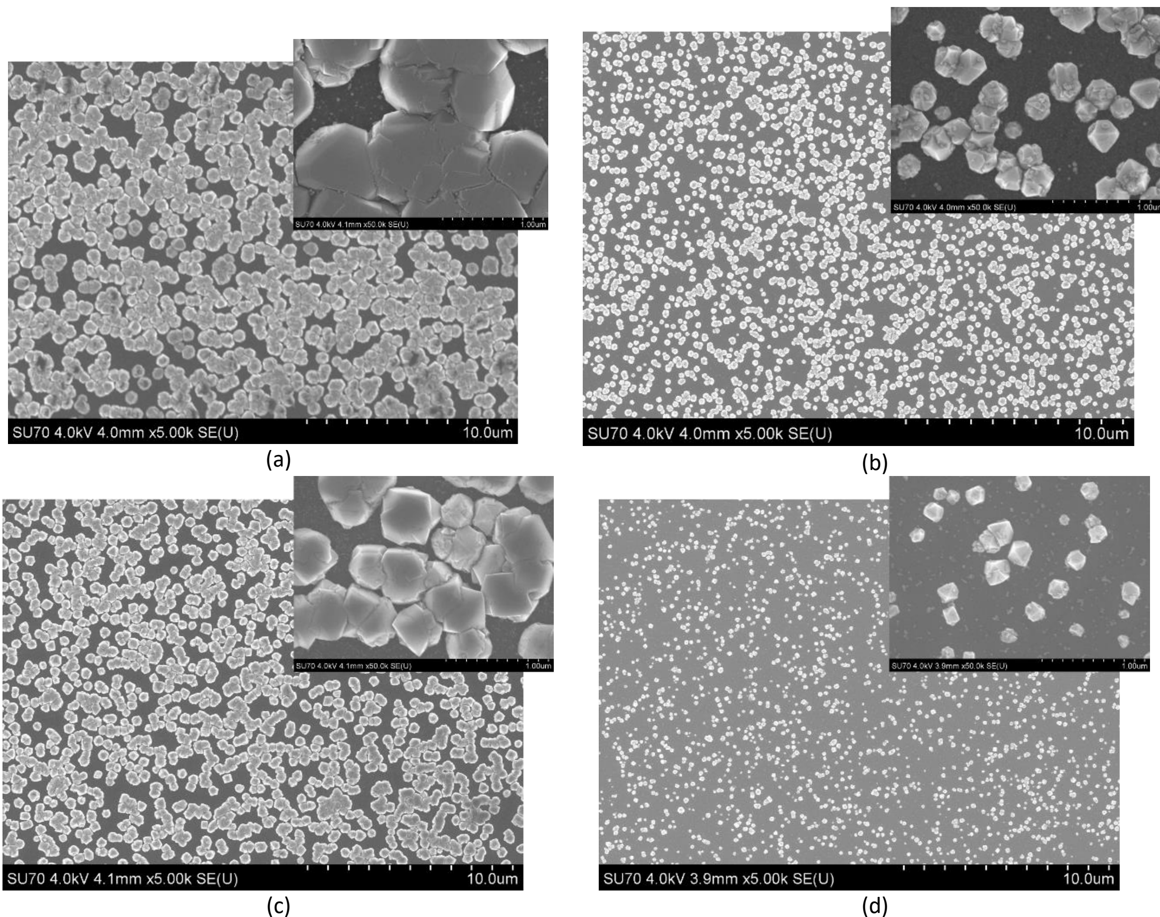

Figure 4-17. SEM images of samples (a) POL_PT2_S2_G21, (b) POL_PT2_S2_G22, (c) POL_PT2_S2_G23 and (d) POL_PT2_S2_G24. Insets: details of isolated grains

The subsequent seeding cycles were performed with 4 nm DND and 6-12 µm grit. The four samples from series C (two epitaxial and two polished) received the same PT step (60 minutes at 873 K and 1% CH_4/H_2 ratio). After the PT, the polished samples were seeded with 4 nm DND suspension and the epitaxial samples with 6-12 µm diamond grit. *Figure 4-18* a and c show low magnification images of the surface of the seeded SiC samples (samples POL_PT2_S3 and EPI_PT3_S4). These samples did not undergo growth and were used to measure the nucleation density which was found to be 9 and 4 $\times 10^6$ cm^{-2} for DND (POL_PT2_S3) and 6-12 µm grit (EPI_PT3_S4), respectively. The surface of the polished sample shows approximately twice the number of crystals compared to the epitaxial sample, indicating that the polishing of the SiC wafer increases the number of nucleating sites for diamond growth. The inset in *Figure 4-18* a is a magnification of the top-right area of the image where polishing lines of the SiC wafer can be seen. It is interesting to note that these lines were not visible before the PT and seeding procedures. The polishing of hard materials like SiC is routinely performed with diamond grit, starting with large particles and then refining the particle size until the final desired roughness is met. However, even though the final roughness may be very low (<0.3 nm), the final polishing may not remove the deeper defect lines caused by the initial polishing with large diamond grit – these offer improved sites for spontaneous diamond nucleation when the samples received the PT. These polishing lines can also be seen on the nucleation surface of diamond films grown on polished Si substrates [585]. However, and despite these lines, it should be noted that the roughness of both substrates is similar and, as a consequence, the particular

type of substrate is not expected to have any major influence in the morphology and quality of the diamond films. Instead, any meaningful differences can be attributed to the influence of the particular suspension (DND vs. 6-12 µm grit) used to seed the substrates. From *Figure 4-18* b and d, it can be concluded that seeding with both diamond suspensions results in a uniform surface coverage. However, when the seeding is performed with DND suspension the nanoparticles tend to form agglomerates that can be as large as 70 nm on the surface (*Figure 4-18* b). Even though the size of the individual DND particles in the suspension is 4-5 nm, it is known that they tend to form primary aggregates with average sizes below 30 nm that are very difficult to separate by simple sonication. These aggregates have a tendency to further agglomerate due to the inherent tendency to reduce the surface energy [586]. The presence of both primary and secondary aggregates is clearly seen on the surface of the sample seeded with DND suspension. When seeding is performed with the 6-12 µm grit, small diamond particles are chipped off from the larger particles, resulting in a uniform "seeding mat". Some 40-70 nm-sized clusters composed of diamond particles are also present on the SiC surface of this sample (*Figure 4-18* d). A large crystal that grew during the PT step can be seen in the top-left corner of sample seeded with DND (*Figure 4-18* b).

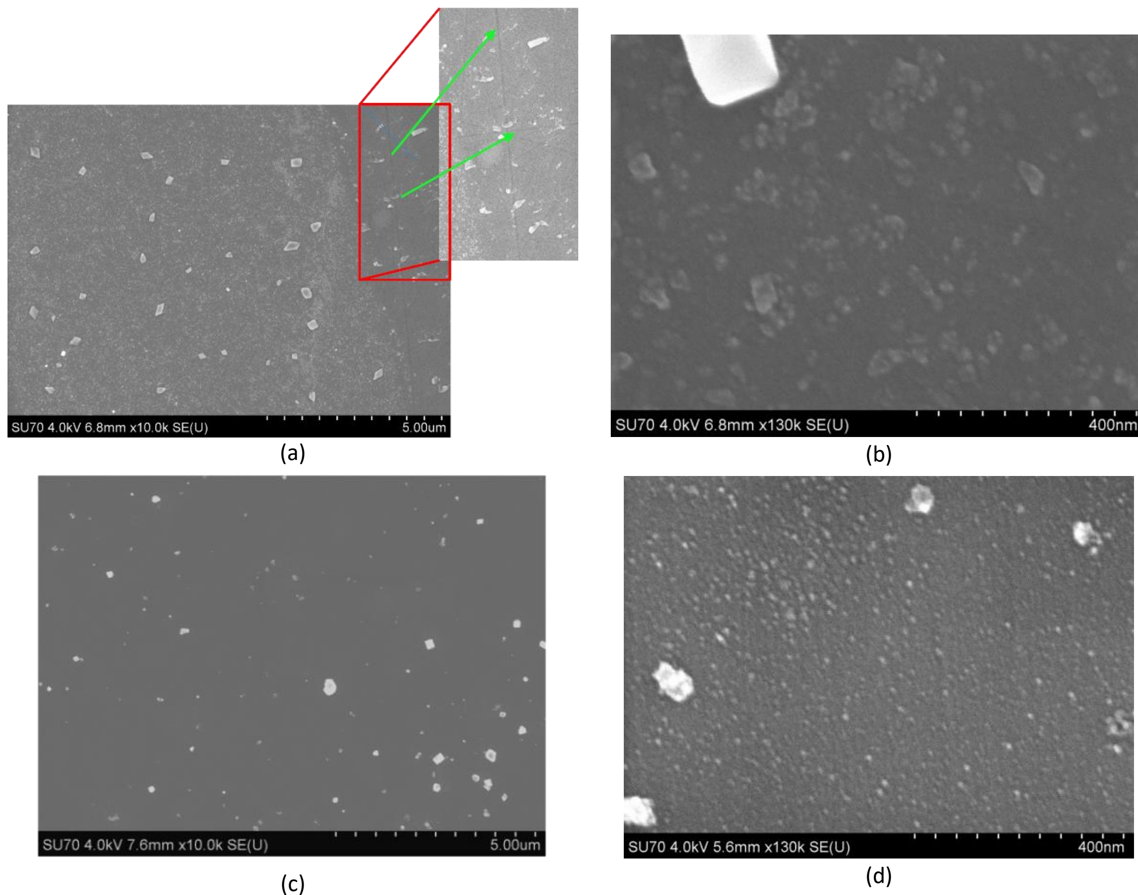

(a) (b) (c) (d)

Figure 4-18 SEM images of samples (a), (b) POL_PT2_S3; (a) inset: visible polishing lines (c), (d) EPI_PT3_S4

The pre-treated and seeded series C samples were again introduced in the system and deposition was carried out for 60 and 180 minutes using the conditions that led to the largest crystals i.e., 773 K and 1% CH_4/H_2 ratio. A polished and an epitaxial (seeded with DND and 6-12 µm diamond particles, respectively) SiC sample were coated in each run. After only 60 minutes of growth at 773 K, the sample seeded with

DND suspension shows a completely coalesced and uniform film (*Figure 4-19* a). On the other hand, the film deposited on the sample seeded with 6-12 µm diamond grit shows about 98-99% coverage; even though it looks very uniform (*Figure 4-19* b) the inset shows a magnified view of a hole. Curiously, the crystals on sample seeded with 6-12 µm are larger than the crystals on sample seeded with DND particles (150-350 nm against 50-100 nm for sample seeded with DND suspension). Recall that in the case of the grit-seeded sample, the surface was covered with a complete layer of diamond nanoparticles that chipped off from the larger diamond particles during the US seeding (*Figure 4-18* d); once under GC, these particles start growing immediately, without any further delay. On the other hand, assuming as before the outer graphitic shell of DND particles, that may delay the effective growth of the diamond seeds, explains the difference in the size of the grains on both samples after 60 minutes' growth. Despite the fact that the film obtained after DND seeding has smaller crystals, it is fully coalesced and no holes can be seen. After 180 minutes' growth, both films are coalesced and uniform (*Figure 4-19* c, d). The grains of sample EPI_PT3_S4_G4 are again slightly larger than the grains of sample POL_PT2_S3_G4 (350-750 nm against 300-550 nm) a difference that was not as marked as after 60 minutes' growth.

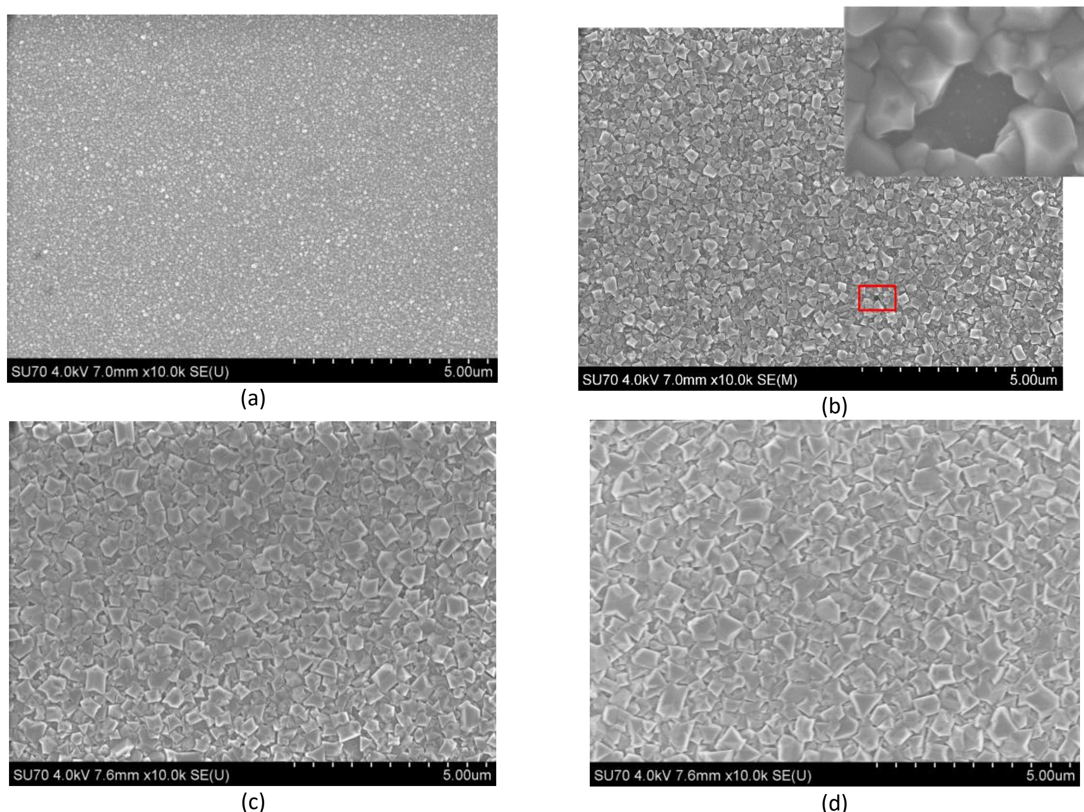

Figure 4-19 SEM images of samples (a) POL_PT2_S3_G3 and (b) EPI_PT3_S4_G3 (60 minutes' growth); (c) POL_PT2_S3_G4 and (d) EPI_PT3_S4_G4 (180 minutes' growth). (a) inset: magnified view of a hole in film on sample POL_PT2_S3_G3

Figure 4-20 a and b show the Raman spectra of the diamond films after 60 and 180 minutes deposition, respectively; the SiC spectrum is included as a reference. Raman spectra were obtained from 5 different locations for each sample and the spectra are quite similar, attesting to the uniformity of the diamond films. After 60 minutes' deposition, and despite being coalesced, the film deposited after DND seeding (POL_PT2_S3_G3) shows a very poor diamond signal, a broad peak with amplitude comparable to the one

of the G-band, centered around 1590 cm^{-1}. On the contrary, the sample EPI_PT3_S4_G3, seeded with 6-12 µm grit, shows a diamond peak centered at ~1333 cm^{-1} and 20 cm^{-1} FWHM; a small band at 1135 cm^{-1} is attributed to the presence of NCD or trans-$[C_2H_2]_n$ and the G-band, if present, is not prominent. It should be noted, however, that the Raman spectrum of the SiC substrate has a band at ~1525 cm^{-1}, which may be partially superimposed on the G band thus hampering its proper identification. The same tendency is observed after 180 minutes' growth; the sharpening of the diamond peak occurs for both samples (FWHM 19 and 16 cm^{-1} for samples seeded with DND and grit, respectively) and the G-band contribution (reflected in the amplitude ratio between the sp^3 peak and the G-band) decreases clearly. Once again, since the superposition of the SiC 1525 cm^{-1} band hampers the accurate determination of the amplitude of the G-band, it was opted to not quantify it. The comparison of the Raman spectra of the different samples suggests that, even though the nucleation density obtained with DND particles may be larger than the one obtained with 6-12 µm grit, seeding with grit improves the quality of the initial layers of the diamond deposits in comparison to seeding with these particular DND particles. Again this can be explained if the DND particles used for seeding have an amorphous C/graphitic shell. DND powders synthesized by detonation contain core particles with a size of 4-5 nm, however these particles are agglomerated in primary, secondary and larger aggregates. The larger and secondary aggregates can be broken down into primary aggregates with diameters of 100-200 nm by US treatments, but the further breaking of these primary aggregates into the 4-5 nm core particles requires a more energetic technique, typically bead milling [587]. This approach, however, introduces contamination from the bead material and creates an sp^2 shell on the surface of the DND core particles [542, 550]. As previously thought, this indeed seems to be the case with the DND particles used in this study. These results outline the importance of using DND particles that have been further processed to remove the outer shell when the quality of the diamond film at the interface is of utmost importance, as is the case when passivation of electronic devices is required.

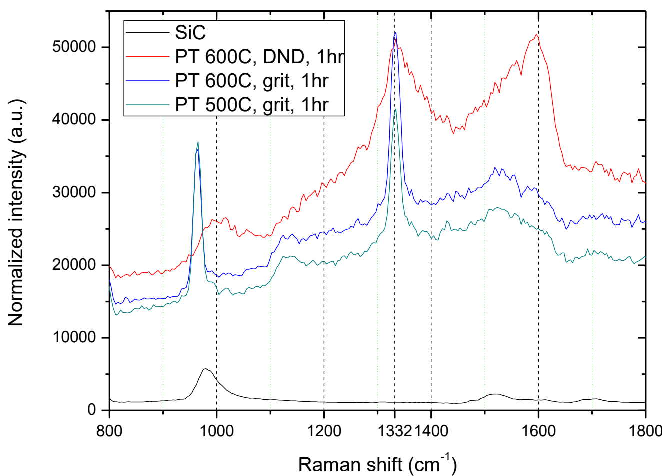

(a)

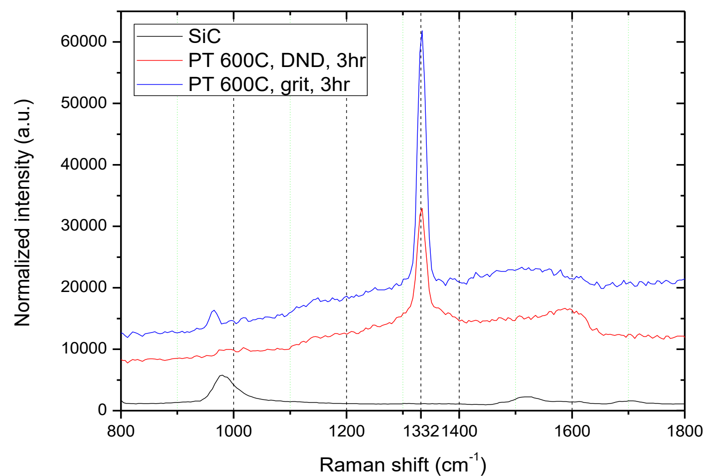

(b)

Figure 4-20 Raman spectra of samples (a) POL_PT2_S3_G3, EPI_PT3_S4_G3 and EPI_PT4_S5_G5 (60 minutes' growth); (b) POL_PT2_S3_G4 and EPI_PT3_S4_G4 (180 minutes' growth). SiC spectrum shown as a reference

Finally, in order to depict the influence (if any) of the PT temperature, an epitaxial SiC substrate was given PT for 60 minutes at 773 K. Seeding was performed with 6-12 µm diamond grit and diamond was deposited at 773 K for 60 minutes (sample EPI_PT4_S5_G5). SEM images (*Figure 4-21*) reveal the diamond film is not coalesced and the crystal size is between 125-225 nm, whereas the crystal size of the sample

prepared under similar conditions but with PT performed at 873 K (EPI_PT3_S4_G3) was somewhat larger (150-350 µm). It is known that the C atoms in the PT film act as an additional C supply during the initial stages of diamond growth, promoting lateral growth and the film coalescence [53]. On the other hand, the PT film thickness increases with temperature, meaning that for a lower deposition temperature the amount of C incorporated in the PT film is lower. As a consequence, and even though the deposition conditions were similar for both EPI_PT3_S4_G3 and EPI_PT4_S5_G5, the total supply of C atoms in the case of sample EPI_PT4_S5_G5 was smaller and the film did not coalesce fully in 60 minutes. The Raman spectrum of sample EPI_PT4_S5_G5 (*Figure 4-20* a) is similar to the Raman spectrum of sample EPI_PT3_S4_G3 .This suggests that the conditions of a particular PT cycle play a vital role in the incubation time of the diamond film (as the C content of the PT film increases, the grains coalesce faster, thus decreasing coalescence time) but do not influence the quality (almost identical FWHM values in *Table 4-5*) of the final deposits.

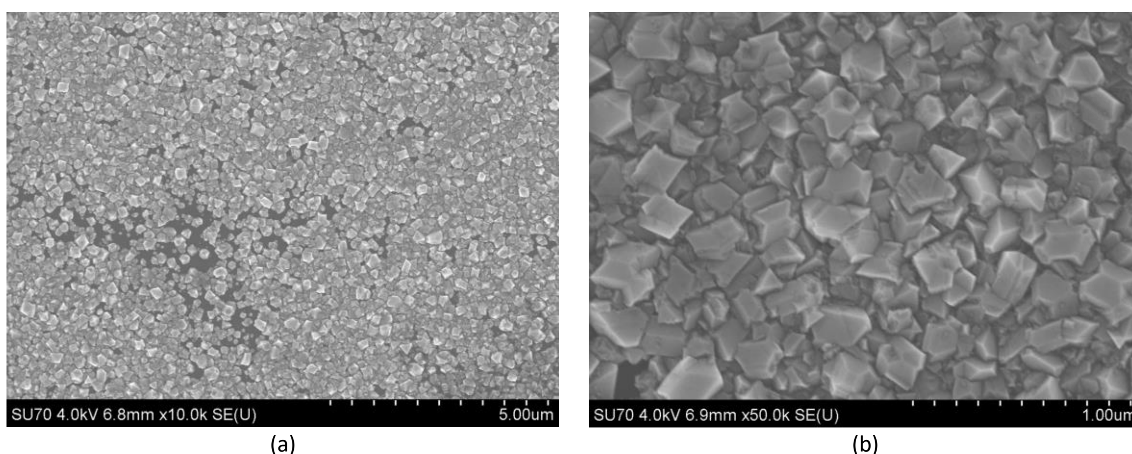

(a) (b)

Figure 4-21 (a, b) SEM images of sample EPI_PT4_S5_G5

In summary, diamond films were deposited on SiC substrates using HFCVD at temperatures as low as 773 K; seeding was performed with 4-5 nm DND, 6-12 and 50-60 µm diamond suspensions. Some of the substrates were partially covered during the PT step with a Si piece; SEM images suggest that this piece induced the trapping of activated species immediately below the edges of the Si piece, which in turn cause the deposited films to be highly non-homogeneous. Lower deposition temperatures (773 K) induce the lateral growth of the diamond crystals, in comparison to higher temperatures (873 K). Seeding with 40-60 µm grit was not effective, since the SiC substrates only showed isolated crystals. On the contrary, after 60 minutes CVD at 773 K the sample seeded with DND showed a completely coalesced diamond film but isolated small holes could be seen in the sample seeded with 6-12 µm. After 180 minutes of deposition however, both films were uniform and completely coalesced- the quality of the film obtained with 6-12 µm seeding, in fact, was considerably better than the quality of the one obtained with DND seeding (FWHM of 16 and 19 cm^{-1} after 180 minutes' deposition, respectively), suggesting that the DND seeds used in this study had an outer sp^2 shell. If DND is to be used for its higher nucleation densities, it must be ensured that such an outer shell is absent. The temperature at which the PT film was formed was also shown to have an impact in the incubation time of the diamond deposits: an increase in the PT temperature leads to a larger incorporation of carbon atoms in the PT film and a consequent decrease in the incubation time. Hence, the best films were obtained using the 6-12 µm grit, high PT and low growth

temperatures (873 K and 1% CH_4/H_2 ratio for PT, 773 K and 1% CH_4/H_2 ratio for growth) for a total of 180 minutes.

4.4.4 Experimental details- Diamond on GaN

One of the major issues limiting diamond CVD onto GaN is the lack of stability of GaN under typical diamond CVD process conditions. Due to rapid etching of GaN in H_2 plasma [588], diamond deposition on epitaxial GaN film is not a straightforward task. It has, however, been demonstrated that it is possible to deposit continuous diamond films onto GaN substrates by HFCVD, using multistep processes involving N_2 addition to inhibit decomposition of the GaN. However, the diamond films are low quality, porous and have poor adherence [589]. Also, the high thermal resistances at the interfaces between the GaN and diamond can offset the very benefit of a diamond film. The reduction of the GaN–diamond thermal interface resistance is required to obtain the expected benefits of using the high thermal conductivity diamond [590]. NCD layers have been successfully deposited on GaN to fabricate AlGaN/GaN HEMTs [591, 592], however, the thermal conductivity of NCD is lower than their counterpart in high-quality diamond films (PCD, for example), meaning that the latter approach does not take full advantage of diamond's superior thermal properties. Alternatively, the deposition of high-quality diamond films usually requires the deposition of interlayers that compromise the heat extraction from the devices hotspots.
In this work the growth of PCD films on GaN substrates by HFCVD was obtained without the use of an interlayer; using instead low temperature GC. This optimization of the growth process was made by carrying out a systematic variation of growth parameters and analysis of their effects on film properties. The challenges of growing PCD on GaN were addressed using a multi-pronged deposition approach that involved optimum HFCVD conditions as well as post growth cooling times.
A total of 17 GaN-on-sapphire substrates were used for this study and depositions were performed Ta filaments. As the aim of the study was to achieve low temperature diamond growth, preference was given to Ta filaments over W. Ta needs longer for its conversion to a carbide [540], allowing for it to be used several times and for experimental conditions to remain unchanged from one run to the other. This is an advantage over W filaments which become brittle after a single use. When compared to the other HF material used for low temperature growth, Re, Ta also shows much lesser ppm contamination when used [387]. As Ta is carbide forming, carburization of the HF was carried out without samples in the system following the conditions as described in the beginning of this chapter. The samples were cleaned using solvent cleaning 1 and 2 before undergoing P1. Seeding was performed after the PT step using two kinds of suspensions: (i) Grit- 0.2 g of 6-12 µm diamond grit dispersed in 20 ml C_2H_5OH and (ii) ND- water based 6 nm ND suspension. ND suspensions have been known to be more effective that µm sized diamond particles under some circumstances [460] and the decision to use it in addition to the grit was thus taken to address the challenge of direct growth on GaN. DND was not used in this study because of its known sp^2 outer shell, which results in higher incubation time and delayed initial growth. For these studies on GaN, it is necessary to reduce the incubation time and initiate growth of diamond sooner rather than later to prevent deterioration of the GaN as much as possible. To address the problem of adhesion of PCD films to the GaN substrates the cooling from deposition temperature to ambient temperature was allowed to occur slowly over the duration of 60 minutes. The deposition parameters are listed in *Table 4-6*. Post deposition, the samples were analysed using SEM and Raman spectroscopy.

<table>
<tr><th rowspan="2">Series</th><th rowspan="2">Sample ID</th><th colspan="3">PT</th><th rowspan="2">Pressure (kPa)</th><th rowspan="2">Seeding</th><th colspan="3">GC</th><th rowspan="2">Pressure (kPa)</th><th rowspan="2">Rate of cooling (°C/min)</th><th rowspan="2">FWHM (cm^{-1}) of sp^3 diamond peak</th></tr>
<tr><th>CH_4/H_2 (%)</th><th>Temperature (K)</th><th>Duration (min)</th><th>CH_4/H_2 (%)</th><th>Temperature (K)</th><th>Duration (min)</th></tr>
<tr><td rowspan="3">A1(a)</td><td>GaN_A1_1a</td><td>1</td><td rowspan="9">673</td><td rowspan="9">90</td><td rowspan="17">5</td><td rowspan="3">ND</td><td>1</td><td rowspan="9">673</td><td rowspan="9">120</td><td rowspan="17">5</td><td rowspan="6">10</td><td>11</td></tr>
<tr><td>GaN_A1_3a</td><td>3</td><td>3</td><td>44</td></tr>
<tr><td>GaN_A1_5a</td><td>5</td><td>5</td><td>87</td></tr>
<tr><td rowspan="3">A2</td><td>GaN_A2_1</td><td>1</td><td rowspan="3">Grit</td><td>1</td><td></td></tr>
<tr><td>GaN_A2_3</td><td>3</td><td>3</td><td></td></tr>
<tr><td>GaN_A2_5</td><td>5</td><td>5</td><td></td></tr>
<tr><td rowspan="3">A1</td><td>GaN_A1_1</td><td>1</td><td rowspan="3">ND</td><td>1</td><td rowspan="3">5</td><td></td></tr>
<tr><td>GaN_A1_3</td><td>3</td><td>3</td><td></td></tr>
<tr><td>GaN_A1_5</td><td>5</td><td>5</td><td></td></tr>
<tr><td rowspan="4">B1</td><td>GaN_B1_1a</td><td>1</td><td rowspan="4">773</td><td rowspan="4">90</td><td rowspan="4">ND</td><td>1</td><td rowspan="4">773</td><td rowspan="4">120</td><td>10</td><td></td></tr>
<tr><td>GaN_B1_1</td><td>1</td><td>1</td><td rowspan="3">6</td><td></td></tr>
<tr><td>GaN_B1_3</td><td>3</td><td>3</td><td>18</td></tr>
<tr><td>GaN_B1_5</td><td>5</td><td>5</td><td></td></tr>
<tr><td rowspan="4">C1</td><td>GaN_C1_1a</td><td>1</td><td rowspan="4">873</td><td rowspan="4">90</td><td rowspan="4">ND</td><td>1</td><td rowspan="4">873</td><td rowspan="4">120</td><td>10</td><td></td></tr>
<tr><td>GaN_C1_1</td><td>1</td><td>1</td><td rowspan="3">7</td><td></td></tr>
<tr><td>GaN_C1_3</td><td>3</td><td>3</td><td>15</td></tr>
<tr><td>GaN_C1_5</td><td>5</td><td>5</td><td>46.8</td></tr>
</table>

Table 4-6 Deposition conditions used for diamond growth on GaN samples

4.4.5 Results and discussion- Diamond on GaN

Samples of series A1(a) and A2 were seeded with ND suspensions and grit suspensions respectively; they received PT and growth at 673 K, at varying CH_4 ratios. Corresponding samples of each series, for example, GaN_A1_1a and GaN_A2_1, underwent PT and growth in the same cycle. Comparing samples GaN_A1_1a and GaN_A2_1, and GaN_A1_3a and GaN_A2_3, using optical microscopy (images not shown), it was clear that the ND suspensions resulted in better films- for the same duration of deposition, the film on A1_1a were more coalesced than the films on A2_1. The SEM images of samples GaN_A1_1a and GaN_A2_1 (*Figure 4-22*) are shown where this is evidenced by more extensive gaps in the diamond film where it failed to close in the latter case. This led to the decision of using ND suspensions exclusively to achieve the optimization of the remaining parameters of the CVD process. It is possible that these ND particles did not have the sp^2 outer shell that was encountered in the DND suspensions.

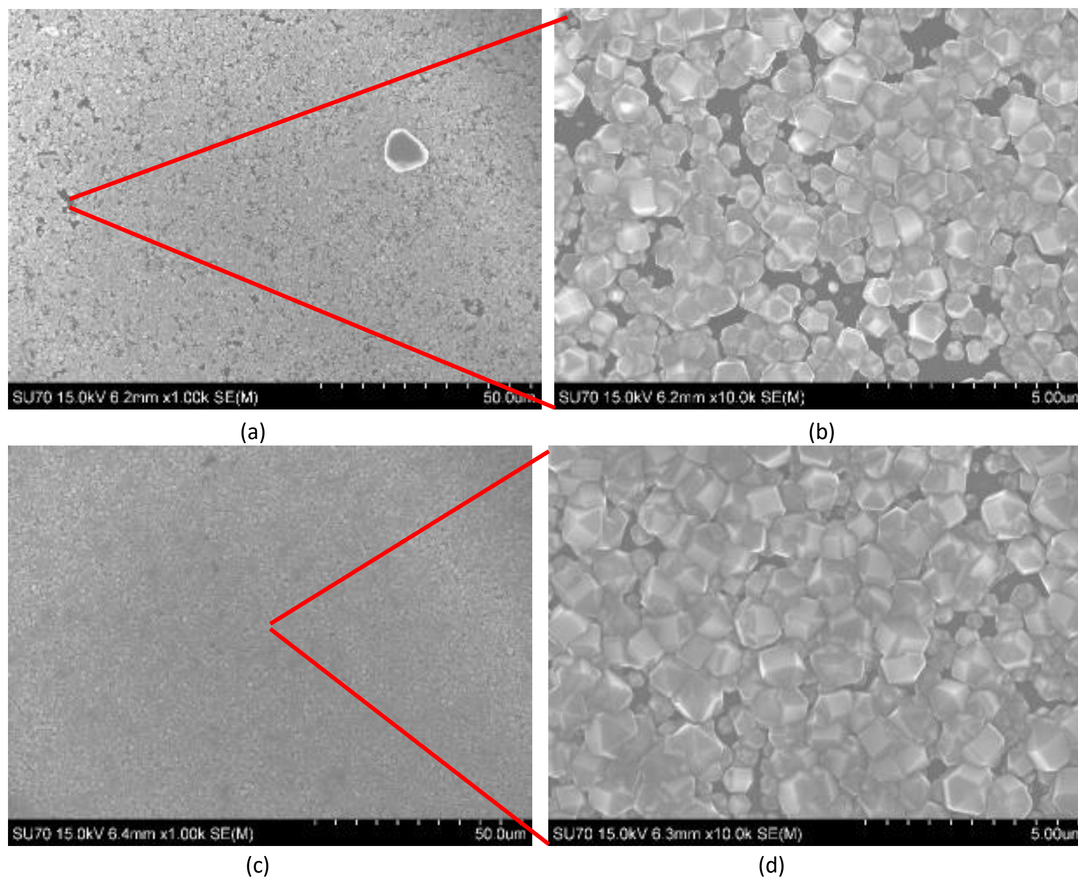

Figure 4-22 SEM images of samples GaN_A2_1 (a,b) and GaN_A1_1a (c,d)

For the next set of experiments, PT and growth was carried out for CH_4/H_2 ratios ranging from 1-5%, for the same temperature- i.e., 673 K (*Table 4-6*), but seeded only with ND suspensions. A higher CH_4/H_2 ratio at low growth temperature is expected to increase the sp^2/sp^3 ratio [433], however, the decision to carry out this set of experiments (A1_3a and A1_5a) was to attempt low temperature growth on GaN, with minimum damage to the substrate surface, as GaN has been known to degrade at higher deposition temperatures [593]. However, the films obtained for this set of experiments were of very poor quality. In the Raman spectra of these films (*Figure 4-23*), a gradual decrease in the intensity of the sp^3 peak, and a corresponding increase in the G-band of graphite was observed in samples A1_1a through A1_5a. Sample A1_3a and A1_5a show a very poor diamond signal, with a broad peak, with amplitude comparable to the one of the G-band, centered around 1551 and 1554 cm^{-1}, respectively; both films also show bands centered at 1370 and 1379 cm^{-1}, the D-band of graphite. On the contrary, the sample A1_1a shows a diamond peak centered at ≈1329 cm^{-1} and 11 cm^{-1} FWHM; and a small band at around 1150 cm^{-1}, signifying NCD. The presence of non-sp^3 components of the films are also marked by the bands centered at 1371, 1450 and 1560 cm^{-1} attributed to D-band of graphite, trans-$(C_2H_2)_n$ (at grain boundaries) and the G-band of graphite respectively. The presence of sp^2 C in the film maybe because of the low growth temperatures used in this round of experiments. It must be noted that the GaN peak at around 734 cm^{-1} (not shown) was noted in A1_1a- signifying that the film was not totally coalesced.

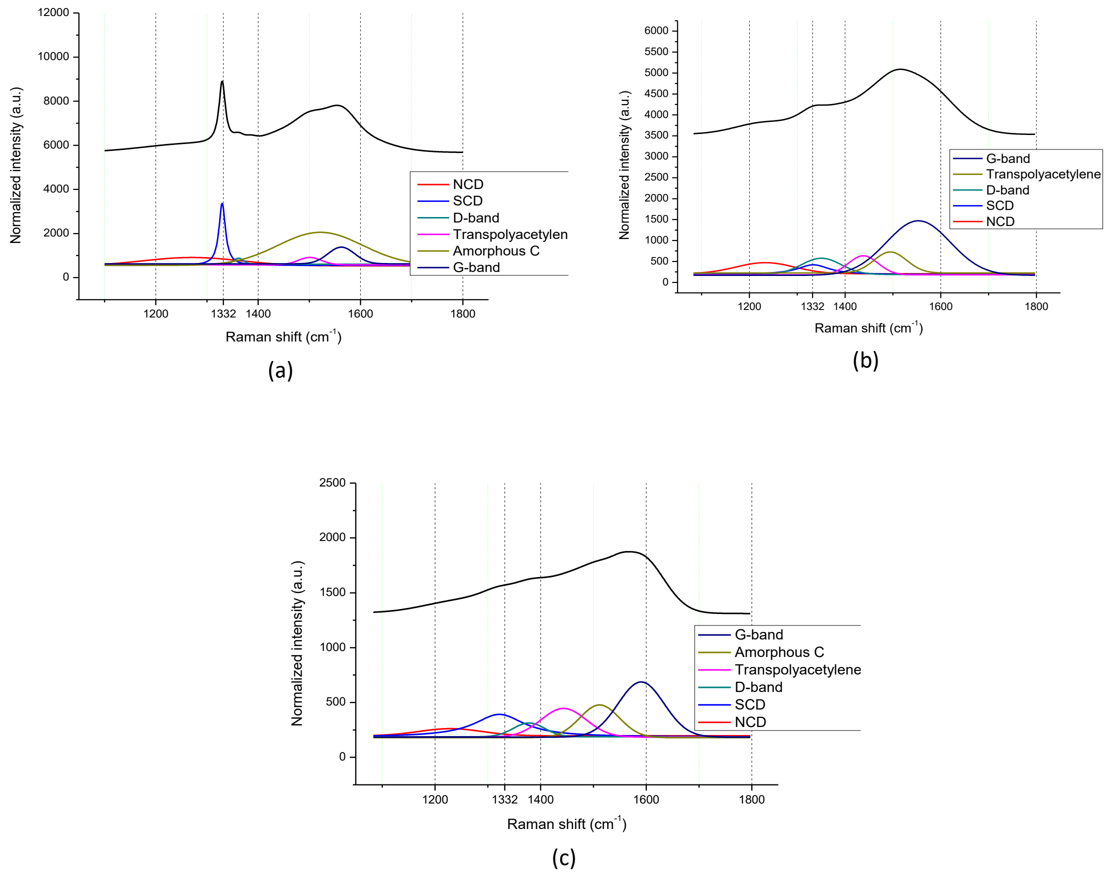

Figure 4-23 Raman spectra of samples (a) A1_1a (b) A1_3a and (c) A1_5a. Also detected was the 734 cm^{-1} of GaN (not shown)

The next set of experiments were on samples of the series A1_1a, B1_1a and C1_1a, i.e., PT/growth at 1% CH_4/H_2 but temperatures of 673, 773 and 873 K. These films showed increasingly better film quality as the temperature was increased, however, due to the mismatch between the thermal expansion coefficients between GaN and PCD (1×10^{-6} K^{-1} for PCD [70] and 3.7×10^{-6} K^{-1} for GaN [107]), the films of samples GaN_B1_1a and GaN_C1_1a delaminated after deposition (*Figure 4-24*).

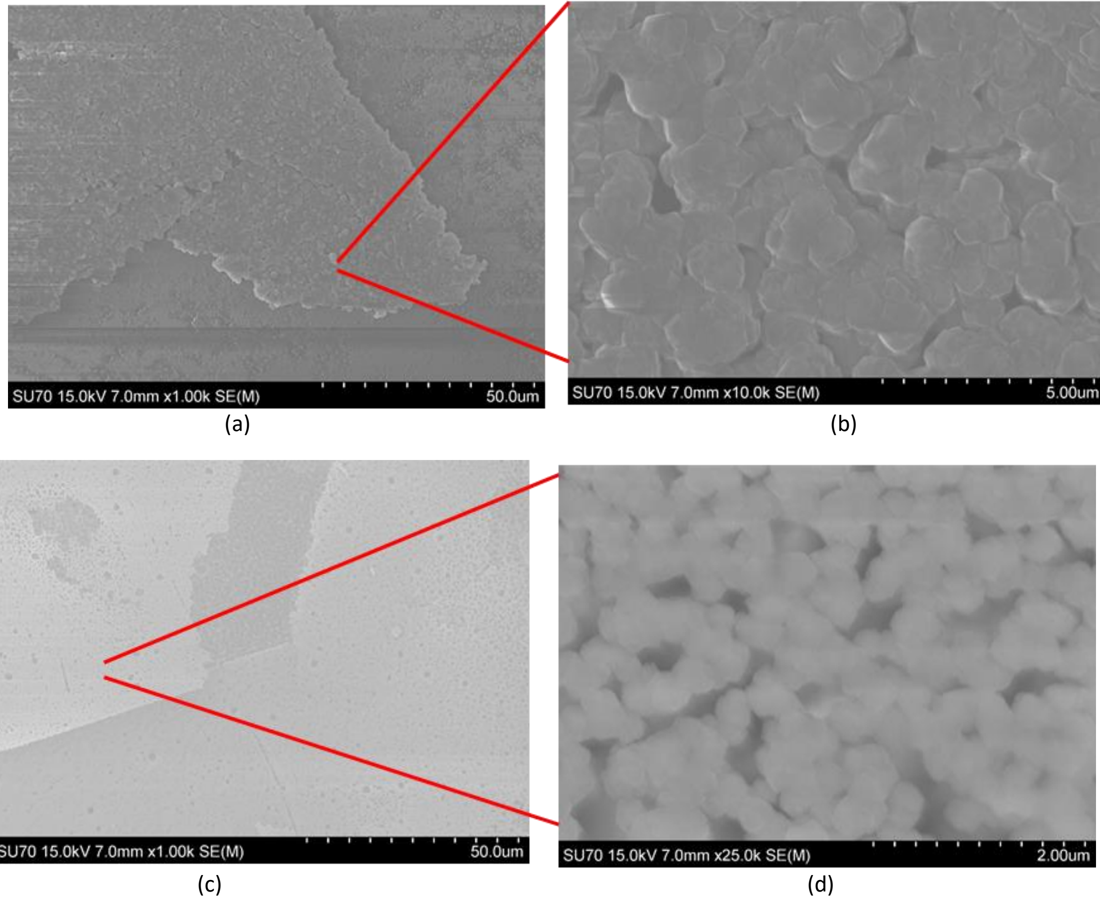

Figure 4-24 SEM images of samples GaN_B1_1a (a,b) and GaN_C1_1a (c,d), showing delamination of film with increasing temperature

As it was seen that better quality films were obtained with increasing temperatures- films at higher temperatures, although delaminated, were completely coalesced and showed uniform crystal quality- further experiments, were carried out with a longer duration of cooling post deposition at the rate of 5 to 7 °C/minute with the idea that increasing the rate of cooling could help reduce the thermal stress at the interface of the film and GaN substrate and improve the adhesion of films deposited at higher temperatures.

However, delamination at higher temperatures was not the only issue. The GaN substrates that underwent growth at higher temperatures, that is, B1_1a and C1_1a also showed degradation of the substrate itself, observable at spots on the GaN substrate where film had delaminated. The typical "etch pits" that have been reported in literature [593] when direct diamond growth has been attempted on GaN were observed (*Figure 4-25*). Although GaN itself has a high melting temperature (around 2773 K [594]), when it is placed at high temperatures in a H_2 plasma, such as in conditions typical of CVD diamond growth, it shows considerable degradation due to etching that results from the gaseous decomposition of the underlying GaN. Possible reasons for this as reported in literature are reactions at high temperature between N and Ga with H_2 to form NH_3 and GaH respectively [593]. As a H_2 rich plasma was indicated to be the reason for this surface damage, along with increasing cooling time, growth was carried out at increasing CH_4 ratios. Although higher CH_4 ratios are associated with poorer diamond quality (low sp^3/sp^2

ratio)[433], it also results in higher growth rates. As a compromise however, by raising the corresponding deposition temperature, a reasonably good sp^3/sp^2 ratio might be obtained [584].

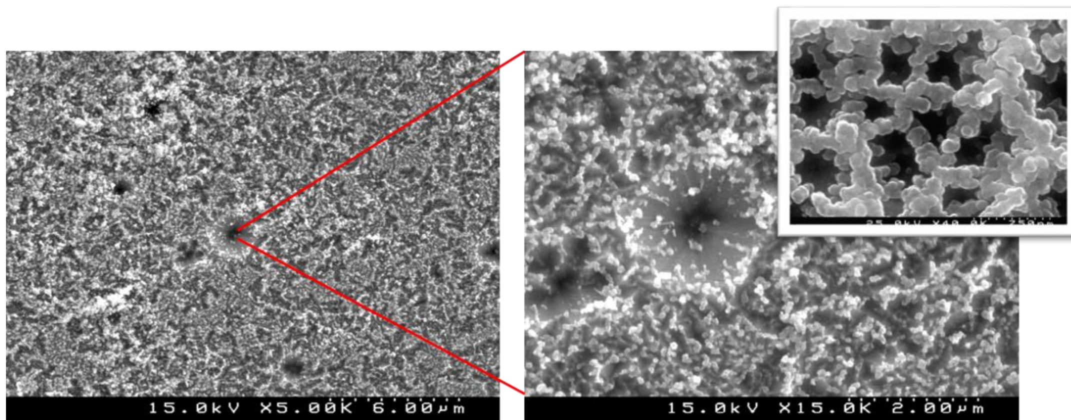

Figure 4-25 SEM images at low (left) and high (right) magnification of exposed GaN surface of sample GaN_C1_1a, inset at 40k magnification shows detail of pit

Therefore, the next series of experiments, A1, B1 and C1, the CH_4/H_2 ratio was increased from 1 to 3 and 5 %, in two independent sets of experiments. For the set of experiments, A1_3, and A1_5 while it was expected that increasing the ratio of CH_4 would prevent extensive degradation of the GaN substrate, the opposite was in fact observed. As the amount of CH_4 in the plasma increased from 1 to 5%, the substrate surface became more porous- GaN_A1_3 and GaN_A1_5 substrates were covered with diamond but prominent holes in the film were observed through which gaseous decomposition of the GaN substrate had taken place. *Figure 4-26* shows this increasing density of these etch pits for samples A1_3 and A1_5. Since these experiments were carried out at low temperatures, the likelihood of the aforementioned reactions of H_2 with Ga and N, to have taken place seems highly unlikely. At low temperatures, between 300 to 500°C, the CH_4/H_2 plasma however has been reported, and actually used, to perform etching in GaN device fabrication- wherein an increase in the damage rate was found with increasing CH_4 concentration with a saturation at 10% [595]. It is possible that this is what happened to the GaN samples in this work for this set of samples.

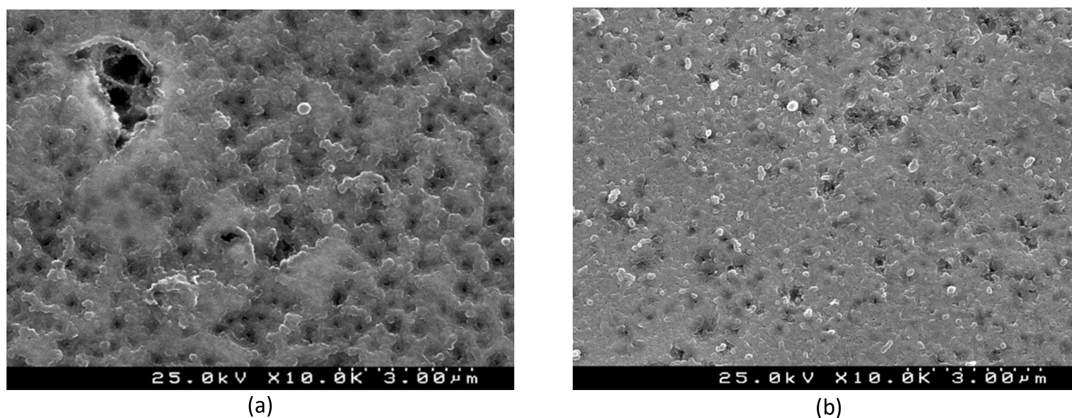

(a) (b)

Figure 4-26 SEM images of (a) GaN_A1_3 (b) GaN_A1_5 at the same magnification

An interesting trend is observed when high CH_4 ratios in the plasma is juxtaposed with increasing the substrate temperature. For the same ratio of CH_4, increasing substrate temperature leads to a reduction in the density of holes in the film, corresponding to pits where GaN is etched. For example, in the two samples, GaN_A1_5 and GaN_B1_5 *(Figure 4-27* a and b) observing the image of one such pit at the same magnification, the overgrowth of diamond on the sample grown at higher temperature is evident- this might be possible due to the higher growth rates achieved for higher substrate/deposition temperatures for diamond CVD [584]. At even higher temperatures, i.e., 873 K, for example, in the case of sample GaN_C1_5, the surface of GaN was completely covered with a coalesced diamond film (*Figure 4-27* c)- however, the film at this high CH_4/H_2 ratio do not show good diamond quality as is evidenced in its Raman spectrum (*Figure 4-28*)- peak centered at 1332 cm^{-1} has a large FWHM (46.8 cm^{-1}), and the spectrum is dominated by the sp^2 signal from the film (D and G bands of graphite at 1350 and 1550 cm^{-1} respectively, as well as amorphous C band at 1480 cm^{-1}). This series of experiments served as an indication of how using an optimum combination of CH_4/H_2 ratio and temperature might be useful in obtaining conformal, good quality diamond films on GaN.

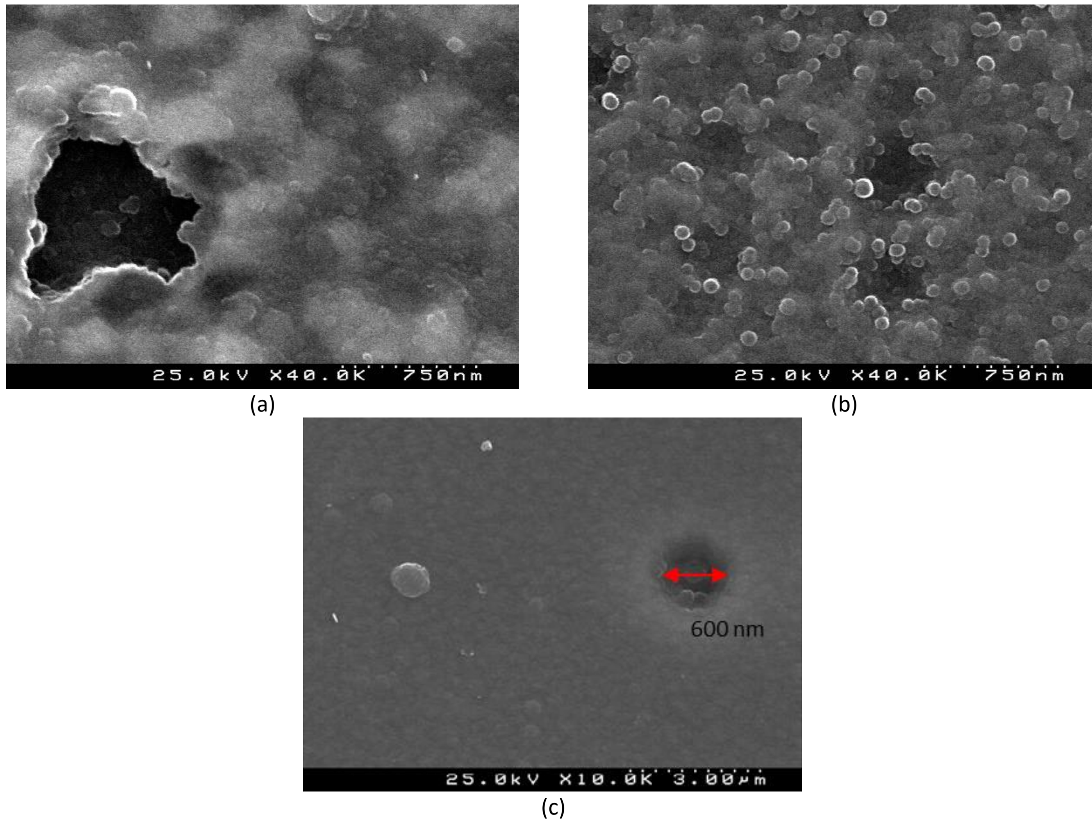

Figure 4-27 SEM images of etch pit at same magnification for (a) GaN_A1_5 and (b) GaN_B1_5 and at low magnification for (c) GaN_C1_5

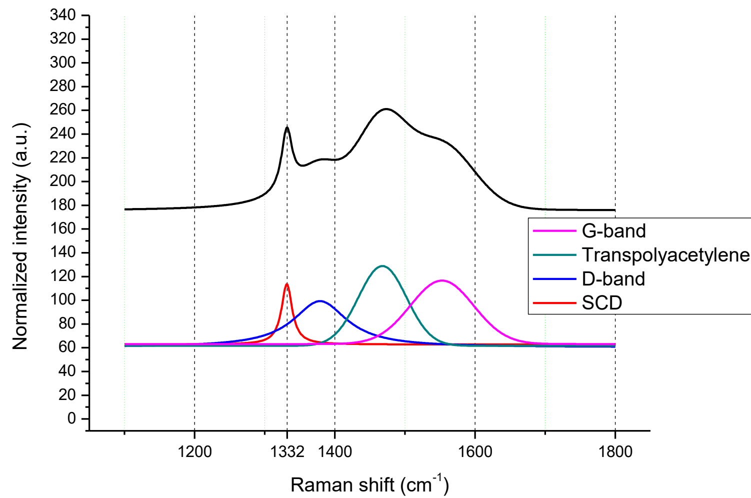

Figure 4-28 Raman spectrum of sample GaN_C1_5

Having optimized the cooling time to ensure that films did not delaminate, the samples GaN_B1_3 and GaN_C1_3 showed the best characteristics. The good quality of the diamond in the film, from the Raman spectrum (*Figure 4-29*) and the large crystal size, as can be seen from the SEM images (*Figure 4-30*, a and b) in sample GaN_B1_3, deposited at 773 K, with a CH_4/H_2 ratio of 3% attest to its quality. SEM images and Raman spectra were obtained from 5 different locations for each sample and the spectra are quite similar, attesting to the uniformity of the diamond films.

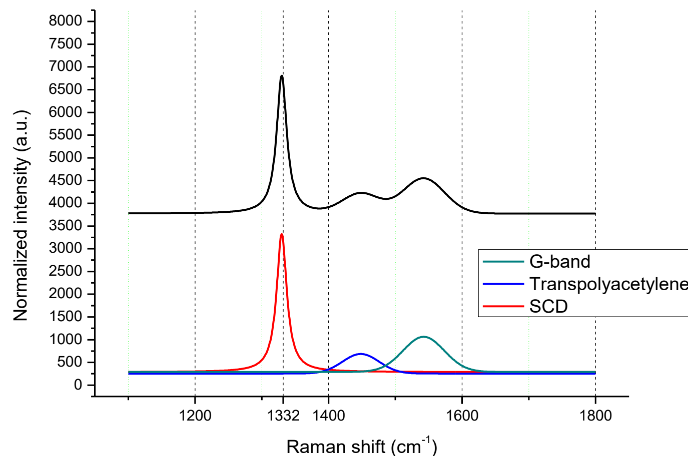

Figure 4-29 Raman spectrum of sample GaN_B1_3

GaN_C1_3, deposited at 873 K, with a CH_4/H_2 ratio of 3%, was also completely covered in diamond- the SEM images show a cauliflower growth that is more typical of UNCD diamond (*Figure 4-30*, c and d)- characterized by a very fine, uniform grain size (3–5 nm on average) and a small but non-negligible amount of sp^2 bonded C at atomically abrupt grain boundaries [596]; the Raman spectra attest to the same. Due to the higher deposition temperatures, however, there was also sporadic degradation of the substrate, as can be seen in *Figure 4-30* c.

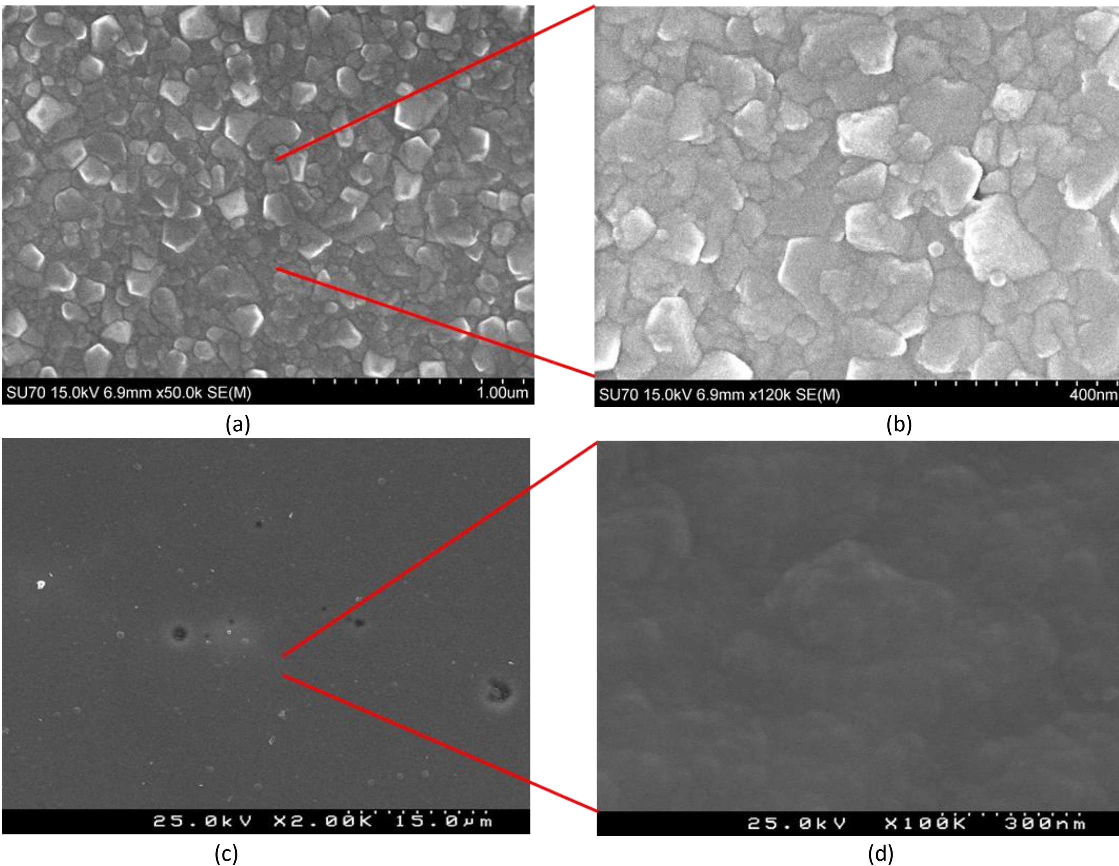

Figure 4-30 SEM images of GaN_B1_3 at (a) 50kx and (b) 120kx magnification and GaN_C1_3 at (c) 2kx and (d) 100kx magnification

In summary- attaining good quality diamond films on GaN is not a straightforward process. Conditions typical of HFCVD for good quality films on Si, such as high temperature (above 873 K) causes extensive degradation of the substrate; high CH_4/H_2 ratios as well cause etching of the substrate. Such damage is characterised by "etching pits" clearly visible in high magnification SEM images. In order to ensure that the substrate of GaN is not damaged, a balance of optimum temperature and CH_4/H_2 ratio was reached- the best films were obtained at low temperature- 500°C, with a CH_4/H_2 ratio of 3%. ND suspension was found to be more effective at seeding when compared to the grit suspensions. Delamination of the coalesced films was prevented by an extensive cooling step post growth using rates between 5 to 10 °C/minute.

4.4.5.1 Near-junction coating of a GaN HEMT device

Ascertaining the optimum conditions of diamond on GaN was not the only scope of this work. The obtained optimum conditions were used to coat a GaN HEMT device. The high breakdown voltages and current handling capabilities of GaN HEMTs allows one to obtain a ten-fold increase in RF power for the same device size when compared to GaAs devices [597]. However that the ultimate power and performance of GaN technology cannot be exploited in real applications due to thermal limitations has also been well documented [598-600]. The high power density in GaN HEMTs translates to MW/cm^2 at the device gate region [601]. Using diamond to increase the heat conductance near the GaN device junction can be a solution to this critical problem. Heat reduction can improve device reliability, reduce

leakage currents, increase lifetime and enable higher channel mobility [602]. Although for this purpose, NCD on GaN has been investigated [601], PCD on GaN results have been more rare. PCD films were deposited directly on GaN HEMTs supplied by a manufacturer, at 400 °C using an HFCVD system (*Figure 4-31* a). It is to be noted that the temperature used here was 100°C lower than the optimum conditions obtained in the previous section; the reason behind this is the configuration of the HFCVD system used in this part of study. When these depositions were made, the thermocouple measuring the substrate temperature was in contact with the bottom surface of the substrate as opposed to all other experiments made in this work, where the substrate thermocouple touched the top surface of the substrate. Due to thermal dissipation through the substrate itself, it is expected that the actual substrate temperature and the measured temperature are not identical, the latter being lower. In the resulting PCD film, the diamond peak centered at 1332 cm^{-1} is easily identified in the Raman spectrum (results not shown). Figure 4-*31* b and c show the surface of the as-supplied and diamond-coated dice, respectively.

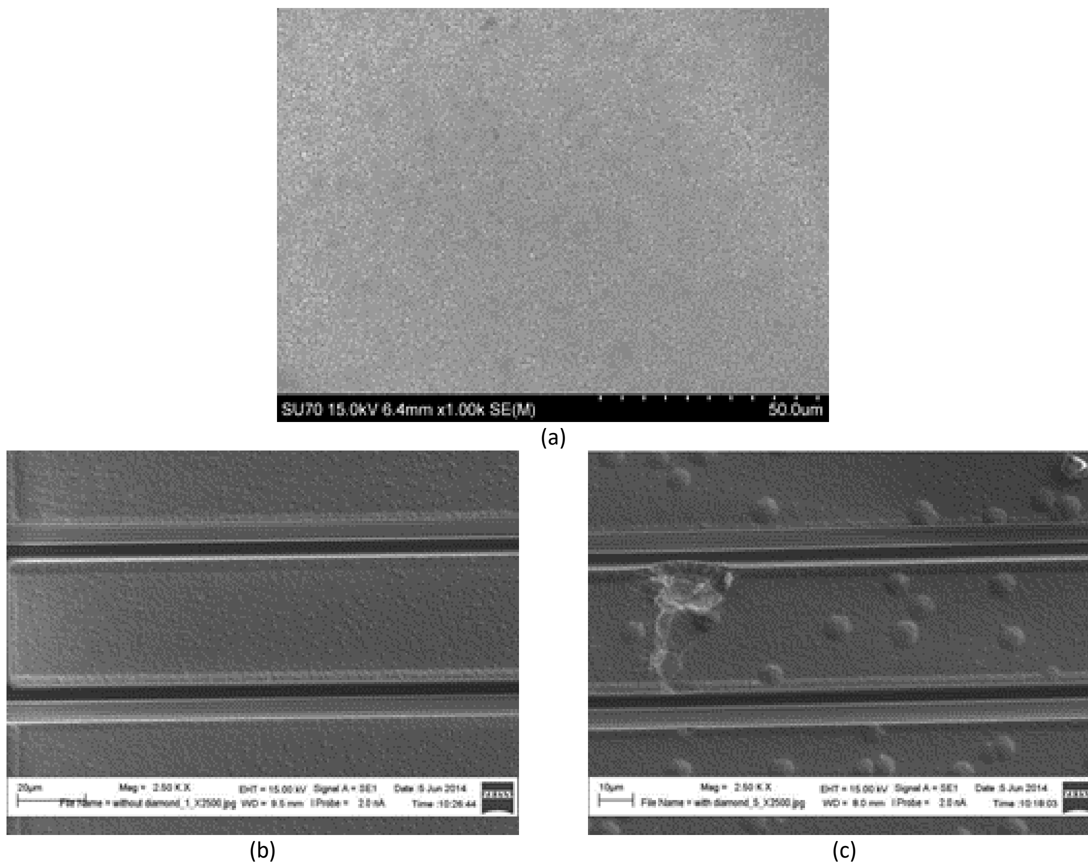

Figure 4-31 SEM images of (a) diamond grown on GaN (b) as-supplied HEMT die (c) diamond coated HEMT

The I-V characteristics of both devices are shown in *Figure 4-32*. Apart from a general decrease in the current for a given voltage, the device performance was not degraded; in conclusion, a GaN HEMT was successfully coated with PCD and it survived the deposition conditions.

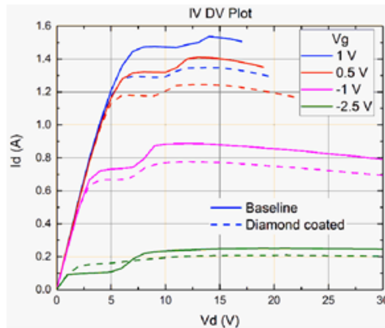

Figure 4-32 I-V characteristics of the as-supplied and diamond-coated dice

4.5 Doped diamond films on SiC

SiC was accidentally discovered by Berzelius [603] in his attempt to produce synthetic diamond, an ironic twist of fate from the perspective of this work that involves the fabrication of heterojunctions that combine the two. High thermal conductivity, optical transmittance, and mechanical hardness are also characteristic properties of SiC; utilising CVD, PCD films as a topside thermal contact for it could be pivotal for providing stable device characteristics in the HPHT and high switching frequency device operating regime that next-generation power converter circuits will mandate. The challenge in fabricating diamond with n-type conductivity in order to fabricate p-n junctions of diamond, can be addressed, in one way, with the fabrication of heterostructures of B-doped diamond and N-doped SiC [604, 605]; there does remain the challenge of a significant difference in the energy gaps of SiC and diamond that results in a high-energy barrier for electrons at the hetero-interface, which could hamper the electron transfer into the diamond, which can however be addressed with post-fabrication processes.

Heterojunctions exhibit useful electronic properties because of the discontinuities in the local band structure at the interface. In order to have a useful heterojunction, the lattice constants of the two materials must be well matched, as in the case of 4H-SiC [606] and diamond [607], since lattice mismatch can introduce dislocations and result in interface states. In addition, technological challenges, such as the difficulty in relating the conduction mechanism in these junctions to a pre-determined band structure, or the causal variety of defect levels present in CVD-grown diamond, justify fundamental experimental study for characterizing the interface behaviour itself and the parameters that affect it. Good B-doped film quality itself, in addition to lattice matching and band engineering requirements, is also a necessary condition in order to utilize CVD diamond films for power electronics applications. The device performance depends on the crystal quality of grown diamond films and its surface termination, metal/diamond junction characteristics, and geometrical factors [608]; and as has been discussed before, the diamond / SiC interface quality remains a crucial parameter for a good electrical performance as it influences the rectifying ratio, as well as the leakage currents at the interface. The work presented in this section is the optimization of BDD films on SiC substrates, as well as the experimental details involved in the optimization of ohmic contacts for BDD.

4.5.1 Experimental details- BDD deposition

P-type B-doped PCD films were deposited on the top side of 5 mm × 5 mm n-type 4H-SiC samples purchased from Cree Inc. using HFCVD. Carrier concentration on the top epitaxial layer of the SiC was 1×10^{16} cm^{-3} and bulk resistivity was ≤ 0.025 Ω cm. A total of 16 SiC samples were used for this study; they underwent in addition to solvent cleaning steps, SC1, oxide clean and SC2. The protocol P1 as well as P2 were followed for this study, in order to compare the effect of NNP on BDD deposition. 3 methods were

used for seeding (i) ND- water based 6 nm ND suspension (ii) grit- 0.2 g of 6-12 µm diamond grit in 20 ml C_2H_5OH and (iii) scratch- manual scratching method (by pressing the sample against a tissue with diamond particles). The scratch method has been used previously with success for BDD films for the same system set-up [487] and was included in the seeding techniques used here The BDD deposition was followed by a 60 minutes long cooling step. The B doping source, B_2O_3 diluted in C_2H_5OH (B/C ratio 10000 ppm) was set to evaporate at the rate of 0.25 µl/min; this value remain unchanged for all experiements in this section of the work. The evaporated B-source was dragged by Ar at different flow rates, at different CH_4/H_2 gas ratios and system pressures, in a custom made HFCVD system [487]. In order to achieve a higher B incorporation efficiency, a relatively higher substrate temperature was used [609], and W filaments were chosen for this purpose. As W is a carbide forming metal, carburization was carried out following the steps detailed in section 4.1. Also used were higher deposition pressure, as the pressure is known to improve crystalline quality of the films [610] which in turn directly influences efficient B incorporation. The deposition conditions are listed in (*Table 4-7*). The films were characterized with SEM and Raman.

<table>
<tr><th rowspan="2">Sample ID</th><th colspan="3">PT</th><th>Pressure (kPa)</th><th rowspan="2">Seeding</th><th colspan="3">GC</th><th rowspan="2">Pressure (kPa)</th></tr>
<tr><th>CH_4/H_2 (%)</th><th>Temperature (K)</th><th>Duration (min)</th><th></th><th>$CH_4/Ar/H_2$ (%)</th><th>Temperature (K)</th><th>Duration (min)</th></tr>
<tr><td>A1/A1'</td><td>1</td><td rowspan="6">993</td><td rowspan="8">90</td><td rowspan="6">4.5</td><td rowspan="3">ND</td><td>1/8/100</td><td rowspan="6">993</td><td rowspan="8">240</td><td rowspan="6">4.5</td></tr>
<tr><td>A2/A2'</td><td>2</td><td>2/8/100</td></tr>
<tr><td>A3/A3'</td><td>3</td><td>3/8/100</td></tr>
<tr><td>A4/A4'</td><td>3</td><td>scratch</td><td>3/8/100</td></tr>
<tr><td>A5/A5’</td><td>2</td><td>grit</td><td>2/8/100</td></tr>
<tr><td>A6/A6’</td><td>1</td><td rowspan="3">ND</td><td>1/10/100</td></tr>
<tr><td>B1/B1’</td><td>2</td><td rowspan="2">1023</td><td rowspan="2">9.0</td><td>2/8/100</td><td rowspan="2">1023</td><td rowspan="2">9.0</td></tr>
<tr><td>B2/B2’</td><td>3</td><td>3/8/100</td></tr>
</table>

Table 4-7 Deposition conditions used for BDD growth on SiC samples- Samples not given PT are marked with '

4.5.2 Results and discussion- BDD deposition

The main parameters that were varied in this study, to study their effect on the properties of the BDD deposited were- PT (given or not), type of seeding, Ar (consequently, rate of flow of dopant) and CH_4 ratio in plasma and chamber pressure during deposition. Each of these factors profoundly influenced the characteristics of the respective films.

Figure 4-33 shows SEM images of deposited films of series A (deposited at 4.5 kPa)- images revealed that after 240 minutes of deposition, samples seeded with the ND suspension, both with and without PT, i.e., A1/A1’ (*Figure 4-33*, a), A2/A2’ and A3/A3’, as well as those seeded with diamond grit, i.e., A5/A5’ (*Figure 4-33*, b) were covered with coalesced and highly adherent PCD films, with an average crystal size of 600 nm. On the contrary, for scratch seeded samples, only A4 was covered with a coalesced film where as A4’, without PT, showed areas where the film was not fully coalesced yet (*Figure 4-33*, d).

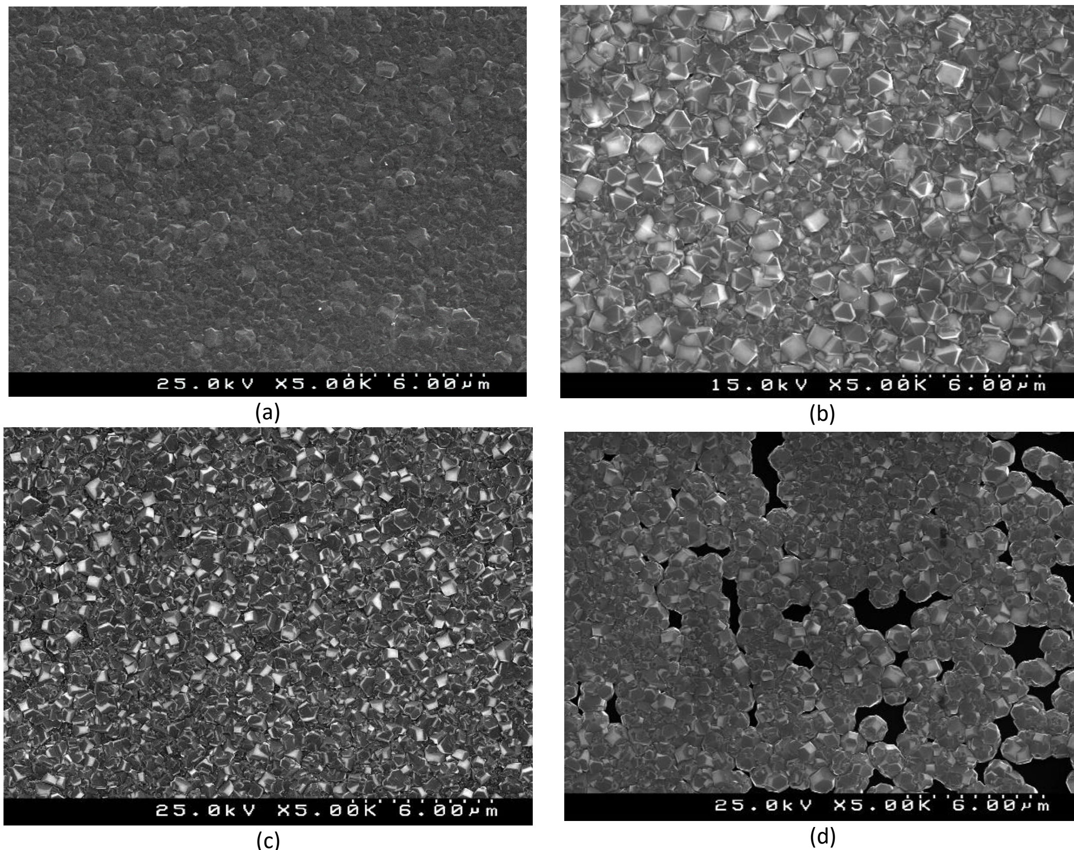

Figure 4-33 SEM images of samples (a) A1’ (b) A5’ (c) A4 (d) A4’

These results are not surprising since it is known that the exposure of the substrates to diamond GC before the seeding step increases nucleation density and decreases coalescence time [53], and although its effectiveness was not obvious in the ND and samples (where films were uniform and coalesced in both cases, with and without PT), for scratch samples, its effectiveness was evident from the coalesced films obtained on samples that received PT. This is especially evident when comparing the Raman spectra of these samples- sample A4’, on which the film was not completely coalesced, showed a strong presence of the 4H-SiC peak at 764 cm^{-1} [611, 612] in its Raman spectrum (FWHM 3.42 cm^{-1}) compared to the wider peak at the same position on sample A4 (FWHM 8.79 cm^{-1}) (*Figure 4-34*). The presence and consequent FWHM of the SiC peaks for both samples is due to the structural distribution of the underlying SiC- a sharper peak signifying crystalline material and a wider peak, in general, amorphous material. In this case, the presence of the sharper peak on sample A4’, at 764 cm^{-1} is from the epitaxial SiC of the substrate, where the films did not fully coalesce. The peak detected at 975 cm^{-1} is of BC [470, 613], signifying B incorporation in the film.

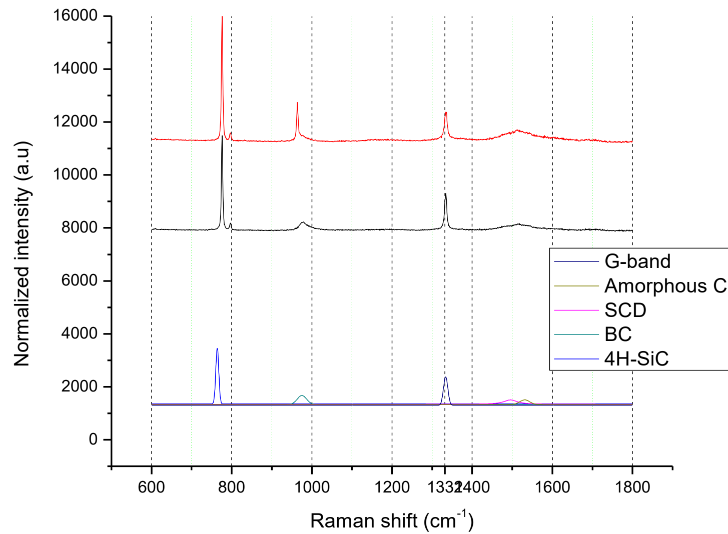

Figure 4-34 Raman spectrum of sample A4’ (red) and A4 (black), with the sharp peak at 764 cm^{-1} of 4H-SiC, fitting shown at the bottom of the plot

For BDD PCD films, beside the peak of BC, the incorporation of B in the film is also typically manifested as a shift in the sp^3 diamond peak from 1332 cm^{-1} towards higher values [535]. In addition, the sharp peak of sp^3 diamond, when obtained for BDD, usually signifies that the spectra has been collected from the [1 0 0] face of the diamond crystal [488] where B incorporation is less efficient; the addition of B takes place preferentially at the [1 1 1] facet. Hence, the spectrum of a BDD sample that has a high amount of incorporated B shows some typical features- a peak of BC, a shifted or reduced sp^3 diamond peak, and a dominant signal of disorder from grain boundaries. The Raman spectra (*Figure 4-35*) of samples A3 and A3’, for example give more insight into the characteristics of the film. Both A3 and A3’ showed the peak of sp^3 diamond (FWHM 5.89 and 8.56 cm^{-1} respectively)- however, in both cases it was displaced to 1334.63 and 1334.3 cm^{-1} for A3 and A3’ respectively. Some conclusions can be drawn from this- the sharp peak implies that the spectra were collected from the [1 0 0] facet of the grains. The displacement of the peak from 1332 cm $^{-1}$ of sp^3 diamond shows some B incorporation; this happened to a greater extent in A3 (2.63 cm^{-1} for sample with PT) than in A3’ (2.3 cm^{-1} for sample without PT). In both cases, the spectra showed contribution of the disordered C- amorphous C at around 1500 cm^{-1} and the G-band of graphite at around 1530 cm^{-1}. These bands however, are typically present in hetero-epitaxial CVD diamond films and cannot be used to infer about the incorporation of B in this case. However, both films showed the BC peak- sample A3 at 977.51 cm^{-1} and A3’ at 963.86 cm^{-1}- from which we can infer more definitively, the B incorporation in the films. The BC peak of A3 has a higher FWHM (11.63 cm^{-1}) than A3’ (9.99 cm^{-1})- signifying a greater disorder, possibly due to greater incorporation of B in the film, for the sample that received PT.

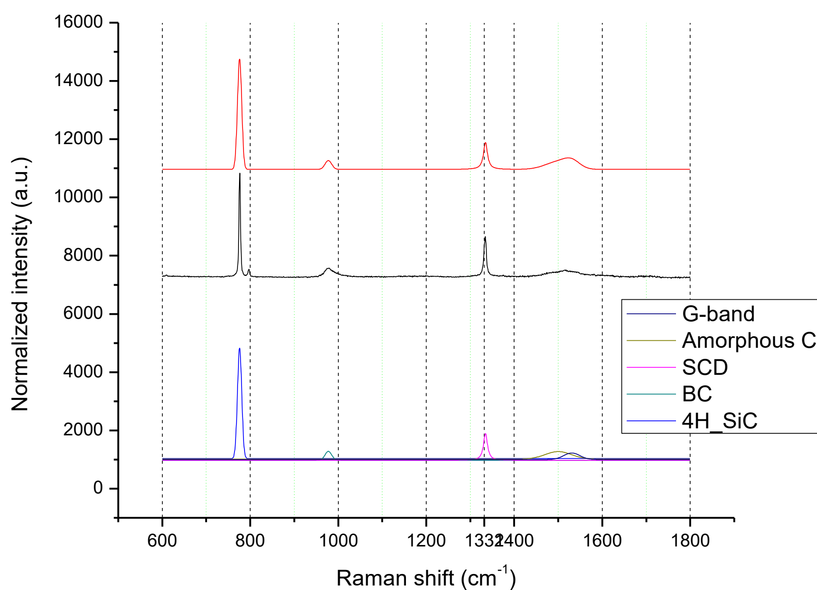

Figure 4-35 Raman spectra of samples A3' (red) and A3 (black)- fitting shown at the bottom of the plot

Between samples A2 and A5, both of which received PT, and were deposited in the same run, under the same deposition conditions, the main difference was in the kind of seeding suspension that was used to seed them. To recall, A2 was seeded in ND suspension and A5 in diamond grit. The SEM images of these two samples reveal clear differences between the films- the film on sample A5 was microcrystalline where as A2 revealed a NCD film, with some larger crystals (*Figure 4-36*). These larger crystals are a few microns in size and are thus not remnants of the ND suspension. A possible explanation of these artefacts are the non-uniform dispersion of the ND particles during seeding, leading to regions where MCD facets have preferentially grown. When compared to sample A5, A2 thus had a more non-uniform nucleation density.

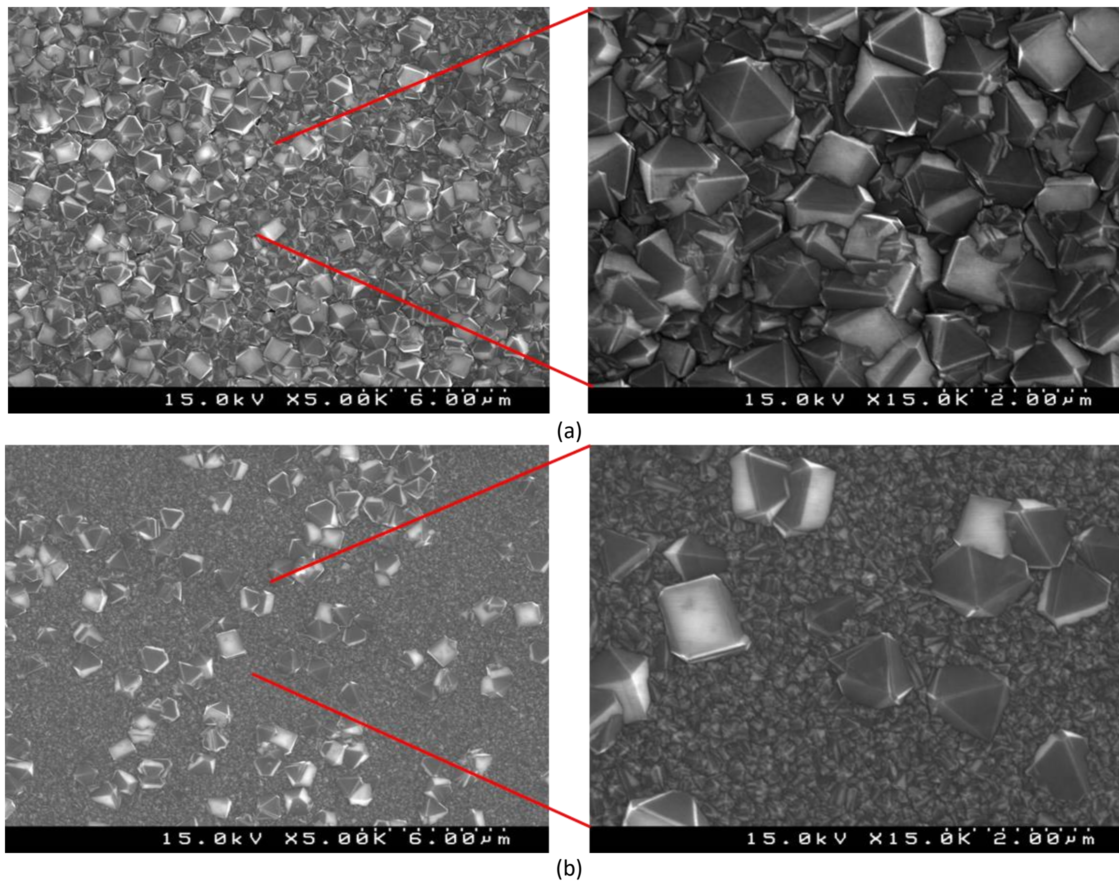

Figure 4-36 SEM images of sample (a) A5 (b) A2

To study the effect of the deposition pressure on the quality of the BDD, samples corresponding to the same PT, seeding and deposition conditions from series A and B were compared- for example, samples A3 and B2 received the same treatment, but the pressure was 4.5 kPa for A3 and 9 kPa for B2. Again, SEM images of the two reveal stark differences. Growth at low pressure growth leads to significantly smaller crystal size as can be seen, comparing images at higher magnification – a and b of *Figure 4-37*. As deposition pressure increases, so does the grain size, from a few nanometres at 4.5 kPa to a few microns at 9 kPa. The edges and corners of the diamond grains become more trenched, that shows growth happening in more number of steps, forming more step edges [376]. The number of surface defects also seems to reduce with increasing pressure; this may be a sign of increased B doping efficiency, as increasing B incorporation in film has been noted to induce a reduction in the density of defects [614, 615].

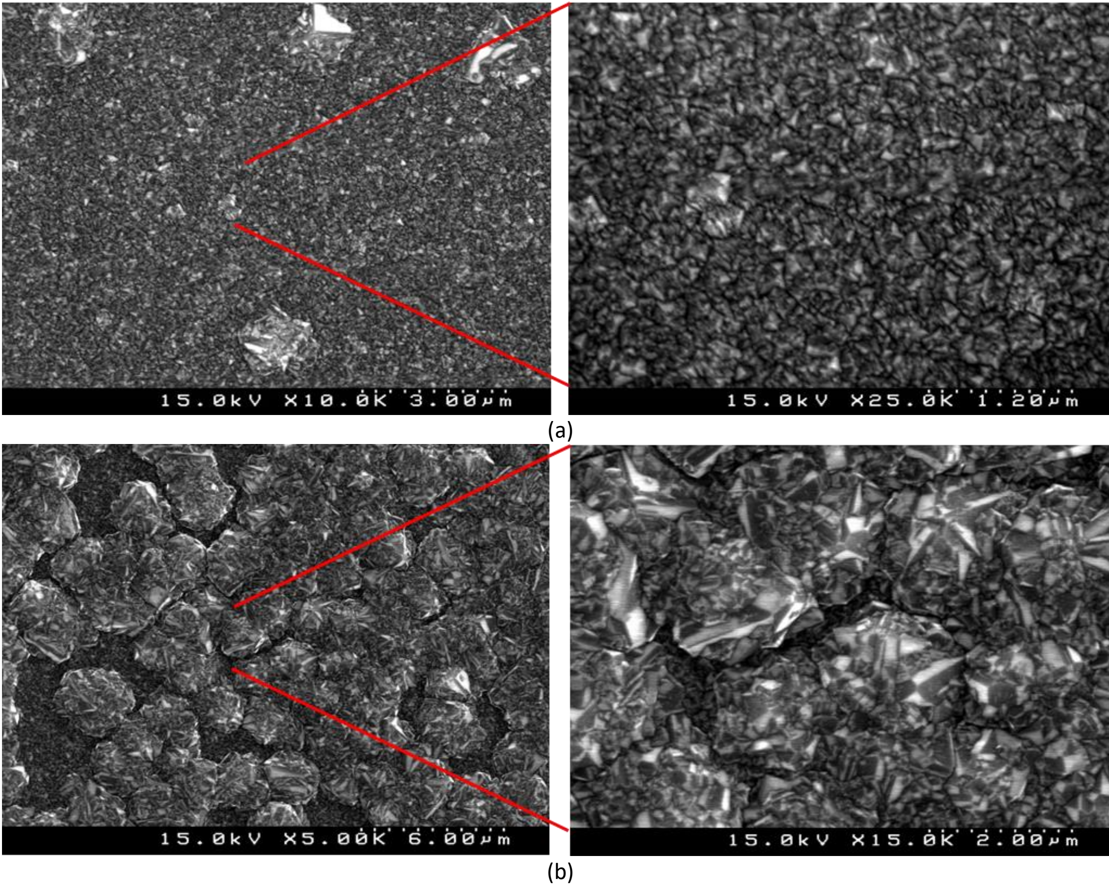

Figure 4-37 SEM images of samples (a) A3 (b) B2

At high deposition pressure, the effect of the PT on samples is also evident. Comparing 2 samples that received all the same conditions of growth but one received PT and the other did not- i.e. samples B2 (*Figure 4-37*, b) and B2' (*Figure 4-38*)- it can be seen that the trenches observed in B2 are not present in present in B2'- growth took in place in lesser number of steps, and by correlation [615], it is possible that the lack of PT results in a lower B incorporation in to the film.

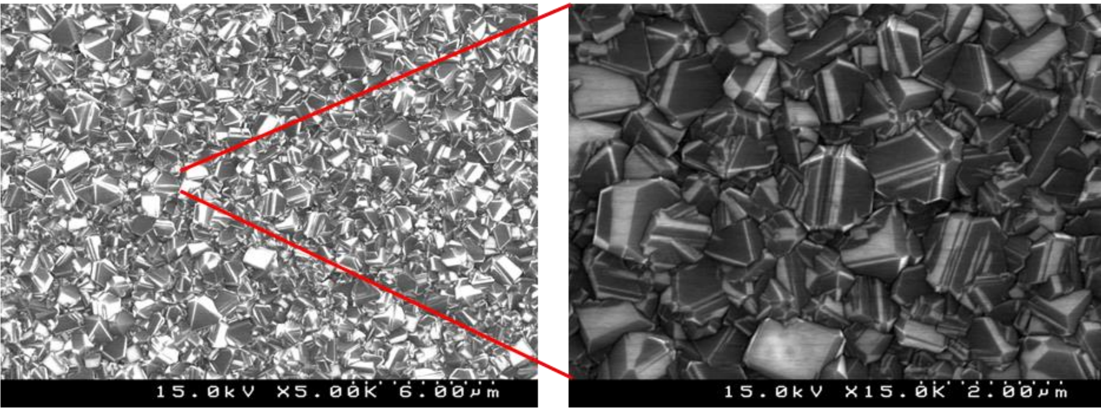

Figure 4-38 SEM image of sample B2'

To study the effect of the CH_4 ratio in the plasma on film characteristics, it is useful to compare the SEM images of samples B1 and B2, at the same magnification- an increased CH_4 amount in the plasma leads to significantly smaller crystal size in BDD (*Figure 4-39*). These samples were grown with the same flow rate of Ar, yet sample B1 was covered in MCD whereas B2 in NCD. This effect of decreasing crystal size with increasing CH_4 ratio occurs in the presence of a chemically inert gas such as Ar- the role of the Ar in the gas mixture appears to increase the degree of dissociation of CH_4, as a result of which, within limits, the conditions of growth in the HFCVD chamber are more likely to induce NCD growth [423, 424].

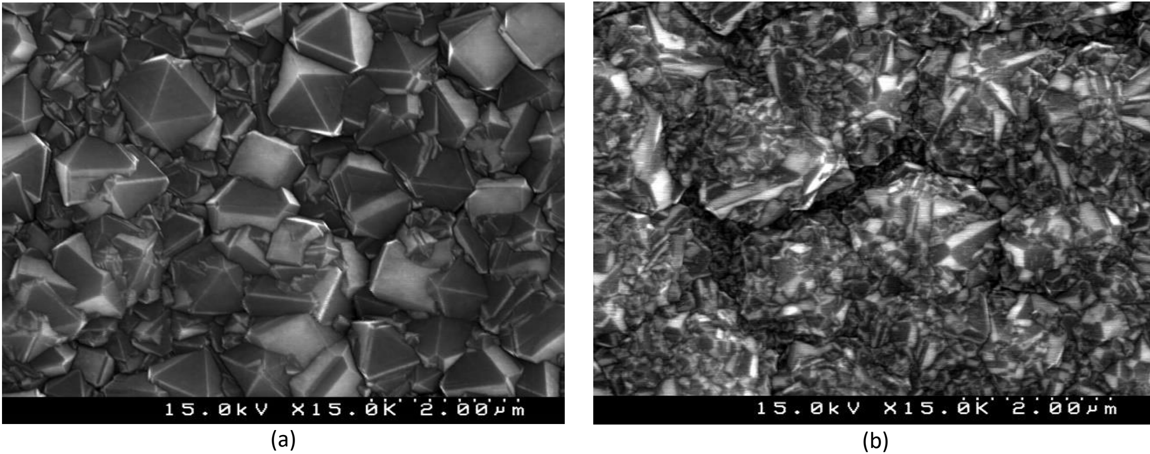

Figure 4-39 SEM images of samples (a) B1 and (b) B2

To study the effect of the Ar ratio in the plasma, which determines the flow rate of the dopant during the deposition process, on film characteristics, it is useful to compare the SEM images of samples A1 and A6 at the same magnification (*Figure 4-40*)- Ar flow significantly influences the crystal size of the BDD film. A higher Ar flow seems to inhibit the lateral growth of the film as is evidenced from the high number of artefacts on the surface of sample A6. As the rate of flow of Ar increases, for the other conditions remaining the same, the amount of B available in the deposition chamber for incorporation into the films increases. It has been seen that film quality (content of diamond) decreases with increased B incorporation [616]. It is also known that increased B incorporation reduces the growth rate of diamond [488]; these two factors might be in conjunction, a possible explanation for the lack of lateral growth in films with higher Ar flow rate. However, it is not possible at the moment to confirm this effect without further study into the film growth mechanisms.

This section thus concludes some of the important insights obtained with respect to the growth of BDD films on SiC substrates, using HFCVD. How the HFCVD parameters affect the characteristics of the film has been discussed.

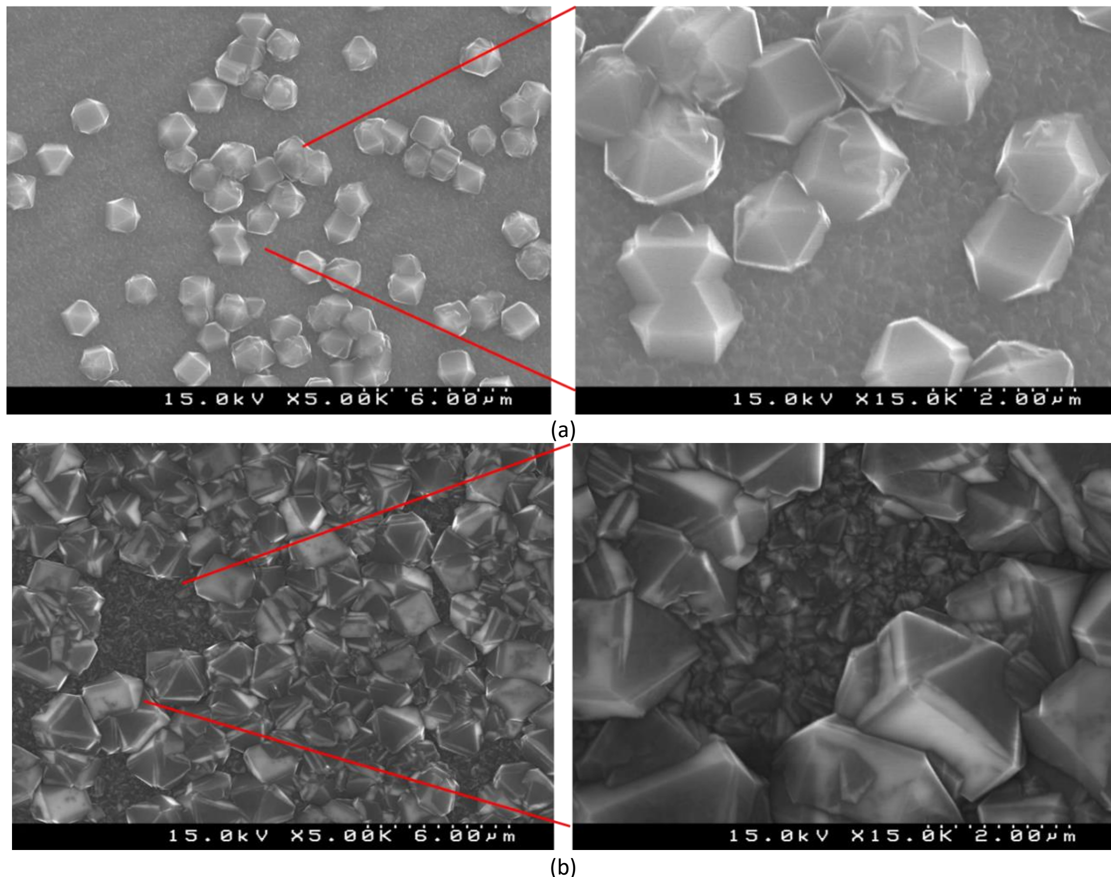

Figure 4-40 SEM images of samples (a) A6 (b) A1

4.5.3 Ohmic contacts to BDD

To fully exploit the material properties of semiconductors and junctions between them, one of the most frequently encountered problems in the development of a new material(s) for electronic device applications must be addressed- the fabrication of suitable high quality metal contacts, since the properties of the electrical contacts directly contribute to the active device performance, and thereby determine the commercial importance of a device, stable physical and electrical characteristics over a wide range of temperature of these contacts is a necessity, making this research challenge particularly relevant [617]. For WBG semiconductors this is specifically true- in order for them to be successfully utilized in applications where smaller band gap materials are unsuitable, contacts that are thermally stable at high temperatures (>300 °C) are required. In the case of diamond, one needs to consider that the semiconducting behaviour of diamond maybe due to doping or surface termination; in addition, the type of diamond as well, in terms of its crystal and morphological characteristics- that is, whether it SCD or PCD, in order to fabricate suitable metal contacts to it.

The barrier height of different metal contacts on SCD has been measured using various techniques, and the reported values of barrier height are all in the range of 1.5-2 eV, independent of the metal [618-621]. In general, a potential barrier is developed at metal-semiconductor interfaces that is due to the difference in the work functions of the two materials or due to the presence of interface states that results in Fermi level pinning. Presumably due to the covalent nature of diamond which offers a high density of surface states, it has been concluded that the Fermi level is strongly pinned at the diamond surface [138] and

gives rise to the phenomenon of a metal-insensitive barrier height, the mechanism which governs the electric charge transfer at the metal-diamond interfaces has, however, not been completely elucidated [617]. However, although lack of this knowledge prevents an establishment of the values of contact resistivities of ohmic contacts and SBH for Schottky contacts, a careful examination of the various contact-fabrication methods is quite helpful to understand important factors which determine the properties of these contacts. Many researchers have been involved in the research and development of metal contacts on polycrystalline, type II B, and homo-epitaxial diamond films and reviews of the early work can be found in [5, 622-624].

Diamond has a high ionization potential, that sets up intrinsic barriers for the contacts on p-type material hindering ohmic behaviour [625]. Thus in order to obtain a good ohmic contact on lightly to moderately doped semiconducting diamond, it is necessary to modify the "nature" of a perfect diamond surface so that the voltage drop across the contact itself is negligibly small as compared to that across the active portion of the device. There are several techniques to achieve this as it is generally believed that most materials will yield rectifying contacts on a clean diamond surface- ohmic contacts can be obtained by modifying the interface in some way (i.e., carbide formation, sputtering, etc.) and they involve either processing conditions that promote interfacial reactions, high surface doping concentrations, and/or defect states that enhance tunnelling or thermionic-field emission of carriers across the metal-semiconductor interface [626]. An alternative method to obtain ohmic contacts on diamond is the use of carbide forming metals such as Ti, Mo, and Ta [5, 627-630]. For the annealed contact, a direct correlation has been revealed by real-time photoemission and using X-ray photoelectron spectroscopy (XPS) between the onset of interfacial carbide formation and the change from a rectifying to an ohmic contact at 482 °C [626, 631] and has also been confirmed by transmission electron microscopy (TEM) [617]. It is believed that the carbide formation at the interface creates a diamond surface layer rich in electrically active defects which lower the barrier height of the metal and increase the leakage current.

Diamond films obtained by CVD, in a H_2 rich environment are H-terminated. These films display a surface conductivity [162]. For such films, quantitative measurements of SBH performed utilizing metals with varying electro-negativities indicates a tendency for the SBH and the rectification ratios to decrease as the metal electronegativity increases, i.e., ohmic properties are obtained when metals with higher electronegativity, such as Pt, Au, Pd and Ag, are used and this linear property remained unchanged when the range of voltage was widened (- 20 to + 20 V) [162]- this kind of ohmic contact has never been obtained on oxygenated surfaces. According to these results, H-terminated diamond has the unique property that I-V characteristics can be changed from rectifying to ohmic by changing the electro-negativities of metals. The SBH dependence on metal electronegativity is enhanced on the monohydride diamond [0 0 1] surface, a trend also observed on as-grown B- doped PCD where the contact resistance largely depends on the metal electronegativity [64, 162, 632]. Similar to other diamond films, Ti shows higher-contact resistance on as-grown (hydrogenated) surfaces, but TiC formation after heat treatment reduces the contact resistance to almost the same value as that of the Au contact without heat treatment on as-grown surfaces. A summary of the results in literature related with the formation of ohmic contacts to diamond is presented in *Table 4-8*.

Type of diamond film	Contact metal	Treatment for Linearity (prior to metallization)	References
PCD	• Au • Ag • W • Ti	• Sputtering (mechanical damage)	[628, 633-635]
PCD	• Al/Si	• In-situ selective B-doping • Post metallization anneal	[636]
PCD	• Pt • Ni • $TaSi_2$ • Al	• In-situ selective B-doping	[535, 637]
SCD, PCD	• Ag • Cu • Au	• Ion implantation	[624, 638]
Natural diamond	• Ti/Au	• Doping by solid state diffusion • Post metallization anneal	[639]
PCD	• Al/Si • Ti-Au • TiWN-Au	• Post metallization anneal	[630]
PCD	• Ti • Mo • Au • Ta	• Post metallization anneal	[5, 627, 629]
PCD	• Zr • Ni	• Post metallization anneal	[640]

Table 4-8 Summary of ohmic contacts to SCD, PCD and natural diamond, of p-type conductivity, using various fabrication techniques

4.5.4 Experimental details- Ohmic contacts to BDD

Ohmic contacts were fabricated on samples of series A and B- keeping the state of the art in ohmic contact fabrication to CVD diamond in mind, Au and Au/Pd contacts were deposited onto the samples diamond surface using a SEM sputtering system (E5000), with Au and Au/Pd targets respectively. Pd is known to improve contact adhesion to diamond films [641]. The contact dimensions were maintained utilising a metal mask- they were circular in shape, with a diameter of 2 mm (*Figure 4-41*). The thickness of the contacts was determined by the deposition time, and the correlation established using profilometry. Following optimization, a deposition time of 20 minutes was utilised to obtain contacts of thickness 100 nm.

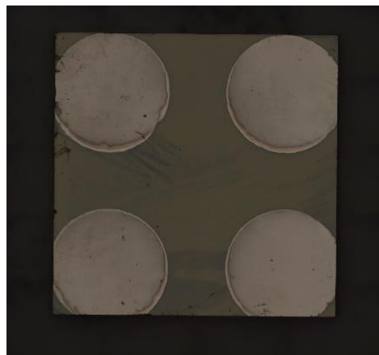

Figure 4-41 Profilometry image of sample with contacts deposited

Half of these metallized samples underwent annealing, post metallization, in a highly pure N_2 atmosphere, at atmospheric pressure, and 973 K for 60 minutes, after which the temperature was increased to 1173 K for 30 minutes. The sample was then cooled slowly, i.e., without any forced cooling in the same N_2 ambient. After the fabrication of contacts, Cu wires were glued using Ag conducting paste, and the samples attached to individual, tailor made PCBs. Resistance measures and IV characteristics were then made using a Keithley 2400. Linearity of the contacts was confirmed and these results are discussed later. Between samples with the same conditions but differing in the Ar flow rate, for example, samples A1 and A6, it was found that a higher flow rate resulted in reduced resistance (signifying a higher doping efficiency; in addition, a similar trend was observed for increasing CH_4 ratios). These results are not presented here, but were utilized to design a second round of experiments- a new set of films (10 in total) following P1 and P2, were made using a higher Ar flow rate (10 sccm) and varying the CH_4 ratio in the plasma. As Ar is the transport gas, it is expected that a high flow rate will favourably affect the B doping efficiency in the films; the CH_4 ratio is also an important parameter affecting B doping efficiency [487]. The parameters can be found listed in *Table 4-9*.

Sample ID	PT (CH_4/H_2)	Seeding	Substrate temperature (K)	Growth ($CH_4/Ar/H_2$)	Pressure (kPa)
BDD_1/BDD_1'	3/100	ND	1023	1/10/100	9.0
BDD_2/BDD_2'				2/10/100	
BDD_3/BDD_3'				3/10/100	
BDD_4/BDD_4'				4/10/100	
BDD_5/BDD_5'				5/10/100	

Table 4-9 Deposition conditions used for second round of BDD growth on SiC samples- samples not given PT are marked with '

4.5.5 Results and discussion- Optimization of ohmic contacts to BDD

To quantify the linearity of the deposited contacts, IV measures were made over a range of voltages- from -5 to +5 V, using a Keithley 2400 (in source V, measure I mode), and 2 probes on a micro-probing station. In order to do this, the device under test (DUT) was connected to the Keithley using the 4 wire sense set-up as illustrated in *Figure 4-42* a and b. The contacts were rectangular, with dimensions 0.5 mm × 5 mm, covering the entire width of the sample.

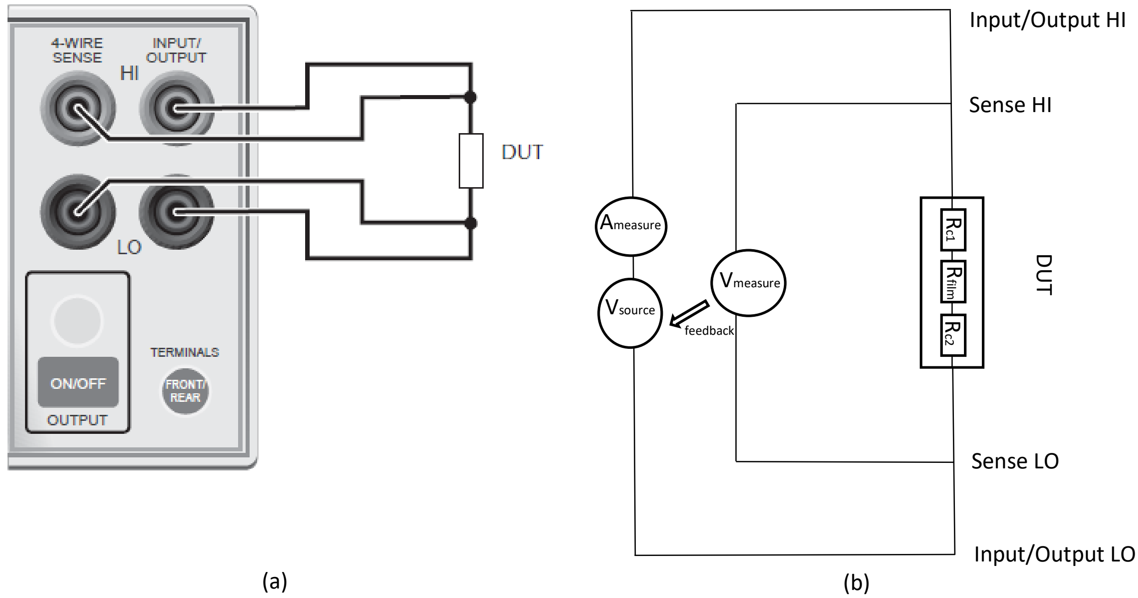

Figure 4-42 (a) 2 wire sense set-up for DUT using a Keithley 2400 (b) Corresponding circuit diagram

Measurements were made by using the Keithley as a voltage source, supplying a linear (for example, from -1 V to +1 V, -5 V to +5 V and -50 V to + 50 V) as well as in a cyclical voltage pulse (for example, from -1 V to + 1 V, and back to – 1V, with and without a time delay between subsequent measurements; and recording the corresponding current (*Figure 4-43*).

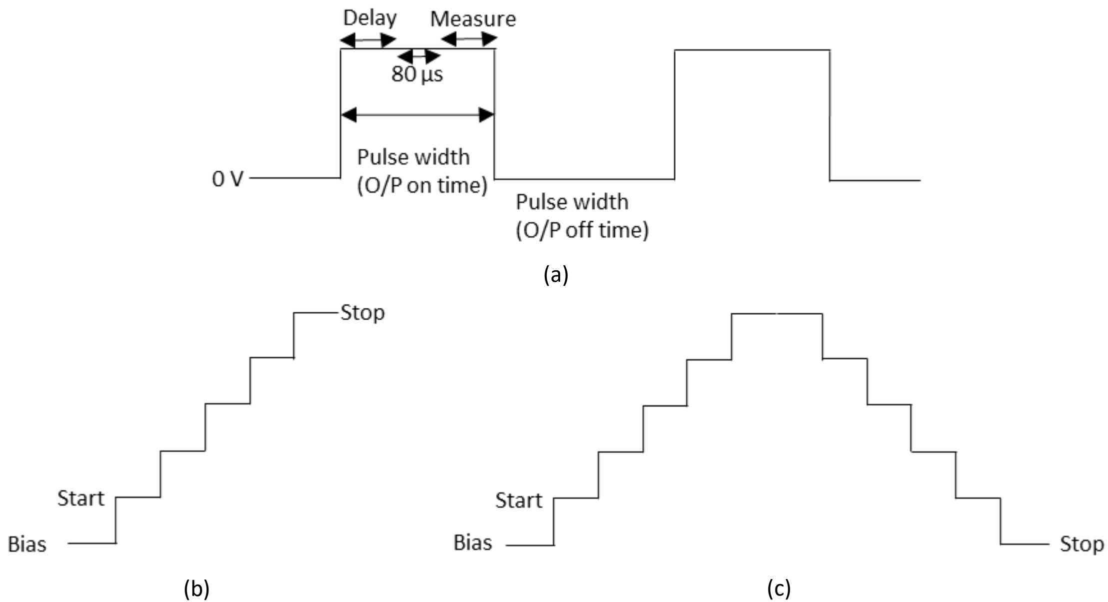

Figure 4-43 (a) Pulse measure timing, with delay, and an overhead of 80µs (b) Linear pulse sweep (c) Cyclical pulse sweep

These measurements were made with both Au and Au-Pd contacts, both before and after annealing. A summary of the samples used for these measurements is presented in *Table 4-10*.

Sample	Contact material	Anneal
A3_Au_ann	Au	Yes
A3_Au		No
A3_AuPd_ann	Au-Pd	Yes
A3_Au		No

Table 4-10 Summary of samples fabricated for ohmic contact characterization

The DUT in these measurements was made up of 3 resistances in series- R_{c1} and R_{c2} (contact resistances) and R_{film} (the resistance of the film). In this way, by making IV measurements, the profile of the DUTs could be measured and compared without calculating and subtracting individual contact resistances. Annealing of the samples clearly influence the electrical characteristics of the contacts- as can be seen from the IV plots (*Figure 4-44*) in the case of Au as well as AuPd contacts, after annealing there is improvement in the linearity of the IV characteristic, thus the ohmic nature of the contact. Between Au and AuPd contacts, it can be seen that for the same that the linearity of the latter is much better than those of Au contacts. For the same voltage, on similar samples, a one order increase in the magnitude of current at the same voltage was also seen for the AuPd when compared to Au contacts.

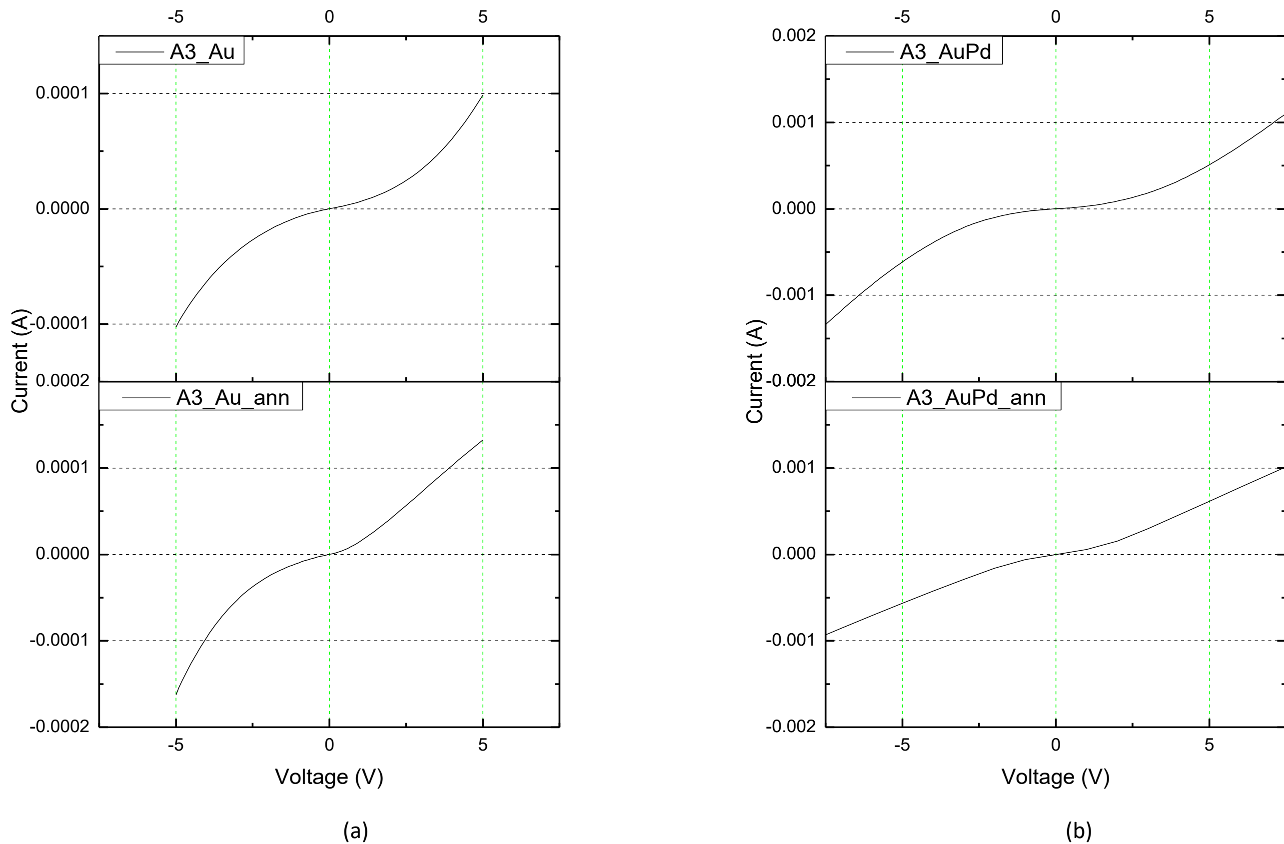

Figure 4-44 IV curves of samples (a) A3_Au and (b) A3_AuPd

From the inferences of the previous IV measurements, AuPd contacts were used for the next set of measurements was made to quantify the resistance of the deposited films. In order to do this, contacts were deposited on samples using the schematic shown in *Figure 4-45* a, and annealed using the aforementioned conditions.

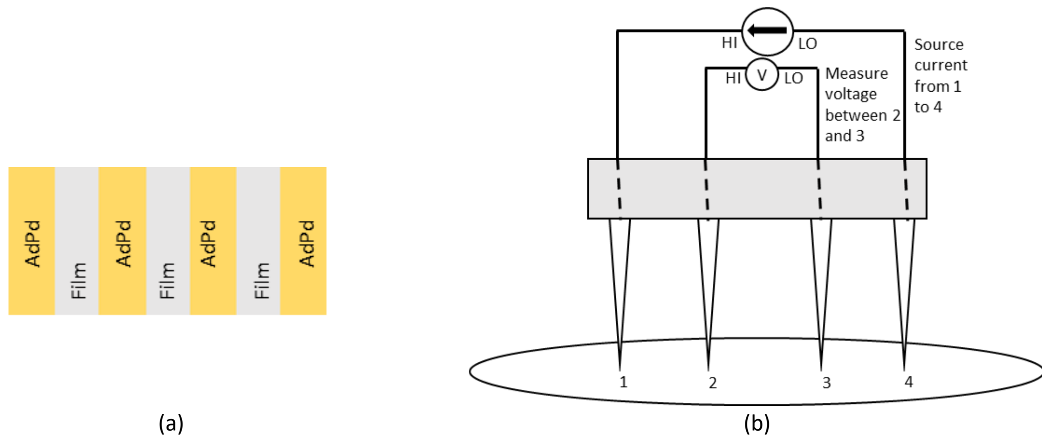

(a) (b)

Figure 4-45 (a) Contacts used for four point probe measurements (b) Measurement set-up for the four point probe technique

The four-point probe method was used to measure resistance of thin films *Figure 4-45* b. Using four probes for thin film measurements allows to eliminate measurement errors due to the probe resistance, the spreading resistance under each probe, and the contact resistance between each metal probe and the semiconductor material under test- i.e., BDD thin films. The four-point probe technique involves bringing four equally spaced probes in contact with a material of unknown resistance; by forcing a DC current between the outer two probes, the voltage difference between the inner two probes is measured (circuit diagram represented in *Figure 4-46*). The resistance is calculated from geometric factors, the source current, and the voltage measurement.

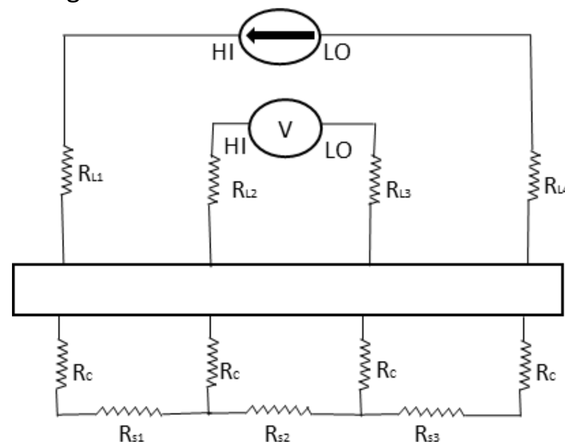

Figure 4-46 Equivalent circuit diagram of 4 point probe set-up where R_s is the sample resistances, R_c is the contact resistance, and R_L the lead resistance

In the derivations for the measurements made using this method, it is assumed that the metal tip is infinitesimally small and that samples are semi-infinite in lateral dimension. For bulk samples where the sample thickness t >>s, the probe spacing, a spherical protrusion of current emanating from the outer probe tips is assumed; for thin films however, whose thickness t <<s, one gets current rings instead of spheres, making the expression for sheet resistance, without correction factors for anisotropy [642]

$$\rho_s = k\left(\frac{V}{I}\right) \tag{4-1}$$

Where k= 4.53 (i.e., $\frac{\pi}{\ln 2}$), and expressed as Ω/square. Note that unlike the resistance, sheet resistance is independent of contact geometries.

Using the Keithley in a source I-measure V mode, I-V measurements were made and using the expression (4-1), sheet resistance of samples of series BDD were calculated. These results are presented in *Table 4-11*. It is seen that PT greatly influences the sheet resistance of the films. In all cases, samples that received PT showed a lower resistance than their counterparts that did not. PT is known to improve the interface quality by increasing the ratio between grains to grain boundaries- by aiding in the dispersion of seeds during US [456] and as discussed before, by promoting lateral growth of films. From these measurements it can be seen that PT also influences favourably the incorporation efficiency of B atoms, reflected in systematically lower value of sheet resistance values of samples that received PT as opposed to those that did not.

Sample	**Average sheet resistance (Ω/square)**		**Ratio of resistance between PT and non-PT samples**
	PT	**No-PT**	
BDD_1/BDD_1'	606	6920	0.09
BDD_2/BDD_2'	127	386	0.33
BDD_3/BDD_3'	0.09	1.73	0.05
BDD_4/BDD_4'	0.366	0.849	0.4
BDD_5/BDD_5'	0.242	0.249	0.97

Table 4-11 Average resistance values of samples of series BDD

In general, with increasing CH_4/H_2 ratio, resistance was found to decrease *Figure 4-47*. This increase in conductivity was noted for both samples with and without PT- samples with PT also had higher current magnitudes (in the order of mA, for all samples) than their counterparts without PT. Since the same contacts were used for all samples, this is not due to a reduction in specific contact resistance (SCR). It is known that the ratio of grain boundaries (more conduction through leakage) to grain (more resistance, if not doped) also increases with increasing CH_4 in the plasma [151]. Therefore, while the decrease in the resistance of BDD films in films with PT might be due to increasing B incorporation efficiency, the decreasing resistance in films of samples without PT is due to increasing leakage current due to increasing non-sp^2 components of the film. In any case, this is a hypothesis and whether the PT did indeed have a positive impact on the B incorporation efficiency, will require the study of the orientation of these films with experimental data from X-ray diffraction (XRD). The effect is also reflected in the way the ratio between the resistance of films with PT to films without PT also increase with increasing CH_4/H_2 ratios, reaching almost unity for samples BDD_5 and BDD_5'. In addition, among PT samples, BDD_3 showed the smallest average resistance but both samples BDD_4 and BDD_5, grown in higher CH_4/H_2 ratio, had average sheet resistivities higher than BDD_3. In case of samples without PT, the decrease in resistance is more linear, from 606 MΩ for BDD_1' to 0.249 MΩ for BDD_5'.

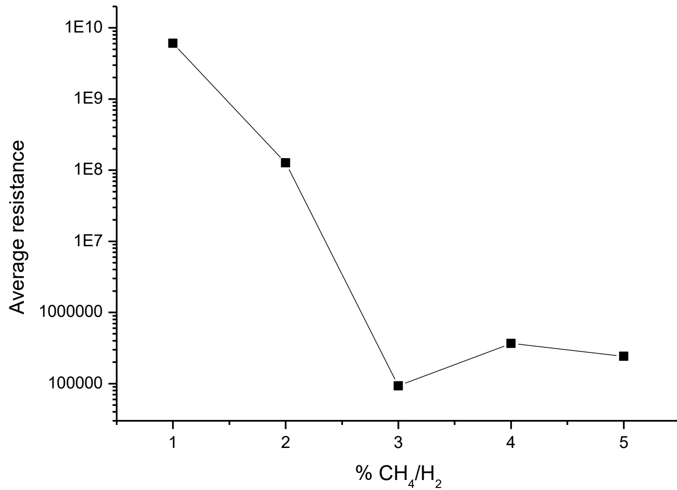

(a)

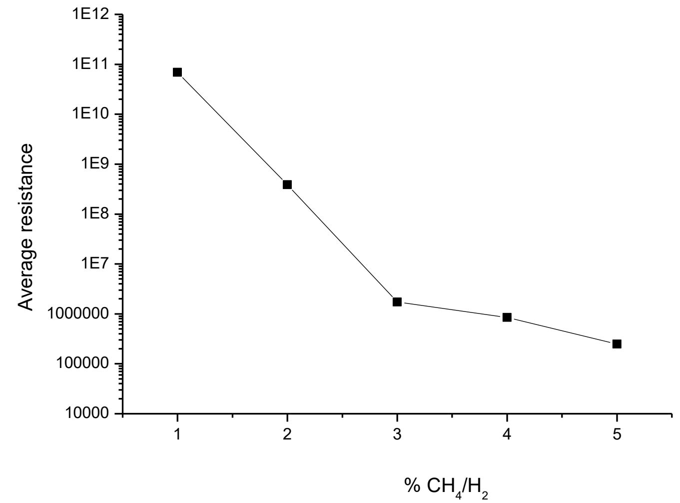

(b)

Figure 4-47 Plot of average resistance and its variation with % of CH_4 for samples of series BDD (a) with PT (b) without PT

4.5.6 SiC-BDD heterojunctions

With the deposition of p-type conductive diamond films on n-type SiC, i.e., samples of series listed in *Table 4-7* and *Table 4-9*, p-n heterojunctions were effectively fabricated. To characterize the behaviour of these heterojunctions, transverse IV measurements need to be made, which require the optimization of ohmic contacts not just to the diamond side, but to the SiC side as well. The microstructural and chemical state of the SiC-metal interface is crucial to the electrical properties of the contacts fabricated on it. Of prime importance is pre-metal-deposition surface preparation, the metal deposition process, choice of metal, and post-deposition annealing, all of which impact the performance of metal-SiC contacts. The pre-metal deposition step usually involves a standard 2-step RCA clean [643-646]. In addition, the chemical nature of the starting SiC surface is strongly dependent on surface polarity, hence it must be noted if the starting surface is the Si face or the C face; it is not uncommon to obtain significantly different results when the same contact process to either of the two faces.

Although the NCD-SiC heterojunction has been investigated, the PCD-SiC heterojunction has not. NCD is highly appropriate for passive applications such as heat spreading, tribology, optical coatings [348, 449, 647, 648], MEMs and NEMs applications [649-652], and B-doped NCD as electrochemical electrodes [653-655]; however, it is not appropriate for active electronic device applications [449]. This is because B-doped NCD is unable to realise high mobility values due to its small grain sizes, and a high proportion of grain boundaries- the values of carrier mobility for NCD and UNCD remain around 1 $cm^2\ V^{-1}\ s^{-1}$ regardless of doping concentration [449, 656, 657]. In this regard, SCD and large grain size PCD demonstrate a pronounced increase in hole mobility as the B doping level is decreased [449], making them more relevant for active electronic devices applications. With respect to the thermal properties, grain sizes must exceed that of a few tens of nanometres to behave like and exhibit the superior thermal conductivity characteristics of bulk diamond [449, 658]. To the author's knowledge, investigation of PCD films as electrical contacts to SiC has not been made elsewhere and this work explored the fabrication of the same.

4.5.7 Experimental details- SiC-BDD heterojunctions

Since the BDD layers were deposited on the top side of the SiC, ohmic contacts were deposited on the bottom surface of the 2 SiC samples (*Table 4-12*). In order to choose an appropriate contact metal for SiC

a thorough literature survey was made and Ni was chosen as it was found to be the most commonly used one. Ni was evaporated onto the surface using an e-beam evaporator (Edwards Auto 306), using the same mask as was used for the BDD side, till contacts of 300 nm thickness were formed. One of the samples then underwent rapid thermal annealing (RTA) in Ar atmosphere at 900°C for 3 minutes. IV measurements were then made on these two samples using the same set-up as was used for BDD films, i.e., after the fabrication of contacts, Cu wires were glued using Ag conducting paste, and the samples attached to individual, tailor made PCBs. Resistance measures and IV characteristics were then made using a Keithley 2400. The results are discussed later.

Sample	Description
SiC_Ni	Ni contacts
SiC_Ni_ann	Ni contacts, followed by RTA

Table 4-12 Summary of samples fabricated for ohmic contact optimization for SiC

The same procedure was then followed to deposit contacts on the bottom side of the SiC of sample BDD_3 (*Table 4-9*), as it was the sample with the highest value of conductivity. Transverse IV measurements were made, using again a Keithley 2400, and the sample attached to a custom made PCB. Measurements were made at room temperature up to 363 K by placing the sample in a Fitoterm 22E, Aralab furnace.

4.5.8 Results and discussion- SiC-BDD heterojunctions

Similar to contact optimization for BDD, to quantify the linearity of the deposited Ni contacts, IV measures were made over a range of voltages- from -5 V to +5 V, using a Keithley 2400 (in source V, measure I mode), and 2 probes on a micro-probing station [634], as described before (*Figure 4-42* and *Figure 4-43).* These measurements were made on both SiC samples- with and without RTA. Annealing of the samples clearly influence the electrical characteristics of the contacts- as can be seen from the IV plots (*Figure 4-48*), after annealing there is improvement in the linearity of the IV characteristic, thus the ohmic nature of the contact. There was also a significant increase in the magnitude of the current for sample SiC_Ni_ann when compared to SiC_Ni- about 9 orders of magnitude. This is not unexpected as annealing has been known to significantly lower the SCR of the Ni-SiC contact [659].

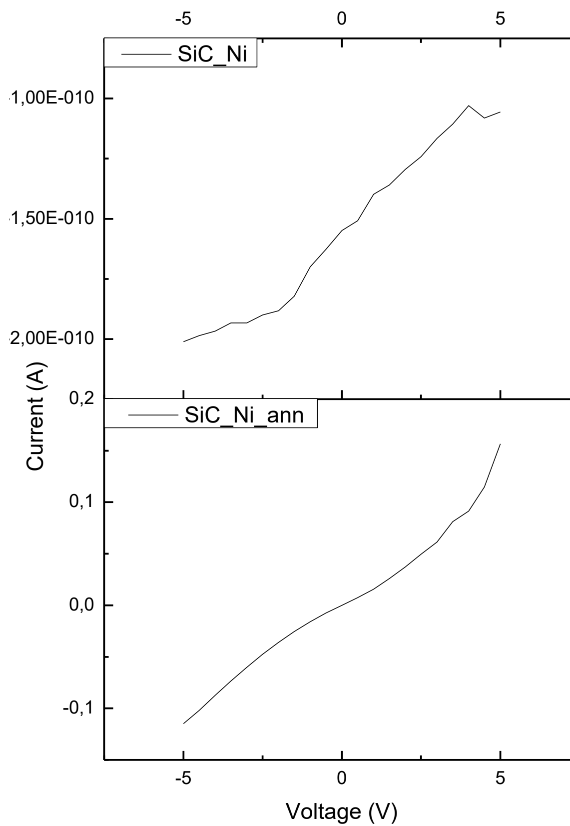

Figure 4-48 IV curves of samples SiC_Ni (top) and SiC_Ni_ann (bottom)

With the optimization of ohmic contacts for both p-type BDD and n-type SiC, diamond-SiC heterojunctions were fabricated, which are expected to show superior performance under high temperatures and powers [660, 661]. The robust characterisations of these heterojunctions, however, was beyond the scope of the current work, but has been enlisted in the future tasks resulting from this thesis.

4.6 Conclusions

In this chapter, the detailed optimization of the fabrication procedures of diamond films for various applications were presented. The novelty of the processes used to obtain these films was also outlined. Certain important future tasks were also identified and these are discussed in the following chapter.

5. Conclusions and future work

5.1 Conclusions

The scientific merit of this work is the optimization of the growth of diamond using HFCVD to deposit diamond on different electronically relevant substrates. It can be thought of as a guidebook for the deposition of diamond for Si, $LiNbO_3$, SiC and GaN. This chapter summarizes the final conclusions of this work.

5.1.1 Influence of the PT film

One of the most important scientific insights obtained in this work was with regards to the PT film that forms an integral part of the NNP. It was an aspect of HFCVD diamond that was investigated for each of the substrates used in this study and it was found to have significant impact in every case. Some general conclusions with respect to its influence can be drawn. For every seeding procedure used in this work (DND, grit, ND suspensions as well as the manual scratch method) samples that received the PT, had films that were coalesced and uniform after the same GC as opposed to samples that did not receive the PT, under the same deposition time. In the case of DMSO suspensions, films were coalesced after just 15 minutes of deposition on Si substrates (section 3.5.3.2). In all of these cases, it was concluded that this was possible because the PT encourages a more uniform distribution of un-agglomerated seeds. The PT also increases the number of diamond seeds that remain attached to the substrate surface after the US seeding. In fact, for substrates seeded with DMSO based suspensions, there was one order of increase in the nucleation density for PT samples compared to no-PT samples (for Si substrates- section 3.5.3.3). It was seen that even at low CH_4/H_2 ratios, PT led to coalesced films with improved qualities as the PT film acts as a C source in the crucial initial moments of film growth (section 4.4.3, for SiC substrates). This aspect of HFCVD growth is particularly important for diamond that is destined to be used for electronics where the crystalline quality of the interface is of prime importance. It also allows one to obtain very thin, fully coalesced diamond films. In two cases- when using grit suspensions (and comparing with other seeding suspensions) for the growth of BDD on SiC, it was seen that samples that received PT showed better crystalline quality- sharper grains, and higher grain to grain boundary ratio. This is an important conclusion for the growth of BDD films- where the usage of NNP has been scarcely investigated. Better crystalline quality is known to improve B incorporation efficiency.

Some particularly relevant insights with respect to the interface of samples that receive the PT were obtained when the Si was etched away to take a direct look at the nucleation surface (section 4.3.2)- this nucleation surface was entirely free of left over seeds and holes as is otherwise noted for the nucleation surfaces obtained using other techniques. This is directly attributable to the NNP. The nucleation surface showed a surface roughness of 2.2 nm and its high crystalline quality is attested by the sharp sp^3 diamond peak observed in its Raman spectrum.

With the exception of one grit size (10-20 µm)- PT was thus able to influence positively, film qualities using all other seeding techniques and for all substrates studied and this is an important conclusion from this work.

5.1.2 Influence of seeding suspensions

Important insight was also obtained with regards to the seeding suspensions used for the treatment of substrates before GC. In all cases where the study was made comparing grit/CH_3OH suspensions and DMSO based DND suspensions, DMSO seeded samples showed higher nucleation densities. It is to be noted that this was found to be true only for DND-DMSO suspensions and not DND-H_2O suspensions (section 3.5.3.2). This inference is relevant when thin, coalesced films of diamond are required and shorter deposition times are to be used- it is beneficial to use DMSO based DND suspensions. However, it is important to note, that in each case, the quality of the film thus obtained had a higher ratio of the non-diamond (sp^2) to diamond (sp^3) phases in the film when compared to grit seeded films. Hence, if the

deposition duration or the thickness of the films are not limitations, grit suspensions are the better option for seeding- in every case when Raman spectra of grit seeded and DND-DMSO (or even, DND- H_2O suspensions) were compared, grit seeded samples showed better crystalline quality and larger grains (sections 3.5.3.3, 4.2.2, 4.2.4, 4.4.3 and 4.5.2). When seeding with grit suspensions, a direct correlation was also found between the grit size and nucleation density and subsequently, grain size of the resulting film- larger grit size leads to smaller nucleation densities and larger grain size in the diamond films.

5.1.3 Other insights

Besides the influence of the NNP and seeding suspensions, some important insights were obtained with respect to growth of diamond on the different substrates. Direct diamond growth was achieved on GaN without use of an inter-layer, a particularly challenging task. Through a process of optimization, the ideal parameters for diamond growth were obtained- using PT, ND based aqueous suspensions, low temperature as well as a CH_4/H_2 ratio of 3%. Using these conditions, a GaN HEMT was coated and the device survived completely the deposition procedure. The addition of a longer cooling step post deposition, at the rate of 5-7 °C / minute was found to be beneficial for prevention of delamination of the films not just for GaN (section 4.4.5) but also $LiNbO_3$ (section 4.2.4)- both substrates with a higher degree of TEC mismatch with CVD diamond.
Another aspect of this study was the low deposition temperature used for the experiments- although higher deposition temperatures are beneficial in some cases (where higher growth rate is desired, section 4.3.1 or improving the incorporation of B in the film, section 4.5.1), higher temperatures are not suitable for substrates such as GaN that undergo degradation under typical high temperature CVD GCs. Obtaining good quality diamond films at low temperature was thus a significant result obtained from this work. Low temperature GC was in fact found to influence positively the desired lateral growth in films during the initial moments (section 4.4.3).
Also investigated in this work were the effects of deposition pressure and flow rate of Ar on the properties of BDD films (section 4.5.2). Some novel procedures were described to obtain patterned diamond growth for SAW dies (section 4.2.3) and all diamond device holders (section 4.3.1).

5.2 Optimization matrices

Using the insights obtained into the HFCVD growth of diamond films on the various substrates and differing conditions, optimization matrices were constructed to summarize the ideal conditions in each case; the tables are listed separately for each substrate investigated in this work. In the following tables, the scoring scheme used, has been:

- +2 - much better than
- +1 - better than
- 0 - equal to
- -1 - worse than
- -2 - much worse than

The “baseline” is defined to be the absence of a system parameter in place, thus its impact on the criteria is nul. In the presence of a system parameter, say presence or absence of NNP or kind of seeding suspension used, a score has been assigned, comparative to the baseline. When a certain parameter has been scored “0”, it implies that its impact on the given criteria was not conclusive- from either not having been studied or from having no effect on said criteria.

Criteria	Baseline	Parameter				
		NNP	Seeding suspension			
			DND/H_2O	DND/DMSO	6-12 μm grit	40-60 μm grit
Seed dispersion	0	+2	+1	+2	+1	+1
Nucleation density	0	+2	+1	+2	+2	+1
Coalesced film	0	+2	-2	+2	+2	+1
Grain size	0	+2	-2	-1	+1	+2
Film quality	0	+2	-2	-1	+2	+2

Table 5-1 Optimization matrix for Si substrates

Criteria	Baseline	Parameter			
		Seeding suspension		PCD conditions	UNCD conditions
		DND/DMSO	Grit		
Coalesced film	0	+2	+1	+2	+2
Grain size	0	-1	+2	+2 (large grain)	-2 (small grain)
Film quality	0	+1	+2	+2	+1
Delamination	0	-2 (no delamination)	-1	+2 (total delamination)	-2 (no delamination)

Table 5-2 Optimization matrix for $LiNbO_3$ substrates (SAW devices)

Criteria	Baseline	Parameter				
		NNP	Seeding suspension			Higher temperature PT/GC (873 K)
			DND/DMSO	6-12 μm grit	40-60 μm grit	
Nucleation density	0	+2	+2	+2	-2	+2
Coalesced film	0	+2	+2	+2	-2	+2
Film quality	0	+2	-1	+2	-2	+2

Table 5-3 Optimization matrix for SiC substrates

Criteria	Baseline	Parameter						
		NNP	Seeding suspension		[CH_4/H_2 (%)]/ [temperature (K)]			Post-growth cooling
			6 nm ND/H_2O	6-12 μm grit	1/673	3/773	5/873	
Coalesced film	0	+2	+2	-2	-1	+2	-1	+2
Film quality	0	+2	+2	-1	-1	+2	-1	0
Delamination	0	0	0	0	0	0	+2 (total delamination)	-2 (no delamination)
Substrate damage	0	0	0	0	+1	-2 (no damage)	+2	0

Table 5-4 Optimization matrix for GaN substrates

Criteria	Baseline	Parameter						
		NNP	Seeding technique			Higher Ar ratio (10sccm)	Higher pressure (9 kPa)	Higher temperature PT/GC (1023 K)
			scratch	6-12 µm grit	6 nm ND/H_2O			
Coalesced film	0	+2	-2	+1	+2	0	0	+2
Film quality	0	+2	-2	+1	+2	0	0	+2
B-doping efficiency	0	+2	0	0	0	+2	+2	+2

Table 5-4 Optimization matrix for BDD on SiC substrates

5.3 Future work

The work of a PhD scholar is rarely finished with the work presented in their thesis- to paraphrase A. Einstein- the more one learns, the more one realizes how much one doesn't know. The investigation presented in the current work answered many questions but also raised a number of them. The following list presents the most relevant questions that warrant continued research and will add to the knowledge base created already in this work-

- From section 3.5.3.3- The curious case of the 10-20 µm grit size- Some anomalous results were obtained with respect to the grit size 10-20 µm, wherein they did not seem to show any apparent influence of the PT; nor did they ascribe to the trends shown by the other grit sizes. Whether this is because of the size of the grit itself, the manufacturing process or perhaps, experimental error, it is a question that might be explored in the future.

- From section 4.2- Investigation of the NNP for UNCD films- UNCD films were successfully deposited on SAW dies in this work. However, the NNP that was the subject of much investigation for the PCD films deposited on other substrates during the course of this work, was not explored for UNCD due to lack of availability of dies. There have been enough indications that the NNP is beneficial for the HFCVD process, as was detailed in section 5.1.1; it might be interesting to see how the PT influences the quality of UNCD films, especially in applications of diamond where UNCD is proved advantageous. Hence one line of work indicated is performing the NNP for SAW dies and characterizing the UNCD films thus formed, by means of comparing them with the films deposited in this work (section 4.2.3). Further study is also required into the origin of the central frequency attenuation that was noted in the diamond-coated dies.

- From section 4.5.5- Influence of PT on B incorporation efficiency- Although PT was found to reduce the sheet resistance of films that received the NNP, further studies are needed to gather the experimental data that can be used to explain this phenomenon. Proposed studies include using XRD and Hall effect measurements for the same.

- From section 4.5.7- Electrical properties of the SiC-BDD heterojunctions- The SiC-BDD heterojunctions that were fabricated at the end of this work have not undergone any electrical characterization- since they are expected to perform under high temperature conditions and exhibit high current densities, the IV characterization of these samples is a necessity to validate the fabrication process. Such characterization should be performed under both high voltage and high temperature conditions and has been identified as one of the most important tasks to be performed in the near future.

6. Bibliography

1. McCarthy, J.R., *Fire in the Earth: The Story of the Diamond*. 1942: Harper & brothers.
2. Hazen, R.M., *The diamond makers*. 1999: Cambridge University Press.
3. James, M. *Introduction to Carbon*. 2002; Available from: http://www.chm.bris.ac.uk/webprojects2002/mjames/carbon.html.
4. Buberman, G.S., *THE BAND STRUCTURE OF DIAMOND.* Soviet Physics Uspekhi, 1971. **14**(2): p. 180-196.
5. Gildenblat, G.S., S.A. Grot, and A. Badzian, *The electrical properties and device applications of homoepitaxial and polycrystalline diamond films.* Proceedings of the IEEE, 1991. **79**(5): p. 647-668.
6. Anton. 2004; Available from: https://commons.wikimedia.org/wiki/File:Diamonds_glitter.png.
7. Gillespie, R.J., *Fifty years of the VSEPR model.* Coordination Chemistry Reviews, 2008. **252**(12): p. 1315-1327.
8. Klippenstein, S.J., L.B. Harding, and B. Ruscic, *Ab initio computations and active thermochemical tables hand in hand: Heats of formation of core combustion species.* The Journal of Physical Chemistry A, 2017. **121**(35): p. 6580-6602.
9. Nassau, K. and J. Nassau, *The history and present status of synthetic diamond.* Journal of Crystal Growth, 1979. **46**(2): p. 157-172.
10. Glukhovsky, M.Z., *Giant swarms of Precambrian mafic dikes and potential diamond resources of ancient platforms.* Geotectonics, 2006. **40**(1): p. 11-24.
11. Wellman, C.H., P.L. Osterloff, and U. Mohiuddin, *Fragments of the earliest land plants.* Nature, 2003. **425**(6955): p. 282-5.
12. Elrich, E.L. and W.D. Hansel, *Diamond deposits : origin, exploration, and history of discovery*. 2002, Australia: Littleton, CO : Society for Mining, Metallurgy, and Exploration.
13. Amato, I., *Stuff: The materials the world is made of*. 1997: Harpercollins.
14. Ball, P., *Made to measure: New materials for the 21st century*. 1999: Princeton University Press.
15. Hannay, J.B., *Artificial Diamonds.* Nature, 1880. **22**: p. 255.
16. Moissan, H., Compt. Rend. (Paris), 1894. **118**: p. 320.
17. Parson, C., Phil. Trans. A, 1919. **220**: p. 671.
18. Hall, H.T., *Ultra-High-Pressure, High-Temperature Apparatus: the ``Belt''.* Review of Scientific Instruments, 1960. **31**(2): p. 125-131.
19. Wentorf, R.H., *The Behavior of Some Carbonaceous Materials at Very High Pressures and High Temperatures.* The Journal of Physical Chemistry, 1965. **69**(9): p. 3063-3069.
20. Bridgman, P.W., *Collected Experimental Papers of P.W. Bridgman*. 1964, Cambridge, MA: Harvard Univ. Press.
21. Wentorf, R.H., *Diamond growth rates.* The Journal of Physical Chemistry, 1971. **75**(12): p. 1833-1837.
22. Strong, H.M. and R.M. Chrenko, *Diamond growth rates and physical properties of laboratory-made diamond.* The Journal of Physical Chemistry, 1971. **75**(12): p. 1838-1843.
23. Kupriyanov, I.N., et al., *HPHT growth and characterization of diamond from a copper-carbon system.* Diamond and Related Materials, 2016. **69**: p. 198-206.
24. DeCarli, P.S. and J.C. Jamieson, *Formation of Diamond by Explosive Shock.* Science, 1961. **134**(3472): p. 92-92.
25. Angus, J., *Synthetic Diamond: Emerging CVD Science and Technology*, ed. J.D. K Spear. 1994: New York: Wiley.
26. Eversole, W.G., *Synthesis of diamond*, in *https://ia800704.us.archive.org/26/items/indexofpatentsis1962unit/indexofpatentsis1962unit.pdf*, U.S.P. Office, Editor. 1962: United States of America.
27. Lander, J.J. and J. Morrison, *Low energy electron diffraction study of the (111) diamond surface.* Surface Science, 1966. **4**(3): p. 241-246.
28. Angus, J.C., *Diamond synthesis by chemical vapor deposition: The early years.* Diamond and Related Materials, 2014. **49**: p. 77-86.
29. Angus, J.C., H.A. Will, and W.S. Stanko, *Growth of Diamond Seed Crystals by Vapor Deposition.* Journal of Applied Physics, 1968. **39**(6): p. 2915-2922.
30. Spitsyn, B.V. and B.V. Deryaguin, *A technique of diamond growth on a diamond face*, U.S.S.R.P. Office, Editor. 1956: Russia.
31. Spitsyn, B.V., L.L. Bouilov, and B.V. Derjaguin, *Vapor growth of diamond on diamond and other surfaces.* Journal of Crystal Growth, 1981. **52**: p. 219-226.
32. Seiichiro, M., et al., *Vapor Deposition of Diamond Particles from Methane.* Japanese Journal of Applied Physics, 1982. **21**(4A): p. L183.
33. Kamo, M., et al., *Diamond synthesis from gas phase in microwave plasma.* Journal of Crystal Growth, 1983. **62**(3): p. 642-644.
34. Matsumoto, S., *Chemical vapour deposition of diamond in RF glow discharge.* Journal of Materials Science Letters, 1985. **4**(5): p. 600-602.
35. Matsui, Y., S. Matsumoto, and N. Setaka, *TEM—electron energy loss spectroscope study of the diamond particles prepared by the chemical vapour deposition from methane.* Journal of Materials Science Letters, 1983. **2**(9): p. 532-534.

36. Sawabe, A. and T. Inuzuka, *Growth of diamond thin films by electron assisted chemical vapor deposition.* Applied Physics Letters, 1985. **46**(2): p. 146-147.
37. Suzuki, K., et al., *Growth of diamond thin films by dc plasma chemical vapor deposition.* Applied Physics Letters, 1987. **50**(12): p. 728-729.
38. Yasuji, M., et al., *Flame Structure and Diamond Growth Mechanism of Acetylene Torch.* Japanese Journal of Applied Physics, 1989. **28**(9R): p. 1718.
39. Bachmann, P.K., D. Leers, and H. Lydtin, *Towards a general concept of diamond chemical vapour deposition.* Diamond and Related Materials, 1991. **1**(1): p. 1-12.
40. Frenklach, M. and K.E. Spear, *Growth mechanism of vapor-deposited diamond.* Journal of Materials Research, 2011. **3**(1): p. 133-140.
41. Celii, F.G., et al., *Infrared detection of gaseous species during the filament-assisted growth of diamond.* Applied Physics Letters, 1988. **52**(24): p. 2043-2045.
42. Celii, F.G. and J.E. Butler, *Hydrogen atom detection in the filament-assisted diamond deposition environment.* Applied Physics Letters, 1989. **54**(11): p. 1031-1033.
43. Goodwin, D.G. and G.G. Gavillet, *Numerical modeling of the filament-assisted diamond growth environment.* Journal of Applied Physics, 1990. **68**(12): p. 6393-6400.
44. Goodwin, D.G., *Simulations of high-rate diamond synthesis: Methyl as growth species.* Applied Physics Letters, 1991. **59**(3): p. 277-279.
45. McMaster, M.C., et al., *Dependence of the gas composition in a microwave plasma-assisted diamond chemical vapor deposition reactor on the inlet carbon source: CH4 versus C2H2.* Diamond and Related Materials, 1995. **4**(7): p. 1000-1008.
46. Vandenbulcke, L., et al., *Molecular beam mass spectrometry and modelling of CH4–CO2 plasmas in relation with polycrystalline and nanocrystalline diamond deposition.* Diamond and Related Materials, 2010. **19**(7): p. 1103-1116.
47. Joeris, P., I. Schmidt, and C. Benndorf, *Photoluminescence spectroscopy of CVD diamond films.* Diamond and Related Materials, 1996. **5**(6): p. 603-607.
48. Gicquel, A., et al., *Gas temperature measurements by laser spectroscopic techniques and by optical emission spectroscopy.* Diamond and Related Materials, 1996. **5**(3): p. 366-372.
49. Moulin, S. and A.M. Bonnot, *In situ monochromatic and spectroscopic optical investigations of diamond thin film growth.* Diamond and Related Materials, 1994. **3**(4): p. 577-580.
50. Hong, B., et al., *Real-time spectroscopic ellipsometry studies of diamond film growth by microwave plasma-enhanced chemical vapour deposition.* Diamond and Related Materials, 1994. **3**(4): p. 431-437.
51. Fayette, L., et al., *In-situ Raman investigation of diamond films during growth and etching processes.* Diamond and Related Materials, 1994. **3**(4): p. 438-442.
52. Chen, C.-F., et al., *Low temperature growth of diamond films by microwave plasma chemical vapor deposition using CH4 +CO2 gas mixtures.* Diamond and Related Materials, 1994. **3**(4): p. 443-447.
53. Rotter, S.Z. and J.C. Madaleno, *Diamond CVD by a Combined Plasma Pretreatment and Seeding Procedure.* Chemical Vapor Deposition, 2009. **15**(7-9): p. 209-216.
54. Ma, Y., et al., *Effect of bias enhanced nucleation on the nucleation density of diamond in microwave plasma CVD.* Diamond and Related Materials, 1995. **4**(12): p. 1325-1330.
55. Fayette, L., M. Mermoux, and B. Marcus, *Role of the nucleation step in the growth rate of diamond films.* Diamond and Related Materials, 1994. **3**(4): p. 480-485.
56. Sumant, A.V., et al., *Surface composition, bonding, and morphology in the nucleation and growth of ultra-thin, high quality nanocrystalline diamond films.* Diamond and Related Materials, 2007. **16**(4): p. 718-724.
57. Bienk, E.J. and S.S. Eskildsen, *The effect of surface preparation on the nucleation of diamond on silicon.* Diamond and Related Materials, 1993. **2**(2): p. 432-437.
58. Lee, S.T., Z. Lin, and X. Jiang, *CVD diamond films: nucleation and growth.* Materials Science and Engineering: R: Reports, 1999. **25**(4): p. 123-154.
59. Muranaka, Y., H. Yamashita, and H. Miyadera, *Worldwide status of low temperature growth of diamond.* Diamond and Related Materials, 1994. **3**(4): p. 313-318.
60. Gruen, D.M., et al., *Fullerenes as precursors for diamond film growth without hydrogen or oxygen additions.* Applied Physics Letters, 1994. **64**(12): p. 1502-1504.
61. Gruen, D.M., et al., *Buckyball microwave plasmas: Fragmentation and diamond-film growth.* Journal of Applied Physics, 1994. **75**(3): p. 1758-1763.
62. Auciello, O. and A.V. Sumant, *Status review of the science and technology of ultrananocrystalline diamond (UNCD™) films and application to multifunctional devices.* Diamond and Related Materials, 2010. **19**(7): p. 699-718.
63. Nesládek, M., et al., *Investigation of n-doping in CVD diamond using gap states spectroscopy.* Diamond and Related Materials, 1996. **5**(9): p. 1006-1011.

64. Iwasaki, T., et al., *Formation of ohmic contacts on semiconducting diamond grown by chemical vapour deposition.* Diamond and Related Materials, 1994. **3**(1): p. 30-34.
65. Madaleno, J.C. and L. Pereira, *The modulation of electrical carrier transport in metal-MPCVD diamond due to the microcrystalline inhomogeneous barriers.* Diamond and Related Materials, 2005. **14**(3): p. 584-588.
66. Liu, J.J., et al., *Band gap structure and electron emission property of chemical-vapor-deposited diamond films.* Solid-State Electronics, 2001. **45**(6): p. 915-919.
67. Su, Q., et al., *Electrical properties of [100]-oriented CVD diamond film.* Solid-State Electronics, 2005. **49**(6): p. 1044-1048.
68. Yang, W., et al., *DNA-modified nanocrystalline diamond thin-films as stable, biologically active substrates.* Nature materials, 2002. **1**(4): p. 253.
69. Wang, Z.Y., et al., *Study of HPHT single crystal diamond as precision cutting tool material.* Precision Engineering, 2012. **36**(1): p. 162-167.
70. Spear, K.E. and J.P. Dismukes, *Synthetic diamond: emerging CVD science and technology*. Vol. 25. 1994: John Wiley & Sons.
71. Schreck, M., et al., *Large-area high-quality single crystal diamond.* MRS Bulletin, 2014. **39**(6): p. 504-510.
72. Element6. *The Element6 CVD diamond handbook*. Available from: https://e6cvd.com/media/wysiwyg/pdf/E6_CVD_Diamond_Handbook_A5_v10X.pdf.
73. Liang, Q., et al., *Recent advances in high-growth rate single-crystal CVD diamond.* Diamond and Related Materials, 2009. **18**(5): p. 698-703.
74. Chrenko, R.M., *Boron, the Dominant Acceptor in Semiconducting Diamond.* Physical Review B, 1973. **7**(10): p. 4560-4567.
75. Custers, J., *Unusual phosphorescence of a diamond.* Physica, 1952. **18**(8-9): p. 489-496.
76. Hess, P., *The mechanical properties of various chemical vapor deposition diamond structures compared to the ideal single crystal.* Journal of Applied Physics, 2012. **111**(5): p. 051101.
77. Raman, C.V., *THE DIAMOND : ITS STRUCTURE AND PROPERTIES.* Current Science, 1968. **37**(8): p. 211-221.
78. Balmer, R., et al., *Chemical vapour deposition synthetic diamond: materials, technology and applications.* Journal of Physics: Condensed Matter, 2009. **21**(36): p. 364221.
79. Moore, M., *Diamond: Natural*, in *Reference Module in Materials Science and Materials Engineering*. 2016, Elsevier.
80. Mortet, V., O.A. Williams, and K. Haenen, *Diamond: a material for acoustic devices.* physica status solidi (a), 2008. **205**(5): p. 1009-1020.
81. Umezawa, H., *Recent advances in diamond power semiconductor devices.* Materials Science in Semiconductor Processing, 2018. **78**: p. 147-156.
82. Shikata, S., *Single crystal diamond wafers for high power electronics.* Diamond and Related Materials, 2016. **65**: p. 168-175.
83. Yurov, V.Y., et al., *Near-infrared refractive index of synthetic single crystal and polycrystalline diamonds at high temperatures.* Journal of Applied Physics, 2017. **122**(24): p. 243106.
84. Yin, Z., et al., *Optical properties and microstructure of CVD diamond films.* Diamond and Related Materials, 1997. **6**(1): p. 153-158.
85. Wolfe, C.M., N. Holonyak Jr, and G.E. Stillman, *Physical properties of semiconductors*. 1988: Prentice-Hall, Inc.
86. Shaffer, P.T. and R.G. Naum, *Refractive index and dispersion of beta silicon carbide.* JOSA, 1969. **59**(11): p. 1498-1498.
87. Ejder, E., *Refractive index of GaN.* physica status solidi (a), 1971. **6**(2): p. 445-448.
88. Migliori, A., et al., *Diamond's elastic stiffnesses from 322 K to 10 K.* Journal of Applied Physics, 2008. **104**(5): p. 053512.
89. Wortman, J. and R. Evans, *Young's modulus, shear modulus, and Poisson's ratio in silicon and germanium.* Journal of applied physics, 1965. **36**(1): p. 153-156.
90. IOFFE. *Propertiesof SiC*. Available from: http://www.ioffe.ru/SVA/NSM/Semicond/SiC/mechanic.html#Acoustic.
91. IOFFE. *Properties of GaN*. Available from: http://www.ioffe.ru/SVA/NSM/Semicond/GaN/mechanic.html#Acoustic.
92. Novikov, N.V. and S.N. Dub, *Hardness and fracture toughness of CVD diamond film.* Diamond and Related Materials, 1996. **5**(9): p. 1026-1030.
93. Vandeperre, L.J., et al., *The hardness of silicon and germanium.* Acta Materialia, 2007. **55**(18): p. 6307-6315.
94. IOFFE. *Properties of Si*. Available from: http://www.ioffe.ru/SVA/NSM/Semicond/Si/mechanic.html.
95. IOFFE. *Properties of Ge*. Available from: http://www.ioffe.ru/SVA/NSM/Semicond/Ge/mechanic.html#Acoustic.
96. Gomes de Mesquita, A.d., *Refinement of the crystal structure of SiC type 6H.* Acta Crystallographica, 1967. **23**(4): p. 610-617.
97. Yu., G., L. M.E., and R. S.L., *Properties of Advanced SemiconductorMaterials GaN, AlN, SiC, BN, SiC, SiGe* ed. L. M.E., R. S.L., and S. M.S. 2001, New York: John Wiley & Sons, Inc.
98. Hess, P., *The mechanical properties of various chemical vapor deposition diamond structures compared to the ideal single crystal.* Journal of Applied Physics, 2012. **111**(5): p. 3.

99. Djemia, P., et al., *Elastic properties of single crystal diamond made by CVD.* Diamond and Related Materials, 2007. **16**(4): p. 962-965.
100. Wang, S.-F., et al., *Determination of acoustic wave velocities and elastic properties for diamond and other hard materials.* Materials Chemistry and Physics, 2004. **85**(2): p. 432-437.
101. Pomorski, M.l., *Electronic Properties of Single Crystal CVD Diamond and its Suitability for Particle Detection in Hadron Physics Experiments*, in *Physics*. 2008, Universit¨at in Frankfurt am Main: Frankfurt.
102. Glassbrenner, C. and G.A. Slack, *Thermal conductivity of silicon and germanium from 3 K to the melting point.* Physical Review, 1964. **134**(4A): p. A1058.
103. Sichel, E., *Thermal conductivity of GaN, 25-360 K.* J. Phys. Chem. Solids, 1977. **38**(3): p. 330-330.
104. Burns, R.C., et al., *HPHT growth and x-ray characterization of high-quality type IIa diamond.* Journal of Physics: Condensed Matter, 2009. **21**(36): p. 364224.
105. May, P.W., *Diamond thin films: a 21st-century material.* Philosophical Transactions of the Royal Society of London. Series A: Mathematical, Physical and Engineering Sciences, 2000. **358**(1766): p. 473-495.
106. Li, Z. and R.C. Bradt, *Thermal Expansion and Thermal Expansion Anisotropy of SiC Polytypes.* Journal of the American Ceramic Society, 1987. **70**(7): p. 445-448.
107. Gian, W., M. Skowronski, and G.S. Rohrer, *Structural defects and their relationship to nucleation of GaN thin films.* MRS Online Proceedings Library Archive, 1996. **423**.
108. Löfås, H., et al., *Effective masses and electronic structure of diamond including electron correlation effects in first principles calculations using the GW-approximation.* AIP Advances, 2011. **1**(3): p. 032139.
109. Fong, C., *Methods used for calculating band structures of layered materials*, in *Electrons and Phonons in Layered Crystal Structures*. 1979, Springer. p. 59-144.
110. Jones, R., *Introduction to density functional theory and exchange-correlation energy functionals.* Computational Nanoscience: Do It Yourself, 2006. **31**: p. 45-70.
111. Han, S., L.S. Pan, and D.R. Kania, *Free Carrier Dynamics in Diamond*, in *Diamond: electronic properties and applications*. 2013, Springer Science & Business Media. p. 241-278.
112. Himpsel, F., J. Van der Veen, and D. Eastman, *Experimental bulk energy bands for diamond using h v-dependent photoemission.* Physical Review B, 1980. **22**(4): p. 1967.
113. Roberts, R. and W. Walker, *Optical study of the electronic structure of diamond.* Physical Review, 1967. **161**(3): p. 730.
114. Clark, C.D., et al., *Intrinsic edge absorption in diamond.* Proceedings of the Royal Society of London. Series A. Mathematical and Physical Sciences, 1964. **277**(1370): p. 312-329.
115. Mort, J., M.A. Machonkin, and K. Okumura, *Density of states distribution in diamond thin films.* Applied Physics Letters, 1991. **59**(4): p. 455-457.
116. Landstrass, M., et al., *Device properties of homoepitaxially grown diamond.* Diamond and Related Materials, 1993. **2**(5-7): p. 1033-1037.
117. Volpe, P., et al., *Ultra-sharp boron interfaces for delta doped diamond structures.* physica status solidi (RRL)–Rapid Research Letters, 2012. **6**(2): p. 59-61.
118. Nebel, C.E., *Chapter 6 Transport and defect properties of intrinsic and boron-doped diamond*, in *Semiconductors and Semimetals*, C.E. Nebel and J. Ristein, Editors. 2003, Elsevier. p. 261-324.
119. Isberg, J., et al., *High Carrier Mobility in Single-Crystal Plasma-Deposited Diamond.* Science, 2002. **297**(5587): p. 1670.
120. Gabrysch, M., et al., *Electron and hole drift velocity in chemical vapor deposition diamond.* Journal of Applied Physics, 2011. **109**(6): p. 063719.
121. Nava, F., et al., *Electron effective masses and lattice scattering in natural diamond.* Solid State Communications, 1980. **33**(4): p. 475-477.
122. Reggiani, L., et al., *Hole-drift velocity in natural diamond.* Physical Review B, 1981. **23**(6): p. 3050-3057.
123. Pernot, J., et al., *Hall hole mobility in boron-doped homoepitaxial diamond.* Physical Review B, 2010. **81**(20): p. 205203.
124. Pan, L., et al., *Electrical transport properties of undoped CVD diamond films.* Science, 1992. **255**(5046): p. 830-833.
125. Pan, L., et al., *Electrical properties of high quality diamond films.* Diamond and Related Materials, 1993. **2**(5-7): p. 820-824.
126. Collins, A. and A. Williams, *The nature of the acceptor centre in semiconducting diamond.* Journal of Physics C: Solid State Physics, 1971. **4**(13): p. 1789.
127. Sadanori, Y., et al., *High-Quality B-Doped Homoepitaxial Diamond Films using Trimethylboron.* Japanese Journal of Applied Physics, 1998. **37**(10A): p. L1129.
128. Butler, J.E., et al., *Nanometric diamond delta doping with boron.* physica status solidi (RRL) – Rapid Research Letters, 2017. **11**(1): p. 1600329.
129. Vavilov, V., A. Gippius, and E. Konorova, *Electron and optical processes in diamond.* Moscow Izdatel Nauka, 1985.
130. Koizumi, S., et al., *Growth and characterization of phosphorus doped n-type diamond thin films.* Diamond and related materials, 1998. **7**(2-5): p. 540-544.

131. Koizumi, S., T. Teraji, and H. Kanda, *Phosphorus-doped chemical vapor deposition of diamond.* Diamond and Related Materials, 2000. **9**(3-6): p. 935-940.
132. Koizumi, S., et al., *Growth and characterization of phosphorous doped {111} homoepitaxial diamond thin films.* Applied physics letters, 1997. **71**(8): p. 1065-1067.
133. Gheeraert, E., et al., *n-Type doping of diamond by sulfur and phosphorus.* Diamond and related materials, 2002. **11**(3-6): p. 289-295.
134. Nesladek, M., et al., *N-type P-doped polycrystalline diamond.* physica status solidi (a), 2003. **199**(1): p. 77-81.
135. Katagiri, M., et al., *Lightly phosphorus-doped homoepitaxial diamond films grown by chemical vapor deposition.* Applied physics letters, 2004. **85**(26): p. 6365-6367.
136. Smith, S.D. and W. Taylor, *Optical Phonon Effects in the Infra-red Spectrum of Acceptor Centres in Semiconducting Diamond.* Proceedings of the Physical Society, 1962. **79**(6): p. 1142.
137. Williams, A., E. Lightowlers, and A. Collins, *Impurity conduction in synthetic semiconducting diamond.* Journal of Physics C: Solid State Physics, 1970. **3**(8): p. 1727.
138. Baker, S.M., G.R. Rossman, and J.D. Baldeschwieler, *Observation of surface charge screening and Fermi level pinning on a synthetic, boron-doped diamond.* Journal of Applied Physics, 1993. **74**(6): p. 4015-4019.
139. Baskaran, G., *Resonating valence bond mechanism of impurity band superconductivity in diamond.* Journal of Superconductivity and Novel Magnetism, 2008. **21**(1): p. 45-49.
140. Šopík, B., *Model for the boron-doping dependence of the critical temperature of superconducting boron-doped diamond.* New Journal of Physics, 2009. **11**(10): p. 103026.
141. Boeri, L., J. Kortus, and O. Andersen, *Three-Dimensional M g B 2-Type Superconductivity in Hole-Doped Diamond.* Physical review letters, 2004. **93**(23): p. 237002.
142. Klein, T., et al., *Metal-insulator transition and superconductivity in boron-doped diamond.* Physical Review B, 2007. **75**(16): p. 165313.
143. Glesener, J.W., *Hole capture in boron-doped diamond.* Applied physics letters, 1994. **64**(2): p. 217-219.
144. Mamin, R.F. and T. Inushima, *Conductivity in boron-doped diamond.* Physical Review B, 2001. **63**(3): p. 033201.
145. Inushima, T., R.F. Mamin, and H. Shiomi, *Impurity band structure of boron-doped homoepitaxial diamond.* Physical Review B, 2009. **79**(4): p. 045210.
146. Karna, S.K., Y. Vohra, and S.T. Weir, *Optical and Electrical Characterization of Boron-Doped Diamond.* arXiv preprint arXiv:1210.7846, 2012.
147. Benabdesselam, M., et al., *Characterization of B-doped polycrystalline diamond films using thermally stimulated luminescence.* Diamond and Related Materials, 2007. **16**(4): p. 805-808.
148. Bourgoin, J., B. Massarani, and R. Visocekas, *Thermally stimulated luminescence and conductivity in boron-doped diamonds.* Physical Review B, 1978. **18**(2): p. 786.
149. Orton, J. and M. Powell, *The Hall effect in polycrystalline and powdered semiconductors.* Reports on Progress in Physics, 1980. **43**(11): p. 1263.
150. Muto, Y., et al., *Electrical conduction in undoped diamond films prepared by chemical vapor deposition.* Applied physics letters, 1991. **59**(7): p. 843-845.
151. Mendes, J.C., et al., *Small signal analysis of MPCVD diamond Schottky diodes.* Diamond and Related Materials, 2019. **93**: p. 131-138.
152. Plano, M., et al., *Thickness dependence of the electrical characteristics of chemical vapor deposited diamond films.* Applied physics letters, 1994. **64**(2): p. 193-195.
153. Graebner, J., et al., *Anisotropic thermal conductivity in chemical vapor deposition diamond.* Journal of applied physics, 1992. **71**(11): p. 5353-5356.
154. Graham, R. and K. Ravi, *Cathodoluminescence investigation of impurities and defects in single crystal diamond grown by the combustion-flame method.* Applied Physics Letters, 1992. **60**(11): p. 1310-1312.
155. Landstrass, M. and K.V. Ravi, *Resistivity of chemical vapor deposited diamond films.* Applied Physics Letters, 1989. **55**(10): p. 975-977.
156. Rezek, B., et al., *Fermi level on hydrogen terminated diamond surfaces.* Applied Physics Letters, 2003. **82**(14): p. 2266-2268.
157. Challinger, S., et al., *Construction of the Energy Band Diagram of Hydrogen Terminated Diamond and Silicon Nanowires.* physica status solidi c, 2017. **14**(12): p. 1700152.
158. Hitoshi, U., et al., *High-Performance Diamond Metal-Semiconductor Field-Effect Transistor with 1 µm Gate Length.* Japanese Journal of Applied Physics, 1999. **38**(11A): p. L1222.
159. Hayashi, K., et al., *Investigation of the effect of hydrogen on electrical and optical properties in chemical vapor deposited on homoepitaxial diamond films.* Journal of applied physics, 1997. **81**(2): p. 744-753.
160. Nebel, C., B. Rezek, and A. Zrenner, *2D-hole accumulation layer in hydrogen terminated diamond.* physica status solidi (a), 2004. **201**(11): p. 2432-2438.

161. Pakes, C.I., J.A. Garrido, and H. Kawarada, *Diamond surface conductivity: Properties, devices, and sensors.* MRS Bulletin, 2014. **39**(6): p. 542-548.
162. Kawarada, H., *Hydrogen-terminated diamond surfaces and interfaces.* Surface Science Reports, 1996. **26**(7): p. 205-259.
163. Vermeulen, L., et al., *Ultrafast photoconductive response of semiconducting diamond.* Solid State Communications, 1981. **38**(12): p. 1223-1225.
164. Young, J.F., et al., *Subnanosecond time-resolved photoconductive response of semiconducting diamond.* Applied Physics Letters, 1983. **42**(5): p. 434-436.
165. Bezrukov, G., et al., *Some Electrical and Optical Properties of Synthetic Semiconducting Diamonds Doped with Boron.* SOVIET PHYSICS SEMICONDUCTORS-USSR, 1970. **4**(4): p. 587-&.
166. Shenai, K., R.S. Scott, and B.J. Baliga, *Optimum semiconductors for high-power electronics.* IEEE transactions on Electron Devices, 1989. **36**(9): p. 1811-1823.
167. Johnson, E., *Physical limitations on frequency and power parameters of transistors.* RCA Rev., 1965. **26**: p. 163-177.
168. Keyes, R., *Figure of merit for semiconductors for high-speed switches.* Proceedings of the IEEE, 1972. **60**(2): p. 225-225.
169. Baliga, B.J., *Power semiconductor device figure of merit for high-frequency applications.* IEEE Electron Device Letters, 1989. **10**(10): p. 455-457.
170. *6 - Circuits and applications*, in *Power Electronics Device Applications of Diamond Semiconductors*, S. Koizumi, et al., Editors. 2018, Woodhead Publishing. p. 383-431.
171. Umezawa, H., Y. Kato, and S.-i. Shikata, *1 Ω on-resistance diamond vertical-Schottky barrier diode operated at 250° C.* Applied Physics Express, 2012. **6**(1): p. 011302.
172. Blank, V., et al., *Power high-voltage and fast response Schottky barrier diamond diodes.* Diamond and Related Materials, 2015. **57**: p. 32-36.
173. Trew, R.J., J.-B. Yan, and P.M. Mock, *The potential of diamond and SiC electronic devices for microwave and millimeter-wave power applications.* Proceedings of the IEEE, 1991. **79**(5): p. 598-620.
174. Planson, D., et al. *Wide bandgap semiconductors for ultra high voltage devices. Design and characterization aspects*. in *2014 International Semiconductor Conference (CAS)*. 2014. IEEE.
175. Rouger, N., N. Donato, and F. Udrea, *6.2 Diamond devices in power converters: needs.* Power Electronics Device Applications of Diamond Semiconductors, 2018: p. 400.
176. Koizumi, S., C. Nebel, and M. Nesladek, *Physics and applications of CVD diamond*. 2008: John Wiley & Sons.
177. Sussmann, R.S., *CVD diamond for electronic devices and sensors*. Vol. 26. 2009: John Wiley & Sons.
178. Traore, A., et al., *Zr/oxidized diamond interface for high power Schottky diodes.* Applied Physics Letters, 2014. **104**(5): p. 052105.
179. Umezawa, H., et al., *Characterization of leakage current on diamond Schottky barrier diodes using thermionic-field emission modeling.* Diamond and related materials, 2006. **15**(11-12): p. 1949-1953.
180. Tarelkin, S., et al., *Power diamond vertical Schottky barrier diode with 10 A forward current.* physica status solidi (a), 2015. **212**(11): p. 2621-2627.
181. Kimoto, T. and Y. Yonezawa, *Current status and perspectives of ultrahigh-voltage SiC power devices.* Materials Science in Semiconductor Processing, 2018. **78**: p. 43-56.
182. Chicot, G., D. Eon, and N. Rouger, *Optimal drift region for diamond power devices.* Diamond and Related Materials, 2016. **69**: p. 68-73.
183. Dunlap, W.C. and R.L. Watters, *Direct Measurement of the Dielectric Constants of Silicon and Germanium.* Physical Review, 1953. **92**(6): p. 1396-1397.
184. Choyke, W.J. and L. Patrick, *Luminescence of Donor-Acceptor Pairs in Cubic SiC.* Physical Review B, 1970. **2**(12): p. 4959-4965.
185. Bougrov, V., et al., *Properties of Advanced Semiconductor Materials GaN, AlN, InN, BN, SiC, SiGe.* Eds. Levinshtein ME, Rumyantsev SL, Shur MS, John Wiley & Sons, Inc., New York, 2001: p. 1-30.
186. Himpsel, F.J., et al., *Quantum photoyield of diamond(111)---A stable negative-affinity emitter.* Physical Review B, 1979. **20**(2): p. 624-627.
187. Vermeeren, V., et al., *DNA sensors with diamond as a promising alternative transducer material.* Sensors, 2009. **9**(7): p. 5600-5636.
188. Chelnokov, V. and A. Syrkin, *High temperature electronics using SiC: actual situation and unsolved problems.* Materials Science and Engineering: B, 1997. **46**(1-3): p. 248-253.
189. Bormashov, V.S., et al., *Electrical properties of the high quality boron-doped synthetic single-crystal diamonds grown by the temperature gradient method.* Diamond and Related Materials, 2013. **35**: p. 19-23.
190. Dorkel, J. and P. Leturcq, *Carrier mobilities in silicon semi-empirically related to temperature, doping and injection level.* Solid-State Electronics, 1981. **24**(9): p. 821-825.
191. Ottaviani, G., et al., *Hole drift velocity in high-purity Ge between 8 and 220 K.* Journal of Applied Physics, 1973. **44**(6): p. 2917-2918.
192. Mnatsakanov, T.T., et al., *Carrier mobility model for GaN.* Solid-State Electronics, 2003. **47**(1): p. 111-115.

193. Werner, M., et al., *The diamond Irvin curve.* Diamond and Related Materials, 1997. **6**(2): p. 308-313.
194. Li, S.S. and W.R. Thurber, *The dopant density and temperature dependence of electron mobility and resistivity in n-type silicon.* Solid-State Electronics, 1977. **20**(7): p. 609-616.
195. Jacoboni, C., et al., *Electron drift velocity and diffusivity in germanium.* Physical Review B, 1981. **24**(2): p. 1014.
196. Jacoboni, C., et al., *A review of some charge transport properties of silicon.* Solid-State Electronics, 1977. **20**(2): p. 77-89.
197. Ferry, D.K., *High-field transport in wide-band-gap semiconductors.* Physical Review B, 1975. **12**(6): p. 2361-2369.
198. Vassilevski, K.V., et al., *Experimental determination of electron drift velocity in 4H-SiC p/sup+/-nn/sup+/avalanche diodes.* IEEE Electron Device Letters, 2000. **21**(10): p. 485-487.
199. Khurgin, J., Y.J. Ding, and D. Jena, *Hot phonon effect on electron velocity saturation in GaN: A second look.* Applied Physics Letters, 2007. **91**(25): p. 252104.
200. Gordon Davies, I., *Properties and growth of diamond.* INSPEC publication, Institution of Electrical Engineers, 1994.
201. Pan, L.S. and D.R. Kania, *Diamond: electronic properties and applications*. 2013: Springer Science & Business Media.
202. Wang, J.J., et al., *Comparison of field-effect transistors on polycrystalline and single-crystal diamonds.* Diamond and Related Materials, 2016. **70**: p. 114-117.
203. Huang, B.r. and D.K. Reinhard, *Electric field-dependent conductivity of polycrystalline diamond thin films.* Applied Physics Letters, 1991. **59**(12): p. 1494-1496.
204. Boettger, E., et al., *Investigation of the high-field conductivity and dielectric strength of nitrogen containing polycrystalline diamond films.* Journal of Applied Physics, 1995. **77**(12): p. 6332-6337.
205. Yamasaki, S. and R.J. Nemanich, *3.2 Strategies for diamond power device applications.* Power Electronics Device Applications of Diamond Semiconductors, 2018: p. 200.
206. Sze, S.M. and K.K. Ng, *Physics of semiconductor devices*. 2006: John wiley & sons.
207. Kyuregyan, A. and S. Yurkov, *Room-temperature avalanche breakdown voltages of p-n# 3 junctions made of Si, Ge, SiC, GaAs, GaP, and InP.* Soviet Physics--Semiconductors(English Translation), 1989. **23**(10): p. 1126-31.
208. Anjos, V., et al. *Thermal lens technique for the determination of SiC thermo-optical properties*. in *Materials science forum*. 2006. Trans Tech Publ.
209. Umezawa, H., et al., *Increase in reverse operation limit by barrier height control of diamond Schottky barrier diode.* IEEE Electron Device Letters, 2009. **30**(9): p. 960-962.
210. Baliga, B.J., *High Voltage Silicon Carbide Devices.* MRS Proceedings, 2011. **512**: p. 77.
211. Ohta, H., et al., *Vertical GaN p-n Junction Diodes With High Breakdown Voltages Over 4 kV.* IEEE Electron Device Letters, 2015. **36**(11): p. 1180-1182.
212. Davis, R.F., et al., *Critical evaluation of the status of the areas for future research regarding the wide band gap semiconductors diamond, gallium nitride and silicon carbide.* Materials Science and Engineering: B, 1988. **1**(1): p. 77-104.
213. Söderberg, S., A. Gerendas, and M. Sjöstrand, *Factors influencing the adhesion of diamond coatings on cutting tools.* Vacuum, 1990. **41**(4): p. 1317-1321.
214. Ramasubramanian, K., N. Arunachalam, and M.S.R. Rao, *A Study on CVD Diamond Coated Cutting Tools Wear Performance using Vibration and Acoustic Emission Signals.* Procedia CIRP, 2018. **72**: p. 1415-1420.
215. (R), D.T. *CVD coated cutting tools*. Available from: https://www.datron.com/tools/diamond-coated-cutting-tools.php.
216. Zou, L., et al., *Thermochemical Wear of Single Crystal Diamond Catalyzed by Ferrous Materials at Elevated Temperature.* Crystals, 2017. **7**(4): p. 116.
217. Materials, D., *Applications of CVD diamond.*
218. GFD. *Diamond coated scalpels and razor blades*. Available from: https://en.blades.diamaze-gfd.com/51.html.
219. Neto, V.F., et al., *Performance of sub-micron diamond films coated on mould inserts for plastic injection moulding.* Journal of Materials Science, 2008. **43**(10): p. 3392-3399.
220. Wilkins, B. *Home Audio 800 series*. Available from: https://www.bowerswilkins.com/eu-en/home-audio/800-series.
221. Miller, A.J., et al., *Diamond coatings for IR window applications.* Diamond and Related Materials, 1997. **6**(2): p. 386-389.
222. Bachmann, P.K. and D.U. Wiechert, *CVD Diamond for X-ray Windows and Lithography Mask Membranes*, in *Low-Pressure Synthetic Diamond: Manufacturing and Applications*, B. Dischler and C. Wild, Editors. 1998, Springer Berlin Heidelberg: Berlin, Heidelberg. p. 207-222.
223. Neto, V.F., et al., *Evaluation of diamond coatings on optical fibre sensors for biological use.* J Nanosci Nanotechnol, 2011. **11**(6): p. 5408-12.
224. Alberto, N., et al., *Diamond-coated fiber Bragg grating through the hot filament chemical vapor process for chemical durability improvement.* Applied Optics, 2017. **56**(6): p. 1603-1609.
225. Rogers, J.A., et al., *Printable, flexible and stretchable diamond for thermal management*. 2013, Google Patents.
226. Simpson, M., *Thermal management of electronic components using synthetic diamond*. 1997, Google Patents.
227. Rotter, S.Z. and S.L. Heidger, *Integrated diamond carrier for laser bar arrays*. 2009, Google Patents.

228. Rotter, S.Z. and S.L. Heidger, *Integrated diamond carrier method for laser bar arrays*. 2008, Google Patents.
229. Kim, T.-H., et al., *Printable, Flexible, and Stretchable Forms of Ultrananocrystalline Diamond with Applications in Thermal Management.* Advanced Materials, 2008. **20**(11): p. 2171-2176.
230. Fabis, P.M., D. Shum, and H. Windischmann. *Thermal modeling of diamond-based power electronics packaging*. in *Fifteenth Annual IEEE Semiconductor Thermal Measurement and Management Symposium (Cat. No.99CH36306)*. 1999.
231. Li, W., et al., *Thermal conductivity of diamond nanowires from first principles.* Physical Review B, 2012. **85**(19): p. 195436.
232. Zhang, Z., H. Schneider, and P. Tounsi, *A promising solution using CVD diamond for efficient cooling of power devices.* Materials Science and Engineering: B, 2012. **177**(15): p. 1358-1361.
233. Schneider, H., et al. *Study of CVD diamond films for thermal management in power electronics*. in *2007 European Conference on Power Electronics and Applications*. 2007.
234. Wang, A., M.J. Tadjer, and F. Calle, *Simulation of thermal management in AlGaN/GaN HEMTs with integrated diamond heat spreaders.* Semiconductor Science and Technology, 2013. **28**(5): p. 055010.
235. Goyal, V., et al., *Direct Low-Temperature Integration of Nanocrystalline Diamond with GaN Substrates for Improved Thermal Management of High-Power Electronics.* Advanced Functional Materials, 2012. **22**(7): p. 1525-1530.
236. Pomeroy, J., et al. *Achieving the best thermal performance for GaN-on-diamond*. in *2013 IEEE Compound Semiconductor Integrated Circuit Symposium (CSICS)*. 2013. IEEE.
237. Govindaraju, N. and R.N. Singh, *Processing of nanocrystalline diamond thin films for thermal management of wide-bandgap semiconductor power electronics.* Materials Science and Engineering: B, 2011. **176**(14): p. 1058-1072.
238. Kyatam, S., et al. *Thermal Analysis of high power LEDs using different PCB materials*. in *Circuit Theory and Design (ECCTD), 2017 European Conference on*. 2017. IEEE.
239. Bezotosnyi, V.V., et al., *Thermal Regime of High-power Laser Diodes.* Physics Procedia, 2015. **72**: p. 399-404.
240. Zweben, C. *CVD diamond for microelectronic and optoelectronic thermal management applications*. Available from: http://www.eoc-inc.com/Diamonds/thermal%20management%20case%20study.pdf.
241. Kyatam, S., et al., *Thermal management of photonic integrated circuits: impact of holder material and epoxies.* Applied Optics, 2019. **58**(22): p. 6126-6135.
242. Morgan, D.P. *History of SAW devices*. in *Frequency Control Symposium, 1998. Proceedings of the 1998 IEEE International*. 1998. IEEE.
243. Mortet, V., et al., *Study of aluminium nitride/freestanding diamond surface acoustic waves filters.* Diamond and Related Materials, 2003. **12**(3-7): p. 723-727.
244. Nakahata, H., et al., *Diamond-based surface acoustic wave devices.* Semiconductor Science and Technology, 2003. **18**(3): p. S96.
245. Shikata, S.-i., et al., *Simulation of characteristics of KNbO3/diamond surface acoustic wave.* Diamond and Related Materials, 2005. **14**(2): p. 167-172.
246. Chen, J.J., et al., *Deposition of high-quality zinc oxide thin films on diamond substrates for high-frequency surface acoustic wave filter applications.* Thin Solid Films, 2005. **485**(1): p. 257-261.
247. Higaki, K., et al. *High frequency SAW filter on diamond*. in *1997 IEEE MTT-S International Microwave Symposium Digest*. 1997.
248. Nakahata, H., et al. *Fabrication of high frequency SAW filters from 5 to 10 GHz using SiO/sub 2//ZnO/diamond structure*. in *2000 IEEE Ultrasonics Symposium. Proceedings. An International Symposium (Cat. No.00CH37121)*. 2000.
249. Dogheche, E., et al., *High-frequency surface acoustic wave devices based on LiNbO3⁄diamond multilayered structure.* Applied Physics Letters, 2005. **87**(21): p. 213503.
250. Masatou, I., et al., *Synthesis and Surface Acoustic Wave Property of Aluminum Nitride Thin Films Fabricated on Silicon and Diamond Substrates Using the Sputtering Method.* Japanese Journal of Applied Physics, 2001. **40**(8R): p. 5065.
251. Salut, R., et al. *Fabrication of GHz range oscillators stabilized by nano-carbon-diamond-based surface acoustic wave resonators*. in *2009 IEEE International Ultrasonics Symposium*. 2009.
252. Shikata, S., et al., *Improvements of Diamond SAW Device Characteristics and Applications to Communication Systems.* New Diamond and Frontier Carbon Technology, 2005. **15**(6): p. 349-361.
253. Yang, W., et al., *DNA-modified nanocrystalline diamond thin-films as stable, biologically active substrates.* Nature Materials, 2002. **1**: p. 253.
254. Varney, M.W., et al., *Polycrystalline-Diamond MEMS Biosensors Including Neural Microelectrode-Arrays.* Biosensors, 2011. **1**(3): p. 118.
255. March, G., T. Nguyen, and B. Piro, *Modified Electrodes Used for Electrochemical Detection of Metal Ions in Environmental Analysis.* Biosensors, 2015. **5**(2): p. 241.
256. Bénédic, F., et al., *Surface acoustic wave devices based on nanocrystalline diamond and aluminium nitride.* Diamond and Related Materials, 2004. **13**(2): p. 347-353.
257. Bénédic, F., et al., *Very high frequency SAW devices based on nanocrystalline diamond and aluminum nitride layered structure achieved using e-beam lithography.* Diamond and Related Materials, 2008. **17**(4-5): p. 804-808.

258. Lamara, T., et al., *Freestanding CVD diamond elaborated by pulsed-microwave-plasma for ZnO/diamond SAW devices.* Diamond and related materials, 2004. **13**(4-8): p. 581-584.
259. Elmazria, O., et al., *Effect of diamond nucleation process on propagation losses of AlN/diamond SAW filter.* IEEE transactions on ultrasonics, ferroelectrics, and frequency control, 2004. **51**(12): p. 1704-1709.
260. Elmazria, O., et al., *High velocity SAW using aluminum nitride film on unpolished nucleation side of free-standing CVD diamond.* IEEE transactions on ultrasonics, ferroelectrics, and frequency control, 2003. **50**(6): p. 710-715.
261. Jagannadham, K., M.J. Lance, and T.R. Watkins, *Growth of diamond film on single crystal lithium niobate for surface acoustic wave devices.* Journal of Vacuum Science & Technology A, 2004. **22**(4): p. 1105-1109.
262. Touloukian, Y., et al., *Thermal expansion: nonmetallic solids. IFI*. 1977, Plenum New York.
263. Jagannadham, K., T.R. Watkins, and M.J. Lance, *Interfacial characterization and residual stress analysis in diamond films on LiNbO3.* Journal of Vacuum Science & Technology A, 2006. **24**(6): p. 2105-2112.
264. Lee, T.-C., et al., *Surface acoustic wave applications of lithium niobate thin films.* Applied Physics Letters, 2003. **82**(2): p. 191-193.
265. Rabson, T.A., et al., *Lithium niobate thin films on diamond/silicon substrates for surface acoustic wave filter device applications.* Integrated Ferroelectrics, 2001. **41**(1-4): p. 81-90.
266. Dogheche, E., et al., *Thick LiNbO 3 layers on diamond-coated silicon for surface acoustic wave filters.* Applied physics letters, 2002. **81**(7): p. 1329-1331.
267. Ishihara, M., et al., *Preparation of lithium niobate thin films on diamond-coated silicon substrate for surface acoustic devices.* Diamond and related materials, 2003. **12**(10-11): p. 1809-1813.
268. Lam, H., J. Dai, and H. Chan, *Orientation controllable deposition of LiNbO3 films on sapphire and diamond substrates for surface acoustic wave device application.* Journal of crystal growth, 2004. **268**(1-2): p. 144-148.
269. Baryshev, S.V., et al. *Developing field emission electron sources based on ultrananocrystalline diamond for accelerators*. in *2016 29th International Vacuum Nanoelectronics Conference (IVNC)*. 2016.
270. Yamaguchi, H., et al., *Electron emission from conduction band of diamond with negative electron affinity.* Physical Review B, 2009. **80**(16): p. 165321.
271. Diederich, L., et al., *Electron emission and NEA from differently terminated, doped and oriented diamond surfaces.* Diamond and Related Materials, 1999. **8**(2): p. 743-747.
272. Yamada, T., et al. *Field emission mechanism of n-type semiconducting diamond with negative electron affinity*. in *2011 24th International Vacuum Nanoelectronics Conference*. 2011.
273. Kleshch, V.I., A.N. Obraztsov, and S.T. Purcell. *Field emission from diamond needles produced by CVD growth*. in *2015 28th International Vacuum Nanoelectronics Conference (IVNC)*. 2015.
274. Kumar, N., H. Schmidt, and X. Chenggang. *Flat panel displays based on nano-crystalline diamond thin films*. in *IEE Colloquium on Diamond in Electronics and Optics*. 1993.
275. Auciello, O., et al. *Ultrananocrystalline diamond (UNCD) films for field emission-based science and devices*. in *25th International Vacuum Nanoelectronics Conference*. 2012.
276. Madaleno, J.C., et al., *Electron field emission from patterned nanocrystalline diamond coated a-SiO2 micrometer-tip arrays.* Applied Physics Letters, 2008. **92**(2): p. 023113.
277. Nemanich, R.J., et al., *CVD diamond—Research, applications, and challenges.* MRS Bulletin, 2014. **39**(6): p. 490-494.
278. Dorsch, O., et al., *Piezoresistive effect of boron-doped diamond thin films.* Diamond and Related Materials, 1993. **2**(5): p. 1096-1099.
279. Kasu, M. and T. Oishi. *Diamond devices for RF applications*. in *2016 URSI Asia-Pacific Radio Science Conference (URSI AP-RASC)*. 2016.
280. Aslam, M., et al., *Piezoresistivity in vapor-deposited diamond films.* Applied physics letters, 1992. **60**(23): p. 2923-2925.
281. Yamamoto, A. and T. Tsutsumoto, *Piezoresistive effect of CVD polycrystalline diamond films.* Diamond and related Materials, 2004. **13**(4-8): p. 863-866.
282. Davidson, J., et al., *Polycrystalline diamond pressure microsensor.* Diamond and related Materials, 1996. **5**(1): p. 86-92.
283. Werner, M., O. Dorsch, and E. Obermeier, *High-temperature pressure sensor using p-type diamond piezoresistors.* Diamond and related materials, 1995. **4**(5-6): p. 873-876.
284. Davidson, J., et al., *Diamond as an active sensor material.* Diamond and related Materials, 1999. **8**(8-9): p. 1741-1747.
285. Werner, M., et al. *Review on diamond based piezoresistive sensors*. in *IEEE International Symposium on Industrial Electronics. Proceedings. ISIE'98 (Cat. No. 98TH8357)*. 1998. IEEE.
286. Sumant, A.V., et al., *MEMS/NEMS based on mono-, nano-, and ultrananocrystalline diamond films.* MRS Bulletin, 2014. **39**(6): p. 511-516.
287. Auciello, O., et al. *Science and technology of piezoelectric/diamond heterostructures for monolithically integrated high performance MEMS/NEMS/CMOS devices*. in *2008 17th IEEE International Symposium on the Applications of Ferroelectrics*. 2008.
288. Zalazar, M., et al., *Integration of piezoelectric aluminum nitride and ultrananocrystalline diamond films for implantable biomedical microelectromechanical devices.* Applied Physics Letters, 2013. **102**(10): p. 104101.

289. Lebedeva, A. and G. Alagashev. *Capacitive RF MEMS switches using ultrananocrystalline diamond films*. in *Proceedings of the 2014 IEEE NW Russia Young Researchers in Electrical and Electronic Engineering Conference*. 2014.
290. Liao, M., et al., *Nanoelectromechanical switch fabricated from single crystal diamond: Experiments and modeling.* Diamond and Related Materials, 2012. **24**: p. 69-73.
291. Liao, M., et al., *Suspended Single-Crystal Diamond Nanowires for High-Performance Nanoelectromechanical Switches.* Advanced Materials, 2010. **22**(47): p. 5393-5397.
292. Tapper, R.J., *Diamond detectors in particle physics.* Reports on Progress in Physics, 2000. **63**(8): p. 1273.
293. Trischuk, W., et al., *Diamond Particle Detectors for High Energy Physics.* Nuclear and Particle Physics Proceedings, 2016. **273-275**: p. 1023-1028.
294. Oh, A., *Diamond particle detectors systems in high energy physics.* Journal of Instrumentation, 2015. **10**(04): p. C04038.
295. Buttar, C., et al., *A study of radiotherapy dosimeters based on diamond grown by chemical vapour deposition.* Diamond and Related Materials, 2000. **9**(3-6): p. 965-969.
296. De Boer, W., et al., *Radiation hardness of diamond and silicon sensors compared.* physica status solidi (a), 2007. **204**(9): p. 3004-3010.
297. Adam, W., et al., *Radiation hard diamond sensors for future tracking applications.* Nuclear Instruments and Methods in Physics Research Section A: Accelerators, Spectrometers, Detectors and Associated Equipment, 2006. **565**(1): p. 278-283.
298. Trischuk, W. *Recent Advances in Diamond Detectors*. in *34th International Conference on High Energy Physics*. 2008. PA, USA.
299. Schmid, G., et al., *A neutron sensor based on single crystal CVD diamond.* Nuclear Instruments and Methods in Physics Research Section A: Accelerators, Spectrometers, Detectors and Associated Equipment, 2004. **527**(3): p. 554-561.
300. Einaga, Y., J.S. Foord, and G.M. Swain, *Diamond electrodes: Diversity and maturity.* MRS Bulletin, 2014. **39**(6): p. 525-532.
301. Hess, A.E., et al., *Diamond-on-Polymer Microelectrode Arrays Fabricated Using a Chemical Release Transfer Process.* Journal of Microelectromechanical Systems, 2011. **20**(4): p. 867-875.
302. Kiran, R., et al., *Multichannel Boron Doped Nanocrystalline Diamond Ultramicroelectrode Arrays: Design, Fabrication and Characterization.* Sensors, 2012. **12**(6): p. 7669.
303. Bitziou, E., D. O'Hare, and B.A. Patel, *Simultaneous Detection of pH Changes and Histamine Release from Oxyntic Glands in Isolated Stomach.* Analytical Chemistry, 2008. **80**(22): p. 8733-8740.
304. Suzuki, A., et al., *Fabrication, Characterization, and Application of Boron-Doped Diamond Microelectrodes for in Vivo Dopamine Detection.* Analytical Chemistry, 2007. **79**(22): p. 8608-8615.
305. Fierro, S., et al., *In vivo assessment of cancerous tumors using boron doped diamond microelectrode.* Scientific Reports, 2012. **2**: p. 901.
306. Wort, C.J.H. and R.S. Balmer, *Diamond as an electronic material.* Materials Today, 2008. **11**(1): p. 22-28.
307. Kohn, E. and A. Denisenko, *Concepts for diamond electronics.* Thin Solid Films, 2007. **515**(10): p. 4333-4339.
308. Bormashov, V.S., et al., *Thin large area vertical Schottky barrier diamond diodes with low on-resistance made by ion-beam assisted lift-off technique.* Diamond and Related Materials, 2017. **75**: p. 78-84.
309. Kumaresan, R., H. Umezawa, and S. Shikata, *Vertical structure Schottky barrier diode fabrication using insulating diamond substrate.* Diamond and Related Materials, 2010. **19**(10): p. 1324-1329.
310. Umezawa, H., et al., *High temperature application of diamond power device.* Diamond and Related Materials, 2012. **24**: p. 201-205.
311. Umezawa, H., et al., *Characterization of Schottky barrier diodes on a 0.5-inch single-crystalline CVD diamond wafer.* Diamond and Related Materials, 2010. **19**(2): p. 208-212.
312. Traoré, A., et al., *Zr/oxidized diamond interface for high power Schottky diodes.* Applied Physics Letters, 2014. **104**(5): p. 052105.
313. Rashid, S.J., et al., *Numerical Parameterization of Chemical-Vapor-Deposited (CVD) Single-Crystal Diamond for Device Simulation and Analysis.* IEEE Transactions on Electron Devices, 2008. **55**(10): p. 2744-2756.
314. Brezeanu, M., et al. *On-State Behaviour of Diamond M-i-P Structures*. in *2006 International Semiconductor Conference*. 2006.
315. Suzuki, M., *High voltage diamond pin diodes: Feasibility study on ultimate properties of diamond toward ultimate power devices.* OYO BUTURI, 2016. **85**(3): p. 218-222.
316. Makino, T., et al., *Diamond Schottky-pn diode without trade-off relationship between on-resistance and blocking voltage.* physica status solidi (a), 2010. **207**(9): p. 2105-2109.
317. Blank, V.D., et al., *Power high-voltage and fast response Schottky barrier diamond diodes.* Diamond and Related Materials, 2015. **57**: p. 32-36.
318. Ikeda, K., et al., *Thermally Stable Schottky Barrier Diode by Ru/Diamond.* Applied Physics Express, 2009. **2**(1): p. 011202.
319. Kubovic, M., et al., *Diamond merged diode.* Diamond and Related Materials, 2007. **16**(4): p. 1033-1037.

320. Looi, H.J., et al., *Progress towards high power thin film diamond transistors.* Diamond and Related Materials, 1999. **8**(2): p. 966-971.
321. Prins, J.F., *Bipolar transistor action in ion implanted diamond.* Applied Physics Letters, 1982. **41**(10): p. 950-952.
322. Aleksov, A., A. Denisenko, and E. Kohn, *Prospects of bipolar diamond devices.* Solid-State Electronics, 2000. **44**(2): p. 369-375.
323. Kato, H., et al., *Diamond bipolar junction transistor device with phosphorus-doped diamond base layer.* Diamond and Related Materials, 2012. **27-28**: p. 19-22.
324. Das, K., *Diamond and silicon carbide heterojunction bipolar transistor*. 1994, Google Patents.
325. Kasu, M., et al., *Diamond-based RF power transistors: Fundamentals and applications.* Diamond and Related Materials, 2007. **16**(4-7): p. 1010-1015.
326. Wang, Y.-F., et al., *Normally-off hydrogen-terminated diamond field-effect transistor with Al2O3 dielectric layer formed by thermal oxidation of Al.* Diamond and Related Materials, 2018. **81**: p. 113-117.
327. Liu, J., et al., *Design and fabrication of high-performance diamond triple-gate field-effect transistors.* Scientific Reports, 2016. **6**: p. 34757.
328. Kazuyuki, H., et al., *High-Performance P-Channel Diamond Metal–Oxide–Semiconductor Field-Effect Transistors on H-Terminated (111) Surface.* Applied Physics Express, 2010. **3**(4): p. 044001.
329. Hitoshi, U., et al., *RF Diamond Transistors: Current Status and Future Prospects.* Japanese Journal of Applied Physics, 2005. **44**(11R): p. 7789.
330. Russell, S.A.O., et al., *Hydrogen-Terminated Diamond Field-Effect Transistors With Cutoff Frequency of 53 GHz.* IEEE Electron Device Letters, 2012. **33**(10): p. 1471-1473.
331. Liu, J., et al., *Logic circuits with hydrogenated diamond field-effect transistors.* IEEE Electron Device Letters, 2017. **38**(7): p. 922-925.
332. Denisenko, A. and E. Kohn, *Diamond power devices. Concepts and limits.* Diamond and related materials, 2005. **14**(3-7): p. 491-498.
333. Shiomi, H., et al., *Pulse-doped diamond p-channel metal semiconductor field-effect transistor.* IEEE Electron Device Letters, 1995. **16**(1): p. 36-38.
334. Aleksov, A., et al., *Diamond junction FETs based on δ-doped channels.* Diamond and Related Materials, 1999. **8**(2): p. 941-945.
335. Gildenblat, G.S., et al., *High-temperature thin-film diamond field-effect transistor fabricated using a selective growth method.* IEEE Electron Device Letters, 1991. **12**(2): p. 37-39.
336. Aleksov, A., et al., *Diamond diodes and transistors.* Semiconductor Science and Technology, 2003. **18**(3): p. S59-S66.
337. El-Hajj, H., et al., *Diamond MISFET based on boron delta-doped channel.* Diamond and Related Materials, 2008. **17**(7): p. 1259-1263.
338. Pang, L.Y.S., et al., *High temperature polycrystalline diamond metal-insulator-semiconductor field-effect-transistor.* Diamond and Related Materials, 1997. **6**(2): p. 333-338.
339. Tessmer, A.J., K. Das, and D.L. Dreifus, *Polycrystalline diamond field-effect transistors.* Diamond and Related Materials, 1992. **1**(2): p. 89-92.
340. Gurbuz, Y., et al., *Diamond semiconductor technology for RF device applications.* Solid-State Electronics, 2005. **49**(7): p. 1055-1070.
341. Ha, D., et al. *Highly manufacturable 7nm FinFET technology featuring EUV lithography for low power and high performance applications*. in *2017 Symposium on VLSI Technology*. 2017.
342. IBM. 2017; Available from: https://www.ibm.com/blogs/think/2017/06/5-nanometer-transistors/.
343. Baccarani, G., M.R. Wordeman, and R.H. Dennard, *Generalized scaling theory and its application to a ¼ micrometer MOSFET design.* IEEE Transactions on Electron Devices, 1984. **31**(4): p. 452-462.
344. del Alamo, J.A., *Nanometre-scale electronics with III–V compound semiconductors.* Nature, 2011. **479**: p. 317.
345. Nelson, R., *IJTAG, heterogeneous integration headline ITC.* EE-Evaluation Engineering, 2015. **54**(12): p. 24-25.
346. Mazellier, J., et al. *First demonstration of heat dissipation improvement in CMOS technology using Silicon-On-Diamond (SOD) substrates*. in *2009 IEEE International SOI Conference*. 2009.
347. Aleksov, A., et al., *Silicon-on-diamond: An advanced silicon-on-insulator technology.* Diamond and Related Materials, 2005. **14**(3-7): p. 308-313.
348. Rabarot, M., et al., *Silicon-On-Diamond layer integration by wafer bonding technology.* Diamond and related materials, 2010. **19**(7-9): p. 796-805.
349. Aleksov, A., et al., *Silicon-on-Diamond—An engineered substrate for electronic applications.* Diamond and related materials, 2006. **15**(2-3): p. 248-253.
350. Annamalai, N., et al., *Radiation response of silicon on diamond (SOD) devices.* IEEE Transactions on Nuclear Science, 1993. **40**(6): p. 1780-1786.
351. Landstrass, M. and D. Fleetwood, *Total dose radiation hardness of diamond-based silicon-on-insulator structures.* Applied physics letters, 1990. **56**(23): p. 2316-2318.

352. Jeong, W., et al. *True 7nm Platform Technology featuring Smallest FinFET and Smallest SRAM cell by EUV, Special Constructs and 3rdGeneration Single Diffusion Break*. in *2018 IEEE Symposium on VLSI Technology*. 2018.
353. Mocuta, A., et al. *Enabling CMOS Scaling Towards 3nm and Beyond*. in *2018 IEEE Symposium on VLSI Technology*. 2018.
354. Qiu, C., et al., *Scaling carbon nanotube complementary transistors to 5-nm gate lengths.* Science, 2017. **355**(6322): p. 271-276.
355. Petrone, N., et al., *Graphene Field-Effect Transistors with Gigahertz-Frequency Power Gain on Flexible Substrates.* Nano Letters, 2013. **13**(1): p. 121-125.
356. Dürkop, T., et al., *Extraordinary mobility in semiconducting carbon nanotubes.* Nano letters, 2004. **4**(1): p. 35-39.
357. Yu, J., et al., *Graphene-on-diamond devices with increased current-carrying capacity: carbon sp2-on-sp3 technology.* Nano letters, 2012. **12**(3): p. 1603-1608.
358. Pesetski, A.A., et al., *Carbon nanotube field effect transistor*. 2010, Google Patents.
359. Rodriguez, S., et al., *RF performance projections of graphene FETs vs. silicon MOSFETs.* ECS Solid State Letters, 2012. **1**(5): p. Q39-Q41.
360. Verma, R., S. Bhattacharya, and S. Mahapatra, *Physics-Based Solution for Electrical Resistance of Graphene Under Self-Heating Effect.* IEEE Transactions on Electron Devices, 2013. **60**(1): p. 502-505.
361. Zhao, F., et al., *Graphene-nanodiamond heterostructures and their application to high current devices.* Scientific reports, 2015. **5**: p. 13771.
362. Carvalho, A.F., et al., *Simultaneous CVD synthesis of graphene-diamond hybrid films.* Carbon, 2016. **98**: p. 99-105.
363. Berman, D., et al., *Metal-induced rapid transformation of diamond into single and multilayer graphene on wafer scale.* Nature communications, 2016. **7**: p. 12099.
364. Tumilty, N., et al., *Synthesis of carbon nanotubes on single crystal diamond.* Carbon, 2010. **48**(11): p. 3027-3032.
365. Fisher, K.A.G., et al., *Frequency and bandwidth conversion of single photons in a room-temperature diamond quantum memory.* Nature Communications, 2016. **7**: p. 11200.
366. England, D.G., et al. *A Quantum Light-Matter Beamsplitter in Diamond*. in *Conference on Lasers and Electro-Optics*. 2017. San Jose, California: Optical Society of America.
367. Yoshiaki Mokuno, H.Y.a.A.C., *Diamond wafer technologies for semiconductor device applications- Single crystal diamond wafers*, in *Power Electronics Device Applications of Diamond Semiconductors*, S. Koizumi, et al., Editors. 2018, Woodhead Publishing. p. 41-57.
368. Tallaire, J.A.a.A., *Diamond wafer technologies for semiconductor device applications- Growth of thick CVD diamond films on different crystalline orientations: defects and doping*, in *Power Electronics Device Applications of Diamond Semiconductors*, S. Koizumi, et al., Editors. 2018, Woodhead Publishing. p. 1-27.
369. Teraji, T., *Diamond wafer technologies for semiconductor device applications- Homoepitaxial growth of ultrahigh purity diamond films*, in *Power Electronics Device Applications of Diamond Semiconductors*, S. Koizumi, et al., Editors. 2018, Woodhead Publishing. p. 27-40.
370. Arnault, M.S.a.J.-C., *Diamond wafer technologies for semiconductor device applications- Heteroepitaxy of diamond on Ir/metal-oxide/ Si substrates*, in *Power Electronics Device Applications of Diamond Semiconductors*, S. Koizumi, et al., Editors. 2018, Woodhead Publishing. p. 58-80.
371. Junya Yaita, T.I.a.M.H., *Diamond wafer technologies for semiconductor device applications- Heteroepitaxy of diamond on SiC*, in *Power Electronics Device Applications of Diamond Semiconductors*, S. Koizumi, et al., Editors. 2018, Woodhead Publishing. p. 81-97.
372. *2 - Doping and semiconductor characterizations*, in *Power Electronics Device Applications of Diamond Semiconductors*, S. Koizumi, et al., Editors. 2018, Woodhead Publishing. p. 99-189.
373. Magyar, A., et al., *Synthesis of luminescent europium defects in diamond.* Nature Communications, 2014. **5**: p. 3523.
374. Isberg, J., et al., *Generation, transport and detection of valley-polarized electrons in diamond.* Nature Materials, 2013. **12**: p. 760.
375. Ashfold, M.N., et al., *What [plasma used for growing] diamond can shine like flame?* Chemical Communications, 2017. **53**(76): p. 10482-10495.
376. Van Enckevort, W., et al., *CVD diamond growth mechanisms as identified by surface topography.* Diamond and Related Materials, 1993. **2**(5-7): p. 997-1003.
377. Hsu, W.L., *Gas phase kinetics during microwave plasma assisted diamond deposition: Is the hydrocarbon product distribution dictated by neutral-neutral interactions?* Journal of Applied Physics, 1992. **72**(7).
378. Sommer, M. and F.W. Smith, *Activity of tungsten and rhenium filaments in CH4/H2 and C2H2/H2 mixtures: Importance for diamond CVD.* Journal of Materials Research, 2011. **5**(11): p. 2433-2440.
379. Rye, R.R., *Hot filament activated chemical vapor deposition of carbon: Film growth and filament reactions.* Journal of Applied Physics, 1994. **76**.
380. Kobashi, K., *Chapter 4 - Other Reactors*, in *Diamond Films*, K. Kobashi, Editor. 2005, Elsevier Science Ltd: Oxford. p. 25-27.

381. Ohtake, N. and M. Yoshikawa, *Diamond film preparation by arc discharge plasma jet chemical vapor deposition in the methane atmosphere.* Journal of the Electrochemical Society, 1990. **137**(2): p. 717-722.
382. Takashi, K. and K. Ken-ichi, *Effects of Oxygen on CVD Diamond Synthesis.* Japanese Journal of Applied Physics, 1987. **26**(9R): p. 1429.
383. Liou, Y., et al., *The effect of oxygen in diamond deposition by microwave plasma enhanced chemical vapor deposition.* Journal of Materials Research, 2011. **5**(11): p. 2305-2312.
384. Kapoor, S., M.A. Kelly, and S.B. Hagström, *Synthesis of diamond films using sequential chemistry: Enhanced growth rate by atomic oxygen.* Journal of Applied Physics, 1995. **77**(12): p. 6267-6272.
385. Jansen, F., M.A. Machonkin, and D.E. Kuhman, *The deposition of diamond films by filament techniques.* Journal of Vacuum Science and Technology A: Vacuum, Surfaces and Films, 1990. **8**(5): p. 3785-3790.
386. Hinneberg, H.J., M. Eck, and K. Schmidt, *Hot-filament-grown diamond films on Si: characterization of impurities.* Diamond and Related Materials, 1992. **1**(7): p. 810-813.
387. Mehta Menon, P., et al., *Filament metal contamination and Raman spectra of hot filament chemical vapor deposited diamond films.* Diamond and Related Materials, 1999. **8**(1): p. 101-109.
388. Nesmeianov, A.N., *Vapour pressure of the elements*. 1963: Pion.
389. Singh, J., *Nucleation and growth mechanism of diamond during hot-filament chemical vapour deposition.* Journal of Materials Science, 1994. **29**(10): p. 2761-2766.
390. Mankelevich, Y.A., A.T. Rakhimov, and N.V. Suetin, *Two-dimensional simulation of a hot-filament chemical vapor deposition reactor.* Diamond and Related Materials, 1996. **5**(9): p. 888-894.
391. Olivas-Martínez, M., et al., *A computational model for the hot-filament chemical vapour deposition process to produce diamond films.* Modelling and Simulation in Materials Science and Engineering, 2007. **15**(3): p. 237.
392. Harris, S.J., A.M. Weiner, and T.A. Perry, *Measurement of stable species present during filament-assisted diamond growth.* Applied Physics Letters, 1988. **53**(17): p. 1605-1607.
393. Harris, S.J., A.M. Weiner, and T.A. Perry, *Filament-assisted diamond growth kinetics.* Journal of Applied Physics, 1991. **70**(3): p. 1385-1391.
394. Harris, S.J. and A.M. Weiner, *Diamond growth rates vs. acetylene concentrations.* Thin Solid Films, 1992. **212**(1): p. 201-205.
395. Wu, C.H., et al., *A study of gas chemistry during hot-filament vapor deposition of diamond films using methane/hydrogen and acetylene/hydrogen gas mixtures.* Journal of Applied Physics, 1990. **68**(9): p. 4825-4829.
396. Schäfer, L., et al., *Atomic hydrogen concentration profiles at filaments used for chemical vapor deposition of diamond.* Applied Physics Letters, 1991. **58**(6): p. 571-573.
397. Celii, F.G. and J.E. Butler, *Direct monitoring of CH3 in a filament-assisted diamond chemical vapor deposition reactor.* Journal of Applied Physics, 1992. **71**(6): p. 2877-2883.
398. Gat, R. and J.C. Angus, *Hydrogen atom recombination on tungsten and diamond in hot filament assisted deposition of diamond.* Journal of Applied Physics, 1993. **74**(10): p. 5981-5989.
399. Ashfold, M.N.R., et al., *Unravelling aspects of the gas phase chemistry involved in diamond chemical vapour deposition.* Physical Chemistry Chemical Physics, 2001. **3**(17): p. 3471-3485.
400. Butler, J., et al., *Understanding the chemical vapor deposition of diamond: recent progress.* Journal of Physics: Condensed Matter, 2009. **21**(36): p. 364201.
401. Moore, G.E. and F.C. Unterwald, *Thermal Dissociation of Hydrogen.* The Journal of Chemical Physics, 1964. **40**(9): p. 2639-2652.
402. Jansen, F., I. Chen, and M.A. Machonkin, *On the thermal dissociation of hydrogen.* Journal of Applied Physics, 1989. **66**(12): p. 5749-5755.
403. Dandy, D.S. and M.E. Coltrin, *Effects of temperature and filament poisoning on diamond growth in hot filament reactors.* Journal of Applied Physics, 1994. **76**.
404. Connell, L.L., et al., *Spatially resolved atomic hydrogen concentrations and molecular hydrogen temperature profiles in the chemical-vapor deposition of diamond.* Journal of Applied Physics, 1995. **78**(6): p. 3622-3634.
405. Gracio, J., Q. Fan, and J. Madaleno, *Diamond growth by chemical vapour deposition.* Journal of Physics D: Applied Physics, 2010. **43**(37): p. 374017.
406. James E. Butler, R.L.W., *Thin film diamond growth mechanisms.* Philosophical Transactions of the Royal Society of London. Series A: Physical and Engineering Sciences, 1993. **342**(1664): p. 209-224.
407. Ohmagari, S., et al., *Lifetime and migration length of B-related admolecules on diamond {100}-surface: Comparative study of hot-filament and microwave plasma-enhanced chemical vapor deposition.* Journal of Crystal Growth, 2017. **479**: p. 52-58.
408. Ogura, M., et al., *Misorientation-angle dependence of boron incorporation into (001)-oriented chemical-vapor-deposited (CVD) diamond.* Journal of Crystal Growth, 2011. **317**(1): p. 60-63.
409. Yamamoto, T., et al., *Toward highly conductive n-type diamond: Incremental phosphorus-donor concentrations assisted by surface migration of admolecules.* Applied Physics Letters, 2016. **109**(18): p. 182102.

410. Frenklach, M. and H. Wang, *Detailed surface and gas-phase chemical kinetics of diamond deposition.* Physical Review B, 1991. **43**(2): p. 1520-1545.
411. May, P.W. and Y.A. Mankelevich, *Simulations of CVD Diamond Film Growth: 2D Models for the identities and concentrations of gas-phase species adsorbing on the surface.* MRS Proceedings, 2011. **1282**: p. mrsf10-1282-a03-02.
412. Debye, P., *Interferenz von röntgenstrahlen und wärmebewegung.* Annalen der Physik, 1913. **348**(1): p. 49-92.
413. Harris, S.J., *Mechanism for diamond growth from methyl radicals.* Applied Physics Letters, 1990. **56**(23): p. 2298-2300.
414. G, G.D. and B.J. E, *Theory of diamond chemical vapor deposition: Handbook of Industrial Diamonds and Diamond Films*, ed. M.A. Prelas. 1997: New York: Dekker.
415. Tamura, H., et al., *First-principle study on reactions of diamond (100) surfaces with hydrogen and methyl radicals.* Physical Review B, 2000. **62**(24): p. 16995-17003.
416. Larsson, K., *Adsorption of hydrocarbon species on a stepped diamond (111) surface.* Physical Review B, 1997. **56**(23): p. 15452-15458.
417. Seshan, V., et al., *Hydrogen termination of CVD diamond films by high-temperature annealing at atmospheric pressure.* The Journal of Chemical Physics, 2013. **138**(23): p. 234707.
418. Oliver, A.W. and B.J. Richard, *Surface conductivity on hydrogen terminated diamond.* Semiconductor Science and Technology, 2003. **18**(3): p. S34.
419. May, P. 2018; Available from: http://www.chm.bris.ac.uk/pt/diamond/growthmodel.htm.
420. May, P.W. and Y.A. Mankelevich, *From Ultrananocrystalline Diamond to Single Crystal Diamond Growth in Hot Filament and Microwave Plasma-Enhanced CVD Reactors: a Unified Model for Growth Rates and Grain Sizes.* The Journal of Physical Chemistry C, 2008. **112**(32): p. 12432-12441.
421. Faust Jr, J. and H. John, *Growth facets on III–V intermetallic compounds.* Journal of Physics and Chemistry of Solids, 1962. **23**(8): p. 1119-1122.
422. Angus, J.C. and C.C. Hayman, *Low-Pressure, Metastable Growth of Diamond and Diamondlike Phases.* Science, 1988. **241**(4868): p. 913.
423. May, P.W., M.N.R. Ashfold, and Y.A. Mankelevich, *Microcrystalline, nanocrystalline, and ultrananocrystalline diamond chemical vapor deposition: Experiment and modeling of the factors controlling growth rate, nucleation, and crystal size.* Journal of Applied Physics, 2007. **101**(5): p. 053115.
424. May, P.W. and Y.A. Mankelevich, *Experiment and modeling of the deposition of ultrananocrystalline diamond films using hot filament chemical vapor deposition and Ar∕CH4∕H2 gas mixtures: A generalized mechanism for ultrananocrystalline diamond growth.* Journal of Applied Physics, 2006. **100**(2): p. 024301.
425. Rodgers, W.J., et al., *Three-dimensional kinetic Monte Carlo simulations of diamond chemical vapor deposition.* The Journal of Chemical Physics, 2015. **142**(21): p. 214707.
426. May, P.W., et al., *Simplified Monte Carlo simulations of chemical vapour deposition diamond growth.* Journal of Physics: Condensed Matter, 2009. **21**(36): p. 364203.
427. Ferrari, A.C. and J. Robertson, *Raman spectroscopy of amorphous, nanostructured, diamond–like carbon, and nanodiamond.* Philosophical Transactions of the Royal Society of London. Series A: Mathematical, Physical and Engineering Sciences, 2004. **362**(1824): p. 2477-2512.
428. Knight, D.S. and W.B. White, *Characterization of diamond films by Raman spectroscopy.* J. Mat.Res., 1989. **4**: p. 385-393.
429. Roy, M., et al., *Detection of nanophase at the surface of HFCVD grown diamond films using surface enhanced Raman spectroscopic technique.* Diamond and related materials, 2002. **11**(11): p. 1858-1862.
430. Poferl, D.J., N.C. Gardner, and J.C. Angus, *Growth of boron-doped diamond seed crystals by vapor deposition.* Journal of Applied Physics, 1973. **44**(4): p. 1428-1434.
431. Rawles, R.E., et al., *Mechanism of surface smoothing of diamond by a hydrogen plasma.* Diamond and Related Materials, 1997. **6**(5): p. 791-795.
432. Ali, M. and M. Ürgen, *Switching dynamics of morphology-structure in chemically deposited carbon films – A new insight.* Carbon, 2017. **122**: p. 653-663.
433. Ali, M. and M. Ürgen, *Surface morphology, growth rate and quality of diamond films synthesized in hot filament CVD system under various methane concentrations.* Applied Surface Science, 2011. **257**(20): p. 8420-8426.
434. Frenklach, M., *Monte Carlo simulation of hydrogen reactions with the diamond surface.* Physical Review B, 1992. **45**(16): p. 9455-9458.
435. Drift, A.V.D., *Evolutionary selection: a principle governing growth orientation in vapour-deposited layers.* Phillips Res. Rep., 1967. **22**.
436. Mitura, S.w., *Nucleation of diamond powder particles in an RF methane plasma.* Journal of Crystal Growth, 1987. **80**(2): p. 417-424.
437. Buerki, P.R. and S. Leutwyler, *Homogeneous nucleation of diamond powder by CO2 -laser-driven gas-phase reactions.* Journal of Applied Physics, 1991. **69**(6): p. 3739-3744.

438. Liu, H. and D.S. Dandy, *Studies on nucleation process in diamond CVD: an overview of recent developments.* Diamond and Related Materials, 1995. **4**(10): p. 1173-1188.
439. Gouzman, I., et al., *Influence of substrate nature on the d.c.-glow discharge induced nucleation of diamond.* Diamond and Related Materials, 1999. **8**(2): p. 132-138.
440. Badzian, A.R. and T. Badzian, *Nucleation and growth phenomena in chemically vapor-deposited diamond coatings.* Surface and Coatings Technology, 1988. **36**(1): p. 283-293.
441. George, M.A., et al., *Investigation of nucleation and growth processes of diamond films by atomic force microscopy.* Journal of Applied Physics, 1994. **76**(7): p. 4099-4106.
442. Wolter, S.D., et al., *Textured growth of diamond on silicon via in situ carburization and bias-enhanced nucleation.* Applied Physics Letters, 1993. **62**(11): p. 1215-1217.
443. Wolter, S.D., et al., *The nucleation of highly oriented diamond on silicon via an alternating current substrate bias.* Applied Physics Letters, 1996. **68**(25): p. 3558-3560.
444. Tang, C. and D.C. Ingram, *The effect of ultrasonic pre-treatment on nucleation density of chemical vapor deposition diamond.* Journal of Applied Physics, 1995. **78**(9): p. 5745-5749.
445. Avigal, Y. and A. Hoffman, *A new method for nucleation enhancement of diamond.* Diamond and Related Materials, 1999. **8**(2): p. 127-131.
446. Chakk, Y., R. Brener, and A. Hoffman, *Mechanism of diamond formation on substrates abraded with a mixture of diamond and metal powders.* Diamond and Related Materials, 1996. **5**(3): p. 286-291.
447. Geis, M.W., *Growth of textured diamond films on foreign substrates from attached seed crystals.* Applied Physics Letters, 1989. **55**(6): p. 550-552.
448. Fox, O.J., et al., *Electrospray deposition of diamond nanoparticle nucleation layers for subsequent CVD diamond growth.* Mater. Res. Soc. Symp. Proc., 2010. **1203**: p. 17-27.
449. Williams, O.A., *Nanocrystalline diamond.* Diamond and Related Materials, 2011. **20**(5): p. 621-640.
450. Spear, K.E., *Handbook of industrial diamonds and diamond films*. 1998.
451. Dennig, P.A. and D.A. Stevenson, *Influence of substrate topography on the nucleation of diamond thin films.* Applied Physics Letters, 1991. **59**(13): p. 1562-1564.
452. Zhang, T., et al., *Effect of mechanical pretreatment on nucleation and growth of HFCVD diamond films on cemented carbide tools with a complex shape.* International Journal of Refractory Metals and Hard Materials, 2019. **84**: p. 105016.
453. Ascarelli, P. and S. Fontana, *Dissimilar grit-size dependence of the diamond nucleation density on substrate surface pretreatments.* Applied Surface Science, 1993. **64**(4): p. 307-311.
454. Rotter, S., *Applications of conformal CVD diamond films.* Israel journal of chemistry, 1998. **38**(1-2): p. 135-140.
455. Iijima, S., Y. Aikawa, and K. Baba, *Early formation of chemical vapor deposition diamond films.* Applied physics letters, 1990. **57**(25): p. 2646-2648.
456. Mukherjee, D., et al., *HFCVD nanostructured diamond films deposited by a combination of seeding suspensions and novel nucleation process.* International Journal of Surface Science and Engineering, 2017. **11**(3): p. 225-240.
457. Stoner, B.R., et al., *Characterization of bias-enhanced nucleation of diamond on silicon by invacuo surface analysis and transmission electron microscopy.* Physical Review B, 1992. **45**(19): p. 11067-11084.
458. Robertson, J., *Mechanism of bias-enhanced nucleation and heteroepitaxy of diamond on Si.* Diamond and Related Materials, 1995. **4**(5): p. 549-552.
459. Maillard-Schaller, E., et al., *Local heteroepitaxy of diamond on silicon (100):mA study of the interface structure.* Physical Review B, 1997. **55**(23): p. 15895-15904.
460. Buijnsters, J.G., L. Vázquez, and J.J. ter Meulen, *Substrate pre-treatment by ultrasonication with diamond powder mixtures for nucleation enhancement in diamond film growth.* Diamond and Related Materials, 2009. **18**(10): p. 1239-1246.
461. Buchkremer-Hermanns, H., H. Ren, and H. Weiβ, *Optimization of diamond nucleation and growth using MW-PACVD method.* Diamond and Related Materials, 1996. **5**(3): p. 312-316.
462. Demuynck, L., et al., *Mechanisms of CVD diamond nucleation and growth on mechanically scratched and virgin Si(100) surfaces.* Diamond and Related Materials, 1997. **6**(2): p. 235-239.
463. Butler, J.E. and A.V. Sumant, *The CVD of Nanodiamond Materials.* Chemical Vapor Deposition, 2008. **14**(7-8): p. 145-160.
464. Madaleno, J.C. and L. Pereira, *Electrical Imaging Map on Polycrystalline Diamond Films and Diodes and Structural Relationship Obtained by Micro-Raman.* Materials Science Forum, 2006. **514-516**: p. 48-52.
465. Cleri, F., et al., *On the electrical activity ofsp2-bonded grain boundaries in nanocrystalline diamond.* Europhysics Letters (EPL), 1999. **46**(5): p. 671-677.
466. Liu, W.L., et al., *Thermal conduction in nanocrystalline diamond films: Effects of the grain boundary scattering and nitrogen doping.* Applied Physics Letters, 2006. **89**(17): p. 171915.
467. Waite, M.M. and S.I. Shah, *X-ray photoelectron spectroscopy of initial stages of nucleation and growth of diamond thin films during plasma assisted chemical vapor deposition.* Applied Physics Letters, 1992. **60**(19): p. 2344-2346.

468. Ohmagari, S., et al., *Low resistivity p+ diamond (100) films fabricated by hot-filament chemical vapor deposition.* Diamond and Related Materials, 2015. **58**: p. 110-114.
469. Deneuville, A., *Chapter 4 Boron doping of diamond films from the gas phase*, in *Semiconductors and Semimetals*, C.E. Nebel and J. Ristein, Editors. 2003, Elsevier. p. 183-238.
470. Ekimov, E., et al., *High-pressure synthesis and characterization of superconducting boron-doped diamond.* Science and Technology of Advanced Materials, 2006. **7**(sup1): p. S2-S6.
471. Kudryavtsev, O., et al., *Fluorescence and Raman Spectroscopy of Doped Nanodiamonds.* Journal of Applied Spectroscopy, 2018. **85**(2): p. 295-299.
472. Yamada, H., *10 - Diamond*, in *Single Crystals of Electronic Materials*, R. Fornari, Editor. 2019, Woodhead Publishing. p. 331-350.
473. Johan, F.P., *Ion implantation of diamond for electronic applications.* Semiconductor Science and Technology, 2003. **18**(3): p. S27.
474. Fontaine, F., et al., *Boron implantation/in situ annealing procedure for optimal p -type properties of diamond.* Applied Physics Letters, 1996. **68**(16): p. 2264-2266.
475. Kalish, R., et al., *Doping of polycrystalline diamond by boron ion implantation.* Applied Physics Letters, 1994. **64**(19): p. 2532-2534.
476. Srimongkon, K., et al., *Boron inhomogeneity of HPHT-grown single-crystal diamond substrates: Confocal micro-Raman mapping investigations.* Diamond and Related Materials, 2016. **63**: p. 21-25.
477. Sun, F.-H., et al., *Improvement of adhesive strength and surface roughness of diamond films on Co-cemented tungsten carbide tools.* Diamond and Related Materials, 2003. **12**(3-7): p. 711-718.
478. Issaoui, R., et al., *Growth of thick heavily boron-doped diamond single crystals: Effect of microwave power density.* Applied Physics Letters, 2010. **97**(18): p. 182101.
479. Fischer, A.E., Y. Show, and G.M. Swain, *Electrochemical Performance of Diamond Thin-Film Electrodes from Different Commercial Sources.* Analytical Chemistry, 2004. **76**(9): p. 2553-2560.
480. Xu, J., et al., *Peer Reviewed: Boron-Doped Diamond Thin-Film Electrodes.* Analytical Chemistry, 1997. **69**(19): p. 591A-597A.
481. Goeting, C., et al., *Boron-doped diamond electrodes: Growth, surface characterisation and sono-electrochemical applications.* NEW DIAMOND AND FRONTIER CARBON TECHNOLOGY, 1999. **9**(3): p. 207-228.
482. Fhaner, M., et al., *Improvements in the formation of boron-doped diamond coatings on platinum wires using the novel nucleation process (NNP).* Diamond and Related Materials, 2011. **20**(2): p. 75-83.
483. Srikanth, V.V.S.S., P. Sampath Kumar, and V.B. Kumar, *A Brief Review on the In Situ Synthesis of Boron-Doped Diamond Thin Films.* International Journal of Electrochemistry, 2012. **2012**: p. 7.
484. Haubner, R., S. Bohr, and B. Lux, *Comparison of P, N and B additions during CVD diamond deposition.* Diamond and Related Materials, 1999. **8**(2): p. 171-178.
485. Gonon, P., et al., *Raman study of diamond films deposited by MPCVD: effect of the substrate position.* Thin Solid Films, 1995. **256**(1): p. 13-22.
486. Gonon, P., et al., *Chemical vapor deposition of B-doped polycrystalline diamond films: Growth rate and incorporation efficiency of dopants.* Journal of Applied Physics, 1995. **78**(12): p. 7404-7406.
487. Neto, M., et al., *Surface modifications on as-grown boron doped CVD diamond films induced by the B2O3–ethanol–Ar system.* Diamond and Related Materials, 2016. **64**: p. 89-96.
488. Hartmann, P., et al., *Diamond growth with boron addition.* International Journal of Refractory Metals and Hard Materials, 1998. **16**(3): p. 223-232.
489. Spicka, H., et al., *Investigations of the incorporation of B, P and N into CVD-diamond films by secondary ion mass spectrometry.* Diamond and Related Materials, 1996. **5**(3): p. 383-387.
490. Gheeraert, E., A. Deneuville, and J. Mambou, *Influence of diborane on the growth rate and phase stability of diamond films1This paper was presented at the European Materials Research Society 1997 Meeting, Symposium A: Fullerenes and Carbon based Materials, Strasbourg, France, June 1997.1.* Carbon, 1999. **37**(1): p. 107-111.
491. Wurzinger, P., et al., *Investigation of the boron incorporation in polycrystalline CVD diamond films by TEM, EELS and Raman spectroscopy.* Diamond and Related Materials, 1997. **6**(5-7): p. 763-768.
492. Kavan, L., et al., *Boron-doped Diamond Electrodes: Electrochemical, Atomic Force Microscopy and Raman Study towards Corrosion-modifications at Nanoscale.* Electrochimica Acta, 2015. **179**: p. 626-636.
493. Samlenski, R., et al., *Characterisation and lattice location of nitrogen and boron in homoepitaxial CVD diamond.* Diamond and Related Materials, 1996. **5**(9): p. 947-951.
494. Kaboli, S. and P.C. Burnley, *Direct observations of crystal defects in polycrystalline diamond.* Materials Characterization, 2018. **142**: p. 154-161.
495. Nazari, M., et al., *Optical characterization and thermal properties of CVD diamond films for integration with power electronics.* Solid-State Electronics, 2017. **136**: p. 12-17.

496. Fabisiak, K., et al., *The influence of working gas on CVD diamond quality.* Materials Science and Engineering: B, 2012. **177**(15): p. 1352-1357.
497. Heiderhoff, R., et al., *Correlation of the electrical, thermal, and optical properties of CVD diamond films by scanning microscopy techniques.* Diamond and Related Materials, 1995. **4**(5): p. 645-651.
498. Sodngam, P., et al. *The study of P-type and N-type diamond crystals synthesis by hot filament chemical vapor deposition*. in *2017 14th International Conference on Electrical Engineering/Electronics, Computer, Telecommunications and Information Technology (ECTI-CON)*. 2017.
499. Faili, F., et al. *Physical and Thermal Characterization of CVD Diamond: A Bottoms-up Review*. in *2017 16th IEEE Intersociety Conference on Thermal and Thermomechanical Phenomena in Electronic Systems (ITherm)*. 2017.
500. Saparin, G.V., *Microcharacterization of CVD diamond films by scanning electron microscopy: morphology, structure and microdefects.* Diamond and Related Materials, 1994. **3**(11): p. 1337-1351.
501. P.W. May, J.A.S., K. N. Rosser, *785nm Raman spectroscopy of CVD diamond films* Diamond and Related Materials, 2008. **17**: p. 199-203.
502. May, P.W., et al., *Simulations of polycrystalline CVD diamond film growth using a simplified Monte Carlo model.* Diamond and Related Materials, 2010. **19**(5): p. 389-396.
503. *Raman spectroscopy in carbons: from nanotubes to diamond.* *special issue* Phil. Trans. R. Soc. London A 2004.
504. M. A. Tamor and W.C.V. Raman, *"Fingerprinting" of amorphous carbon films.* Journal of Applied Physics, 1994. **76**: p. 3823-3830.
505. Ferrari, A.C. and D.M. Basko, *Raman spectroscopy as a versatile tool for studying the properties of graphene.* Nature nanotechnology, 2013. **8**(4): p. 235.
506. Ramaswamy, C., *Raman Effect in Diamond.* Nature, 1930. **125**: p. 704.
507. Steven Prawer, R.J.N., *Raman spectroscopy of diamond and doped diamond.* Phil. Trans. R. Soc. London A, 2004. **362**: p. 2537-2565.
508. Robertson, Fox, and Martin, *Two types of diamond.* Philosophical Transactions of the Royal Society of London. Series A, Containing Papers of a Mathematical or Physical Character, 1933. **232**(707-720): p. 463-535.
509. Nayar, P.G.N., *The lattice and electronic spectrum of diamond.* Proceedings of the Indian Academy of Sciences - Section A, 1942. **15**(5): p. 293-309.
510. Chen, K.H., et al., *Micro-Raman for diamond film stress analysis.* Diamond and Related Materials, 1995. **4**(4): p. 460-463.
511. Windischmann, H. and K.J. Gray, *Stress measurement of CVD diamond films.* Diamond and Related Materials, 1995. **4**(5): p. 837-842.
512. Ascarelli, P., et al., *Relation between the HFCVD diamond growth rate, the line-width of Raman spectrum and the particle size.* Diamond and Related Materials, 1995. **4**(4): p. 464-468.
513. Mermoux, M., et al., *In situ Raman monitoring of the growth of diamond films in plasma-assisted CVD reactors.* Diamond and Related Materials, 1995. **4**(5): p. 745-749.
514. von Kaenel, Y., J. Stiegler, and E. Blank, *Evolution of the density of graphite-like defects during CVD diamond growth.* Diamond and Related Materials, 1995. **4**(7): p. 972-976.
515. Fayette, L., et al., *Analysis of the fine structure of the Raman line and of X-ray reflection profiles for textured CVD diamond films.* Diamond and Related Materials, 1995. **4**(11): p. 1243-1250.
516. Mossbrucker, J. and T.A. Grotjohn, *Determination of local crystal orientation of diamond using polarized Raman spectra.* Diamond and Related Materials, 1996. **5**(11): p. 1333-1343.
517. Alers, P., H.E. Hintermann, and I. Hayward, *Correlations between Raman scattering and thermal expansion behavior for CVD and natural diamond.* Thin Solid Films, 1995. **259**(1): p. 14-17.
518. Mortet, V., et al., *Analysis of heavily boron-doped diamond Raman spectrum.* Diamond and Related Materials, 2018. **88**: p. 163-166.
519. Mortet, V., et al., *Insight into boron-doped diamond Raman spectra characteristic features.* Carbon, 2017. **115**: p. 279-284.
520. Volodin, V.A., et al., *Raman scattering in boron doped nanocrystalline diamond films: Manifestation of Fano interference and phonon confinement effect.* Solid State Communications, 2018. **276**: p. 33-36.
521. Kuntumalla, M.K., et al., *Raman scattering of nitrogen incorporated diamond thin films grown by hot filament chemical vapor deposition.* Thin Solid Films, 2018. **653**: p. 284-292.
522. Zolkin, A., et al., *Characteristics of the Raman spectra of diamond-like carbon films. Influence of methods of synthesis.* Materials Today: Proceedings, 2017. **4**(11, Part 1): p. 11480-11485.
523. Bachmann, P.K., et al., *Raman and X-ray studies of polycrystalline CVD diamond films.* Diamond and Related Materials, 1994. **3**(11): p. 1308-1314.
524. Kunishige, E., et al., *Local Structures of Carbon Thin Films Synthesized by the Hot Filament Chemical Vapor Deposition Method X-Ray-Absorption Near-Edge Structure and Raman Spectroscopic Studies.* Japanese Journal of Applied Physics, 1991. **30**(5R): p. 1073.

525. Rudigier, M. and R. Haubner, *Characterisation of diamond coatings with different morphologies by Raman spectroscopy using various laser wavelengths.* Analytical and Bioanalytical Chemistry, 2012. **403**(3): p. 675-681.
526. Sails, S.R., et al., *Monitoring the quality of diamond films using Raman spectra excited at 514.5 nm and 633 nm.* Diamond and Related Materials, 1996. **5**(6): p. 589-591.
527. Leeds, S.M., et al., *Use of different excitation wavelengths for the analysis of CVD diamond by laser Raman spectroscopy.* Diamond and Related Materials, 1998. **7**(2): p. 233-237.
528. Jackman, R.B., J. Beckman, and J.S. Foord, *The growth of nucleation layers for high-quality diamond CVD from an r.f. plasma.* Diamond and Related Materials, 1995. **4**(5): p. 735-739.
529. Hiramatsu, M., et al., *Formation of diamond and nanocrystalline diamond films by microwave plasma CVD.* Thin Solid Films, 2002. **407**(1): p. 18-25.
530. A.C. Ferrari, J.R., *Interpretation of Raman spectra of disordered and amorphous carbon.* Phys. Rev. B, 2000. **61**: p. 14095-14107.
531. Birrell, J., et al., *Interpretation of the Raman spectra of ultrananocrystalline diamond.* Diamond and Related Materials, 2005. **14**(1): p. 86-92.
532. Ferrari, A.C. and J. Robertson, *Origin of the 1150 cm-1 Raman mode in nanocrystalline diamond.* Physical Review B, 2001. **63**(12): p. 121405.
533. R.E. Shroder, R.J.N., J.T. Glass, *Analysis of the composite structures in diamond thin films by Raman spectroscopy.* Phys. Rev. B, 1990. **41**: p. 3738-3745.
534. Adamopoulos, G., et al., *Hydrogen content estimation of hydrogenated amorphous carbon by visible Raman spectroscopy.* Journal of applied physics, 2004. **96**(11): p. 6348-6352.
535. Nishimura, K., K. Das, and J. Glass, *Material and electrical characterization of polycrystalline boron-doped diamond films grown by microwave plasma chemical vapor deposition.* Journal of applied physics, 1991. **69**(5): p. 3142-3148.
536. Ushizawa, K., et al., *Boron concentration dependence of Raman spectra on {100} and {111} facets of B-doped CVD diamond.* Diamond and Related Materials, 1998. **7**(11): p. 1719-1722.
537. Haubner, R. and M. Rudigier, *Raman Characterisation of Diamond Coatings Using Different Laser Wavelengths.* Physics Procedia, 2013. **46**: p. 71-78.
538. Gheeraert, E., et al., *Effect of boron incorporation on the “quality” of MPCVD diamond films.* Diamond and Related Materials, 1993. **2**(5-7): p. 742-745.
539. Pruvost, F., E. Bustarret, and A. Deneuville, *Characteristics of homoepitaxial heavily boron-doped diamond films from their Raman spectra.* Diamond and Related Materials, 2000. **9**(3): p. 295-299.
540. Okoli, S., R. Haubner, and B. Lux, *Carburization of tungsten and tantalum filaments during low-pressure diamond deposition.* Surface and Coatings Technology, 1991. **47**(1): p. 585-599.
541. Touloukian, Y.S. and D.P. DeWitt, *Thermal radiative properties: Nonmetallic solids.* 1972.
542. Shenderova, O., S. Hens, and G. McGuire, *Seeding slurries based on detonation nanodiamond in DMSO.* Diamond and Related Materials, 2010. **19**(2-3): p. 260-267.
543. Schwan, J., et al., *Raman spectroscopy on amorphous carbon films.* Journal of Applied Physics, 1996. **80**(1): p. 440-447.
544. Nemanich, R.J. and S.A. Solin, *First- and second-order Raman scattering from finite-size crystals of graphite.* Physical Review B, 1979. **20**(2): p. 392-401.
545. Robertson, J. and E.P. O’Reilly, *Electronic and atomic structure of amorphous carbon.* Physical Review B, 1987. **35**(6): p. 2946-2957.
546. Ferrari, A.C., S.E. Rodil, and J. Robertson, *Interpretation of infrared and Raman spectra of amorphous carbon nitrides.* Physical Review B, 2003. **67**(15): p. 155306.
547. Menon, P.M., et al., *Filament metal contamination and Raman spectra of hot filament chemical vapor deposited diamond films.* Diamond and related materials, 1999. **8**(1): p. 101-109.
548. Almeida, F.A., et al., *Interfaces in Nano-/Microcrystalline Multigrade CVD Diamond Coatings.* ACS Applied Materials & Interfaces, 2013. **5**(22): p. 11725-11729.
549. Haynes, W.M., *CRC handbook of chemistry and physics*. 2014: CRC press.
550. Ōsawa, E., *Monodisperse single nanodiamond particulates.* Pure and Applied Chemistry, 2008. **80**(7): p. 1365-1379.
551. Turner, S., et al., *Determination of size, morphology, and nitrogen impurity location in treated detonation nanodiamond by transmission electron microscopy.* Advanced functional materials, 2009. **19**(13): p. 2116-2124.
552. Bogdanowicz, R., et al., *Improved surface coverage of an optical fibre with nanocrystalline diamond by the application of dip-coating seeding.* Diamond and Related Materials, 2015. **55**: p. 52-63.
553. Nakahata, H., et al., *Theoretical study on SAW characteristics of layered structures including a diamond layer.* IEEE Transactions on Ultrasonics, Ferroelectrics, and Frequency Control, 1995. **42**(3): p. 362-375.
554. Ishihara, M., et al., *Preparation of AlN and LiNbO3 thin films on diamond substrates by sputtering method.* Diamond and related materials, 2002. **11**(3-6): p. 408-412.
555. Lee, T.-C., et al., *Surface acoustic wave applications of lithium niobate thin films.* Applied physics letters, 2003. **82**(2): p. 191-193.

556. Hickernell, F.S., *High-reliability SAW bandpass filters for space applications.* IEEE transactions on ultrasonics, ferroelectrics, and frequency control, 1988. **35**(6): p. 652-656.
557. Meier, H., T. Baier, and G. Riha. *Miniaturization and advanced functionalities of SAW devices*. in *Ultrasonics Symposium, 2000 IEEE*. 2000. IEEE.
558. Ruppel, C.C., L. Reindl, and R. Weigel, *SAW devices and their wireless communications applications.* IEEE microwave magazine, 2002. **3**(2): p. 65-71.
559. Al-Sarawi, S.F., D. Abbott, and P.D. Franzon, *A review of 3-D packaging technology.* IEEE Transactions on Components, Packaging, and Manufacturing Technology: Part B, 1998. **21**(1): p. 2-14.
560. Semenov, O., A. Vassighi, and M. Sachdev, *Impact of self-heating effect on long-term reliability and performance degradation in CMOS circuits.* IEEE transactions on device and materials reliability, 2006. **6**(1): p. 17-27.
561. Chung, D.D., *Materials for electronic packaging*. 1995: Elsevier.
562. Eden, R.C., *Application of diamond substrates for advanced high density packaging.* Diamond and Related Materials, 1993. **2**(5): p. 1051-1058.
563. Pickrell, D. and D. Hoover, *Chemical Vapor Deposition of Diamond for Electronic Packaging Applications.* Inside ISHM, 1991: p. 11-15.
564. Su, Q., et al., *Efficient CVD diamond film/alumina composite substrate for high density electronic packaging application.* Diamond and Related Materials, 2006. **15**(10): p. 1550-1554.
565. Xiangwei, Z., et al., *The fabrication of all-diamond packaging panels with built-in interconnects for wireless integrated microsystems.* Journal of Microelectromechanical Systems, 2004. **13**(3): p. 396-405.
566. Mallik, A.K., et al., *Property mapping of polycrystalline diamond coatings over large area.* Journal of Advanced Ceramics, 2014. **3**(1): p. 56-70.
567. Sumant, A.V., et al., *Surface composition, bonding, and morphology in the nucleation and growth of ultra-thin, high quality nanocrystalline diamond films.* Diamond and Related Materials, 2007. **16**(4-7): p. 718-724.
568. Rahman, A. and R. Reif. *Thermal analysis of three-dimensional (3-D) integrated circuits (ICs)*. in *Proceedings of the IEEE 2001 International Interconnect Technology Conference (Cat. No.01EX461)*. 2001.
569. Heinrich, W., *The flip-chip approach for millimeter wave packaging.* IEEE Microwave Magazine, 2005. **6**(3): p. 36-45.
570. Jin, Y., et al. *Next generation eWLB (embedded wafer level BGA) packaging*. in *2010 12th Electronics Packaging Technology Conference*. 2010. IEEE.
571. Kweon, D.W., J.Y. Lee, and D. Kim, *The growth kinetics of diamond films deposited by hot-filament chemical vapor deposition.* Journal of Applied Physics, 1991. **69**(12): p. 8329-8335.
572. Storms, E., *The Refractory Carbides, Acad.* Press, NY, 1967.
573. Windischmann, H. and G.F. Epps, *Free-standing diamond membranes: optical, morphological and mechanical properties.* Diamond and Related Materials, 1992. **1**(5): p. 656-664.
574. Huang, A.Q. *Wide bandgap (WBG) power devices and their impacts on power delivery systems*. in *2016 IEEE International Electron Devices Meeting (IEDM)*. 2016. IEEE.
575. Lin, H., *Market and Technology Trends in WBG Materials for Power Electronics Applications.* CS MANTECH Conference, Scottsdale, Arizona, USA, May 18th - 21st, 2015.
576. Fraga, M.A., M. Bosi, and M. Negri, *Silicon carbide in microsystem technology—thin film versus bulk material*, in *Advanced Silicon Carbide Devices and Processing*. 2015, IntechOpen.
577. Silva, A.G., et al., *Growth of aluminum oxide on silicon carbide with an atomically sharp interface.* Journal of Vacuum Science & Technology A: Vacuum, Surfaces, and Films, 2017. **35**(1): p. 01B142.
578. Usman, M., et al., *Improving the quality of Al2O3/4H-SiC interface for device applications.* Materials Science in Semiconductor Processing, 2018. **81**: p. 118-121.
579. Roccaforte, F., et al., *Challenges for energy efficient wide band gap semiconductor power devices.* physica status solidi (a), 2014. **211**(9): p. 2063-2071.
580. Ozpineci, B. and L.M. Tolbert, *Comparison of wide-bandgap semiconductors for power electronics applications*. 2004: United States. Department of Energy.
581. Pearton, S.J., et al., *Fabrication and performance of GaN electronic devices.* Materials Science and Engineering: R: Reports, 2000. **30**(3–6): p. 55-212.
582. Dow, H.S., W.S. Kim, and J.W. Lee, *Thermal and electrical properties of silicon nitride substrates.* AIP Advances, 2017. **7**(9): p. 095022.
583. Hallén, A., et al., *Passivation of SiC device surfaces by aluminum oxide.* IOP Conference Series: Materials Science and Engineering, 2014. **56**: p. 012007.
584. Salgueiredo, E., et al., *HFCVD diamond deposition parameters optimized by a Taguchi Matrix.* Vacuum, 2011. **85**(6): p. 701-704.
585. Mallik, A.K., et al., *Detonation nanodiamond seeding technique for nucleation enhancement of CVD diamond–some experimental insights.* Advances In Ceramic Science And Engineering, 2014. **3**: p. 36-45.
586. Mochalin, V.N., et al., *The properties and applications of nanodiamonds.* Nature nanotechnology, 2012. **7**(1): p. 11.

587. Williams, O.A., et al., *Enhanced diamond nucleation on monodispersed nanocrystalline diamond.* Chemical Physics Letters, 2007. **445**(4-6): p. 255-258.
588. Sugino, T., et al., *Field emission from GaN surfaces roughened by hydrogen plasma treatment.* Applied Physics Letters, 2001. **78**(21): p. 3229-3231.
589. al., P.W.M.e., *Deposition of CVD diamond onto GaN.* Diamond & Related Materials, 2006. **15**: p. 526-530.
590. Jungwan Cho, Z.L., Elah Bozorg-Grayeli, Takashi Kodama, Daniel Francis, Felix Ejeckam, Firooz Faili, Mehdi Asheghi, and Kenneth E. Goodson, *Improved Thermal Interfaces of GaN–Diamond Composite Substrates for HEMT Applications.* IEEE TRANSACTIONS ON COMPONENTS, PACKAGING AND MANUFACTURING TECHNOLOGY, 2013. **3**(1): p. 79-85.
591. Tadjer, M.J., et al., *Reduced Self-Heating in AlGaN/GaN HEMTs Using Nanocrystalline Diamond Heat-Spreading Films.* IEEE Electron Device Letters, 2012. **33**(1): p. 23-25.
592. Meyer, D.J., et al., *Large-signal RF performance of nanocrystalline diamond coated AlGaN/GaN high electron mobility transistors.* IEEE Electron Device Letters, 2014. **35**(10): p. 1013-1015.
593. May, P., et al., *Deposition of CVD diamond onto GaN.* Diamond and Related materials, 2006. **15**(4-8): p. 526-530.
594. Porowski, S., *Growth and properties of single crystalline GaN substrates and homoepitaxial layers.* Materials Science and Engineering: B, 1997. **44**(1-3): p. 407-413.
595. Kako, T., et al., *Elevated-temperature etching of gallium nitride (GaN) in dual-frequency capacitively coupled plasma of CH4/H2 at 300–500 °C.* Vacuum, 2018. **156**: p. 219-223.
596. Klauser, F., et al., *Raman studies of nano-and ultra-nanocrystalline diamond films grown by hot-filament CVD.* Chemical Vapor Deposition, 2010. **16**(4-6): p. 127-135.
597. Micovic, M., et al. *High frequency GaN HEMTs for RF MMIC applications*. in *2016 IEEE International Electron Devices Meeting (IEDM)*. 2016.
598. Won, Y., et al., *Fundamental cooling limits for high power density gallium nitride electronics.* IEEE Transactions on Components, Packaging and Manufacturing Technology, 2015. **5**(6): p. 737-744.
599. Guggenheim, R. and L. Rodes. *Roadmap review for cooling high-power GaN HEMT devices*. in *2017 IEEE International Conference on Microwaves, Antennas, Communications and Electronic Systems (COMCAS)*. 2017. IEEE.
600. Anderson, T.J., et al. *Nanocrystalline Diamond for near Junction Heat Spreading in GaN Power HEMTs*. in *2013 IEEE Compound Semiconductor Integrated Circuit Symposium (CSICS)*. 2013.
601. Sandhu, R., et al. *Diamond Materials for GaN HEMT near Junction Heat Removal*. in *2012 IEEE Compound Semiconductor Integrated Circuit Symposium (CSICS)*. 2012.
602. Neudeck, P.G., R.S. Okojie, and L.-Y. Chen, *High-temperature electronics-a role for wide bandgap semiconductors?* Proceedings of the IEEE, 2002. **90**(6): p. 1065-1076.
603. Berzelius, J.J., *Untersuchungen über die Flussspathsäure und deren merkwürdigsten Verbindungen.* Annalen der Physik, 1824. **77**(6): p. 169-230.
604. Weishart, H., V. Heera, and W. Skorupa, *n-type conductivity in high-fluence Si-implanted diamond.* Journal of applied physics, 2005. **97**(10): p. 103514.
605. Park, Y.-S., *SiC materials and devices*. Vol. 52. 1998: Academic Pr.
606. Persson, C. and U. Lindefelt, *Relativistic band structure calculation of cubic and hexagonal SiC polytypes.* Journal of Applied Physics, 1997. **82**(11): p. 5496-5508.
607. W. Paszkowicz, P.P., W. Łasochac, I. Margiolaki, M. Brunelli, A. Fitch, *Lattice Parameter of Polycrystalline Diamond in the Low-Temperature Range.* ACTA PHYSICA POLONICA A 2010. **117**(2): p. 323-327.
608. Verona, C., et al., *Gate-Source Distance Scaling Effects in H-Terminated Diamond MESFETs.* Electron Devices, IEEE Transactions on, 2015. **62**(4): p. 1150-1156.
609. Macpherson, J.V., *A practical guide to using boron doped diamond in electrochemical research.* Physical Chemistry Chemical Physics, 2015. **17**(5): p. 2935-2949.
610. Zhang, T., et al., *The deposition parameters in the synthesis of CVD microcrystalline diamond powders optimized by the orthogonal experiment.* Journal of Crystal Growth, 2015. **426**: p. 15-24.
611. Wasyluk, J., et al., *Raman Investigation of Different Polytypes in SiC Thin Films Grown by Solid-Gas Phase Epitaxy on Si (111) and 6H-SiC Substrates.* Materials Science Forum, 2010. **645-648**: p. 359-362.
612. Nakashima, S.-i., et al., *Raman characterization of damaged layers of 4H-SiC induced by scratching.* AIP Advances, 2016. **6**(1): p. 015207.
613. Tallant, D.R., et al., *Boron carbide structure by Raman spectroscopy.* Physical Review B, 1989. **40**(8): p. 5649-5656.
614. Tokuda, N., et al., *The role of boron atoms in heavily boron-doped semiconducting homoepitaxial diamond growth — Study of surface morphology.* Diamond and Related Materials, 2007. **16**(2): p. 409-411.
615. Wang, Z.L., et al., *Influence of growth pressure on the electrical properties of boron-doped polycrystalline diamond films.* Applied Surface Science, 2009. **255**(23): p. 9522-9525.
616. Ferreira, N., et al., *Residual stresses and crystalline quality of heavily boron-doped diamond films analysed by micro-Raman spectroscopy and X-ray diffraction.* Carbon, 2003. **41**(6): p. 1301-1308.

617. Tachibana, T. and J.T. Glass, *Electrical Contacts to Diamond*, in *Diamond: Electronic Properties and Applications*. 1995, Springer. p. 319-348.
618. Bell, M.D. and W.J. Leivo, *Rectification, photoconductivity, and photovoltaic effect in semiconducting diamond.* Physical Review, 1958. **111**(5): p. 1227.
619. Glover, G., *The CV characteristics of Schottky barriers on laboratory grown semiconducting diamonds.* Solid-State Electronics, 1973. **16**(9): p. 973-978.
620. Mead, C. and T. McGill, *Schottky barrier heights on p-type diamond and silicon carbide (6H).* Physics Letters A, 1976. **58**(4): p. 249-251.
621. Himpsel, F., P. Heimann, and D. Eastman, *Schottky barriers on diamond (1 1 1).* Solid State Communications, 1980. **36**(7): p. 631-633.
622. Das, K., et al., *A review of the electrical characteristics of metal contacts on diamond.* Thin Solid Films, 1992. **212**(1): p. 19-24.
623. Moazed, K., J. Zeidler, and M. Taylor, *A thermally activated solid state reaction process for fabricating ohmic contacts to semiconducting diamond.* Journal of Applied Physics, 1990. **68**(5): p. 2246-2254.
624. Venkatesan, V. and K. Das, *Ohmic contacts on diamond by B ion implantation and Ti-Au metallization.* IEEE electron device letters, 1992. **13**(2): p. 126-128.
625. Porter, L.M., et al., *4.03 - Contacts to Wide-Band-Gap Semiconductors*, in *Comprehensive Semiconductor Science and Technology*, P. Bhattacharya, R. Fornari, and H. Kamimura, Editors. 2011, Elsevier: Amsterdam. p. 44-85.
626. Tachibana, T., B.E. Williams, and J.T. Glass, *Correlation of the electrical properties of metal contacts on diamond films with the chemical nature of the metal-diamond interface. II. Titanium contacts: A carbide-forming metal.* Physical Review B, 1992. **45**(20): p. 11975-11981.
627. Gildenblat, G.S., et al., *High-temperature Schottky diodes with thin-film diamond base.* IEEE Electron Device Letters, 1990. **11**(9): p. 371-372.
628. Collins, A., E. Lightowlers, and A. Williams, *Formation of electrical contacts on insulating and semiconducting diamonds.* Diamond Res., 1970: p. 19-22.
629. Moazed, K., R. Nguyen, and J.R. Zeidler, *Ohmic contacts to semiconducting diamond.* IEEE electron device letters, 1988. **9**(7): p. 350-351.
630. Werner, M., et al., *The effect of metallization on the ohmic contact resistivity to heavily B-doped polycrystalline diamond films.* IEEE Transactions on Electron Devices, 1995. **42**(7): p. 1344-1351.
631. Evans, D.A., et al., *Diamond-metal contacts: interface barriers and real-time characterization.* J Phys Condens Matter, 2009. **21**(36): p. 364223.
632. Kawaguchi, G., et al., *Dependence of contact resistance on metal electronegativity for B-doped diamond films.* Journal of applied physics, 1994. **75**(10): p. 5165-5170.
633. Tachibana, T., B.E. Williams, and J.T. Glass, *Correlation of the electrical properties of metal contacts on diamond films with the chemical nature of the metal-diamond interface. I. Gold contacts: A non-carbide-forming metal.* Physical Review B, 1992. **45**(20): p. 11968-11974.
634. Collins, A., E. Lightowlers, and P. Dean, *Role of phonons in the oscillatory photoconductivity spectrum of semiconducting diamond.* Physical Review, 1969. **183**(3): p. 725.
635. Collins, A. and E. Lightowlers, *Photothermal ionization and photon-induced tunneling in the acceptor photoconductivity spectrum of semiconducting diamond.* Physical Review, 1968. **171**(3): p. 843.
636. Werner, M., et al., *Electrical characterization of Al/Si ohmic contacts to heavily boron doped polycrystalline diamond films.* Journal of Applied Physics, 1996. **79**(5): p. 2535-2541.
637. Nishimura, K., et al., *Electrical contacts to polycrystalline B doped diamond films.* MRS Online Proceedings Library Archive, 1989. **162**.
638. Prins, J.F., *Preparation of ohmic contacts to semiconducting diamond.* Journal of Physics D: Applied Physics, 1989. **22**(10): p. 1562.
639. Tsai, W., et al. *Boron doping of diamond via solid state diffusion*. in *New Diamond Science and Technology*. 1991.
640. Davydova, M., et al., *Characteristics of zirconium and niobium contacts on boron-doped diamond.* Diamond and Related Materials, 2018. **83**: p. 184-189.
641. Wang, W., et al., *Palladium Ohmic contact on hydrogen-terminated single crystal diamond film.* Diamond and Related Materials, 2015. **59**: p. 90-94.
642. Miccoli, I., et al., *The 100th anniversary of the four-point probe technique: the role of probe geometries in isotropic and anisotropic systems.* Journal of Physics: Condensed Matter, 2015. **27**(22): p. 223201.
643. Cheng, J. and B. Tsui, *Effects of Rapid Thermal Annealing on Ar Inductively Coupled Plasma-Treated n-Type 4H-SiC Schottky and Ohmic Contacts.* IEEE Transactions on Electron Devices, 2018. **65**(9): p. 3739-3745.
644. Zhang, X., et al. *Study on simultaneous formation of ohmic contacts on p- and n- type 4H-SiC using Ni/Ti/Al ternary system*. in *2014 12th IEEE International Conference on Solid-State and Integrated Circuit Technology (ICSICT)*. 2014.

645. Pham, H.V., et al. *Impact of temperature on electrical performance of Ni film on n-type 4H-SÌC contacts in terms of micropipes density*. in *2018 2nd International Conference on Recent Advances in Signal Processing, Telecommunications & Computing (SigTelCom)*. 2018.
646. Jiang, S., X. Li, and Z. Chen, *Role of W in W/Ni Bilayer Ohmic Contact to n-Type 4H-SiC From the Perspective of Device Applications.* IEEE Transactions on Electron Devices, 2018. **65**(2): p. 641-647.
647. Lions, M., et al., *Ultra-thin nanocrystalline diamond films (< 100 nm) with high electrical resistivity.* physica status solidi (RRL)–Rapid Research Letters, 2009. **3**(6): p. 205-207.
648. Chandler, G. and J. Zimmer. *Enhancing SOI with thin film diamond*. in *SOI Conference, 2008. SOI. IEEE International*. 2008. IEEE.
649. Sillero, E., et al., *Static and dynamic determination of the mechanical properties of nanocrystalline diamond micromachined structures.* Journal of Micromechanics and Microengineering, 2009. **19**(11): p. 115016.
650. Gaidarzhy, A., et al., *High quality factor gigahertz frequencies in nanomechanical diamond resonators.* Applied Physics Letters, 2007. **91**(20): p. 203503.
651. Krauss, A., et al., *Ultrananocrystalline diamond thin films for MEMS and moving mechanical assembly devices.* Diamond and Related Materials, 2001. **10**(11): p. 1952-1961.
652. Huff, M.A., D.A. Aidala, and J.E. Butler, *MEMS applications using diamond thin films.* Solid State Technology, 2006. **49**(4): p. 45-48.
653. Martin, H.B., et al., *Hydrogen and oxygen evolution on boron-doped diamond electrodes.* Journal of the Electrochemical Society, 1996. **143**(6): p. L133-L136.
654. Stotter, J., et al., *Comparison of the electrical, optical, and electrochemical properties of diamond and indium tin oxide thin-film electrodes.* Chemistry of materials, 2005. **17**(19): p. 4880-4888.
655. Stotter, J., et al., *Optical and electrochemical properties of optically transparent, boron-doped diamond thin films deposited on quartz.* Analytical Chemistry, 2002. **74**(23): p. 5924-5930.
656. Gajewski, W., et al., *Electronic and optical properties of boron-doped nanocrystalline diamond films.* Physical Review B, 2009. **79**(4): p. 045206.
657. Williams, O.A., et al., *n-Type conductivity in ultrananocrystalline diamond films.* Applied Physics Letters, 2004. **85**(10): p. 1680-1682.
658. Philip, J., et al., *Elastic, mechanical, and thermal properties of nanocrystalline diamond films.* Journal of Applied Physics, 2003. **93**(4): p. 2164-2171.
659. Lu, W., et al., *Ohmic contact properties of Ni/C film on 4H-SiC.* Solid-State Electronics, 2003. **47**(11): p. 2001-2010.
660. Tadjer, M.J., et al., *On the high curvature coefficient rectifying behavior of nanocrystalline diamond heterojunctions to 4H-SiC.* Applied Physics Letters, 2010. **97**(19): p. 193510.
661. Tadjer, M.J., et al., *Nanocrystalline diamond films as UV-semitransparent Schottky contacts to 4H-SiC.* Applied Physics Letters, 2007. **91**(16): p. 163508.

7. Appendix

Throughout the study, various characterization instruments were employed for analysing the morphology and quality of the films. Instruments were also used for the control and measure of process parameters during the HFCVD. The following table gathers the details about the instruments for the ease of reference for the reader.

Instrument	Purpose	Resolution /limits of accuracy	Type/Brand	Additional information
HFCVD				
Mass flow controllers	Determine flow rates of pre-cursor			
B-evaporation		1%	Brooks 9861	
Gases		1%	Brooks 5850 EM	
Thermocouple	Measure substrate temperature		standard type K (chromel-alumel)	
Pyrometer	Measure filament temperature		Impac Infrared 140	
Seeding				
Ultrasound bath	Ultrasonic agitation for seeding	N/A	TekMotion (15l)	Operates at 40 kHz, power 760 W
Morphological characterization				
Optical microscope	Preliminary observation		Eclipse E200 upright	Observation under brightfield, epi-fluorescence, darkfield, phase contrast, simple polarizing
Optical profilometer	Measure features, roughness		Sensofar S Neox	5 measurements per spot
SEM	High-magnification imaging		Hitachi SU70 instrument or Leo Supra 35	
Ellipsometry			AutoSE (HORIBA Scientific)	Total of 218 points in wavelength interval 450-850 nm, an incidence angle of 70°, a signal quality of 50, a measurement spot area of 250×250 m^2
Quality				
Raman spectroscope	Spectra of CVD diamond		Yobin Yvon HR800	514.5 nm Ar+ laser focused to a 1 µm-diameter spot and with 5 mW incident beam power. The spectral resolution was 2 cm^{-1} and the spectra were calibrated using the 1332.2 cm^{-1} line of a SCD
Electrical				
Network analyser	Measure S-parameters of SAW devices		Agilent ENA5071B	
Sourcemeter	IV-measurements		Keithley 2400	
Others				
E-beam evaporation			Edwards Auto 306	
RTA			SEMCO	
Sputtering			Quorum E600	

Table A-1 Instrumental details